CO$_2$ Chemistry

Edited by Walter Leitner and Thomas E. Müller

Imprint

CO$_2$ Chemistry

Thomas E. Müller[*1] and Walter Leitner[*2]

Editorial

Address:
[1]CAT Catalytic Center, RWTH Aachen University, Worringerweg 2, 52074 Aachen, Germany and [2]Lehrstuhl für Technische Chemie und Petrolchemie, ITMC, RWTH Aachen University, Worringerweg 1, 52074 Aachen, Germany

Email:
Thomas E. Müller[*] - Thomas.Mueller@catalyticcenter.rwth-aachen.de;
Walter Leitner[*] - Walter.Leitner@itmc.rwth-aachen.de

* Corresponding author

This article is part of the Thematic Series "CO$_2$ Chemistry".

Guest Editors: W. Leitner and T. E. Müller

It is our pleasure to introduce this Thematic Series on CO$_2$ chemistry for the Beilstein Journal of Organic Chemistry (BJOC). Today's growing demand for energy, materials and chemicals has prompted renewed interest in CO$_2$ chemistry. More resource-efficient chemical processes are being implemented, while we are facing the change from a fossil fuel-based society to one that must rely on the sustainable use of renewable resources. Although there are many ways to harness renewable energy resources, much of the needed materials and chemicals will continue to be carbon-based.

One of the most abundant renewable resources of carbon is carbon dioxide (Figure 1). Carbon capture technologies are being implemented [1] to capture a part of the yearly anthropogenic CO$_2$ emission of 36,600 million metric tons of CO$_2$ [2]. If only a fraction of the captured CO$_2$ stream could be made available for chemical production, a significant contribution to the annual production of carbon-based materials and chemicals could be supplied. Here, we offer the reader to relate these figures with the annual production of polymeric materials of 280 million metric tons [3]. Remarkably, 110 million metric tons of CO$_2$ per year for producing urea, methanol and salicylic

acid are industrial reality today. These applications clearly illustrate the path forward. Due to the abundant availability of pure CO$_2$ gas streams [1], it is only logical to promote a more widespread use of carbon dioxide as chemical feedstock. Notably, the use of CO$_2$ for manufacturing materials and chemicals is still in its infancy.
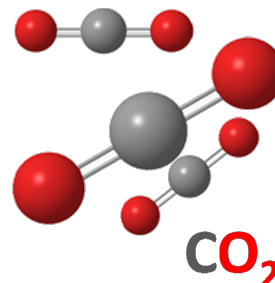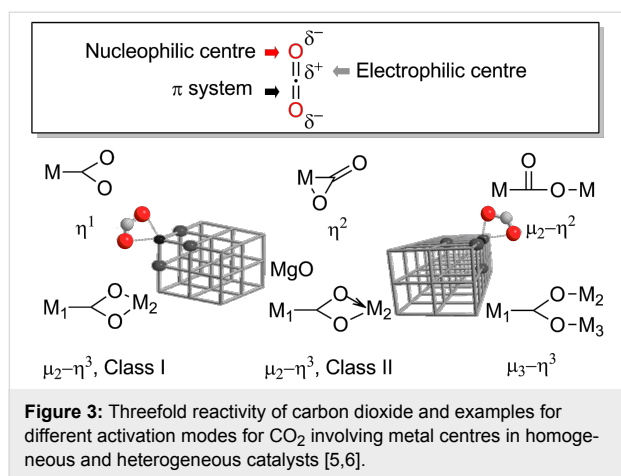

Figure 1: The carbon dioxide molecule.

Carbon dioxide (CO$_2$) has long stirred the fascination of chemists. A rich chemistry has evolved utilizing this molecule in chemical synthesis [4]. Hitherto the low reactivity of the CO$_2$

molecule poses significant challenges to the utilization of carbon dioxide in industrial applications. Thus, the CO_2 molecule is commonly perceived to be highly inert. This perception clearly stems from the high chemical stability of carbon dioxide. However, the reactivity of the CO_2 molecule may be underestimated. Carbon dioxide is isoelectronic to highly reactive molecules such as isocyanates and ketenes (Figure 2). This implies that reactivity and kinetic limitations may be encountered much less frequently in the chemical conversion of carbon dioxide than generally assumed.

Figure 2: Examples of highly reactive molecules that are isoelectronic to carbon dioxide.
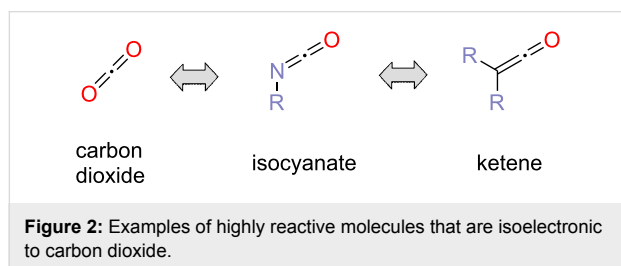
To overcome its thermodynamically low level, additional energy is required to activate the CO_2 molecule. The threefold reactivity (Figure 3) of CO_2 with a nucleophilic oxygen atom, an electrophilic carbon atom and a π system provides the chemist with many options. Likewise, a rich coordination chemistry to metal centres has been reported for CO_2 [5,6]. A forthcoming path is the reaction of CO_2 to form energy-rich intermediates that can subsequently transfer the CO_2 molecule to target substrates [7]. The use of efficient catalysts is often another requisite to direct the reaction pathways with high selectivity to yield the desired target products and to overcome kinetic limitations associated with certain slow elementary steps.

Figure 3: Threefold reactivity of carbon dioxide and examples for different activation modes for CO_2 involving metal centres in homogeneous and heterogeneous catalysts [5,6].

This Thematic Series on CO_2 chemistry presents intriguing approaches regarding different methodologies to activate carbon dioxide. One emerging field is the electrochemical fixation of CO_2, which can be applied in the synthesis of carboxylic acids [8]. Also highly interesting is the combination of enzymatic and photocatalytic approaches for activating CO_2 [9]. Bifunctional catalyst systems are frequently needed and well-understood in the synthesis of cyclic carbonates [10]. Activation of carbon dioxide by inserting it into metal-alkoxide bonds allows for subsequent applications in polymer synthesis such as the copolymerisation of carbon dioxide with epoxides and other co-monomers [11]. Here, the catalysis with cobalt complexes still presents surprising effects [12]. More efficient systems for CO_2 capture are being developed on the basis of amine-functionalised ionic liquids where zwitterionic adduct formation is the key to higher efficiency [13]. Furthermore, many physical properties of carbon dioxide are outstanding, making supercritical carbon dioxide a solvent like no other [14].

Altogether, the articles in this Thematic Series present a remarkable overview of opportunities in the field of CO_2 chemistry from many of its top practitioners. These opportunities are harbingers of the many additional reactions, reactivity modes and catalysts that remain to be discovered. Exploiting carbon dioxide to create economic value will be the driving force for the more widespread use of this fascinating molecule. In the long term, we envision mankind creating an anthropogenic carbon loop where CO_2 released at the end of the life span of carbon-based goods of everyday life is again employed in the production of new materials and chemicals.

We are highly grateful to the authors for their excellent contributions towards making this Thematic Series as successful as the previous editions.

Thomas E. Müller and Walter Leitner

Aachen, April 2015

References

1. Markewitz, P.; Kuckshinrichs, W.; Leitner, W.; Linssen, J.; Zapp, P.; Bongartz, R.; Schreiber, A.; Müller, T. E. *Energy Environ. Sci.* **2012,** *5,* 7281. doi:10.1039/c2ee03403d
2. Canadell, J. G.; Le Quére, C.; Raupach, M. R.; Field, C. B.; Buitenhuis, E. T.; Ciais, P.; Conway, T. J.; Gillett, N. P.; Houghton, R. A.; Marland, G. *Proc. Natl. Acad. Sci. U. S. A.* **2007,** *104,* 18866–18870. doi:10.1073/pnas.0702737104
3. *Plastics - The Facts;* PlasticsEurope Association of Plastics Manufacturers: Brussels, Belgium, 2012.
4. Peters, M.; Köhler, B.; Kuckshinrichs, W.; Leitner, W.; Markewitz, P.; Müller, T. E. *ChemSusChem* **2011,** *4,* 1216. doi:10.1002/cssc.201000447
5. Chiesa, M.; Giamello, E. *Chem. – Eur. J.* **2007,** *13,* 1261. doi:10.1002/chem.200600792
6. Gibson, D. H. *Chem. Rev.* **1996,** *96,* 2063. doi:10.1021/cr940212c

7. Elmas, S.; Subhani, M. A.; Vogt, H.; Leitner, W.; Müller, T. E. *Green Chem.* **2013,** *15,* 1356. doi:10.1039/c3gc40147b

8. Matthessen, R.; Fransaer, J.; Binnemans, K.; De Vos, D. E. *Beilstein J. Org. Chem.* **2014,** *10,* 2484. doi:10.3762/bjoc.10.260

9. Aresta, M.; Dibenedetto, A.; Baran, T.; Angelini, A.; Łabuz, P.; Macyk, W. *Beilstein J. Org. Chem.* **2014,** *10,* 2556. doi:10.3762/bjoc.10.267

10. Martín, C.; Kleij, A. W. *Beilstein J. Org. Chem.* **2014,** *10,* 1817. doi:10.3762/bjoc.10.191

11. Jeon, J. Y.; Eo, S. C.; Varghese, J. K.; Lee, B. Y. *Beilstein J. Org. Chem.* **2014,** *10,* 1787. doi:10.3762/bjoc.10.187

12. Elmas, S.; Subhani, M. A.; Leitner, W.; Müller, T. E. *Beilstein J. Org. Chem.* **2015,** *11,* 42. doi:10.3762/bjoc.11.7

13. Yang, Z.-Z.; He, L.-N. *Beilstein J. Org. Chem.* **2014,** *10,* 1959. doi:10.3762/bjoc.10.204

14. Peach, J.; Eastoe, J. *Beilstein J. Org. Chem.* **2014,** *10,* 1878. doi:10.3762/bjoc.10.196

Copolymerization and terpolymerization of carbon dioxide/propylene oxide/phthalic anhydride using a (salen)Co(III) complex tethering four quaternary ammonium salts

Jong Yeob Jeon, Seong Chan Eo, Jobi Kodiyan Varghese and Bun Yeoul Lee[*]

Open Access

Abstract

The (salen)Co(III) complex **1** tethering four quaternary ammonium salts, which is a highly active catalyst in CO_2/epoxide copolymerizations, shows high activity for propylene oxide/phthalic anhydride (PO/PA) copolymerizations and PO/CO_2/PA terpolymerizations. In the PO/PA copolymerizations, full conversion of PA was achieved within 5 h, and strictly alternating copolymers of poly(1,2-propylene phthalate)s were afforded without any formation of ether linkages. In the PO/CO_2/PA terpolymerizations, full conversion of PA was also achieved within 4 h. The resulting polymers were gradient poly(1,2-propylene carbonate-*co*-phthalate)s because of the drift in the PA concentration during the terpolymerization. Both polymerizations showed immortal polymerization character; therefore, the molecular weights were determined by the activity (g/mol-**1**) and the number of chain-growing sites per **1** [anions in **1** (5) + water (present as impurity) + ethanol (deliberately fed)], and the molecular weight distributions were narrow (M_w/M_n, 1.05–1.5). Because of the extremely high activity of **1**, high-molecular-weight polymers were generated (M_n up to 170,000 and 350,000 for the PO/PA copolymerization and PO/CO_2/PA terpolymerization, respectively). The terpolymers bearing a substantial number of PA units (f_{PA}, 0.23) showed a higher glass-transition temperature (48 °C) than the CO_2/PO alternating copolymer (40 °C).

Introduction

Carbon dioxide (CO_2) can be utilized to prepare aliphatic polycarbonates through coupling reactions with epoxides [1-6]. The pioneering work for this copolymerization was introduced by Inoue in 1969 [7]. Eventually, a highly active and efficient cata-lyst was developed based on the concept of combining (salen)Co(III) units with quaternary ammonium salts in a molecule [8-12]. The highly efficient catalyst (**1** in Scheme 1) showed a high turnover frequency (TOF, 16,000 h^{-1}), high

Scheme 1: Synthesis of poly(propylene carbonate) (PPC) using catalyst **1**.
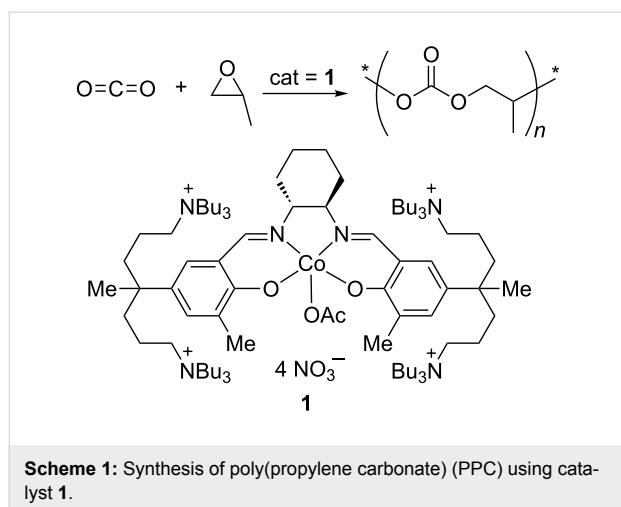
molecular weight (M_n, up to 300,000), and good selectivity (>99%). These promising performances motivated to construct a continuous-process pilot plant in industry [13]. Currently, many hurdles in the preparation of **1** on a large scale have been overcome, and an economical synthesis on the 100 kg scale has been achieved [14-16], along with precise control of the molecular weight and chain topology, facilitating the applications of these attractive materials [14,17-19]. Now, the production of poly(propylene carbonate) (PPC) using catalyst **1** is at the stage of the final decision regarding a commercial investment. Another success story using double metal cyanide (DMC) catalysts has been reported recently [20]. The DMC catalysts provided low-molecular-weight CO_2/PO copolymers containing significant numbers of ether linkages [21,22].

PO and ethylene oxide (EO) are bulk chemicals produced annually on the million-ton scale, and the focus in industry has been on CO_2/PO and CO_2/EO copolymerizations. Catalyst **1** is also highly active in CO_2/EO copolymerizations [23]. Even though the CO_2/PO or CO_2/EO copolymer itself shows some advantageous properties such as biodegradability, good adhesiveness, good barrier properties, and clean burning properties, the incorporation of a third monomer has also been pursued to improve the properties and hence facilitate its use in more widespread applications. For example, the terpolymerization of CO_2/PO/cyclohexene oxide (CHO) was successful, providing resins, of which the glass-transition temperatures (T_g) were modulated in the range of 50–100 °C according to the mole fraction of the incorporated CHO [24,25]. However, the feeding of a third monomer such as CHO gives rise to intrinsic problems in terms of commercial operation. The third monomer is not completely consumed, and the remaining CHO should be recovered and recycled, which is a severe burden because of its high boiling point (130 °C). Moreover, the toxic CHO should be removed completely from the resin for use in our daily life. In this work,

we demonstrate the complete incorporation of the third monomer of phthalic anhydride (PA) in CO_2/PO copolymerizations using catalyst **1**.

Results and Discussion
PO/PA copolymerizations
Alternating copolymerizations of epoxides and cyclic anhydrides using a diiminate zinc catalyst as well as a chromium(III) salen complex have been reported [26,27]. Long reaction times (>10 h) were needed to reach full conversion, and the average molecular weights were in the region of several ten thousand. When a zinc glutarate catalyst was used in PO/PA copolymerization, significant numbers of ether linkages were generated through consecutive PO incorporation [28].

When PA (1.00 g) and PO (10.4 g) were reacted using catalyst **1** (3.0 mg; **1**/PA/PO = 1:3,750:100,000) at 80 °C for 3 h, 100% conversion of PA was achieved (entry 1 in Table 1). The ^{1}H NMR spectrum indicated that no PA remained in the resulting solution, and that the generated polymer was strictly alternating with no ether linkages (Scheme 2, Figure 1(A)). The isolated polymer mass was 1.39 g, in exact agreement with that calculated (1.39 g) on the basis of full conversion of 1.0 g PA to the strictly alternating PO/PA copolymer. Three aromatic signals were observed in the ^{1}H NMR spectra at 7.71, 7.68, and 7.50 ppm in 1:1:2 ratios (Figure 1(A)). The OCH(Me) signal was observed at 5.35 ppm, while the CH_2O signal was observed at 4.3–4.5 ppm. When a larger amount of PA (2.0 g) was added, the conversion of PA was 76% after 3 h (Table 1, entry 2) and 96% after 4.5 h (Table 1, entry 3), but full conversion of PA was achieved after running the copolymerization for 5.0 h (Table 1, entry 4). When 3.0 g PA was added, the conversion of PA was very low (16%), and after polymerization, a lot of unreacted PA was deposited as a solid. The solubility of PA in PO was limited; 3.0 g of PA might not dissolve fully in 10 g of PO even at a high temperature of 80 °C. Catalyst residues were removed completely through filtration with a short pad of silica gel after the polymerization. After filtration, the light orange solution became colorless, and the isolated polymer was also colorless (see Supporting Information File 1). If PA was not fully converted, the polymers were obtained as admixtures with unreacted PA (Table 1, entries 2 and 3).
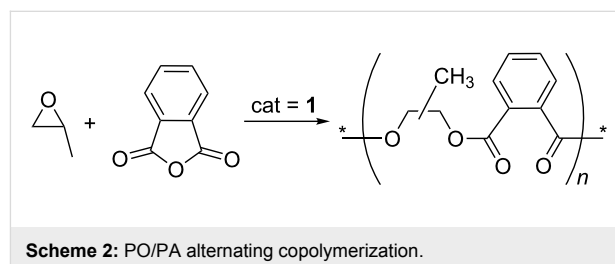

Scheme 2: PO/PA alternating copolymerization.

Table 1: PO/PA alternating copolymerization results with catalyst **1**.[a]

Entry	PA (g)	EtOH (mg)	Time (h)[b]	PA conversion (%)	Yield[c] (g)	Activity (Kg/g-cat)	M_n[d]	M_w/M_n[d]	T_g[e] (°C)
1	1.0	0	3.0	100	1.39 (1.39)	0.46	59,000	1.61	65
2	2.0	0	3.0	76	(2.2)	(0.73)	80,000	1.26	62
3	2.0	0	4.5	96	(2.7)	(0.90)	116,000	1.27	65
4	2.0	0	5.0	100	2.70 (2.78)	0.90	167,000	1.21	65
5	2.0	5.0	5.0	100	2.70 (2.78)	0.90	17,000	1.43	63
6	2.0	10	5.0	100	2.63 (2.78)	0.88	11,000	1.42	60
7	2.0	15	5.0	100	2.54 (2.78)	0.84	9,000	1.40	58
8	2.0	20	5.0	100	2.48 (2.78)	0.83	6,000	1.40	55

[a]Polymerization conditions: PO (10.4 g, 180 mmol), catalyst **1** (3.0 mg, 1.8 µmol), temperature (80 °C). [b]Including heating time of ca. 50 min. [c]Values in parentheses calculated from the conversion. [d]Determined on GPC using a polystyrene standard. [e]Determined on DSC.
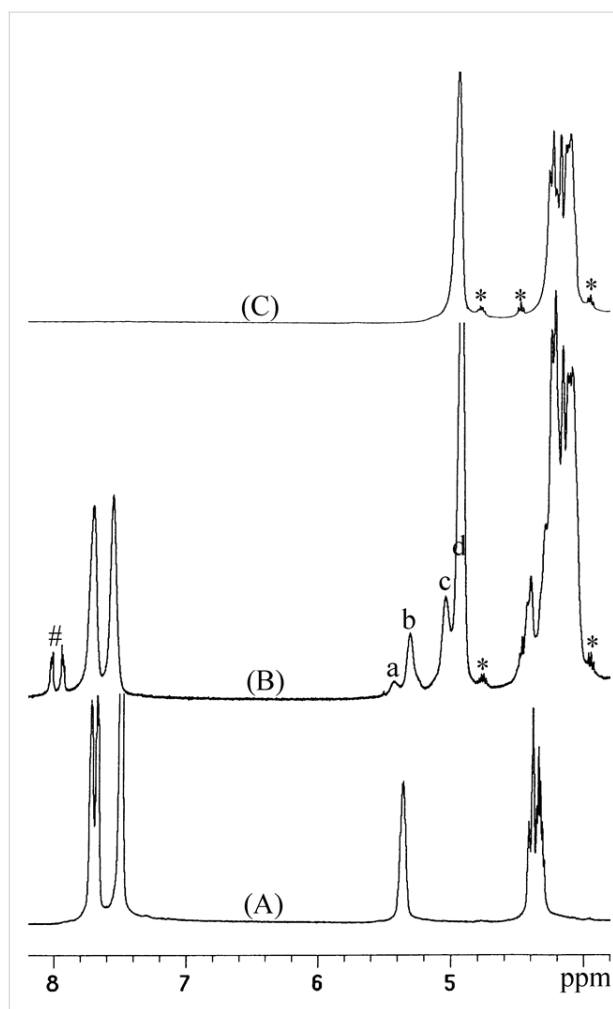

Figure 1: ^{1}H NMR spectrum of crude products in the PO/PA alternating polymerization (A, entry 1 in Table 1), PO/CO$_2$/PA terpolymerization (B, entry 3 in Table 2), and CO$_2$/PO alternating copolymerization (C) ("a" signal for ester-C*H*(Me)CH$_2$-ester; "b" signal for ester-C*H*(Me)CH$_2$-carbonate; "c" signal for ester-CH$_2$C*H*(Me)-carbonate; "d" signal for carbonate-CH$_2$C*H*(Me)-carbonate; "*" signals for propylene carbonate; "#" signals for unreacted PA).

At the full conversion of 1.0 g PA, the number average molecular weight (M_n) of the resulting polymer was 59,000 (Table 1, entry 1). Upon increasing the PA feed amount to 2.0 g and achieving full conversion, a high-molecular-weight polymer with M_n = 167,000 was obtained (Table 1, entry 4). As the reaction time (and consequently, the PA conversion) increased, the number average molecular weight (M_n) increased gradually with a narrow molecular weight distribution (M_w/M_n ca. 1.2) preserved in all cases, indicating living or immortal polymerization (Table 1, entries 2–4). Bimodal distributions were observed in the GPC curves (Figure 2). The peak molecular weight in the high-molecular-weight mode was always twice that in the low-molecular-weight mode. The chains in the high-molecular-weight mode were attributed to those grown biaxially from water, which was present as an impurity, while those in the low-molecular-weight mode were grown from the nitrate and acetate anions in **1**. The numbers of polymer chains generated per **1**, which was calculated from the yield (g) and M_n values [yield/(M_n × (mole of **1**)], were 13, 15, 13, and 9 for the samples in Table 1, entries 1–4, respectively. These numbers were roughly in agreement with the sum of the number of anions in **1** (5) and the number of water molecules per **1** present as an impurity (8, 10, 8, and 4, respectively). The portion of the high-molecular-weight mode (that is, the portion of chains grown from water molecules) relative to the portion of the low-molecular-weight mode decreased in the GPC curves in the order of entries 2, 3, and 4 (see Supporting Information File 1). This order was in accord with the number of water molecules calculated above from the yield and M_n values (10, 8, and 4, respectively). These observations indicated that the polymer chains grew uniformly from the anions in **1** and water molecules with immortal polymerization character. Water molecules might be incorporated into the polymerization system from various sources such as PO, CO$_2$ gas, catalyst, and the reactor surface. The amount fluctuated batch by batch in the lab scale polymerization.
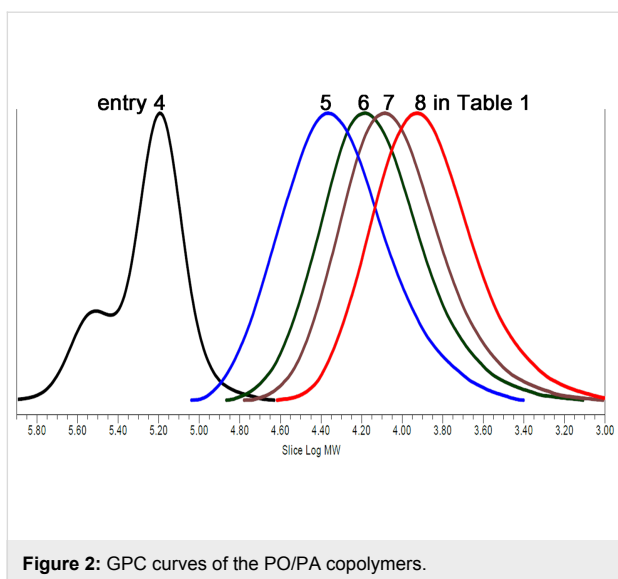
Figure 2: GPC curves of the PO/PA copolymers.

Upon the addition of ethanol, which was expected to act as a chain-transfer agent, the M_n values decreased significantly and were regulated precisely by the amount of ethanol fed (Table 1, entries 5–8). With 5.0 mg of ethanol fed at the PA feeding of 2.0 g, full PA conversion was achieved by running for 5 h, and the M_n value of the resulting polymer was 17,000, indicating that the ethanol worked well as a chain-transfer agent (Table 1, entry 5). As the amount of ethanol was increased to 10, 15, and 20 mg, full conversions were also achieved in 5 h, and the M_n values decreased systematically to 11,000, 9,000, and 6,000, respectively. The number of polymer chains per **1**, calculated from the yield and M_n values [yield/(M_n × (mole of **1**)], were 92, 141, 173, and 259 for the samples obtained with 5, 10, 15, and 20 mg ethanol feeding, respectively. These numbers were in rough agreement with the sum of the number of ethanol molecules per **1** (60, 120, 180, and 240, respectively) and the number of anions in **1** (5). The polymer chains were grown uniformly from the fed ethanol and the anions in **1** with immortal polymerization character. The portion of the chains grown biaxially from impurity water molecules was relatively small, and unimodal distributions were observed when ethanol was fed. The T_g value of the PO/PA copolymer was 65 °C when the molecular weight was high (mostly M_n > 80000, Table 1, entries 1–4), and decreased gradually from 63 °C to 55 °C as M_n was lowered from 17,000 to 6,000 (Table 1, entries 5–8).

PO/CO₂/PA terpolymerizations

The terpolymerization of CHO/CO_2/diglycolic anhydride using a diiminate zinc catalyst has been reported. Here, the block copolymer of poly(ester-*block*-carbonate) was formed through the faster reaction of CHO/anhydride coupling, and after complete conversion of the anhydride, the carbonate block was grown by CO_2/CHO coupling [29]. Porphyrin Al or Cr(III) complexes also generated block copolymers in PO/CO_2/PA terpolymerizations [30]. The terpolymerizations of CHO/CO_2/ PA and PO/CO_2/maleic anhydride using a zinc glutarate catalyst have also been reported, where random copolymers containing some ether linkages were generated [28,31].

When CO_2 gas was also pressurized under the PO/PA copolymerization conditions [PA (1.00 g), PO (10.4 g), **1** (3.0 mg; **1**/ PA/PO = 1:3,750:100,000), 80 °C, 3 h], all the fed PA was consumed (entry 4, Table 2). No signals due to unreacted PA were observed in the ^{1}H NMR spectrum of the resulting crude product dissolved in THF-d_8, in which both PA and the resulting polymer were freely soluble. Upon shortening the reaction time to 1.5, 2.0, and 2.5 h, unreacted PA signals were observed at 8.0 and 7.9 ppm along with the resulting polymer signals (Figure 1(B)). In all cases, negligible amounts of propylene carbonate were generated (less than 2 mol % per consumed PO) and no ether linkages were formed (Scheme 3). The conversions of PA were calculated simply from the ^{1}H NMR spectra by using the formula $(I_{7.5-7.8})/(I_{7.5-7.8} + I_{7.9-8.1})$, where I is the integrated value of the region defined by the subscript. As the reaction time increased, the PA conversion increased (Table 2, entries 1–4), and full conversion of PA was achieved with the formation of 6.5 g of polymer at a reaction time of 3.0 h (including the heating time of ca. 50 min). The formation of 6.5 g of polymer corresponded to a commercially acceptable high activity of 2.2 kg-polymer/g-catalyst. The CO_2 pressure decreased monotonously from 35 to 32 bar up to the cutoff time of 3 h, indicating that the catalyst was not deactivated during the polymerization. The turnover number (TON = mole of consumed PO/mole of **1**) and turnover frequency (TOF) at the full PA conversion were calculated to be 32,000 and 12,000 h⁻¹, so the performance of **1** was not deteriorated by feeding PA. In the absence of PA (that is, in CO_2/PO copolymerizations), catalyst **1** showed a TOF of approximately 16,000 h⁻¹.
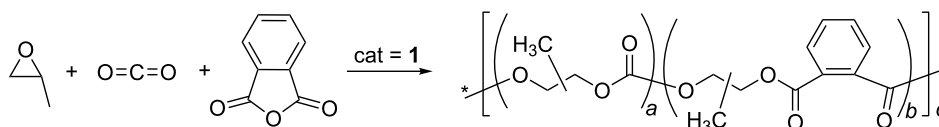
Scheme 3: CO₂/PO/PA terpolymerization.

Table 2: CO_2/PO/PA terpolymerization results with catalyst **1**.[a]

Entry	PA (g)	EtOH (mg)	Time (h)[b]	PA Conversion (%)	f_{PA}[c]	Yield[d] (g)	Activity (Kg/g-cat.)	M_n[e]	M_w/M_n[e]	T_g[f] (°C)
1	1.0	0	1.5	38	0.12	(2.5)	(0.83)	115,000	1.22	29, 69
2	1.0	0	2.0	68	0.23	(2.5)	(0.83)	215,000	1.33	48
3	1.0	0	2.5	91	0.15	(4.7)	(1.6)	198,000	1.40	44
4	1.0	0	3.0	100	0.11	6.5 (7.0)	2.2	381,000	1.27	41
5	2.0	0	1.5	31	0.31	(1.8)	(0.60)	87,000	1.20	24, 73
6	2.0	0	2.0	86	0.39	(4.2)	(1.4)	193,000	1.22	43
7	2.0	0	3.0	100	0.23	7.3 (7.4)	2.4	354,000	1.23	48
8	1.0	5.0	1.5	50	0.18	(2.2)	(0.73)	19,000	1.08	25, 67
9	1.0	10	1.5	59	0.19	(2.6)	(0.87)	10,000	1.06	25, 72
10	1.0	15	1.5	63	0.22	(2.4)	(0.80)	8,000	1.07	25, 69
11	1.0	20	1.5	63	0.25	(2.2)	(0.73)	5,000	1.05	14
12	1.0	15	2.0	80	0.18	(3.6)	(1.2)	11,000	1.03	28
13	1.0	15	2.5	100	0.13	5.7 (5.9)	1.9	16,000	1.03	39
14	1.0	15	3.0	100	0.12	6.4 (6.3)	2.1	19,000	1.03	39
15	1.0	15	4.0	100	0.10	7.0 (7.6)	2.3	26,000	1.04	38
16	2.0	15	3.0	100	0.24	6.6 (7.2)	2.2	22,000	1.05	43

[a]Polymerization conditions: PO (10.4 g, 180 mmol), catalyst **1** (3.0 mg, 1.8 µmol), CO_2 (35 bar), 80 °C. [b]Including heating time of ca. 50 min. [c]Mole fraction of PA in the polymers determined by ^1H NMR spectroscopy. [d]Values in parentheses calculated from conversion and f_{PA}. [e]Determined on GPC using a polystyrene standard. [f]Determined on DSC.

Catalyst residues could also be removed completely by filtration through a short pad of silica gel to provide colorless polymers (see Supporting Information File 1). The catalyst residue should be removed thoroughly because it is not only toxic, but also leads to the thermal instability of the products [32]. It was not easy to separate the generated polymer and the unreacted PA; the polymers were obtained admixed with the unreacted PA unless 100% conversion of PA was reached.

The pattern of the aromatic signals in the ^1H NMR spectra was different from that observed for the alternating PO/PA copolymer: just two broad signals were observed at 7.71 and 7.57 ppm (Figure 1(B)). Four OCH(Me) signals were observed at 5.45, 5.30, 5.10, and 4.95 ppm. The large signal at 4.95 ppm (marked "d" in Figure 1(B)) was assigned unambiguously to the carbonate-CH(Me)CH$_2$-carbonate signal through comparison with the spectrum of PPC (Figure 1(C)). The signals at 5.30 ppm (marked "b") and 5.10 ppm (marked "c") were assigned to ester-CH(Me)CH$_2$-carbonate and ester-CH$_2$CH(Me)-carbonate, respectively. A comparatively small signal was observed at 5.45 ppm (marked "a"), which was assigned to ester-CH(Me)CH$_2$-ester. The mole fractions of PA in the polymers (f_{PA}) were determined from the ^1H NMR spectra using the equation $f_{PA} = [(I_{7.5-7.8})/4]/I_{4.8-5.4}$, where $I_{7.5-7.8}$ and $I_{4.8-5.4}$ are the integrated values in the region 7.5–7.8 ppm (benzene-H signal) and 4.8–5.4 ppm (OCHMe
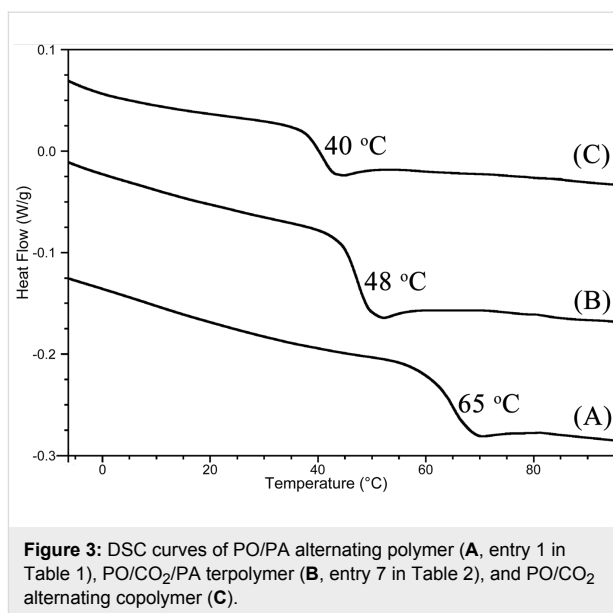
signal), respectively. The yields calculated from the conversion (*c*) and f_{PA} [yield (g) = (206.19 × *y* + 102.08 × *y* × (1 − f_{PA})/f_{PA}), where *y* is the number of moles of consumed PA, that is, *y* = (fed PA (g) × *c*)/148.12], were in good agreement with the measured weights of the isolated polymers at full PA conversion (Table 2, entries 4, 7, 13–16). The f_{PA} values decreased gradually from 0.23 to 0.11 upon increasing the reaction time from 2.0 to 3.0 h (Table 2, entries 2–4). The CO_2 concentration was almost unchanged at the pressure of 35–33 bar, whereas the free PA concentration in solution was gradually depleted, resulting in lower f_{PA} values with increased polymerization times. A deviation was observed at a very early reaction time of 1.5 h (Table 2, entry 1), where the f_{PA} value was low (0.12) even at a high PA concentration. This deviation might be attributed to the uncontrolled reaction temperature. The bomb reactor was warmed slowly using a hot oil bath (80 °C), reaching the desired temperature (80 °C) in ca. 50 min. If the small portion of chains grown during the warming time is ignored, the generated polymers should be gradient poly(1,2-propylene carbonate-*co*-phthalate). The chains grown in the early stages were enriched with PA units, while those grown at a later stage were enriched with or composed solely of carbonate units. When the fed PA amount was doubled to 2.0 g, polymers with higher PA mole fractions were generated (Table 2, entries 5–7). Upon running the reaction for 3.0 h, full conversion of PA was also achieved (Table 2, entry 7). The f_{PA} value at this full conver-

sion was 0.23, which was twice that attained at the PA feeding of 1.0 g. Related stereogradient CO_2/PO copolymers have been reported, in which one end of the polymer chain is enriched with the *R*-isomer of PO, while the other is enriched with the *S*-isomer [33,34]. A related copolymer composed of aliphatic polycarbonate and aromatic polyester units [poly(1,4-butylene terephthalate-*co*-carbonate)], prepared by condensation polymerization of 1,4-butanediol, dimethyl terephthalate, and dimethyl carbonate, has also been reported recently [35,36].

When ethanol (5.0 mg, 60 equiv/**1**) was fed as a chain-transfer agent with 1.0 g PA, faster PA consumption was observed (Table 2, entry 8). At the initial stage of 1.5 h including a heating time of ca. 50 min, the PA conversion was 50% with a high f_{PA} value (0.18) compared with that in the absence of ethanol (PA conversion, 38%; f_{PA}, 0.12). The PA conversions at the identical reaction time of 1.5 h increased gradually from 50% to 63% upon increasing the ethanol feeding amount from 5.0 to 20 mg, and the f_{PA} values also increased gradually from 0.18 to 0.25 (entries 8–11). Because of the faster PA consumption, full PA conversion was achieved in 2.5 h (entry 13). At this full conversion, the polymerization solution was stirrable because of the formation of a low-molecular-weight polymer. By running the polymerization for a further 1.0 or 2.0 h, the yields increased further from 5.7 g to 6.4 and 7.0 g, respectively (entries 14, 15). During the additional polymerization time after full PA conversion, only the carbonate units were grown, resulting in the formation of a block copolymer. One side of the block copolymer was gradient poly(1,2-propylene phthalate-*co*-carbonate), while the other side was poly(1,2-propylene carbonate). When 2.0 g of PA was fed along with 15 mg of ethanol, full conversion of PA was achieved in 3.0 h and the f_{PA} value (0.24) was almost twice that attained at a PA feed of 1.0 g (entry 16).

When a substantial number of PA units (f_{PA}, 0.23) was incorporated in PO/CO_2/PA terpolymers, a high T_g of 48 °C was observed (entries 2 and 7), which was higher than that of the PO/CO_2 alternating copolymer (40 °C), but lower than that of the PO/PA alternating polymer (65 °C) (Figure 3). With a small number of incorporated PA units (f_{PA}, ca. 0.1), T_g was similar to that of the PO/CO_2 alternating copolymer (entries 4, 13–15). For the polymers generated at the early stage (1.5 h), two T_g signals were observed at 25 °C and ca. 70 °C (entries 1, 5, 8–10).

In the polymerization reaction, the nitrate and acetate anions in **1** became chain-growing carbonate or alkoxide anions [14,17]. In the presence of protic compounds such as water (present as an impurity) or alcohols (deliberately added), reversible proton exchange reactions occur rapidly between the chain-growing

Figure 3: DSC curves of PO/PA alternating polymer (**A**, entry 1 in Table 1), PO/CO_2/PA terpolymer (**B**, entry 7 in Table 2), and PO/CO_2 alternating copolymer (**C**).

anions and protic compounds, resulting in uniform chain growth not only from the protic compounds but also from the anions in **1**. In all cases, when the polymerizations were carried out without the deliberate addition of a chain-transfer agent (Table 2, entries 1–7), bimodal GPC curves were observed (see Supporting Information File 1). Polymer chains in the high-molecular-weight mode were grown biaxially from water, while those in the low-molecular-weight mode were grown from the anions in **1**. The ratio of the two modes was different for each entry. A very small amount of catalyst **1** was fed under the polymerization conditions employed (**1**/PO = 1:100,000), so the number of impurity water molecules was not negligible, and varied in the range of the same order of the number of anions in **1**, even with thorough drying of PO and CO_2. High-molecular-weight polymers with M_n 381,000 and 354,000 were obtained at the full conversions of 1.0 g and 2.0 g PA, respectively (Table 2, entries 4 and 7). The molecular weights were controlled by the amount of ethanol fed as a chain-transfer agent. At the feeding amount of 15 mg of ethanol (180 equiv per **1**) and full conversion of PA (Table 2, entries 13–16), low-molecular-weight polymers with M_n 16,000–26,000 were generated. The numbers of polymer chains generated per **1** under those conditions were calculated to be 198, 187, 145, and 167, respectively, roughly in agreement with the number of ethanol molecules (180 equiv per **1**). For the feeding of a large amount of ethanol (180 equiv per **1**), the number of polymer chains grown biaxially from the water molecules was negligible, and very narrow unimodal distributions were observed with M_w/M_n of ca. 1.05 in the GPC curves.

Scheme 4 shows the PA incorporation process in the PO/CO_2/ PA terpolymerizations. In addition to the direct attack of the

alkoxide anion on PA, another PA consumption process might operate in the presence of the chain transfer agent such as deliberated added ethanol or impurity water. In this process, PA directly reacted with the formed OH chain terminus, leading to incorporation of PA without the action of the catalyst. This process made the PA conversion faster, consequently helping to achieve the full conversion of PA.

Scheme 4: PA incorporation process in PO/CO$_2$/PA terpolymerization.
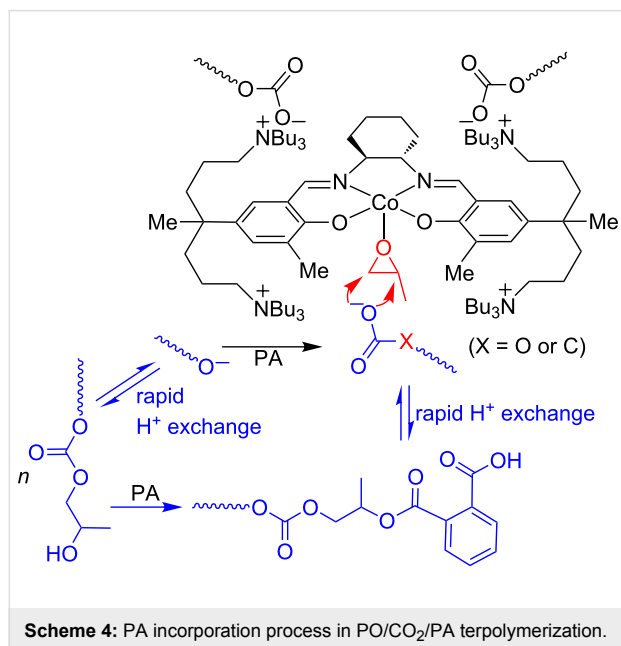
Conclusion

The (salen)Co(III) complex **1** tethering four quaternary ammonium salts, which is a highly active catalyst for CO$_2$/PO copolymerization, worked efficiently as a catalyst in both PO/PA copolymerizations and CO$_2$/PO/PA terpolymerizations. An attractive feature in view of commercial application is that full conversion of PA could be achieved within 5 h in both polymerizations, even under the conditions of a high feeding amount of PA (2.0 g PA/10 g PO) and a very small feeding amount of catalyst **1** (3.0 mg). No ether linkages were formed in either of the polymerizations to afford poly(1,2-propylene phthalate) or poly(1,2-propylene phthalate-*co*-carbonate). The latter had a gradient composition with one end enriched with PA units and the other enriched with carbonate units. Both showed immortal polymerization character: the molecular weights of the resulting polymer were controlled precisely by the activity (g/mol-**1**) and the number of chain-growing sites per **1** [anions in **1** (5) + water (present as impurity) + ethanol (deliberately fed)], and the molecular weight distributions were narrow (M_w/M_n, 1.05–1.5). Because of the high activity of **1**, polymers with very high molecular weights were generated (M_n up to 170,000 and 350,000 for PO/PA copolymerization and CO$_2$/PO/PA terpolymerization, respectively). The terpolymer bearing a substantial

number of PA units (f_{PA}, 0.23) showed a higher T_g value (48 °C) than the CO$_2$/PO alternating copolymer (40 °C).

Experimental

General remarks. CO$_2$ gas (99.999% purity) was dried through storage in a column of molecular sieves 3Å at a pressure of 30 bar. PO was dried by stirring over CaH$_2$ and then vacuum-transferred to a reservoir. PA was purchased from Aldrich and purified by recrystallization in ethyl acetate. ^{1}H NMR (400 MHz) and ^{13}C NMR (100 MHz) spectra were recorded on a Varian Mercury Plus 400 instrument. Gel permeation chromatography (GPC) was performed in THF at 40 °C using a Waters Millennium apparatus with polystyrene standards. The T_g data were determined from a second heating at a heating rate of 10 °C/min by differential scanning calorimetry (DSC) using a Thermal Analysis Q10 instrument.

Typical procedure for PO/PA alternating copolymerizations. A bomb reactor (ca. 50 mL) was assembled inside a glove box after being charged with **1** (3.0 mg, 1.8 μmol), PO (10.4 g, 179 mmol), and PA (and ethanol as a chain-transfer agent). The reactor was immersed in a hot oil bath (80 °C). After running of the polymerization for a given time, the reactor was cooled to room temperature. An aliquot was taken to measure the PA conversion by ^{1}H NMR spectroscopy. The polymer solution was filtered over a short pad of silica gel to remove the catalyst residue. The silica gel pad was washed with methylene chloride (10 mL × 2). The colorless filtrates were combined. The solvent was removed using a rotary evaporator, and the residual solvent was removed completely by keeping the isolated lump in a vacuum oven overnight at 100 °C. When the PA conversion was not 100%, the polymer was obtained admixed with unreacted PA. For DSC studies, small pieces of the polymer lump admixed with the unreacted PA were dissolved in a copious amount of CH$_2$Cl$_2$, and the resulting solution was eluted through a relatively long pad of silica gel.

Typical procedure for PO/CO$_2$/PA terpolymerizations. A bomb reactor (ca. 50 mL) was assembled inside a dry box after being charged with **1** (3.0 mg, 1.8 μmol), PO (10.4 g, 179 μmol), and PA (and ethanol as a chain-transfer agent). The CO$_2$ gas was pressurized to 25 bar at room temperature, and the reactor was then immersed in a hot oil bath (80 °C). When the temperature inside the bomb reactor reached the bath temperature, the pressure was 35 bar. After running of the polymerization for a given time, the reactor was cooled to room temperature through immersion in an ice bath. CO$_2$ gas was released and the reactor was opened. An aliquot was taken to measure the PA conversion by ^{1}H NMR spectroscopy. The catalyst removal and work-up procedures were as described for the PO/PA alternating copolymerizations.

Supporting Information

Supporting Information File 1
^{1}H NMR spectra, ^{13}C NMR spectra, GPC curves, and the pictures of the isolated polymers in PO/PA alternating polymerizations and PO/CO_2/PA terpolymerizations. [http://www.beilstein-journals.org/bjoc/content/supplementary/1860-5397-10-187-S1.pdf]

Acknowledgements

References

1. Darensbourg, D. J.; Wilson, S. J. *Green Chem.* **2012,** *14,* 2665–2671. doi:10.1039/c2gc35928f
2. Lu, X.-B.; Ren, W.-M.; Wu, G.-P. *Acc. Chem. Res.* **2012,** *45,* 1721–1735. doi:10.1021/ar300035z
3. Klaus, S.; Lehenmeier, M. W.; Anderson, C. E.; Rieger, B. *Coord. Chem. Rev.* **2011,** *255,* 1460–1479. doi:10.1016/j.ccr.2010.12.002
4. Kember, M. R.; Buchard, A.; Williams, C. K. *Chem. Commun.* **2011,** *47,* 141–163. doi:10.1039/c0cc02207a
5. Luinstra, G. A. *Polym. Rev.* **2008,** *48,* 192–219. doi:10.1080/15583720701834240
6. Coates, G. W.; Moore, D. R. *Angew. Chem., Int. Ed.* **2004,** *43,* 6618–6639. doi:10.1002/anie.200460442
7. Inoue, S.; Koinuma, H.; Tsuruta, T. *J. Polym. Sci., Part B: Polym. Lett.* **1969,** *7,* 287–292. doi:10.1002/pol.1969.110070408
8. Noh, E. K.; Na, S. J.; S, S.; Kim, S.-W.; Lee, B. Y. *J. Am. Chem. Soc.* **2007,** *129,* 8082–8083. doi:10.1021/ja071290n
9. S, S.; Min, J. K.; Seong, J. E.; Na, S. J.; Lee, B. Y. *Angew. Chem., Int. Ed.* **2008,** *47,* 7306–7309. doi:10.1002/anie.200801852
10. Na, S. J.; S., S.; Cyriac, A.; Kim, B. E.; Yoo, J.; Kang, Y. K.; Han, S. J.; Lee, C.; Lee, B. Y. *Inorg. Chem.* **2009,** *48,* 10455–10465. doi:10.1021/ic901584u
11. Nakano, K.; Kamada, T.; Nozaki, K. *Angew. Chem., Int. Ed.* **2006,** *45,* 7274–7277. doi:10.1002/anie.200603132
12. Ren, W.-M.; Liu, Z.-W.; Wen, Y.-Q.; Zhang, R.; Lu, X.-B. *J. Am. Chem. Soc.* **2009,** *131,* 11509–11518. doi:10.1021/ja9033999
13. Ok, M. A.; Jeon, M. In *ANTEC 2011 plastics: 69th Annual technical Conference Proceedings,* Boston, Massachusetts, USA, May 1–5, 2011; Society of Plastics Engineers, 2011; pp 2134–2139.
14. Cyriac, A.; Lee, S. H.; Varghese, J. K.; Park, E. S.; Park, J. H.; Lee, B. Y. *Macromolecules* **2010,** *43,* 7398–7401. doi:10.1021/ma101259k
15. Jeon, J. Y.; Varghese, J. K.; Park, J. H.; Lee, S. H.; Lee, B. Y. *Eur. J. Org. Chem.* **2012,** 3566–3569. doi:10.1002/ejoc.201200370
16. Min, J.; Seong, J. E.; Na, S. J.; Cyriac, A.; Lee, B. Y. *Bull. Korean Chem. Soc.* **2009,** *30,* 745–748. doi:10.5012/bkcs.2009.30.3.745
17. Cyriac, A.; Lee, S. H.; Lee, B. Y. *Polym. Chem.* **2011,** *2,* 950–956. doi:10.1039/c0py00365d
18. Cyriac, A.; Lee, S. H.; Varghese, J. K.; Park, J. H.; Jeon, J. Y.; Kim, S. J.; Lee, B. Y. *Green Chem.* **2011,** *13,* 3469–3475. doi:10.1039/c1gc15722a
19. Lee, S. H.; Cyriac, A.; Jeon, J. Y.; Lee, B. Y. *Polym. Chem.* **2012,** *3,* 1215–1220. doi:10.1039/c2py00010e
20. Langanke, J.; Wolf, A.; Hofmann, J.; Böhm, K.; Subhani, M. A.; Müller, T. E.; Leitner, W.; Gürtler, C. *Green Chem.* **2014,** *16,* 1865–1870. doi:10.1039/c3gc41788c
21. Varghese, J. K.; Park, D. S.; Jeon, J. Y.; Lee, B. Y. *J. Polym. Sci., Part A: Polym. Chem.* **2013,** *51,* 4811–4818. doi:10.1002/pola.26905
22. Gao, Y.; Gu, L.; Qin, Y.; Wang, X.; Wang, F. *J. Polym. Sci., Part A: Polym. Chem.* **2012,** *50,* 5177–5184. doi:10.1002/pola.26366
23. Jeon, J. Y.; Lee, J. J.; Varghese, J. K.; Na, S. J.; Sujith, S.; Go, M. J.; Lee, J.; Ok, M. A.; Lee, B. Y. *Dalton Trans.* **2013,** *42,* 9245–9254. doi:10.1039/c2dt31854g
24. Seong, J. E.; Na, S. J.; Cyriac, A.; Kim, B. W.; Lee, B. Y. *Macromolecules* **2009,** *43,* 903–908. doi:10.1021/ma902162n
25. Ren, W.-M.; Zhang, X.; Liu, Y.; Li, J.-F.; Wang, H.; Lu, X.-B. *Macromolecules* **2010,** *43,* 1396–1402. doi:10.1021/ma902321g
26. DiCiccio, A. M.; Coates, G. W. *J. Am. Chem. Soc.* **2011,** *133,* 10724–10727. doi:10.1021/ja203520p
27. Jeske, R. C.; DiCiccio, A. M.; Coates, G. W. *J. Am. Chem. Soc.* **2007,** *129,* 11330–11331. doi:10.1021/ja0737568
28. Liu, Y.; Xiao, M.; Wang, S.; Xia, L.; Hang, D.; Cui, G.; Meng, Y. *RSC Adv.* **2014,** *4,* 9503–9508. doi:10.1039/c3ra46343e
29. Jeske, R. C.; Rowley, J. M.; Coates, G. W. *Angew. Chem., Int. Ed.* **2008,** *47,* 6041–6044. doi:10.1002/anie.200801415
30. Bernard, A.; Chatterjee, C.; Chisholm, M. H. *Polymer* **2013,** *54,* 2639–2646. doi:10.1016/j.polymer.2013.02.033
31. Song, P. F.; Xiao, M.; Du, F. G.; Wang, S. J.; Gan, L. Q.; Liu, G. Q.; Meng, Y. Z. *J. Appl. Polym. Sci.* **2008,** *109,* 4121–4129. doi:10.1002/app.28449
32. Varghese, J. K.; Na, S. J.; Park, J. H.; Woo, D.; Yang, I.; Lee, B. Y. *Polym. Degrad. Stab.* **2010,** *95,* 1039–1044. doi:10.1016/j.polymdegradstab.2010.03.006
33. Nakano, K.; Hashimoto, S.; Nakamura, M.; Kamada, T.; Nozaki, K. *Angew. Chem., Int. Ed.* **2011,** *50,* 4868–4871. doi:10.1002/anie.201007958
34. Lee, B. Y.; Cyriac, A. *Nat. Chem.* **2011,** *3,* 505–507. doi:10.1038/nchem.1081
35. Lee, J. J.; Jeon, J. Y.; Park, J. H.; Jang, Y.; Hwang, E. Y.; Lee, B. Y. *RSC Adv.* **2013,** *3,* 25823–25829. doi:10.1039/c3ra45264f
36. Park, J. H.; Jeon, J. Y.; Lee, J. J.; Jang, Y.; Varghese, J. K.; Lee, B. Y. *Macromolecules* **2013,** *46,* 3301–3308. doi:10.1021/ma400360w

License and Terms

Comparing kinetic profiles between bifunctional and binary type of Zn(salen)-based catalysts for organic carbonate formation

Carmen Martín[1] and Arjan W. Kleij[*1,2]

Abstract

Zn(salen) complexes have been employed as active catalysts for the formation of cyclic carbonates from epoxides and CO_2. A series of kinetic experiments was carried out to obtain information about the mechanism for this process catalyzed by these complexes and in particular about the order-dependence in catalyst. A comparative analysis was done between the binary catalyst system Zn(salphen)/NBu₄I and a bifunctional system Zn(salpyr)·MeI with a built-in nucleophile. The latter system demonstrates an apparent second-order dependence on the bifunctional catalyst concentration and thus follows a different, bimetallic mechanism as opposed to the binary catalyst that is connected with a first-order dependence on the catalyst concentration and a monometallic mechanism.
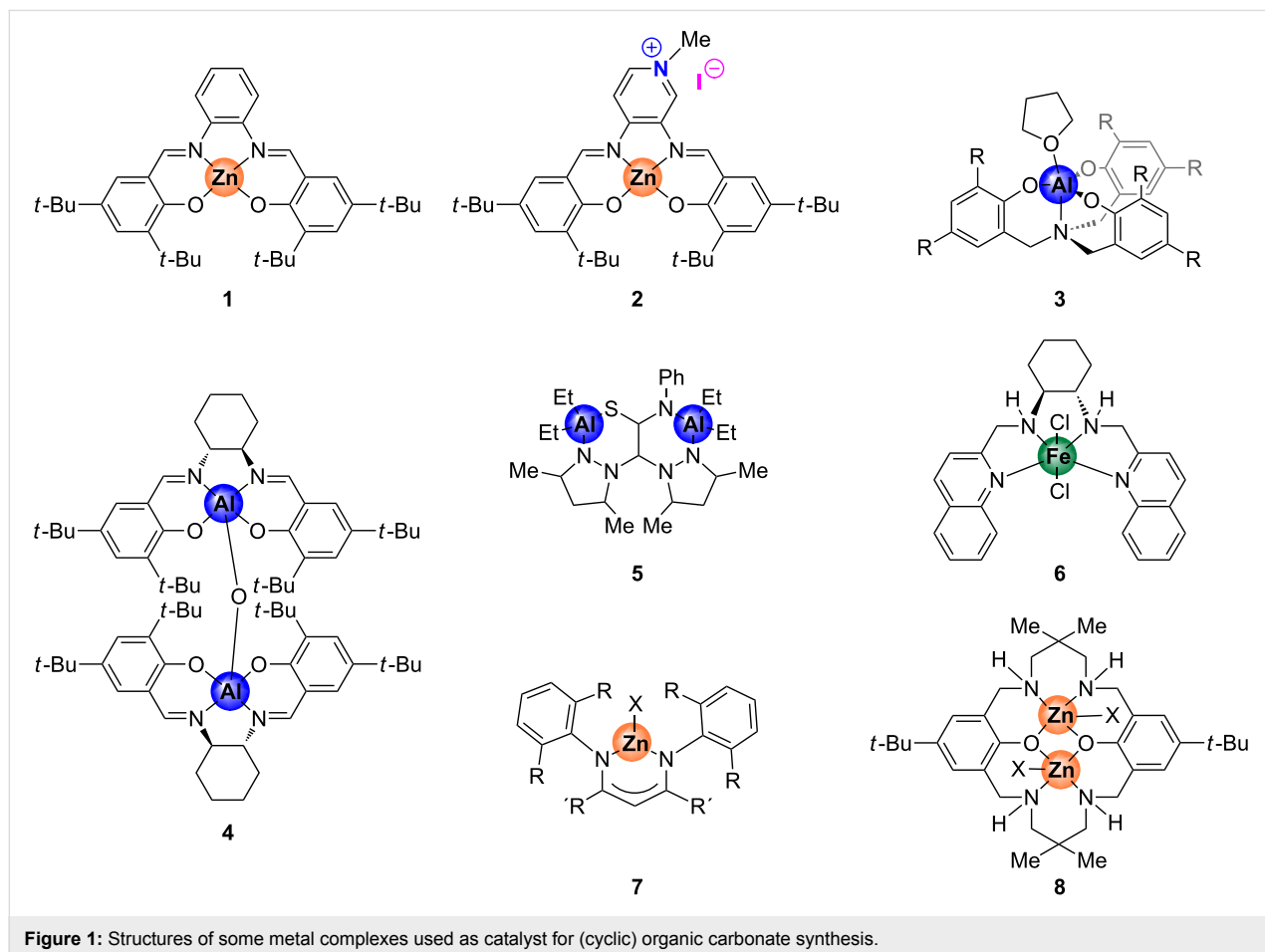
Introduction

Carbon dioxide may be regarded as an ideal, renewable carbon feed stock for the synthesis of organic compounds being also of interest in an industrial context [1-5]. This inexpensive, abundant and nontoxic source of carbon has been extensively used to convert epoxides into their respective cyclic carbonates [6-9] (Scheme 1), that find useful applications as green solvents, precursors towards pharmaceutical intermediates and as electrolytes in lithium ion batteries [1,10,11]. However, energy is

required to activate the kinetically highly stable CO_2 making the use of catalysts a requisite to overcome this limitation and to convert it under more attractive reaction conditions. Over the past years many different catalytic systems have been developed for this kind of process exemplifying the huge interest in the synthesis of cyclic carbonates and these catalysts include quaternary ammonium salts [12], ionic liquids [13,14] and metal-based catalysts [15-21]. In this regard, our group has

shown in previous reports various effective organic [22,23] and metal-based systems [24-29] applied as catalysts for organic carbonate formation. Interestingly, we demonstrated high activity and versatility of cheaper, nontoxic and earth-abundant metal-based complexes based on aluminum [24] and iron [25] amino-triphenolate complexes. Additionally, salen-based Zn complexes were also found to be rather efficient catalyst for this transformation. More specifically, these systems relate to the Zn(salphen) family of complexes [salphen = *N*,*N*'-phenylene-1,2-bis[salicylidene]imine] (Figure 1, **1**) combined with a nucleophilic ammonium halide salt [26,27], or an analogous bifunctional system (Figure 1, **2**) containing a Lewis acidic and nucleophilic center within the same molecule [29].

Scheme 1: Catalytic synthesis of organic (poly)carbonates from epoxides and CO_2.
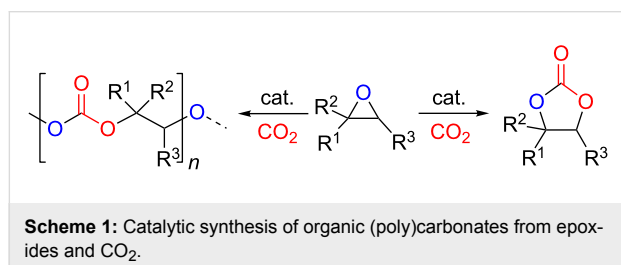
Mechanistic investigations for these CO_2/epoxide coupling reactions are essential to control the process selectivity (cyclic versus polycarbonate formation, Scheme 1) and to improve the activity of the used catalysts. Several computational investigations have been reported in this area focusing on catalysts comprising ionic liquids [30], *N*-heterocyclic carbenes [31], polyphenolic compounds [32], quaternary ammonium salts [33] or metal-containing complexes [34-37]. Also, a detailed theoretical analysis combined with experimental evidences using a Zn(salphen) complex has been reported [36]. Beside these computational activities, experimental studies involving kinetic measurements have also been undertaken with the aim to obtain more insight into the operating mechanism [15,37-45]. Prominent among these studies is the work carried out by North and co-workers [15,39] who described kinetic studies of a binary, dimetallic aluminum–salen complex **4** (see Figure 1) in conjunction with NBu₄Br. Remarkably, a second-order dependence on the concentration of the ammonium salt was determined suggesting that two molecules of NBu₄Br are involved in the rate-determining step: one molecule is supposed to be converted in situ to NBu₃ able to activate CO_2 whereas the other molecule helps to ring-open a coordinated epoxide. This

Figure 1: Structures of some metal complexes used as catalyst for (cyclic) organic carbonate synthesis.
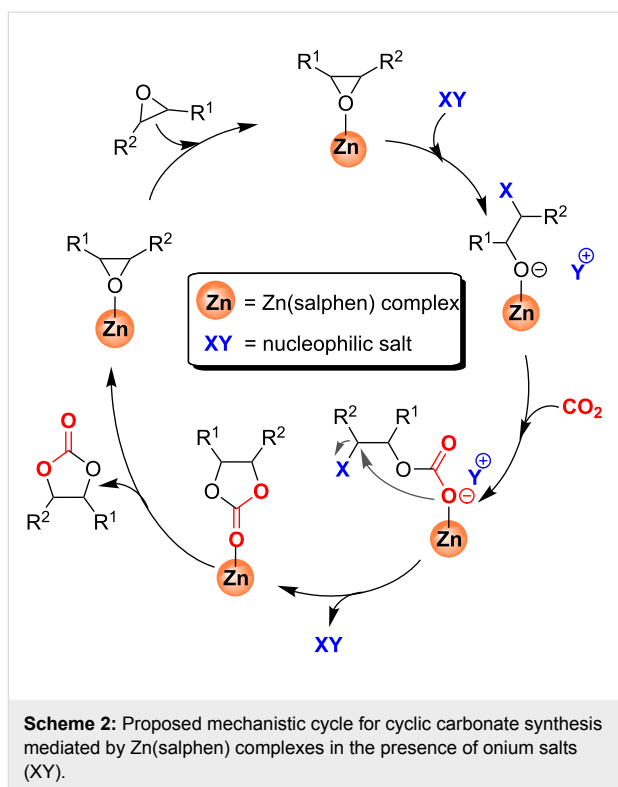
activation mode differs from one reported for the binary system based on Al complex **3**/NBu$_4$I (Figure 1) [37] and the first-order dependence with respect to each catalyst and co-catalyst displayed when the dimetallic aluminum complex **5** (Figure 1) was utilized [40]. Another interesting example was described by Rieger et al. who used a single-component catalyst **6** based on iron (Figure 1) for which a second-order rate dependence was determined indicating a dimetallic reaction mechanism [41]. Of further importance are the efforts from Coates and co-workers [44] and the kinetic studies described by the group of Williams [45]. In each of these latter cases a binuclear mechanism was proposed for the copolymerization reaction of CO_2 and epoxide, establishing a second-order dependence for mononuclear Zn complex **7** (Figure 1) employed by Coates and first-order behavior in the case of the dinuclear Zn complex **8** (Figure 1). However, to the best of our knowledge, reports on comparative kinetic studies between structurally related binary and bifunctional systems are rare [43].

Herein we describe such a kinetic investigation of the mechanism of the coupling between CO_2 and epoxides catalyzed by Zn-based complexes containing salen ligands. A comparative kinetic analysis between the binary system Zn(salphen) **1**/NBu$_4$I and bifunctional, alkylated Zn(salpyr) complex **2** [salpyr = *N,N′*-bis[salicylidene]-3,4-pyridinediamine] has been carried out and the results are in line with the view that the mechanisms by which the organic carbonate product is formed are essentially different and contrasting to previously reported literature [43].

Results and Discussion

We have described the catalytic capability of Zn(salphen) complexes in conjunction with NBu$_4$I for CO_2/epoxide coupling reactions [26-29], proposing for this process the monometallic mechanism depicted in Scheme 2 [26]. Furthermore, a detailed DFT study for this transformation was reported supporting this proposed mechanism [36]. In the catalytic cycle of Scheme 2 first the epoxide coordinates to the Zn center allowing Lewis acid activation following the ring opening by nucleophilic attack of X. Then, carbon dioxide insertion into the metal–oxygen bond takes place and a consecutive cyclisation step (ring closure) occurs to give the cyclic carbonate and regenerates the (binary) catalyst.

In addition, this transformation has also been developed using a structurally related bifunctional Zn catalyst (Figure 1, **2**) [29] showing a different behavior in terms of reactivity with respect to the binary system. Catalysts based on Zn complexes containing the nucleophile anchored onto the ligand framework are less active than "similar" binary-type catalysts based on comparable components. For instance, coupling between 1,2-

Scheme 2: Proposed mechanistic cycle for cyclic carbonate synthesis mediated by Zn(salphen) complexes in the presence of onium salts (XY).

epoxyhexane and CO_2 to afford the cyclic carbonate derivative mediated by binary Zn(salphen) **1**/NBu$_4$I was virtually complete whereas the alkylated Zn(salpyr) complex **2** gave a substantially lower 67% result under similar reaction conditions (0.25 mol % of (co)catalyst, 18 h, 1.0 MPa of CO_2 and 80 °C). On the basis of this difference we decided to investigate the operating mechanisms in more detail through a series of kinetic experiments to obtain more details about the catalytic activation mode of both the binary and bifunctional systems **1**/NBu$_4$I and **2** respectively.

In an attempt to assess the role of the catalyst structure in the synthesis of cyclic carbonates, kinetic measurements as a function of catalyst loading were performed (for more details see experimental section). As benchmark substrate 1,2-epoxyhexane was chosen, and in all studied cases complete selectivity towards the cyclic carbonate was observed under neat conditions. The conversion of the substrate was calculated by ^{1}H NMR spectroscopy of an aliquot taken from the reaction mixture at the initial stage (at low conversion) of the process assuming "steady-state" conditions working in the presence of an excess of CO_2 (see Figure 2). Under these reaction conditions the reaction rate can be defined as Equation 1 and further simplified to Equation 2 since both the CO_2 and epoxide concentration may be considered pseudo constant at the initial stage of the reaction. The natural logarithm of the rate law (Equation 2) results in Equation 3, from which is possible to

Figure 2: Typical ^{1}H NMR spectrum of a sample of a crude mixture in CDCl$_3$ (300 MHz) at rt.
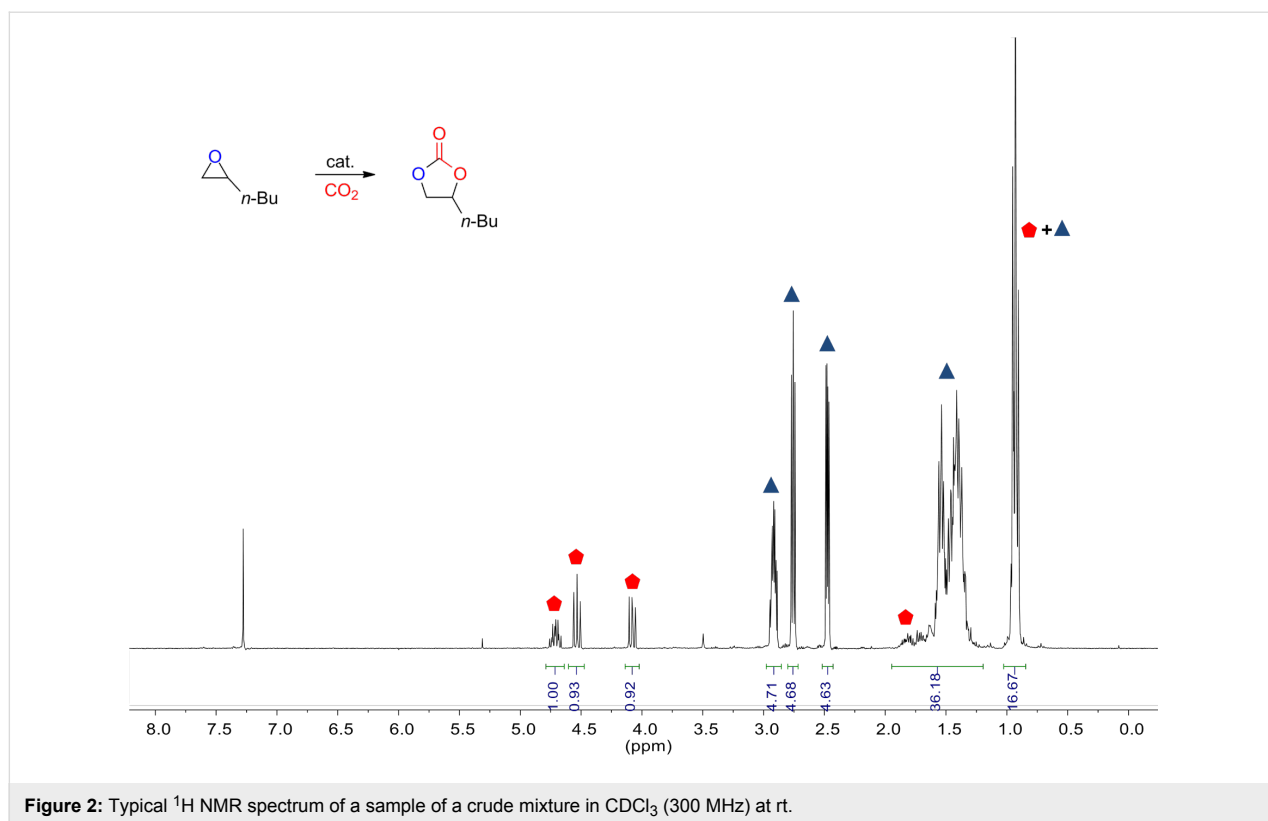
afford the order "c" with respect to the catalyst concentration by examination of a double logarithmic plot.

$$\text{Rate} = k \cdot [\text{CO}_2]^a \cdot [\text{epoxide}]^b \cdot [\text{cat}]^c \qquad (1)$$
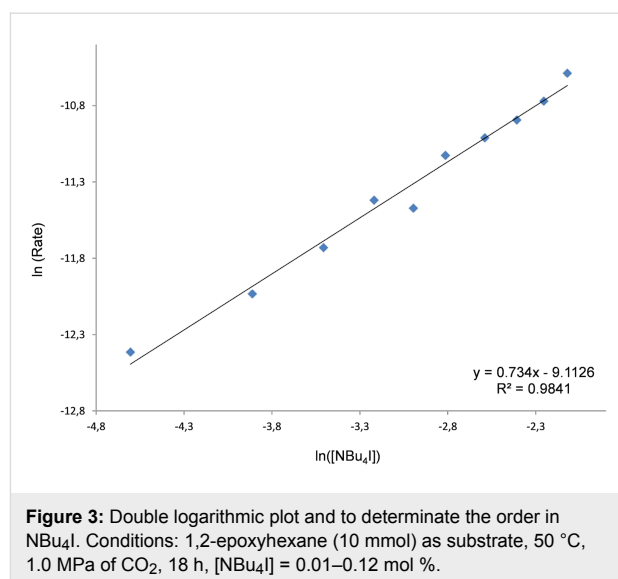
with $[\text{cat}]^c = [\text{Zn}]^d \cdot [\text{I}]^e$ in the binary and $[\text{cat}]^c = [\text{ZnI}]^c$ in the bifunctional system

$$\text{Rate} = k_{\text{obs}} \cdot [\text{cat}]^c, \text{ with } k_{\text{obs}} = [\text{CO}_2]^a \cdot [\text{epoxide}]^b \quad (2)$$

$$\ln(\text{Rate}) = \ln(k_{\text{obs}}) + c \ln[\text{cat}] \qquad (3)$$

Before performing the kinetic experiments with Zn complexes **1** and **2**, the catalytic activity of NBu$_4$I (the "co-catalyst") was first tested where [cat] is equal to [NBu$_4$I]. A linear and well-behaved correlation between ln(Rate) and ln([NBu$_4$I]) was found (Figure 3) with a gradient of 0.734. This apparent first order in [NBu$_4$I] is expected for the synthesis of cyclic carbonates being comparable with that observed for other similar salts [38] with the attack of the nucleophile on the epoxide proposed as the rate-determining step of the mechanism (Scheme 3). This kinetic behavior was evaluated after 18 h at 50 °C in view of the very low catalytic activity of NBu$_4$I being virtually absent at ambient temperature. This fact allowed us to analyze the binary

system and to study the catalytic activity of the binary couple Zn(salphen) **1**/NBu$_4$I since no conversion was observed at 30 °C for NBu$_4$I alone after two hours, whereas a significant conversion is achieved by the binary system under these latter conditions.

Figure 3: Double logarithmic plot and to determinate the order in NBu$_4$I. Conditions: 1,2-epoxyhexane (10 mmol) as substrate, 50 °C, 1.0 MPa of CO$_2$, 18 h, [NBu$_4$I] = 0.01–0.12 mol %.

To evaluate the function of the Zn complex and the NBu$_4$I in the binary catalyst system, three different kinetic experiments
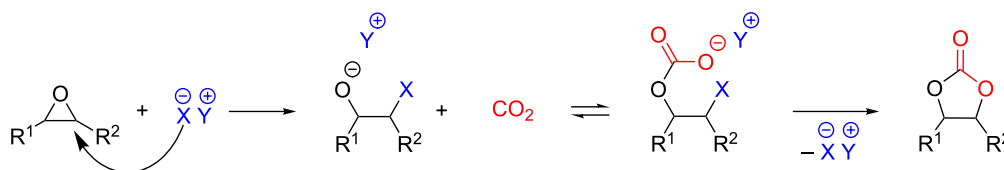
Scheme 3: Proposed mechanism for the formation of cyclic carbonates mediated by an ammonium salt.

were carried out using similar reaction conditions (30 °C, 1 MPa of CO_2, 2 h). Initially, the amount of co-catalyst was fixed at 0.4 mol % whilst the concentration of Zn complex **1** was varied between 0.025–0.225 mol %. In the second series, the concentration of Zn was kept at 0.2 mol %, and altering [NBu$_4$I] from 0.04–0.4 mol %. In both cases the double logarithmic plot showed a linear behavior providing a slope of 0.889 and 0.915 respectively (Figure 4 and Figure 5).
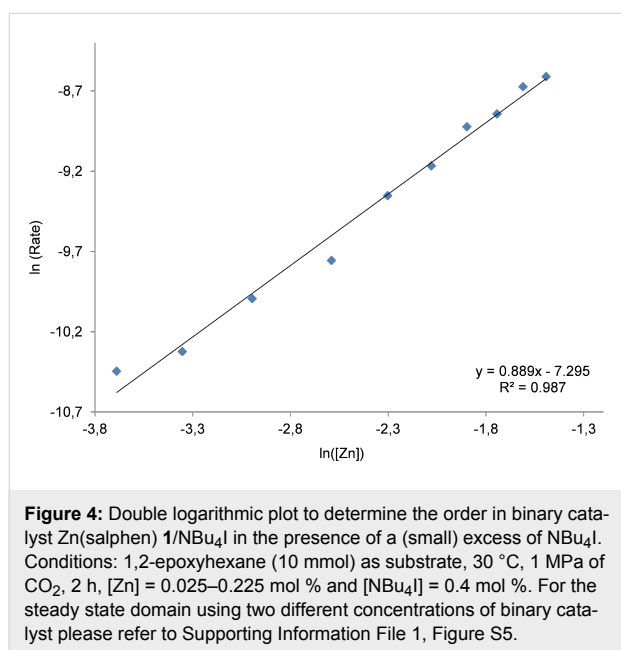

Figure 5: Double logarithmic plot to determine the order in binary catalyst Zn(salphen) **1**/NBu$_4$I in the presence of (a small excess of) Zn(salphen) complex **1**. Conditions: 1,2-epoxyhexane (10 mmol) as substrate, 30 °C, 1 MPa of CO_2, 2 h; [Zn] = 0.2 mol %, [NBu$_4$I] = 0.04–0.4 mol %. For the steady state domain using two different concentrations of binary catalyst please refer to Supporting Information File 1, Figure S5.

Figure 4: Double logarithmic plot to determine the order in binary catalyst Zn(salphen) **1**/NBu$_4$I in the presence of a (small) excess of NBu$_4$I. Conditions: 1,2-epoxyhexane (10 mmol) as substrate, 30 °C, 1 MPa of CO_2, 2 h, [Zn] = 0.025–0.225 mol % and [NBu$_4$I] = 0.4 mol %. For the steady state domain using two different concentrations of binary catalyst please refer to Supporting Information File 1, Figure S5.

The apparent first-order dependence on the binary catalyst system in either case suggests that only one molecule of Zn complex **1** as well as one molecule of ammonium salt is involved in the rate-determining step of the catalytic cycle. Similar results have been reported by Otero and co-workers [40], describing a monometallic mechanism for dimetallic aluminum complex **5** (Figure 1). However, in the literature we can also find different proposals. For instead, North proposed a second-order dependence on NBu$_4$Br when using the binary system **4**/NBu$_4$Br. A double role of the salt was suggested, providing bromide as nucleophile for the ring opening of the co-ordinated epoxide and conversely triethylamine which can activate the CO_2.
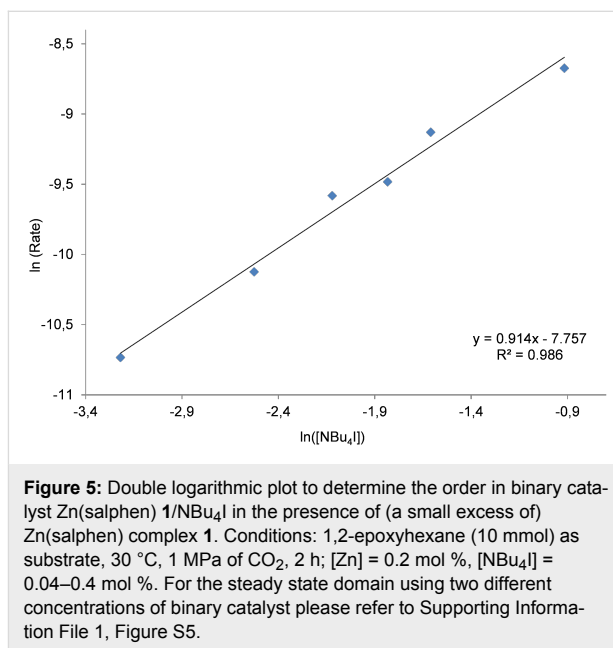
In addition, we also performed kinetic studies using a fixed ratio (1:1) between the Zn(salphen) complex **1** and NBu$_4$I (Figure 6) at different concentrations; also in this case a first-order dependence seems obvious. This result implies that both the Lewis acid and iodide species are important in the rate-determining step, therefore they should not be considered separately. Thus, the first order in catalyst concentration observed in these three different experiments that we performed can be ascribed to the order shown in the catalytic species formed by both the Zn complex **1** and NBu$_4$I.

Next we turned our focus on the bifunctional system **2** (structure presented in Figure 1) to examine the order in **2** as to propose a plausible mechanism for the formation of cyclic carbonates mediated by this system. With this in mind kinetic analysis was undertaken by varying the concentration of **2**. It should be noted that in this case an elevated temperature was required to allow for satisfactory product formation. At lower temperatures (rt) complex **2** in solution is likely present in an aggregated form by means of intermolecular interactions (Figure 7) as was recently demonstrated by Santo Di Bella for a similar Zn(salen) complex comprising ammonium bromide
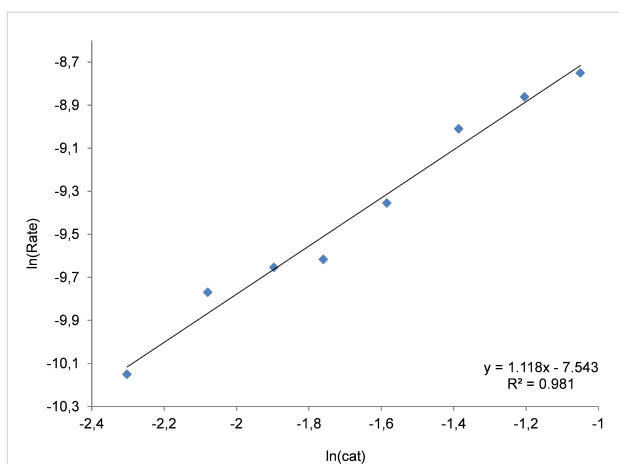
Figure 6: Double logarithmic plot to determine the order with respect to the binary system NBu$_4$I/Zn complex **1**. Conditions: 1,2-epoxy-hexane (10 mmol) as substrate, 30 °C, 1 MPa of CO$_2$, 2 h, [Zn] = [NBu$_4$I] = 0.10–0.35 mol %. For the steady state domain using two different concentrations of binary catalyst please refer to Supporting Information File 1, Figure S5.
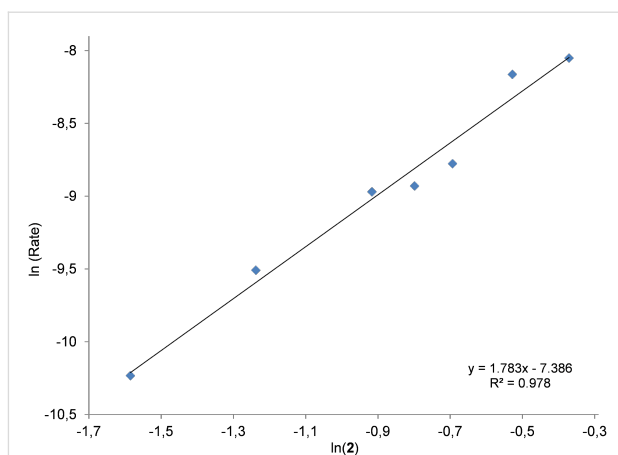

Figure 8: Double logarithmic plot to determine the order in Zn complex **2**. Conditions: 1,2-epoxyhexane (10 mmol) as substrate, 80 °C, 1 MPa of CO$_2$, 2 h; [**2**] = 0.205–0.69 mol %. For the steady state domain using two different concentrations of bifunctional catalyst please refer to Supporting Information File 1, Figure S6.
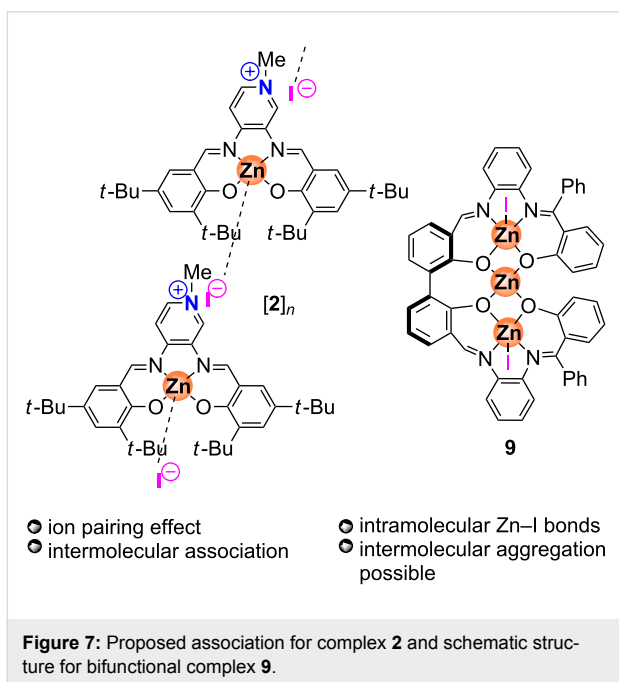

**Figure 7:** Proposed association for complex **2** and schematic structure for bifunctional complex **9**.

functions in the ligand scaffold [46]. The presence of reminiscent Zn–I coordination patterns has also been reported by our group [47]. Another possible barrier to overcome is the (strong) ion-pair effect between the methylpyridinium unit in **2** and the iodide when comparing to the binary system Zn(salphen) **1**/NBu$_4$I. Thus, to potentially break the Zn–I coordinative interaction and to enable both Lewis acid and nucleophilic functions, the reaction had to be heated to at least to 40 °C. A similar behavior was observed in previous work from our group for the trinuclear complex **9** (Figure 7) since high temperatures were

required for the dissociation process of the coordinating iodides [28].

Thus, catalytic experiments for bifunctional complex **2** were finally performed at 80 °C and at a CO$_2$ pressure of 1 MPa. After 2 h, aliquots of the crude reaction mixtures were checked by ^{1}H NMR to determine substrate conversion, and from these data it was possible to correlate the rate with the catalyst concentration in the range 0.205–0.69 mol %. A pseudo-second order was found for the catalytic system indicating a dimetallic reaction mechanism (Figure 8) as was also suggested by Rieger et al. for iron catalyst **6** [41]. This experimental evidence suggests that in the rate-determining step one molecule of the Zn complex **2** may activate the substrate through coordination, while the iodide anion of a second molecule of **2** attacks the co-ordinated epoxide (Scheme 4).

This mechanistic proposal does not seem to be affected by temperature, since the apparent second-order dependence was also found when the kinetic experiments were executed at 50 °C (see Supporting Information File 1, Figure S2 for more details).

To further increase the credibility of a dimetallic mechanism, the bifunctional Zn complex **2** incorporating a methylpyridinium iodide fragment was combined with an external halide source (i.e., NBu$_4$I). At relatively low temperature, such a combination should behave (mostly) as a binary system as complex **2** and NBu$_4$I alone have lethargic activation behavior. Therefore it may be anticipated that a pseudo first-order dependence results from this combination of catalyst components. We thus performed a series of reactions with a constant NBu$_4$I loading (0.6 mol %) while varying the concentration of
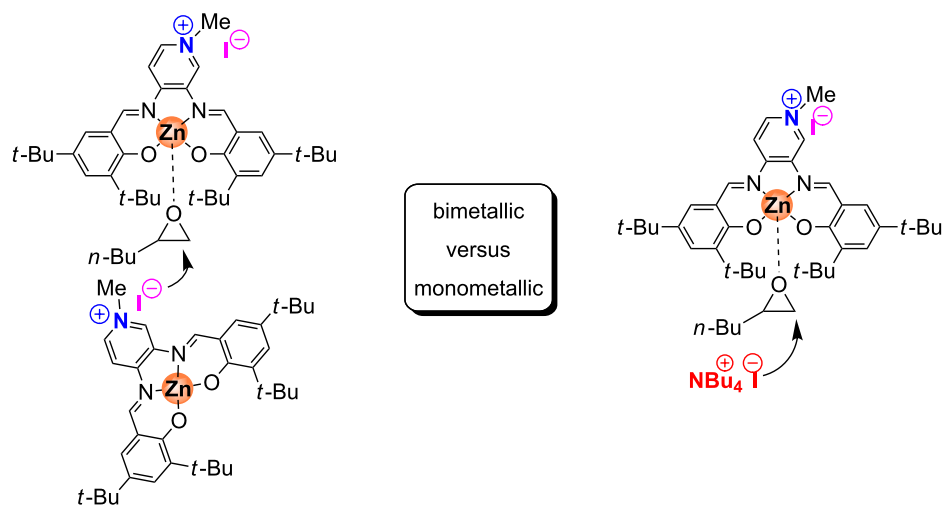
Scheme 4: On the left a dimetallic mechanism proposed for bifunctional catalyst **2** and on the right a monometallic mechanism proposed for binary catalyst **2**/NBu$_4$I are shown.

bifunctional Zn complex **2** (0.1–0.4 mol %). These experiments were carried out at 40 °C, a minimal reaction temperature required for the bifunctional catalyst to provide a sufficiently disaggregated state and thus the required Lewis acid centers for catalytic turnover when combined with NBu$_4$I (Figure 9).
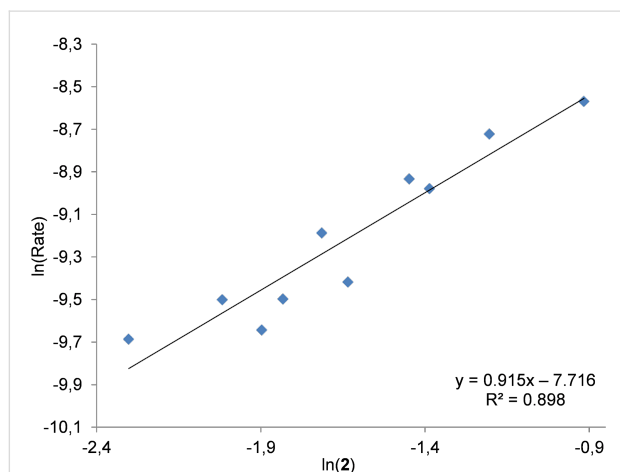

Figure 9: Double logarithmic plot to determine the order with respect to the bifunctional Zn complex **2** in the presence of NBu$_4$I. Conditions: 1,2-epoxyhexane (10 mmol) as substrate, 40 °C, 1 MPa of CO$_2$, 2 h; [**2**] = 0.1–0.4 mol %, [NBu$_4$I] = 0.6 mol % [48].

At this temperature individual catalytic conversions for bifunctional complex **2** and ammonium salt alone (2.0 and 2.6%, respectively) are much lower compared with the combination of both (16.5%). Thus, we can assume that the conversion data observed in these experiments correspond mostly with the in situ formed binary catalyst Zn(salpyr)·MeI **2**/NBu$_4$I. Under these reaction conditions the initial rate is directly proportional

to catalyst concentration and the corresponding double logarithmic plot gives a slope of 0.915 (Figure 9). The effect of the catalyst concentration on the rate for bifunctional complex **2** in the presence or absence of an (external) co-catalyst is markedly different: a pseudo-first order seems apparent for complex **2** in the presence of NBu$_4$I consistent with a monometallic mechanism, whereas for bifunctional complex **2** alone the activation of the substrate requires two molecules of **2** (Scheme 4). This is an interesting observation since in the work from Lu et al. [43] an exact opposite observation was done; the comparison between a bifunctional and binary type Co(salen) catalyst for polycarbonate formation revealed that the bifunctional system displays a first order and the binary system a second order rate relationship.

Conclusion

In summary, kinetic investigations for the addition of CO$_2$ into epoxides mediated by Zn(salen) complexes were performed to obtain a more complete understanding of the reaction mechanism. In particular, the binary system **1**/NBu$_4$I was compared with the structurally related bifunctional system **2** and both were shown to behave differently. A first-order dependence on catalyst concentration for the binary system was found in line with previous computational work on this system [36] while a second-order rate dependence was observed for the bifunctional catalyst **2**. These observations thus support a monometallic mechanism when Zn species **1** and NBu$_4$I are combined, while a bimetallic mechanism seems more likely for the bifunctional complex **2**. The possibility of using this type of alkylammonium halide functionalized ligand in the synthesis of new salpyr-based complexes (M = Co, Cr) allows to reconsider and improve the design of this kind of bifunctional catalyst as to

prepare efficient mediators of both cyclic as well as polycarbonates starting from epoxides and CO_2. In particular the presence of a tethered co-catalyst with a long enough linker between the ligand and the nucleophilic center [49,50] could allow for more efficient combination with the Lewis acid ion thereby creating a higher degree of synergy.

Experimental
General procedures
Carbon dioxide was purchased from PRAXAIR and used without further purification. Epoxide substrate and tetrabutylammonium iodide are commercially available and were used as received. Complexes **1** [51] and **2** [27] were prepared according to literature procedures. NMR spectra were recorded using a Bruker AV-300 spectrometer and referenced to the residual NMR solvent signals.

Typical catalysis procedure
A solution of the respective catalyst in 10 mmol of 1,2-epoxyhexane (1.2 mL, 1.0 g) was transferred to a stainless steel reactor (30 mL). Three cycles of pressurization and depressurization of the reactor with carbon dioxide (0.5 MPa) were carried out to replace all air by CO_2 in the reactor. The final pressure was then adjusted to 1.0 MPa, and the reaction was left stirring at the required temperature for 2 or 18 h, depending on the experiment. Afterwards, the conversion was calculated by ^{1}H NMR spectroscopy of an aliquot of reaction mixture using $CDCl_3$ as solvent. Reactions carried out in the presence or absence of mesitylene as an internal standard gave similar results (see Supporting Information File 1, Table S8 for more details). The carbonate product, 4-butyl-1,3-dioxolan-2-one, has been previously described, therefore its identification was done by comparison with reported data [52]. For a photograph of the reactor see Supporting Information File 1.

Kinetic experiments
For the catalytic studies, the same procedure was used but doing the reaction in an SPR16 Slurry Phase Reactor (Amtec GmbH). The AMTEC vessels were charged with the corresponding catalyst. First a leak test was performed with 1.5 MPa of N_2 to finally reduce the pressure to 0.2 MPa. Then, the reactors were subjected to three cycles of pressurization and depressurization with CO_2 (from 0.4 to 0.2 MPa). Finally 10 mmol of 1,2-epoxyhexane was injected into the reactors and the CO_2 pressure was raised to 1 MPa. Reactions were stirred at the appropriate temperature for two hours. At the end of the process stirring was stopped, reactors were cooled and depressurized. The conversion of the substrate was examined by ^{1}H NMR spectroscopy ($CDCl_3$) of an aliquot taken from the crude reaction mixture. For a photograph of the Amtec reactor system see Supporting Information File 1.

Supporting Information
Further details of experimental procedures, typical ^{1}H NMR spectra for the aliquots taken in the kinetic studies (containing the carbonate product [4-butyl-1,3-dioxolan-2-one]) and photographs of the reactor systems used for the catalytic/kinetic studies are given.

Supporting Information File 1
Experimental procedures, typical ^{1}H NMR spectra for aliquots taken in the kinetic studies and photographs of the reactor systems.
[http://www.beilstein-journals.org/bjoc/content/supplementary/1860-5397-10-191-S1.pdf]

References
1. Sakakura, T.; Choi, J.-C.; Yasuda, H. *Chem. Rev.* **2007,** *107,* 2365–2387. doi:10.1021/cr068357u
2. Aresta, M., Ed. *Carbon Dioxide as Chemical Feedstock;* Wiley-VCH: Weinheim, 2010.
3. Martín, R.; Kleij, A. W. *ChemSusChem* **2011,** *4,* 1259–1263. doi:10.1002/cssc.201100102
4. Kleij, A. W. *ChemCatChem* **2013,** *5,* 113–115. doi:10.1002/cctc.201200462
5. Maeda, C.; Miyazaki, Y.; Ema, T. *Catal. Sci. Technol.* **2014,** *4,* 1482–1497. doi:10.1039/C3CY00993A
6. Decortes, A.; Castilla, A. M.; Kleij, A. W. *Angew. Chem., Int. Ed.* **2010,** *49,* 9822–9837. doi:10.1002/anie.201002087
7. North, M.; Pasquale, R.; Young, C. *Green Chem.* **2010,** *12,* 1514–1539. doi:10.1039/C0GC00065E
8. Pescarmona, P. P.; Taherimehr, M. *Catal. Sci. Technol.* **2012,** *2,* 2169–2187. doi:10.1039/C2CY20365K
9. Whiteoak, C. J.; Kleij, A. W. *Synlett* **2013,** 1748–1756. doi:10.1055/s-0033-1339483
10. Schäffner, B.; Schäffner, F.; Verevkin, S. P.; Börner, A. *Chem. Rev.* **2010,** *110,* 4554–4581. doi:10.1021/cr900393d
11. Shaikh, A.-A. G.; Sivaram, S. *Chem. Rev.* **1996,** *96,* 951–976. doi:10.1021/cr950067i
12. Caló, V.; Nacci, A.; Monopoli, A.; Fanizzi, A. *Org. Lett.* **2002,** *4,* 2561–2563. doi:10.1021/ol026189w
13. Yang, Z.-Z.; He, L.-N.; Miao, C.-X.; Chanfreau, S. *Adv. Synth. Catal.* **2010,** *352,* 2233–2240. doi:10.1002/adsc.201000239
14. Zhao, Y.; Yao, C.; Chen, G.; Yuan, Q. *Green Chem.* **2013,** *15,* 446–452. doi:10.1039/C2GC36612F

15. Clegg, W.; Harrington, R. W.; North, M.; Pasquale, R. *Chem.–Eur. J.* **2010,** *16,* 6828–6843. doi:10.1002/chem.201000030
16. Ren, W.-M.; Wu, G.-P.; Lin, F.; Jiang, J.-Y.; Liu, C.; Luo, Y.; Lu, X.-B. *Chem. Sci.* **2012,** *3,* 2094–2102. doi:10.1039/C2SC20068F
17. Buchard, A.; Kember, M. R.; Sandeman, K. G.; Williams, C. K. *Chem. Commun.* **2011,** *47,* 212–214. doi:10.1039/C0CC02205E
18. Chang, T.; Jin, L.; Jing, H. *ChemCatChem* **2009,** *1,* 379–383. doi:10.1002/cctc.200900135
19. North, M.; Villuendas, P.; Young, C. *Chem.–Eur. J.* **2009,** *15,* 11454–11457. doi:10.1002/chem.200902436
20. Paddock, R. L.; Nguyen, S. T. *Chem. Commun.* **2004,** 1622–1623. doi:10.1039/B401543F
21. Langanke, J.; Greiner, L.; Leitner, W. *Green Chem.* **2013,** *15,* 1173–1182. doi:10.1039/C3GC36710J
22. Whiteoak, C. J.; Henseler, A. H.; Ayats, C.; Kleij, A. W.; Pericàs, M. A. *Green Chem.* **2014,** *16,* 1552–1559. doi:10.1039/C3GC41919C
23. Whiteoak, C. J.; Nova, A.; Maseras, F.; Kleij, A. W. *ChemSusChem* **2012,** *5,* 2032–2038. doi:10.1002/cssc.201200255
24. Whiteoak, C. J.; Kielland, N.; Laserna, V.; Escudero-Adán, E. C.; Martin, E.; Kleij, A. W. *J. Am. Chem. Soc.* **2013,** *135,* 1228–1231. doi:10.1021/ja311053h
25. Whiteoak, C. J.; Martin, E.; Martinez-Belmonte, M.; Benet-Buchholz, J.; Kleij, A. W. *Adv. Synth. Catal.* **2012,** *354,* 469–476. doi:10.1002/adsc.201100752
26. Decortes, A.; Martinez-Belmonte, M.; Benet-Buchholz, J.; Kleij, A. W. *Chem. Commun.* **2010,** *46,* 4580–4582. doi:10.1039/c000493f
27. Decortes, A.; Kleij, A. W. *ChemCatChem* **2011,** *3,* 831–834. doi:10.1002/cctc.201100031
28. Escárcega-Bobadilla, M. V.; Martinez-Belmonte, M.; Martin, E.; Escudero-Adán, E. C.; Kleij, A. W. *Chem.–Eur. J.* **2013,** *19,* 2641–2648. doi:10.1002/chem.201204132
29. Martin, C.; Whiteoak, C. J.; Martin, E.; Martinez-Belmonte, M.; Escudero-Adán, E. C.; Kleij, A. W. *Catal. Sci. Technol.* **2014,** *4,* 1615–1621. doi:10.1039/c3cy01043k
30. Sun, H.; Zhang, D. *J. Phys. Chem. A* **2007,** *111,* 8036–8043. doi:10.1021/jp073873p
31. Ajitha, M. J.; Suresh, C. H. *Tetrahedron Lett.* **2011,** *52,* 5403–5406. doi:10.1016/j.tetlet.2011.08.062
32. Wang, J.-Q.; Sun, J.; Cheng, W.-G.; Dong, K.; Zhang, X.-P.; Zhang, S.-J. *Phys. Chem. Chem. Phys.* **2012,** *14,* 11021–11026. doi:10.1039/C2CP41698K
33. Wang, J.-Q.; Dong, K.; Cheng, W.-G.; Sun, J.; Zhang, S.-J. *Catal. Sci. Technol.* **2012,** *2,* 1480–1484. doi:10.1039/C2CY20103H
34. Man, M. L.; Lam, K. C.; Sit, W. N.; Ng, S. M.; Zhou, Z.; Lin, Z.; Lau, C. P. *Chem.–Eur. J.* **2006,** *12,* 1004–1015. doi:10.1002/chem.200500780
35. Adhikari, D.; Nguyen, S. T.; Baik, M.-H. *Chem. Commun.* **2014,** *50,* 2676–2678. doi:10.1039/C3CC48769E
36. Castro-Gómez, F.; Salassa, G.; Kleij, W. A.; Bo, C. *Chem.–Eur. J.* **2013,** *19,* 6289–6298. doi:10.1002/chem.201203985
37. Whiteoak, C. J.; Kielland, N.; Laserna, V.; Castro-Gómez, F.; Martin, E.; Escudero-Adán, E. C.; Bo, C.; Kleij, W. A. *Chem.–Eur. J.* **2014,** *20,* 2264–2275. doi:10.1002/chem.201302536
38. Kihara, N.; Hara, N.; Endo, T. *J. Org. Chem.* **1993,** *58,* 6198–6202. doi:10.1021/jo00075a011
39. North, M.; Pasquale, R. *Angew. Chem., Int. Ed.* **2009,** *48,* 2946–2948. doi:10.1002/anie.200805451
40. Castro-Osma, J. A.; Lara-Sánchez, A.; North, M.; Otero, A.; Villuendas, P. *Catal. Sci. Technol.* **2012,** *2,* 1021–1026. doi:10.1039/C2CY00517D
41. Dengler, J.-E.; Lehenmeier, M. W.; Klaus, S.; Anderson, C. E.; Herdtweck, H.; Rieger, B. *Eur. J. Inorg. Chem.* **2011,** 336–343. doi:10.1002/ejic.201000861
42. Darensbourg, D. J.; Yarbrough, J. C.; Ortiz, C.; Fang, C. C. *J. Am. Chem. Soc.* **2003,** *125,* 7586–7591. doi:10.1021/ja034863e
43. Liu, J.; Ren, W.-M.; Liu, Y.; Lu, X.-B. *Macromolecules* **2013,** *46,* 1343–1349. doi:10.1021/ma302580s
44. Moore, D. R.; Cheng, M.; Lobkovsky, E. B.; Coates, G. W. *J. Am. Chem. Soc.* **2003,** *125,* 11911–11924. doi:10.1021/ja030085e
45. Jutz, F.; Buchard, A.; Kember, M. R.; Fredriksen, S. B.; Williams, C. K. *J. Am. Chem. Soc.* **2011,** *133,* 17395–17405. doi:10.1021/ja206352x
46. Oliveri, I. P.; Failla, S.; Colombo, A.; Dragonetti, C.; Righetto, S.; Di Bella, S. *Dalton Trans.* **2014,** *43,* 2168–2175. doi:10.1039/C3DT53072H
47. Wezenberg, S. J.; Escudero-Adán, E. C.; Benet-Buchholz, J.; Kleij, A. W. *Chem.–Eur. J.* **2009,** *15,* 5695–5700. doi:10.1002/chem.200900528
48. The scattering in the data is probably a result of the background reactions that are mediated by the bifunctional catalyst **2** and NBu4I alone compared with the combination of both. Note that both higher as well as lower reaction temperatures are not feasible due to the absence of sufficient activity (lower temperatures) and too much interference with background activity by both **2** and NBu4I at higher reaction temperatures.
49. Zhang, X.; Jia, Y.-B.; Lu, X.-B.; Li, B.; Wang, H.; Sun, L.-C. *Tetrahedron Lett.* **2008,** *49,* 6589–6592. doi:10.1016/j.tetlet.2008.09.035
50. Ren, W.-M.; Liu, Z.-W.; Wen, Y.-Q.; Zhang, R.; Lu, X.-B. *J. Am. Chem. Soc.* **2009,** *131,* 11509–11518. doi:10.1021/ja9033999
51. Kleij, A. W.; Kuil, M.; Tooke, D. M.; Lutz, M.; Spek, A. L.; Reek, J. N. H. *Chem.–Eur. J.* **2005,** *11,* 4743–4750. doi:10.1002/chem.200500227
52. Jiang, J.-L.; Gao, F.; Hua, R.; Qiu, X. *J. Org. Chem.* **2005,** *70,* 381–383. doi:10.1021/jo0485785

Supercritical carbon dioxide: a solvent like no other

Jocelyn Peach and Julian Eastoe[*]

Abstract

Supercritical carbon dioxide ($scCO_2$) could be one aspect of a significant and necessary movement towards green chemistry, being a potential replacement for volatile organic compounds (VOCs). Unfortunately, carbon dioxide has a notoriously poor solubilising power and is famously difficult to handle. This review examines attempts and breakthroughs in enhancing the physicochemical properties of carbon dioxide, focusing primarily on factors that impact solubility of polar and ionic species and attempts to enhance $scCO_2$ viscosity.

Introduction

In this day and age, sustainability and renewability are watchwords. This includes focus within the scientific community on the philosophy of green chemistry, a concept encouraging the design of chemically efficient products and processes that reduce or eliminate the use or generation of hazardous substances [1]. This can, in theory, be achieved through the application of a set of 'principles', including reduced use and production of toxic reagents and products, avoidance of auxiliary substances where possible, and minimization of the energy requirements needed for the process, under this umbrella [2]. Attention has been drawn to the potential surrounding by the use of supercritical fluids and carbon dioxide in chemical processing and as a solvent [3], thus replacing the volatile organic compounds (VOCs) that are currently commonly used [4]. These VOCs are environmentally hazardous and notori-

ously difficult to dispose of so a reduction in use would improve the sustainability of many chemical processes. As well as being readily available, cheap, non-flammable, recyclable and unrestricted by the US Environmental Protection Agency (EPA) [3,5-15], supercritical CO_2 ($scCO_2$) is non-toxic so could potentially be used for the production of consumable products, such as pharmaceutical and food products [14] as well as already being an established system for numerous processes [16], including extractions [17], nanoparticle production and modification [18-21] and polymer processing [22-25]. Supercritical fluids also make appealing solvents due to the opportunities for tuning of solvent properties through changes in temperature and pressure; supercritical conditions are also easily reached with CO_2, with critical pressure (P_c) and temperature (T_c) being 72.8 bar and 31.1 °C, respectively.

Unfortunately, scCO$_2$ suffers from a range of inconvenient physicochemical properties ordinarily required for an effective solvent, with a lower viscosity, dielectric constant [26,27] and surface tension in comparison to other common reference solvents. Also, as CO$_2$ is a linear molecule with no net dipole moment there is significant difficulty dissolving polar and ionic species [26].

As well as looking to modify physicochemical properties of scCO$_2$ to increase its appeal as a solvent, the ability to control properties will aid CO$_2$ use in other avenues, including atmospheric CO$_2$ capture, sequestration and storage as well as enhanced oil recovery processes (EOR) [28,29]. Increasing levels of atmospheric CO$_2$ is a substantial challenge faced by scientists, politicians, engineers and economists, and carbon capture and sequestration (CCS) is one of the favoured techniques envisaged for tackling this. The ease and efficiency of both EOR and CCS require the fluid properties to be managed and controlled; both of these techniques would be both economically and technically more viable if the viscosity of CO$_2$ used could be increased (leading to a reduction of viscous fingering during EOR and giving generally more overall control in CCS). The physicochemical properties of CO$_2$ have thus far been managed through the addition of soluble and self-assembling additives, such as surfactants and polymers [11,30-51].

Viscosity of CO$_2$ has been shown to be modifiable through the addition of aggregation and self-assembly of polymers and surfactants; however before internal/aggregated structures can be considered, and therefore viscosity modifiers developed, it is essential to 'crack' the puzzle of solubility, solvophilicity and CO$_2$-philicity.

Review
Solvent compatibility – solubility and solvophilicity

Solubility is the property of a given substance (solute) that allows dissolution in a solvent leading to a homogeneous solution. It is measured in terms of the maximum amount of solute that can be dissolved in a solution at dynamic equilibrium, i.e., until the solution is fully saturated. Solubility can be quantified using either molar units, mol dm^{-3}, or mass per unit volume units, such as g L^{-1}. Solubility range can vary widely, from infinitely soluble (fully miscible) to poorly soluble. The term insoluble is often applied to solutes with very poor solubility, although in actuality there are very few truly insoluble systems. Solubility is determined by the balance of intermolecular forces between solvent and solute, along with the entropy change that occurs on dispersal of the solute, so is therefore dependent on both pressure, temperature and system polarity. Solvophilicity

could be defined as the affinity a solute has for a given solvent, therefore CO$_2$-philicity would represent the affinity a solute has for CO$_2$.

A commonly coined term, 'like dissolves like' is often used in regard to solubility [52], i.e., polar solutes are easily solubilized by polar solvents. Molecular polarity arises from a separation of electrical charge within a molecule that leads to an electric dipole/multipole moment. It is dependent on a difference in electronegativity between the atoms within a compound and the degree of asymmetry in the compound. Point group determination is useful for the prediction of polarity. If individual dipole moments within a molecule cancel each other out, the molecule will not be polar. Any molecule with an inversion centre, a horizontal mirror plane (σ_h), or multiple C_n axes will not have dipole moments and therefore will not be polar, (C_1, C_s, $C_{\infty h}$, $D_{\infty h}$ C_n and C_{nv} do not have a dipole moment). CO$_2$ has a point group of $D_{\infty h}$, so is not polar.

As previously mentioned above, the difficulty observed in solubilisation of polar solutes in carbon dioxide is a substantial problem which must be overcome if the possibility of scCO$_2$ as a solvent is to become a reality. Early studies by Consani and Smith [53] into the solubility of commercially available surfactants in scCO$_2$ showed that the majority are insoluble, with a few non-ionic surfactants showing marginal solubility (out of the 130 or so surfactants tested). Following this discovery efforts have been directed towards the development of CO$_2$-soluble additives. Focus has primarily been in surfactant and polymer design in water-in-CO$_2$ (*w/c*) systems, however, attention is now beginning to expand into other alternative systems, including ionic liquid-in-CO$_2$ systems [54-56] and the production of microstructures such as lamellar and bicontinuous phases [43,48].

Solubility
Surfactants

Surfactant tails – fluorinated surfactants: Fluorine has a high electron affinity and electronegativity, hence fluorocarbons with a carbon number (*n*) that is equal to or greater than 4 have lower boiling points and refractive indices than the corresponding hydrocarbons [57] (different behaviour is observed when *n* < 4). Additionally, fluorocarbons have a larger molecular volume in the liquid state in comparison to corresponding hydrocarbons; therefore the polarizability per volume (α/υ) and the Hildebrand solubility parameter (δ, Equations 1) are significantly smaller than the equivalent hydrocarbons.

$$\delta = \sqrt{\frac{\Delta H_v - RT}{V_m}}$$

(1)

The Hildebrand solubility parameter δ can be used as an indication of solubility of a substance, as it provides a quantifiable estimate of the degree of interaction between materials. The parameters in Equation 1 are enthalpy change through vaporisation (ΔH_v), gas constant R and temperature *T* divided by molar volume (V_m).

As CO_2 also has a low dielectric constant, α/υ and δ, it is expected that fluorocarbons and CO_2 will be more compatible than HCs and CO_2. It can therefore be said that fluorocarbons are more CO_2-philic than the corresponding hydrocarbons. A range of surfactants are discussed throughout this review; the structures of which are displayed in Table 1.

Fluorocarbon-based surfactants have been used frequently in the field due to the high solubility of fluorocarbon chains in liquid and supercritical CO_2. They were first introduced by Hoefling, Enick and Beckmann in 1991, through the synthesis of fluorinated AOT (Aerosol-OT, sodium dioctylsulfosuccinate) analogues and the observation of Windsor II microemulsions [26]. Microemulsions are thermodynamically stable dispersions of two or more immiscible/partially miscible fluids which are stabilised through the addition of amphiphilic molecules, such as surfactants or polymers. The domains created are on the nanometer scale leading to the dispersions being transparent or translucent in appearance. The microemulsion appearance does not alter over time. Following this discovery, a vast array of

Table 1: Structures of CO_2-philic surfactants discussed in this review.

Compound	Structure	Shortened Term	Reference
1		F7H7	[27,58]
2		Di-CF1	[59]
3		Di-CF2	[59]
4		Di-CF3	[59]
5		Di-CF4	[59]
6		di-C5SS	[59]

Table 1: Structures of CO₂-philic surfactants discussed in this review. (continued)

7		Hybrid CF2-AOT4	[59]
8		AOT3	[59]
9		AOT4	[59]
10		TC14	[60]
11		SIS1	[61]
12		TMN-6	[61]
13		AGLU	[62]
14		AOK	[37]
15		AO-Vac	[37]

fluorocarbon surfactants have been investigated and successfully solubilised in dense CO_2 to form *w/c* reverse micelles and microemulsions; this area has been extensively reviewed [36,38,63]. In more recent years, efforts have been made to reduce fluorocarbon use due to the high expense and ensuing environmental hazards [64-67]. Investigations focusing on partially fluorinated hybrid surfactants as a way to reduce fluorine content began in 1994 with the design and synthesis of F7H7, a partially fluorinated surfactant with an *n*-C7 fluorocarbon chain and an *n*-C7 hydrocarbon chain (Table 1, compound **1**) [27,58,68]. Subsequently both surfactant development and the understanding of applications of scCO2 have advanced considerably. Surfactant solubility has been previously expressed in a range of ways based on pressure and temperature phase behaviour studies. The phase instability P_{trans} (cloud point pressure) is the minimum pressure where a dispersion is a stable single transparent phase. It has been used as a measure of surfactant efficiency in CO_2, with a lower P_{trans} being equated to a more efficient surfactant. The *w* value expresses the degree of water uptake or the number of water molecules solubilised by the additive/surfactant being tested in CO_2 and is quantified by the water-to-surfactant ratio (Equation 2). A relationship between *w* value and P_{trans} has been highlighted, with P_{trans} increasing with increased *w* value [45].

$$w = \frac{[\text{water}]}{[\text{surfactant}]} \tag{2}$$

The effects of the surfactant chain length on microemulsion stability and the effects of fluorination have also been investigated, with studies showing that longer surfactant tails lead to increased stability in microemulsions. This is possibly due to increased interfacial activity and the changing of the terminal group from -CF3 to -CF2H reduces ease of microemulsion formation [35,69,70]. A systematic study by Mohamed et al. [59]

identified the minimum amount of fluorine needed in a surfactant to remain CO_2-philic. This was achieved with a controlled range of fluorinated AOT analogues, di-CF*n*, where *n* = 1–4 (with di-CF4 having fully fluorinated C4 groups and di-CF1 having the minimum level of fluorination, Table 1, compounds **2**–**5**), and a HC control analogue (di-C5SS, Table 1, compound **6**) containing no fluorine. The study also looked at the effects of replacing a terminal fluorine atom with hydrogen (*n*-CF3 to *n*-CF2H), hereby introducing a dipole moment at the end of the chain; a property that has strong possibility of decreasing CO_2-philicity. This also leads to a reduction in the levels of fluorine, making the precursors cheaper [61,71]. Overall the study identified important factors for CO_2-philicity as well as several avenues that could potentially be pursued further. A key CO_2-philicity indicator identified was surfactant coverage at the water-CO_2 interface, which can be quantified using surface tension measurements of aqueous solutions and the interface coverage index Φ_{surf}, Equation 3.
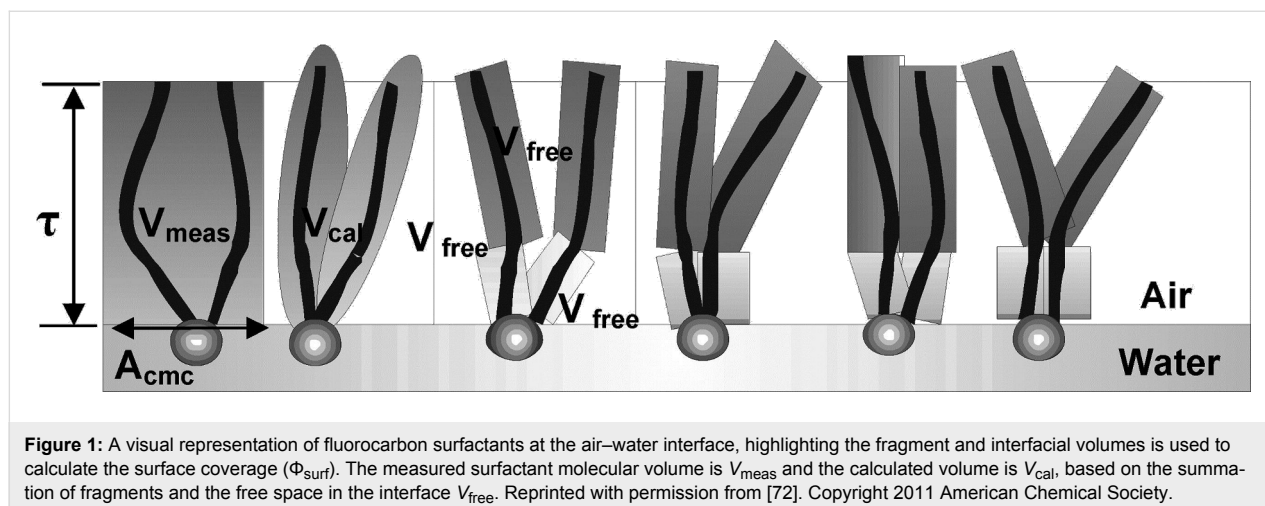
$$\phi_{surf} = \frac{V_{cal}}{V_{meas}} \tag{3}$$

Where V_{meas} is the total fragment volume at the interface and V_{cal} is the volume of surfactants in total. V_{meas} is calculated using the area of surfactant headgroups (A_{cmc}) and the interfacial thickness (τ) [59,72], Equation 4.
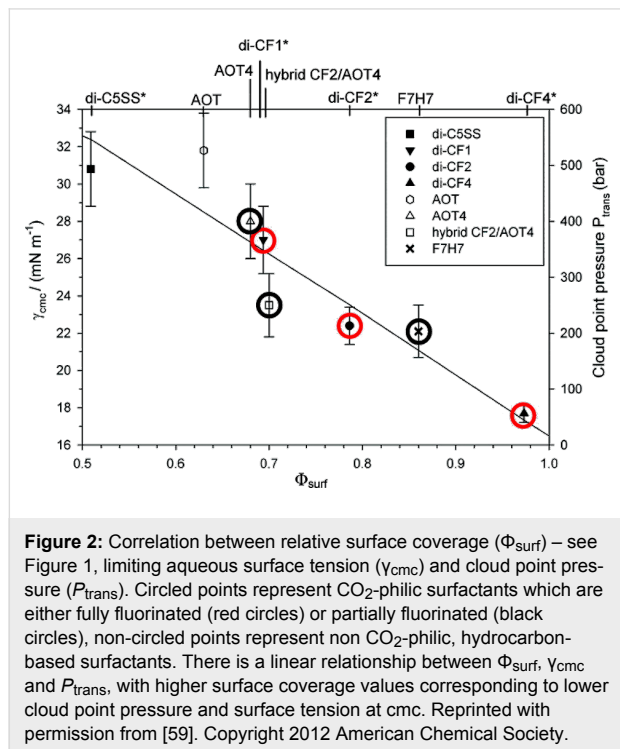
$$V_{meas} = A_{cmc} \times \tau \tag{4}$$

An increased Φ_{surf} value ensured a greater separation at the interface between CO_2 and water, see Figure 1.

A linear relationship between Φ_{surf}, P_{trans} and γ_{cmc} (surface tension of aqueous solutions) has been identified, with Φ_{surf} increasing with decreased P_{trans} and γ_{cmc}. This has been

Figure 1: A visual representation of fluorocarbon surfactants at the air–water interface, highlighting the fragment and interfacial volumes is used to calculate the surface coverage (Φ_{surf}). The measured surfactant molecular volume is V_{meas} and the calculated volume is V_{cal}, based on the summation of fragments and the free space in the interface V_{free}. Reprinted with permission from [72]. Copyright 2011 American Chemical Society.

observed with a range of surfactants, including fully and partially fluorinated and hydrocarbon-based surfactants (Figure 2).

Figure 2: Correlation between relative surface coverage (Φ_{surf}) – see Figure 1, limiting aqueous surface tension (γ_{cmc}) and cloud point pressure (P_{trans}). Circled points represent CO_2-philic surfactants which are either fully fluorinated (red circles) or partially fluorinated (black circles), non-circled points represent non CO_2-philic, hydrocarbon-based surfactants. There is a linear relationship between Φ_{surf}, γ_{cmc} and P_{trans}, with higher surface coverage values corresponding to lower cloud point pressure and surface tension at cmc. Reprinted with permission from [59]. Copyright 2012 American Chemical Society.

Surfactant tails – siloxane, hydrocarbon and oxygenated surfactants: Though the use of fluorocarbons can be significantly reduced through the development of hybrid, semi-fluorinated surfactants, the race toward the development of a non-fluorinated, CO_2 soluble surfactant is of primary focus in this field. These include hydrocarbon based, siloxane based and carbonyl based/oxygenated surfactants (Table 1, compounds **1**–**10**) [13,42,47,60,61].

Trisiloxanes have been identified as stabilisers for emulsions in both water-in-carbon dioxide and carbon dioxide-in-water systems but have yet to be seen to stabilise microemulsions. Investigations were carried out with a range of ethylene oxide (EO) repeat units, with an inversion of emulsion morphology from water-in-carbon dioxide to carbon dioxide-in-water as EO repeat units increased from 2 to 7. There was noteworthy stability at EO7 thought to be due to the strong solvation of the trisiloxanes by CO_2 [47].

Hydrocarbon based surfactants: As previously mentioned, the compatibility of many commercially available hydrocarbon surfactants has been investigated to find that the majority are not CO_2-philic [53], however, efforts to increase CO_2-philicity have been made through intelligent surfactant design and syn-

thesis. Several structural aspects have thus far been identified as increasing CO_2-philicity of hydrocarbon surfactants, including the degree of surfactant tail branching and methylation [49], where increased tail branching and methylation led to increased solvophilicity in carbon dioxide in comparison to linear alkanes. This in turn led to the formation of *w/c* microemulsions with increased stability. It is thought that this is due to weaker interactions between surfactant tails as well as lower surfactant affinity to water thus leading to an improved partition coefficient.

Pitt et al. [73] drew attention to the fact that surfactants with *tert*-butyl chain tips have the lowest surface energies for hydrocarbon surfactants following a systematic study using a range of surfactant types. Following this study, two variations of AOT with *tert*-butyl tipped chains were observed to have low water-CO_2 interfacial tensions (Table 1, compounds **8** and **9**). The presence of reversed micelles was also confirmed with small-angle neutron scattering (SANS) where the *w* value = 0, although phase separation occurred immediately upon water addition [59]. SANS is a non-invasive technique that utilizes elastic neutron scattering at small scattering angles in order to investigate internal sample structure over length scales of ~10 Å–1000 Å. It is used extensively in the field of colloid science due to the ability to identify a range of internal structures, as well as having the capacity to contrast individual components in a multicomponent mixture through selective isotropic (hydrogen/deuterium) labelling. Research around a group of tri-chain surfactants has been carried out through the addition of a third extensively methylated tail in hope to both enhance CO_2 compatibility and to also reduce surface energy [39]. TC14 (sodium 1,4-bis(neopentyloxy)-3-(neopentyloxycarbonyl)-1,4-dioxobutane-2-sulfonate, Table 1, compound **10**) was solubilised in water, heptane and supercritical carbon dioxide and aggregates were characterised with SANS [39,60]. Results from surface tension measurements show that γ decreased as the number of tails increased, which is attributed to hydrocarbon tail packing efficiency balanced against headgroup repulsions, as well as the increase in the number of low energy methyl groups per headgroup. Expectations surrounding the impacts of chain-tip structure on CO_2-philicity also supported data from previous studies [49], with structures having a greater extent of chain-tip branching showing a lower P_{trans} in comparison to those which baring less chain-tip branches [60]. Sagisaka et al. have synthesised and successfully solubilised a hydrocarbon based CO_2-philic surfactant, SIS1 (sodium 2-(4,4-dimethylpentan-2-yl)-5,7,7-trimethyloctyl sulfate, Table 1, compound **11**) [61]. It was designed on the basis that a strongly hydrophobic tail was needed to efficiently solubilise surfactant in CO_2 alongside the discovery that a highly methylated isostearyl unit is highly CO_2-philic following

the successful stabilisation of silver nanoparticles using isostearic acid [74]. It was compared to TMN-6 (Table 1, compound **12**), a non-ionic surfactant with highly branched alkyl tails and around eight oxyethylene units which has previously been reported as solubilising water up to a w_o value of 30 (w_o value is similar to w value, however, uses a corrected water-to-surfactant ratio, where the number of moles of water solubilised by carbon dioxide is taken into account) when temperatures and pressures exceed 55 °C and 210 bar, respectively [75-77]. SIS1 has been observed to achieve a w_o value of 50 but only with high temperature and pressure (55 °C and 210 bar). Both the cmc and the A_{cmc} (the surface area per molecule) of SIS1 were around 1.5 and 1.7 times larger than that of TMN-6 (1.5×10^{-3} mol L^{-1} cf. 8.8×10^{-4} mol L^{-1} and 103 Å^2 cf. 70 Å^2 respectively) resulting potentially from the bulkier isostearyl tail or from the increased electrostatic repulsion from the larger sulfate head group. The surface tension at cmc was marginally lower in SIS1 cf. TMN-6 (25 mN m^{-1} cf. 26 mN m^{-1}, respectively), indicating that SIS1 has a greater ability to lower interfacial tension and therefore a higher solubilizing power in CO$_2$. It is hypothesised that *w/c* microemulsions may be obtained at lower pressures and temperatures if; (i) the CO$_2$-philicity of reversed micelles can be increased, (ii) if there are reduced attractive interactions between micelles or (iii) if the solvent power of CO$_2$ could be tuned to make it more hydrocarbon-like [61]. It was reported that these properties could be modified through co-solvent/co-surfactant addition or by tuning the position and the amount of methyl groups on the surfactant tail [61].
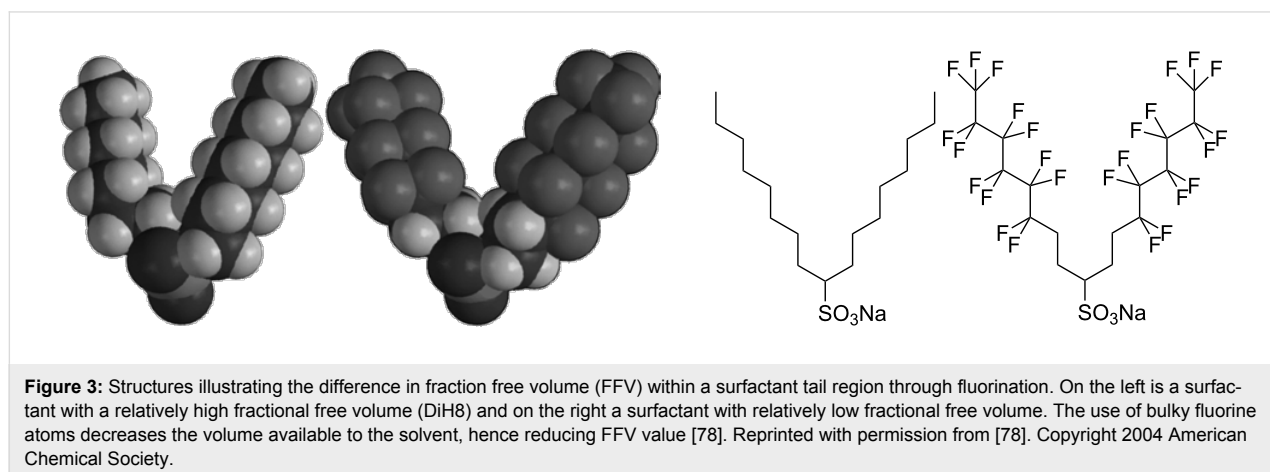
The concept of FFV: A range of different models have been used to attempt to predict and quantify CO$_2$-philicity. One very popular approach is the concept of fraction free volume, or FFV, defined by Johnston et al. [78]. The fractional free volume of an adsorbed monolayer is calculated from surfactant tail geometry and surface coverage, using the surfactant tail volume

(V), the surfactant tail length (t) and the area of the surfactant headgroup at critical micelle concentration (A_{cmc}), Equation 5:

$$\text{FFV} = 1 - \frac{V}{t A_{cmc}} \quad (5)$$

Surfactants with lower FFV values are expected to be effective CO$_2$-philes, corresponding to improved solubility of surfactants and therefore increased stability with the formation of *w/c* microemulsions. The concepts and properties identified as effectively making surfactants soluble in CO$_2$ are known to reduce FFV; fluorinated surfactants have a significantly larger tail volume in comparison to their hydrocarbon counterparts, and hydrocarbon surfactants with increased branching and a larger number of surfactant tails (tri-chain surfactants vs double chain surfactants) have been seen to be more CO$_2$-compatible [39,49,60,73,78]. A reduced value for FFV leads to a more densely packed interfacial film and therefore a decrease in both CO$_2$ and water penetration into the surface layers. Penetration of CO$_2$ into the surfactant film could destabilise the aggregation structures, see Figure 3. Unfortunately the concept of FFV cannot be used exclusively as a measure of CO$_2$-philicity but has served as a useful tool along with P_{trans} and Φ_{surf}, for guiding selection and design of CO$_2$-compatible surfactants.

Oxygenated surfactants: Oxygenated hydrocarbon chain surfactants have also been identified as potential replacements for fluorocarbon surfactants for applications in supercritical carbon dioxide. Kazarian et al. carried out a study investigating the interactions between CO$_2$ and carbonyl groups using FTIR spectroscopy with polymers incorporating electron donating (carbonyl) groups. These polymers showed splitting of the band corresponding to the CO$_2$ v_2 mode, which was not observed in spectra from polymers without electron-donating groups [71]. The splitting is likely to be caused by Lewis acid–base interactions, arising from electron donation from the lone pair of the

Figure 3: Structures illustrating the difference in fraction free volume (FFV) within a surfactant tail region through fluorination. On the left is a surfactant with a relatively high fractional free volume (DiH8) and on the right a surfactant with relatively low fractional free volume. The use of bulky fluorine atoms decreases the volume available to the solvent, hence reducing FFV value [78]. Reprinted with permission from [78]. Copyright 2004 American Chemical Society.

oxygen in a carbonyl group to the electron-deficient carbon atom in CO_2. On this basis carbon dioxide should also interact favourably with other Lewis bases, another potential reason that fluorocarbon surfactants exhibit high solubility in scCO_2 [26,79]. This is also supported by Reilly et al., who indicated that CO_2 is more likely to behave as an electron acceptor over an electron-pair donor, through a study investigating CO_2 interactions with *d*-methanol. Research confirmed that a *d*-methanol–CO_2 complex occurred through Lewis acid–base interactions over hydrogen-bonding interactions [80]. Oxygenated hydrocarbon-based molecules have also been designed for use in CO_2 by Raveendran et al., where selected carbohydrates were solubilised indicating the potential that they hold as alternative CO_2-philic groups (Table 1, compound **13**) [62]. Eastoe et al. stabilised spherical reverse micellar microemulsions (characterised by SANS) with specifically designed AOT analogues; one containing a carbonyl group in each chain along with a *tert*-butyl at the chain tip (AOK, Table 1, compound **14**) and another with twin vinyl acetate oligomeric chains (AO-Vac, Table 1, compound **15**).
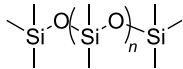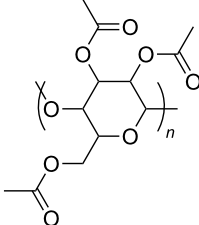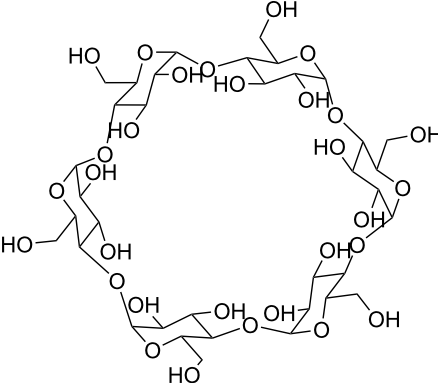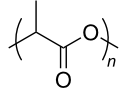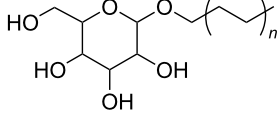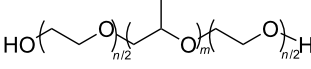
Polymers: Amphiphilic block-copolymers are classic examples of molecules which have an inherent ability to adsorb at interfaces and generate aggregation structures. Polymeric micelles may be generated in water and have been used in a range of applications, including biomedical science for drug delivery [81,82]. Judicial choice of the chemical nature of block components could help drive the formation of structures, such as reverse micelles, in scCO_2. Many of the factors that have been employed to increase CO_2-philicity of small molecule surfactants have reapplied during the design of CO_2-philic polymers. The structures of polymers discussed in this review can be seen in Table 2.

Fluorinated polymers: One of the first polymers reported to be solubilised in CO_2 was Krytox 16350 (Table 2, compound **16**), a perfluoropolyether (PFPE) oil [83] with a molecular weight of 11350 g mol^{-1}. The study showed that polymer solubility decreases with increased molecular weight with lower molecular weight polymers (<15000 g mol^{-1}) showing high solubility in scCO_2. The effects of head group composition and

Table 2: Structures of CO_2-philic polymers discussed in this review.

Compound	Structure	Name	Reference
16		Krytox 16350	[83]
17		Teflon AF	[11,12]
18		Poly(propylene glycol)-diol	[13]
19		Poly(propylene glycol) monobutyl ether	[13]
20		Poly(propylene glycol) acetate	[13]
21		Poly(ether carbonate)	[13]
22		Poly(methyl acrylate)	[84]
23		Poly(vinyl acetate)	[84]

Table 2: Structures of CO_2-philic polymers discussed in this review. (continued)

24		Poly(dimethylsiloxane)	[85,86]
25		Cellulose triacetate	[87]
26		Cyclodextrin	[88]
27		Poly(lactic acid)	[89]
28		Glucopyranoside	[89]
29		Pluronic	[51]

polymer chain length were investigated by Howdle et al. [90]. When the PFPE polymers were in their carboxylic acid form no microemulsions were formed, however, upon the conversion of the headgroups to ammonium carboxylates *w/c* microemulsions were observed. The length of the polymer tail was also shown to affect the ability to form microemulsions. The optimum molecular weight was found to be around 2500 g mol^{-1}, with longer chain lengths being too CO_2-philic, whereas shorter chain lengths were too hydrophilic to disperse extensive quantities of water within reverse micelles [90]. Partially fluorinated analogues, including an ethylene-based copolymer and fluorinated Teflon analogue Teflon AF have also been solubilised in CO_2 (Table 2, compound **17**) [11,12].

Non fluorinated polymers: There has also been a large amount of research around non-fluorinated polymer analogues, for the

same reasons as surfactants, to reduce fluorocarbon use. The identification of Lewis acid–base interactions as a mechanism for solubility in CO_2 has given rise to many potentially CO_2 soluble polymers, including oxygenated and acylated species [26,71,79,80]. The first non-fluorous polymers to be effectively designed and solubilised were poly(propylene glycol)-diol, poly(propylene glycol) monobutyl ether, poly(propylene glycol) acetate and poly(ether carbonate), (Table 2, compounds **18**–**21**) [13]. Beckman et al. developed a set of design rules for CO_2-philic polymers based on both theoretical and experimental approaches [91]. These include (a) chain flexibility (for example, the addition of ether/oxygen linkages can increase the flexibility within the polymer backbone or side chains); (b) free volume, similar to the FFV principle mentioned earlier, with *tert*-butyl groups and other highly branched moieties giving a decrease in free volume; (c) presence of functional groups that

have thermodynamically favourable interactions with CO_2; (d) low crystallinity; this can be decreased by increased branching structures on side chains and finally (e) a low glass transition temperature (T_g) [92]. There are also several factors that have been identified as having a negative impact on polymer solubility, including the presence of amine-functional groups and allyl polymers with a $-CH_2$-spacer between the polymer backbone and the side chain or group [85,91]. These have since been used more as a set of guidelines as opposed to a set of hard-and-fast rules; poly(methyl acrylate) (PMA - Table 2, compound **22**) has a greater degree of acetylation than poly(vinyl acetate) (PVAc - Table 2, compound **23**) but has a much higher melting point and is insoluble in CO_2 [84].

A significant amount of experimental and theoretical work has been carried out on the addition of CO_2-philic moieties to polymer backbones and side groups, including the addition of tertiary amines and pyridine (all analogues tested were insoluble) [91] and siloxanes (poly(dimethylsiloxane) (PDMS, Table 2, compound **24**)), which has the highest solubility of all known non-fluorinated polymers in carbon dioxide [85,86]. There is also promise being seen with organic hydroxylated and oxygenated compounds such as cellulose triacetate [87], cyclodextrins [88], amorphous poly(lactic acid) and glucopyranoside [89] (Table 2, compounds **25**–**28**) as well as polymers with incorporated ether linkages [87].

Beckman and Enick et al. have a large body of both practical and theoretical work around polymer solubility in carbon dioxide [84]. The first reported use of ab initio modelling to design oxygenated hydrocarbon polymers for use in CO_2 was in 2009, where one oligomer and two polymers were synthesised and found to be soluble in CO_2 after ab initio predictions. The molecules OAO, PVMME and PVMEE were derived from the

smaller CO_2-philic moieties MIA, 2MME and 2MEE. It is hoped that other macromolecules could also be designed based on these moieties in time (Figure 4).

Unfortunately, ab initio modelling can be quite limiting as there are interactions and factors that cannot be taken into account. These include effects of temperature, density effects of the solvent, polymer–polymer interactions and the fact that only interactions between polymer segments and the solute can be computed, as the polymer cannot be represented as one macromolecule but instead must be represented in smaller fragments.

The induced micellisation by $scCO_2$ of commercially available Pluronic polymers/poloxamers has also recently been observed at low temperatures [51]. Pluronics are non-ionic triblock copolymers with a central hydrophobic polyoxypropylene (PPO) unit edged by two hydrophilic polyoxyethylene (PEO) units (Table 2, compound **29**). It is hypothesised that the increased hydrophobic interaction of the internal PPO blocks with CO_2 during addition is responsible for the change in morphology. These polymeric micelles differ slightly from those that have been previously reported due to the amphiphilic nature of their cores; ensuring that both non-polar and polar components could be dissolved in the micellar interiors.

Conclusions – factors impacting solubility in CO_2

Significant effort has gone into further understanding the origins and intrinsic properties for both surfactant and polymer solubility in $scCO_2$, which have been highlighted above. These include the inclusion of CO_2-philic moieties which show favourable interactions with CO_2, such as Lewis bases and fluorocarbons. Effort has been made to move away from the use of fluorocarbons in both surfactant and polymer design, but they are still potentially the most CO_2-philic moieties observed thus
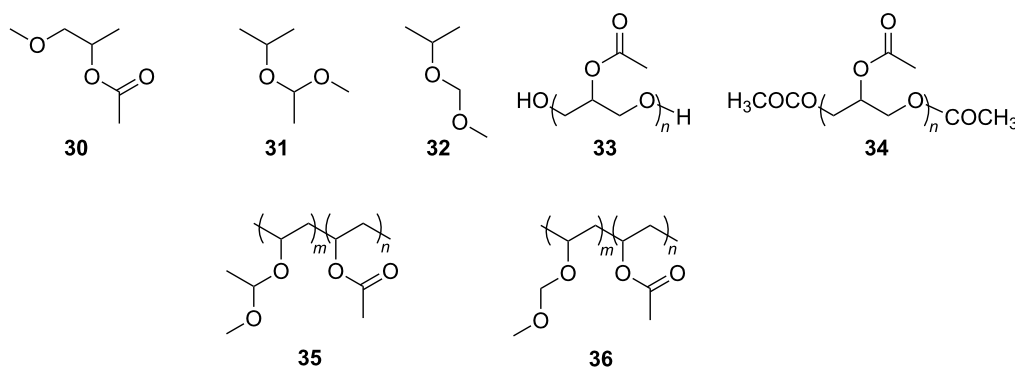

Figure 4: Structures of three CO_2-philic candidates: (**30**) MIA, (**31**) 2MEP and (**32**) 2MMP and the respective polymer candidates they produce: (**33**) -OH terminated oligo(3-acetoxy acetate), OAO, based on MIA; (**34**) -OCOCH$_3$ terminated OAO, also based on MIA; (**35**) PVMEE, poly(vinyl 1-methoxyethyl ether-co-acetate), based on 2MEP and finally (**36**) PVMME, poly(vinyl methoxymethyl ether-co-acetate), based on 2MMP.

far. This is thought to be due to their high molar volume and as well as their lower polarisability volume and solubility parameter, leading fluorocarbons to be more akin to CO_2 (with low dielectric constant) than the respective hydrocarbon counterparts. There has been success in the design and synthesis of non-fluorinated polymers and surfactants, with hydrocarbon based, siloxane based and carbonyl and oxygenated hydrocarbon surfactants and polymers successfully solubilised [11-13,26,83,84,86,91].

Several models for quantifying solubility have also been developed: (A) the concept of Fractional Free Volume. Depending on surface tail geometry and surface coverage calculated using the tail volume and length and the surfactant headgroup, a lower FFV value is expected to be a better CO_2-phile because of a more densely packed interfacial film, leading to increased stability at the interface. (B) Surfactant coverage at the interface (Φ_{surf}). This is a similar property to FFV, but taking into account the fractional fragment volume of surfactant at the interface in respect to the volume of surfactant in the entire system. The fragment volume at the interface is calculated using the interfacial thickness and the area of surfactant headgroups at critical micelle concentration. Increased Φ_{surf} corresponds to greater separation between two phases at the interface.

Viscosifiers for CO_2

Though solubility of additives in CO_2 is a very important factor, the eventual goal would be to have the ability to tune solvent properties with solutes, as is commonly done with regular solvents (e.g., water). As discussed above, a huge amount of research has been carried out around solubility and identifying and quantifying the properties that make any given additive CO_2-philic. Alongside this, work focusing on modification of CO_2 solvent properties has been undertaken; viscosity is one of these key properties, with viscosity enhancing solutes acting through increasing internal structure. The majority of structures observed with surfactants and polymers in CO_2 have been spherical reversed micelles [69], however, other anisotropic surfactant aggregate structures have been observed. Surfactants and polymers that undergo self-assembly and aggregation provide convenient ways to develop structure and affect viscosity. Examples of self-assembly structures that are commonly used to enhance viscosity include ellipsoid and rodlike micelles, worm and lamellar structures, bicontinuous phases and also the formation of gels [32,46,49,50,93-95].

Polymeric CO_2 viscosifiers: Several polymeric thickeners for CO_2 have previously been identified, following investigations into polymer solubility in CO_2 [96,97]. Heller et al. identified poly(1-decene) (P-1-D, Figure 5, compound **37**) as having potential CO_2 viscosifying properties due to its high solubility

in CO_2 [97]. This work has been built on by Zhang et al. along with another low molecular weight, CO_2-philic polymer; poly(vinyl ethyl ether), (PVEE, Figure 5, compound **38**) [98,99].

Figure 5: Structures of poly(1-decene) (37, P-1-D) and. poly(vinyl ethyl ether) (38, PVEE).
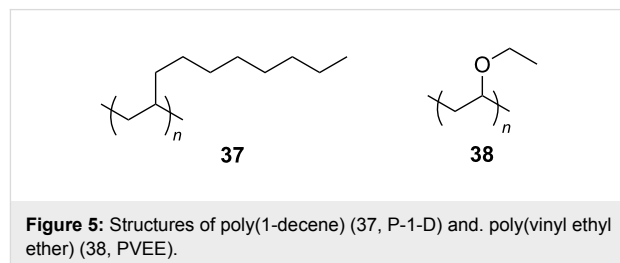
Viscosities of the polymer-thickened CO_2 were measured by capillary viscometry across a range of pressures along with cloud point pressures. Higher P_{trans} values were observed for PVEE systems in comparison to the P-1-D systems, attributed to the presence of the oxygen containing ether group in the polymer (previously established as a group capable of increasing CO_2-philicity and therefore solubility in CO_2) [26,71,79,80]. Results showed that the viscosity of the polymer thickened CO_2 (μCO_2/PVEE) was around 13 to 14 times higher than that of the pure CO_2 (μCO_2) ($\mu CO_2 = 0.048–0.063$ mPa s cf. μCO_2/PVEE $= 0.68–0.95$ mPa s and μCO_2/P-1-D $= 0.70–0.93$ mPa s) at 329.15 K [98]. Enick and Beckman et al. successfully enhanced the viscosity of dense CO_2 by a factor of around 5 to 400 through the addition of fluoroacrylate and styrene copolymers at a range of polymer concentrations (1–5 w/w %) and styrene:fluoroacrylate molar ratios [100]. Cloud point pressures indicated that polymer solubility decreased with increased concentrations of styrene in the polymer chain, due to poor solvency of styrene in CO_2. It was anticipated that π–π stacking between phenyl groups is a main contributor to the viscosity increase, through its provision of a fundamental intermolecular force needed to raise viscosity in a system. The optimum composition of polymers for viscosity enhancement in this study was 29 mol % styrene:71 mol % fluoroacrylate.

Surfactant headgroups – counterion effects: An important area of investigation is salt addition and counterion exchange in surfactant headgroups. The effects of counterion exchange from Na^+ to M^{2+} ions (Mg^{2+}, Ca^{2+}, Co^{2+}, Ni^{2+}, Cu^{2+} and Zn^{2+}) on Aerosol OT in water-in-oil (*w/o*) microemulsions has been investigated [101]. A range of aggregate morphologies was characterised through SANS, with Na(AOT), Mg(AOT)$_2$ and Ca(AOT)$_2$ forming spherical micelles with reduced viscosities of around 2.5 cm^3 g^{-1} in comparison to rod-shaped micelles formed by Co(AOT)$_2$, Ni(AOT)$_2$, Cu(AOT)$_2$ and Zn(AOT)$_2$ which showed a reduced viscosity of between 10 cm^3 g^{-1} and

20 cm^3 g^{-1}. Though this was not a CO_2-water system, AOT has been the basis for many successful CO_2-philic surfactants, so attempts have been made to apply this strategy to CO_2 surfactants.

Work using the fluorinated surfactant anion di-HCF4 changing the normal Na$^+$ counterion for Co^{2+} or Ni^{2+} resulted in an increase of viscosity between 20–90% over shear rates of 6000–10000 s^{-1} at approximately 6–10 wt % with Ni(di-CF4)$_2$ in comparison to the minor viscosity increase seen for the Na$^+$ ion analogue (approximately 10% over the same conditions) [49]. The high pressure viscosity data in this study is combined with high pressure SANS (HP-SANS) characterizations which confirmed the presence of anisotropic microemulsion aggregates, or rod-like micelles, within samples containing Ni^{2+} and Co^{2+} counterions. This phenomenon has also been observed with di-CF3 with the replacement of Na$^+$ with Ni^{2+} and Co^{2+} counterions [8] but not with the tri-branched hydrocarbon chain TC14 analogue for which spherical aggregates were observed [102].

Work around the effects of counterion hydrated radius (r_{hyd}) and critical packing parameter (CPP) on self-assembled morphologies of the CO_2-philic hybrid semi-fluorinated surfactant M-F7H4 (pentadecafluoro-5-dodecyl sulfate) was carried out by Cummings et al. through the substitution of a range of metal counterions (Li-F7H4, K-F7H4, Na-F7H4 and Rb-F7H4) [32]. It is known that r_{hyd} of the M$^+$ ion can impact preferred curvature and therefore impact surfactant morphology, and exchanging counterion induces a change in effective ion size through the hydrated radius (Figure 6).

The study indicated that micelles in water and CO_2 should have a range of geometric packing parameters as a function of M$^+$, as interfacial packing density and limiting the area of the head group at the critical micelle concentration (A_{cmc}) are dependent on the identity of M$^+$ (highlighted through surface tensiometric measurements). Decreases in cmc, A_{cmc} and surface tension were observed with a respective increase in the size of the counter ion (Li$^+$ < K$^+$ < Na$^+$ < Rb$^+$). A_{cmc} is a good approximation of the limiting area per head group in micellar aggregates and can be used to estimate the critical packing parameter, Equation 6.

$$\text{CPP} = V\!\!\bigg/\!\!tA_{cmc} \tag{6}$$

Where V is the surfactant tail volume and t is the maximum extended length of the tail group chains within the micelle. Surfactants with smaller tail volumes (V) and larger head groups (A_{cmc}) will have CPP values of <1 and will self-
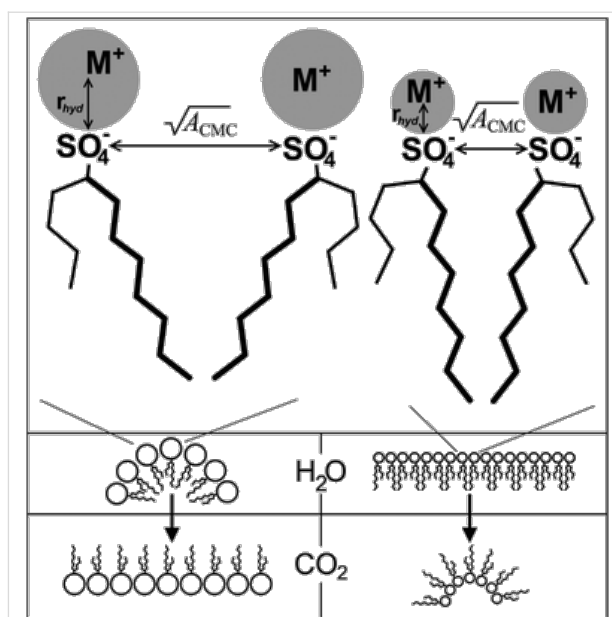

Figure 6: Schematic showing how hydrated cation radius (r_{hyd}) mediates surfactant headgroup repulsions by controlling limiting headgroup area at critical micelle concentration (A_{cmc}). Changes in A_{cmc} and r_{hyd} affect preferred curvature and therefore aggregate morphology in water and scCO$_2$. Reprinted with permission from [32]. Copyright 2012 American Chemical Society.

assemble with a positive surface curvature, whereas those with smaller headgroups and larger tail volumes will have CPP values of >1, giving rise to a negative surface curvature and reverse micelles. As CPP value of a system decreases towards 1.5–1, reversed cylindrical and rod-like reversed micelles are expected to form.

When CPP ≤ 0.33, normal curved spherical aggregates are expected, if 0.33 < CPP < 0.5, ellipsoidal or rod-like aggregates are expected to form and when 0.5 < CPP < 1, lamellar structures are expected to form. SANS was used to characterise morphologies of M-F7H7 at the air-water interface, which were in line with the predictions from CPP values: Li-F7H4 (CPP = 0.26) and K-F7H4 (CPP = 0.44) formed prolate ellipsoids, Na-F7H4 formed rods (CPP = 0.40) and Rb-F7H4 formed vesicles (CPP = 0.52) at w = 12.5 systems. An increase of the w value lead to micellar elongation in the Li$^+$, Na$^+$ and K$^+$ systems and no change in the Rb$^+$ systems. The area of counterion exchange and its impact on surfactant packing in CO_2 has been extensively reviewed by James et al. [41]; readers are referred to this for further information on the subject.

Co-surfactant, salt and additive addition: Methods of viscosity enhancement in general have been reviewed by Trickett et al. with a specific focus on surfactant gel formation through the production of worm-like micelles [50]. Worm-like micelles have been shown to build viscosity through entangling

or cross-linking of the structures, which then generates a structural network and enhance elasticity and viscosity [31,50]. Micellar growth in these systems was induced through the addition of co-surfactants and additives. Though the review does not include gelation in CO_2 systems, it is still worth mentioning due to the inclusion of fluorocarbon and AOT surfactants since AOT derivatives and fluorocarbon surfactants have both been successfully solubilised in dense CO_2. The one-dimensional growth of worm-like micelles has been reported with the addition of cosolvents and salts with a range of surfactants, including anionic, cationic and mixed surfactants, in oil-in-water systems [95].

Salt addition to an amphiphilic system is known to screen the charged surfactant headgroup repulsions, which leads to a reduction of the effective headgroup size [103]. This leads to a reduction in preferred curvature (as described by the CPP model) and therefore the formation of microstructures that favour reduced curvature, such as rod-like micelles. Hydrotropic salts have shown to be successful in elongating spherical reverse micellar structures to form rod-like and ellipsoid microemulsions in alkanes, and also interestingly scCO$_2$ systems [40,94,104]. Extensive work by Hatzopoulos et al. has been carried out to investigate further the impacts of hydrotropic salt structure and water level (*w*) on AOT surfactant microemulsion structure in *w/o* systems [40,105,106]; these findings were used as the basis for designing CO_2-philic analogues. James et al. studied the impacts of *w* value and

hydrotrope concentration in water-in-oil (*w/o*) and in water-in-scCO$_2$ (*w/c*) systems using universal surfactant TC14 [94]. In general, in both *w/c* and *w/o* systems, as w level is increased morphologies transitioned from cylinders to ellipsoids, and finally to spheres. This is accounted for through the decrease of the aqueous concentration of the hydrotrope toward the critical aggregation concentration (cac) with increased water content; when the hydrotrope concentration decreases below the cac, spherical micelles are formed. In this study, a range of hydrotrope structures was also investigated, see Figure 7. It was also discovered that hydrotropes with longer alkyl tails (compound **40** – C$_4$Benz and compound **41** – C$_8$Benz) had the greatest solubilisation capacity, followed by the remaining "long" hydrotropes (compound **43** – PhenC$_5$ and compound **45** – CyclohexC$_5$), which could be due to the destabilizing effects of the rings in the surfactant layers. Hydrotropes with equal numbers of C atoms also had similar upper temperature boundaries (C$_4$Benz, C$_5$Phen and CyclohexC$_5$) [40].

James et al. recently published research around the use of hydrotropes with a universal surfactant TC14 reporting spherical to rod reverse micellar transitions in both *w/o* and *w/c* systems [94]. Impacts of water content, hydrotrope structure and hydrotrope mole fraction (X, Equation 7) were investigated.

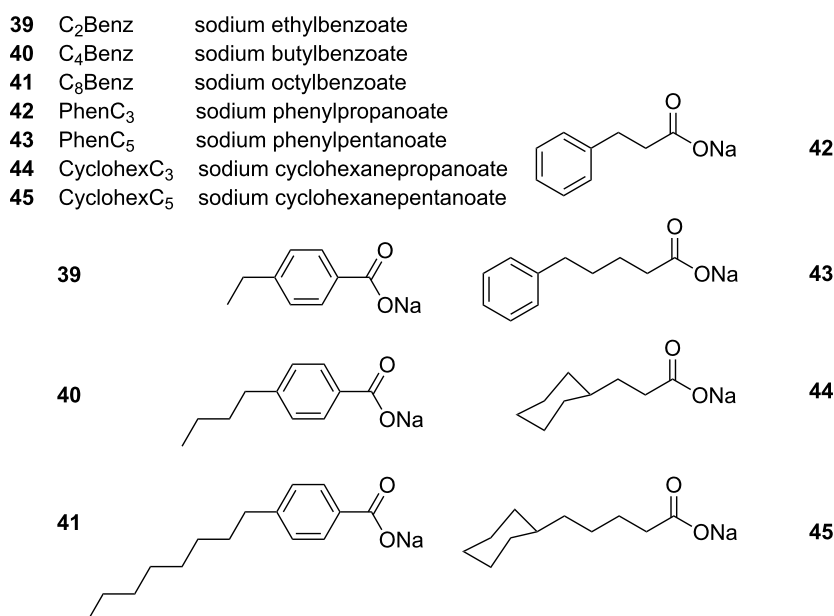$$X = \frac{[\text{hydrotrope}]}{[\text{hydrotrope}] + [\text{surfactant}]} \qquad (7)$$

39	C$_2$Benz	sodium ethylbenzoate
40	C$_4$Benz	sodium butylbenzoate
41	C$_8$Benz	sodium octylbenzoate
42	PhenC$_3$	sodium phenylpropanoate
43	PhenC$_5$	sodium phenylpentanoate
44	CyclohexC$_3$	sodium cyclohexanepropanoate
45	CyclohexC$_5$	sodium cyclohexanepentanoate

Figure 7: Abbreviated names and structures of hydrotropes tested by Hatzopoulos et al. [40,105,107].

Micellar elongation was observed in water-in-oil systems with increased *w* value; though this is the opposite of that which was observed by Hatzopoulos et al. [40], this is attributed to the aqueous concentration of the hydrotrope never reaching the cac, due to the inability of TC14 to stabilise *w* values as high as those observed within AOT microemulsions [42]. Increased hydrotrope mole fraction also lead to increase in micellar elongation and hydrotrope structure was also shown to impact elongation; however, there was no visible trend around the magnitude of elongation and hydrotrope structure (hydrotrope structures investigated include hydrotropes **39–43**, Figure 7). For water-in-CO_2 systems the structure of the hydrotrope was shown to have minimal impact on morphology and higher mole fractions of hydrotrope gave rise to an increase in microemulsion elongation; this was significantly less pronounced than those seen in water-in-oil systems [94].

AOT surfactant organogels have also been induced in isooctane through the addition of trace levels of para-substituted phenols (*p*-ethylphenol and *p*-methylphenol, Figure 8), with reports of vast viscosity enhancements up to ~5 orders of magnitude with phenol addition being as low as 0.1 mol dm^{-3} [93,104,108]. Particularly stiff gels were formed when the surfactant concentration and the phenol concentration were close to 1:1 and softening appeared when the surfactant:phenol ratio moved to around ≥3:1 or ≤1:3; the gels 'melted' when trace amounts of water were added to the system. The gel is thought to be formed through a stacked phenolic structure, with AOT adsorbing onto the external surface. FTIR data indicates that there was hydrogen bonding between AOT and the phenolic species [93,104]. Though AOT is not CO_2-philic, significant developments surrounding AOT, like those made by John et al. are included in this review, in hope that they may shed light on potential CO_2 viscosifiers due to the CO_2-philicity of many AOT analogues.
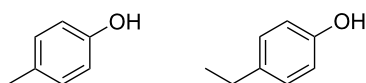
Figure 8: Structures of *para*-methylphenol and *para*-ethylphenol. Para-substituted phenols have been shown to trigger gel formation in AOT w/o systems [94,104] .

Hydrotropic salts have also been shown to increase internal structure through intermolecular π–π interactions. Highly ordered macroscale structures were formed through surfactant self-assembly with the addition of the hydrotropic salt benzylamine hydrochloride (BnNH$_2$·HCl) to a sodium sulfonate surfactant (sodium dodecylbenzene sulfonate, SDBS) [109].

With hydrotrope addition, self-assembly of the surfactant into multilamellar vesicles was observed. Multi-lamellar vesicles consequently transform into ultra-long fibres when [BnNH$_2$·HCl] ≥ [SBDS]. These ultra-long fibres are visible through optical microscopy and can entangle which would lead to an increase in viscosity. The one dimensional fibre growth is attributed to directional forces arising from π–π interactions between the phenyl groups present in both the surfactant and the hydrotrope.

Conclusions – viscosity enhancers in dense CO_2

There is a range of approaches to help develop viscosity in scCO$_2$, most of which surround the principle of building internal structure. Exchange of surfactant counterion has been known to impact viscosity in both water-in-oil and water-in-CO_2 systems; research by Eastoe et al. [101] showed that counterion exchange from Na$^+$ ions to heavier M^{2+} ions lead to the formation of rod-shaped reverse micelles when transition metal analogues were used as opposed to spherical micelles with the use of Na$^+$, Mg^{2+} and Ca^{2+} ions in AOT systems. An increase in reduced viscosity was observed along with the change in morphology. This was then built on through research around counterion exchange in a range of CO_2-philic surfactants, where the same phenomenon was generally observed and accompanied by a significant viscosity increase when M$^+$ ions were exchanged for M^{2+} ions [32,49]. Effective ion size, hydrated ion radius and surfactant critical packing parameters were some of the factors used to explain these phenomena [32,41].

The addition of low molecular weight polymers has shown some promise, with viscosity increases being observed in polymer containing CO_2 in comparison to pure CO_2, which are attributed to strong intermolecular forces arising from π–π interactions of phenyl groups in the polymeric constituent [96-100]. Salt addition to systems is also shown to drive the formation of elongated micelles, leading to increased screening of the surfactant headgroups and reduction in effective headgroup size and therefore favouring a reduced surface curvature. Similarly, the addition of hydrotropic salts and phenols to microemulsions can lead to positive viscosity builds in both water-in-oil and water-in-carbon dioxide systems as observed by Eastoe et al. and John et al. [40,94,104]

## Emerging areas using supercritical CO_2

Bicontinuous and lamellar phases, lamellar liquid crystals and foams: Klostermann et al. has recently reported research around balanced supercritical CO_2 microemulsions; systems where there are equal volumes of carbon dioxide and water [43]. These systems use a polyfluoroether surfactant (poly(ethylene glycol) perfluoroalkyl ether), along with commercially available ethoxylated surfactants Zonyl FSN 100

and Zonyl FSO 100 and NaCl. SANS data and phase behaviour work indicated that these systems follow a bicontinuous structure, with microemulsion domain size increasing with increased pressure [43].

Sagisaka et al. reported the production of water-in-CO$_2$ lamellar structures after a study using fluorinated double-chain anionic surfactants with varied chain lengths. Surfactants with chain length $n = 4$, 6, & 8 were found to form spherical reverse micelles and those with chain length $n = 2$ were found to form lamellar structures (confirmed through SANS). These observations are accounted for through the reduction of CPP with shorter fluorocarbon surfactant tails. The surfactant where $n = 4$ showed the highest solubilizing power out of those tested ($w = 80$); the reason for this is still unclear, although it has been proposed that this is due to the formation of a water-in-CO$_2$ bicontinuous microemulsion (also based of the reduction of CPP value) [48].

Carbon dioxide-in-water (*c*/*w*) foams have been formed with a range of branched non-ionic hydrocarbon surfactants and their viscosities, stabilities and morphologies studied using microscopy and capillary microscopy for potential application in CCS and EOR [110,111]. Surfactant design requirements are more flexible for *c*/*w* foams in comparison than for *w*/*c* microemulsions, due to the lower γ values needed to stabilise *w*/*c* microemulsions [112]. Branching in the surfactant tails was seen to increase foam stability in comparison to linear chain surfactants, through reducing the contact of water and CO$_2$. The greater stability of *c*/*w* films in comparison to air-in-water (*a*/*w*) was attributed to a smaller film size as well as smaller γ and π (surface pressure) values.

Ionic liquid-in-scCO$_2$: Room temperature ionic liquids (ILs) are organic salts composed purely of organic and inorganic ions with a melting point below 100 °C. They have recently received a significant amount of attention, and due to their chemical stability, non-flammability, low toxicity and low volatility are, alongside supercritical CO$_2$, regarded as green solvents [113]. Research has particularly focused around combining ILs with scCO$_2$ to form microemulsions with the hope to combine the advantages of each solvent. Liu et al. have reported the formation of IL-in-CO$_2$ microemulsions using a highly fluorinated surfactant, *N*-ethyl perfluorooctylsulfonamide (compound **49**, Figure 9). Ionic liquids solubilised included 1,1,3,3-tetramethylguanidinium acetate (TMGA, compound **46**, Figure 9), 1,1,3,3-tetramethylguanidinium lactate (TMGL, compound **47**, Figure 9) and 1,1,3,3-tetramethylguanidinium trifluoroacetate (TMGT, compound **48**, Figure 9). Additives such as methyl orange, CoCl$_2$ and HAuCl$_4$ were solubilised within the IL domains, which were shown to be spherical micelles by trans-

Figure 9: Structures of 1,1,3,3-tetramethylguanidinium acetate (**46**), 1,1,3,3-tetramethylguanidinium lactate (**47**), 1,1,3,3-tetramethylguanidinium trifluoroacetate (**48**) and *N*-ethyl perfluorooctylsulfonamide (**49**), as used in IL-in-CO$_2$ microemulsions.
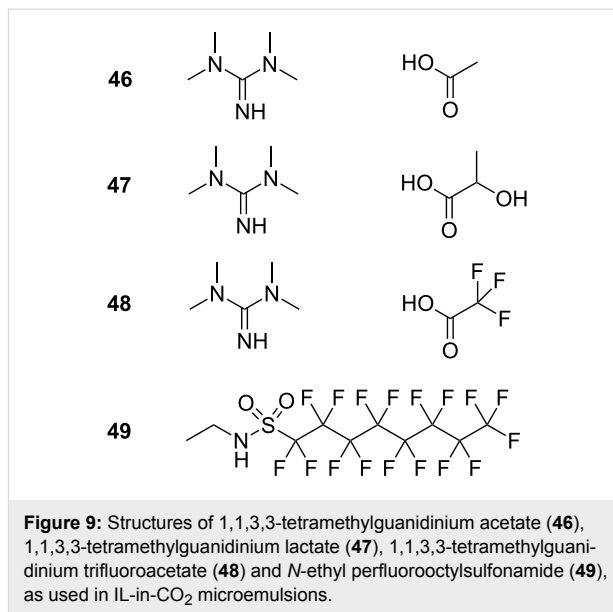
mission electron microscopy (TEM). The group also observed an increase in P_{trans} with increased w value, as expected ($w = 0.1$–0.8) [54].

Chandran et al. have mapped the formation of reverse IL micelles in scCO$_2$ through a computer simulation technique, which also gives evidence for the production of stable IL droplets within a continuous CO$_2$ phase through amphiphilic surfactant addition. This study suggests that microemulsion stability is dependent on ionic liquid anion-surfactant headgroup interactions and that ionic liquid cations play only a minor role [55]. The study was also indicative of the presence of ellipsoidal reverse micelles, which is supported by SANS data previously carried out on a similar IL-in-oil system [56].

Conclusion

Over the last 20 years there have been significant developments surrounding the use of supercritical carbon dioxide, both as an alternative green solvent to volatile organic compounds but also towards the efficiency of carbon dioxide handling with a view to enhance carbon capture and sequestration techniques, as well as enhanced oil recovery. This has come in several forms, through identifying factors that lead to an enhancement of CO$_2$-philicity in additives as well as the development of CO$_2$ viscosifiers. A combination of these breakthroughs may lead to both commercially viable and practical surfactants and additives that will effectively thicken CO$_2$. A myriad of structures has been observed in water-in-CO$_2$ systems, including a range of reverse micellar shapes to bicontinuous phases and lamellar structures. The virtuous properties of scCO$_2$ as a solvent could be enhanced further through the use of IL-in-CO$_2$ systems, thus combining with the positive properties of ILs have as solvents.

Though noteworthy breakthroughs have been made around this area, more work needs to be undertaken to overcome the uncooperative nature of CO_2 to fully utilize it as a solvent and processing medium.

Acknowledgements

References

1. Anastas, P. T.; Warner, J. C. *Green Chemistry: Theory and Practice;* Oxford University Press: New York, 1998.
2. Basics of Green Chemistry - United States Environmental Protection Agency.
3. Eckert, C. A.; Knutson, B. L.; Debenedetti, P. G. *Nature* **1996,** *383,* 313–318. doi:10.1038/383313a0
4. Noyori, R. *Chem. Commun.* **2005,** 1807–1811. doi:10.1039/b502713f
5. Wells, S. L.; DeSimone, J. *Angew. Chem., Int. Ed.* **2001,** *40,* 518–527. doi:10.1002/1521-3773(20010202)40:3<518::AID-ANIE518>3.0.CO;2-4
6. McHugh, M. H.; Krukonis, V. J. *Supercritical Fluid Extractions: Principles and Practice,* 2nd ed.; Butterworth-Heinerman: Boston, 1994.
7. Laintz, K.; Wai, C. M.; Yonker, C. R.; Smith, R. D. *J. Supercrit. Fluids* **1991,** *4,* 194–198. doi:10.1016/0896-8446(91)90008-T
8. DeSimone, J. M.; Guan, Z.; Elsbernd, C. S. *Science* **1992,** *257,* 945–947. doi:10.1126/science.257.5072.945
9. DeSimone, J. M. *Science* **2002,** *297,* 799–803. doi:10.1126/science.1069622
10. Poliakoff, M.; Fitzpatrick, J. M.; Farren, T. R.; Anastas, P. T. *Science* **2002,** *297,* 807–810. doi:10.1126/science.297.5582.807
11. Rindfleisch, F.; DiNoia, T. P.; McHugh, M. A. *J. Phys. Chem.* **1996,** *100,* 15581–15587. doi:10.1021/jp9615823
12. Beyer, C.; Oellrich, L. R.; McHugh, M. A. *Chem. Eng. Technol.* **2000,** *23,* 592–595. doi:10.1002/1521-4125(200007)23:7<592::AID-CEAT592>3.0.CO;2-H
13. Sarbu, T.; Styranec, T.; Beckman, E. J. *Nature* **2000,** *405,* 165–168. doi:10.1038/35012040
14. Subramaniam, B.; Rajewski, R.; Snavely, K. *J. Pharm. Sci.* **1997,** *86,* 885–890. doi:10.1021/js9700661
15. Oakes, R. S.; Clifford, A. A.; Rayner, C. M. *J. Chem. Soc., Perkin Trans. 1* **2001,** 917–941. doi:10.1039/b101219n
16. Aymonier, C.; Loppinet-Serani, A.; Reverón, H.; Garrabos, Y.; Cansell, F. *J. Supercrit. Fluids* **2006,** *38,* 242–251. doi:10.1016/j.supflu.2006.03.019
17. Campbell, M. L.; Apodaca, D. L.; Yates, M. Z.; McCleskey, T. M.; Birnbaum, E. R. *Langmuir* **2001,** *17,* 5458–5463. doi:10.1021/la0104166
18. Ohde, M.; Ohde, H.; Wai, C. M. *Chem. Commun.* **2002,** 2388–2389. doi:10.1039/b205993m
19. Ohde, H.; Hunt, F.; Wai, C. M. *Chem. Mater.* **2001,** *13,* 4130–4135. doi:10.1021/cm010030g
20. Ohde, H.; Rodriguez, J. M.; Ye, X.-R.; Wai, C. M. *Chem. Commun.* **2000,** 2353–2354. doi:10.1039/b005924m
21. Reverchon, E.; Adami, R. *J. Supercrit. Fluids* **2006,** *37,* 1–22. doi:10.1016/j.supflu.2005.08.003
22. Yeo, S.-D.; Kiran, E. *J. Supercrit. Fluids* **2005,** *34,* 287–308. doi:10.1016/j.supflu.2004.10.006
23. Du, L.; Kelly, J. Y.; Roberts, G. W.; DeSimone, J. M. *J. Supercrit. Fluids* **2009,** *47,* 447–457. doi:10.1016/j.supflu.2008.11.011
24. Wood, C. D.; Cooper, A. I.; DeSimone, J. M. *Curr. Opin. Solid State Mater. Sci.* **2004,** *8,* 325–331. doi:10.1016/j.cossms.2005.02.001
25. Cao, L.; Chen, L.; Chen, X.; Zuo, L.; Li, Z. *Polymer* **2006,** *47,* 4588–4595. doi:10.1016/j.polymer.2006.04.039
26. Hoefling, T. A.; Enick, R. M.; Beckman, E. J. *J. Phys. Chem.* **1991,** *95,* 7127–7129. doi:10.1021/j100172a006
27. Harrison, K.; Goveas, J.; Johnston, K. P.; O'Rear, E. A., III. *Langmuir* **1994,** *10,* 3536–3541. doi:10.1021/la00022a028
28. Orr, F. M., Jr.; Taber, J. J. *Science* **1984,** *224,* 563–569. doi:10.1126/science.224.4649.563
29. Plasynski, S. I.; Litynski, J. T.; McIlvried, H. G.; Srivastava, R. D. *Crit. Rev. Plant Sci.* **2009,** *28,* 123–138. doi:10.1080/07352680902776440
30. Cummings, S.; Enick, R.; Rogers, S.; Heenan, R.; Eastoe, J. *Biochimie* **2012,** *94,* 94–100. doi:10.1016/j.biochi.2011.06.021
31. Cummings, S.; Trickett, K.; Enick, R.; Eastoe, J. *Phys. Chem. Chem. Phys.* **2011,** *13,* 1276–1289. doi:10.1039/c003856c
32. Cummings, S.; Xing, D.; Enick, R.; Rogers, S.; Heenan, R.; Grillo, I.; Eastoe, J. *Soft Matter* **2012,** *8,* 7044–7055. doi:10.1039/c2sm25735a
33. DeSimone, J. M.; Keiper, J. S. *Curr. Opin. Solid State Mater. Sci.* **2001,** *5,* 333–341. doi:10.1016/S1359-0286(00)00041-3
34. Dobbs, J. M.; Wong, J. M.; Johnston, K. P. *J. Chem. Eng. Data* **1986,** *31,* 303–308. doi:10.1021/je00045a014
35. Eastoe, J.; Downer, A.; Paul, A.; Steytler, D. C.; Rumsey, E.; Penfold, J.; Heenan, R. K. *Phys. Chem. Chem. Phys.* **2000,** *2,* 5235–5242. doi:10.1039/b005858k
36. Eastoe, J.; Gold, S. *Phys. Chem. Chem. Phys.* **2005,** *7,* 1352–1362. doi:10.1039/b418985j
37. Eastoe, J.; Gold, S.; Rogers, S.; Wyatt, P.; Steytler, D. C.; Gurgel, A.; Heenan, R. K.; Fan, X.; Beckman, E. J.; Enick, R. M. *Angew. Chem., Int. Ed.* **2006,** *45,* 3675–3677. doi:10.1002/anie.200600397
38. Eastoe, J.; Gold, S.; Steytler, D. C. *Langmuir* **2006,** *22,* 9832–9842. doi:10.1021/la060764d
39. Gold, S.; Eastoe, J.; Grilli, R.; Steytler, D. C. *Colloid Polym. Sci.* **2006,** *284,* 1333–1337. doi:10.1007/s00396-006-1519-2
40. Hatzopoulos, M. H.; Eastoe, J.; Dowding, P. J.; Grillo, I. *J. Colloid Interface Sci.* **2013,** *392,* 304–310. doi:10.1016/j.jcis.2012.09.078
41. James, C.; Eastoe, J. *Curr. Opin. Colloid Interface Sci.* **2013,** *18,* 40–46. doi:10.1016/j.cocis.2012.12.004
42. Hollamby, M. J.; Trickett, K.; Mohamed, A.; Cummings, S.; Tabor, R. F.; Myakonkaya, O.; Gold, S.; Rogers, S.; Heenan, R. K.; Eastoe, J. *Angew. Chem., Int. Ed.* **2009,** *48,* 4993–4995. doi:10.1002/anie.200901543
43. Klostermann, M.; Strey, R.; Sottmann, T.; Schweins, R.; Lindner, P.; Holderer, O.; Monkenbusch, M.; Richter, D. *Soft Matter* **2012,** *8,* 797–807. doi:10.1039/c1sm06533e
44. Li, Y.; Park, E. J.; Lim, K. T.; Johnston, K. P.; Green, P. F. *J. Polym. Sci., Part B: Polym. Phys.* **2007,** *45,* 1313–1324. doi:10.1002/polb.21159
45. Liu, Z.-T.; Erkey, C. *Langmuir* **2001,** *17,* 274–277. doi:10.1021/la000947e
46. Nagarajan, R. *Langmuir* **1993,** *9,* 369–375. doi:10.1021/la00026a002

47. da Rocha, S. R. P.; Dickson, J.; Cho, D.; Rossky, P. J.; Johnston, K. P. *Langmuir* **2003,** *19,* 3114–3120. doi:10.1021/la026608y

48. Sagisaka, M.; Iwama, S.; Ono, S.; Yoshizawa, A.; Mohamed, A.; Cummings, S.; Yan, C.; James, C.; Rogers, S. E.; Heenan, R. K.; Eastoe, J. *Langmuir* **2013,** *29,* 7618–7628. doi:10.1021/la400376g

49. Trickett, K.; Xing, D.; Enick, R.; Eastoe, J.; Hollamby, M. J.; Mutch, K. J.; Rogers, S. E.; Heenan, R. K.; Steytler, D. C. *Langmuir* **2010,** *26,* 83–88. doi:10.1021/la902128g

50. Trickett, K.; Eastoe, J. *Adv. Colloid Interface Sci.* **2008,** *144,* 66–74. doi:10.1016/j.cis.2008.08.009

51. Zhang, J.; Han, B.; Zhao, Y.; Li, J.; Yang, G. *Chem.–Eur. J.* **2011,** *17,* 4266–4272. doi:10.1002/chem.201002153

52. Williamson, K. *Macroscale and Microscale Organic Experiments,* 2nd ed.; Lexington: Massachusetts, 1994.

53. Consan, K. A.; Smith, R. D. *J. Supercrit. Fluids* **1990,** *3,* 51–65. doi:10.1016/0896-8446(90)90008-A

54. Liu, J.; Cheng, S.; Zhang, J.; Feng, X.; Fu, X.; Han, B. *Angew. Chem., Int. Ed.* **2007,** *46,* 3313–3315. doi:10.1002/anie.200605019

55. Chandran, A.; Prakash, K.; Senapati, S. *J. Am. Chem. Soc.* **2010,** *132,* 12511–12516. doi:10.1021/ja1055005

56. Eastoe, J.; Gold, S.; Rogers, S. E.; Paul, A.; Welton, T.; Heenan, R. K.; Grillo, I. *J. Am. Chem. Soc.* **2005,** *127,* 7302–7303. doi:10.1021/ja051155f

57. Kissa, E. *Flourinated Surfactants;* Marcell Dekker Inc.: New York, 1994; Vol. 50.

58. Guo, W.; Li, Z.; Fung, B. M.; O'Rear, E. A.; Harwell, J. H. *J. Phys. Chem.* **1992,** *96,* 6738–6742. doi:10.1021/j100195a038

59. Mohamed, A.; Sagisaka, M.; Hollamby, M.; Rogers, S. E.; Heenan, R. K.; Dyer, R.; Eastoe, J. *Langmuir* **2012,** *28,* 6299–6306. doi:10.1021/la3005322

60. Mohamed, A.; Trickett, K.; Chin, S. Y.; Cummings, S.; Sagisaka, M.; Hudson, L.; Nave, S.; Dyer, R.; Rogers, S. E.; Heenan, R. K.; Eastoe, J. *Langmuir* **2010,** *26,* 13861–13866. doi:10.1021/la102303q

61. Sagisaka, M.; Kudo, K.; Nagoya, S.; Yoshizawa, A. *J. Oleo Sci.* **2013,** *62,* 481–488. doi:10.5650/jos.62.481

62. Raveendran, P.; Wallen, S. L. *J. Am. Chem. Soc.* **2002,** *124,* 7274–7275. doi:10.1021/ja025508b

63. Eastoe, J.; Yan, C.; Mohamed, A. *Curr. Opin. Colloid Interface Sci.* **2012,** *17,* 266–273. doi:10.1016/j.cocis.2012.06.006

64. Olsen, G. W.; Church, T. R.; Miller, J. P.; Burris, J. M.; Hanson, K. J.; Lundberg, J. K.; Armitage, J. B.; Herron, R. M.; Medhdizadehkashi, Z.; Nobiletti, J. B.; O'Neill, E. M.; Mandel, J. H.; Zobel, L. R. *Environ. Health Perspect.* **2013,** *111,* 1892–1901.

65. Falandysz, J.; Taniyasu, S.; Gulkowska, A.; Yamashita, N.; Schulte-Oehlmann, U. *Environ. Sci. Technol.* **2006,** *40,* 748–751. doi:10.1021/es051799n

66. Houde, M.; Bujas, T. A. D.; Small, J.; Wells, R. S.; Fair, P. A.; Bossart, G. D.; Solomon, K. R.; Muir, D. C. G. *Environ. Sci. Technol.* **2006,** *40,* 4138–4144. doi:10.1021/es060233b

67. Butenhoff, J. L.; Costa, G.; Elcombe, C.; Farrar, D.; Hansen, K.; Iwai, H.; Jung, R.; Kennedy, G., Jr.; Lieder, P.; Olsen, G.; Thomford, P. *Toxicol. Sci.* **2002,** *69,* 244–257. doi:10.1093/toxsci/69.1.244

68. Guo, W.; Fung, B. M.; O'Rear, E. A. *J. Phys. Chem.* **1992,** *96,* 10068–10074. doi:10.1021/j100203a088

69. Eastoe, J.; Bayazit, Z.; Martel, S.; Steytler, D. C.; Heenan, R. K. *Langmuir* **1996,** *12,* 1423–1424. doi:10.1021/la950546c

70. Sagisaka, M.; Yoda, S.; Takebayashi, Y.; Otake, K.; Kitiyanan, B.; Kondo, Y.; Yoshino, N.; Takebayashi, K.; Sakai, H.; Abe, M. *Langmuir* **2003,** *19,* 220–225. doi:10.1021/la020340t

71. Kazarian, S. G.; Vincent, M. F.; Bright, F. V.; Liotta, C. L.; Eckert, C. A. *J. Am. Chem. Soc.* **1996,** *118,* 1729–1736. doi:10.1021/ja950416q

72. Mohamed, A.; Sagisaka, M.; Guittard, F.; Cummings, S.; Paul, A.; Rogers, S. E.; Heenan, R. K.; Dyer, R.; Eastoe, J. *Langmuir* **2011,** *27,* 10562–10569. doi:10.1021/la2021885

73. Pitt, A. R.; Morley, S. D.; Burbridge, N. J.; Quickenden, E. L. *Colloids Surf., A* **1996,** *114,* 321–335. doi:10.1016/0927-7757(96)03593-5

74. Bell, P. W.; Anand, M.; Fan, X.; Enick, R. M.; Roberts, C. B. *Langmuir* **2005,** *21,* 11608–11613. doi:10.1021/la052392z

75. Sagisaka, M.; Koike, D.; Mashimo, Y.; Yoda, S.; Takebayashi, Y.; Furuya, T.; Yoshizawa, A.; Sakai, H.; Abe, M.; Otake, K. *Langmuir* **2008,** *24,* 10116–10122. doi:10.1021/la8014145

76. Ryoo, W.; Webber, S. E.; Johnston, K. P. *Ind. Eng. Chem. Res.* **2003,** *42,* 6348–6358. doi:10.1021/ie0300427

77. Sagisaka, M.; Fujii, T.; Koike, D.; Yoda, S.; Takebayashi, Y.; Furuya, T.; Yoshizawa, A.; Sakai, H.; Abe, M.; Otake, K. *Langmuir* **2007,** *23,* 2369–2375. doi:10.1021/la062789i

78. Stone, M. T.; Smith, P. G., Jr.; da Rocha, S. R. P.; Rossky, P. J.; Johnston, K. P. *J. Phys. Chem. B* **2004,** *108,* 1962–1966. doi:10.1021/jp036224w

79. Francis, A. W. *J. Phys. Chem.* **1954,** *58,* 1099–1114. doi:10.1021/j150522a014

80. Reilly, J. T.; Bokis, C. P.; Donohue, M. D. *Int. J. Thermophys.* **1995,** *16,* 599–610. doi:10.1007/BF01438845

81. Jones, M.-C.; Leroux, J.-C. *Eur. J. Pharm. Biopharm.* **1999,** *48,* 101–111. doi:10.1016/S0939-6411(99)00039-9

82. Gaucher, G.; Dufresne, M.-H.; Sant, V. P.; Kang, N.; Maysinger, D.; Leroux, J.-C. *J. Controlled Release* **2005,** *109,* 169–188. doi:10.1016/j.jconrel.2005.09.034

83. Enick, R.; Beckman, E.; Yazdi, A.; Krukonis, V.; Schonemann, H.; Howell, J. *J. Supercrit. Fluids* **1998,** *13,* 121–126. doi:10.1016/S0896-8446(98)00043-6

84. Wang, Y.; Hong, L.; Tapriyal, D.; Kim, I. C.; Paik, I.-H.; Crosthwaite, J. M.; Hamilton, A. D.; Thies, M. C.; Beckman, E. J.; Enick, R. M.; Johnson, J. K. *J. Phys. Chem. B* **2009,** *113,* 14971–14980. doi:10.1021/jp9073812

85. Kilic, S.; Michalik, S.; Wang, Y.; Johnson, J. K.; Enick, R. M.; Beckman, E. J. *Ind. Eng. Chem. Res.* **2003,** *42,* 6415–6424. doi:10.1021/ie030288b

86. Xiong, Y.; Kiran, E. *Polymer* **1995,** *36,* 4817–4826. doi:10.1016/0032-3861(95)99298-9

87. Hong, L.; Fisher, M.; Enick, R.; Beckman, E. *Green Chem.* **2008,** *10,* 756–761. doi:10.1039/b800812d

88. Potluri, V. K.; Hamilton, A. D.; Karanikas, C. F.; Bane, S. E.; Xu, J.; Beckman, E. J.; Enick, R. M. *Fluid Phase Equilib.* **2003,** *211,* 211–217. doi:10.1016/S0378-3812(03)00206-1

89. Tapriyal, D.; Wang, Y.; Enick, R. M.; Johnson, J. K.; Crosthwaite, J.; Thies, M. C.; Paik, I. H.; Hamilton, A. D. *J. Supercrit. Fluids* **2008,** *46,* 252–257. doi:10.1016/j.supflu.2008.05.001

90. Loeker, F.; Marr, P. C.; Howdle, S. M. *Colloids Surf., A* **2003,** *214,* 143–150. doi:10.1016/S0927-7757(02)00407-7

91. Kilic, S.; Wang, Y.; Johnson, J. K.; Beckman, E. J.; Enick, R. M. *Polymer* **2009,** *50,* 2436–2444. doi:10.1016/j.polymer.2009.03.012

92. Hong, L. *Identification, Design an Synthesis of Oxygenated Hydrocarbon based CO-soluble Polymers for Chemical and Petroleum Engineering Applications;* University of Pittsburg: Pittsburg, 2006.

93. Tata, M.; John, V. T.; Waguespack, Y. Y.; McPherson, G. L. *J. Am. Chem. Soc.* **1994,** *116,* 9464–9470. doi:10.1021/ja00100a008

94. James, C.; Hatzopoulos, M. H.; Yan, C.; Smith, G. N.; Alexander, S.; Rogers, S. E.; Eastoe, J. *Langmuir* **2014,** *30,* 96–102. doi:10.1021/la404144a

95. Acharya, D. P.; Kunieda, H. *Adv. Colloid Interface Sci.* **2006,** *123–126,* 401–413. doi:10.1016/j.cis.2006.05.024

96. Bae, J.; Irani, C. *Soc. Pet. Eng. Adv. Technol. Ser.* **1993,** *1,* 166–171. doi:10.2118/20467-PA

97. Heller, J. P.; Dandge, D. K.; Card, R. J.; Donaruma, L. G. *Soc. Pet. Eng. J.* **1985,** *25,* 679–686. doi:10.2118/11789-PA

98. Zhang, S.; She, Y.; Gu, Y. *J. Chem. Eng. Data* **2011,** *56,* 1069–1079. doi:10.1021/je1010449

99. Gu, Y.; Zhang, S.; She, Y. *J. Polym. Res.* **2013,** *20,* 61. doi:10.1007/s10965-012-0061-9

100. Huang, Z.; Shi, C.; Xu, J.; Kilic, S.; Enick, R. M.; Beckman, E. J. *Macromolecules* **2000,** *33,* 5437–5442. doi:10.1021/ma992043+

101. Eastoe, J.; Fragneto, G.; Robinson, B. H.; Towey, T. F.; Heenan, R. K.; Leng, F. J. *J. Chem. Soc., Faraday Trans.* **1992,** *88,* 461–471. doi:10.1039/ft9928800461

102. Trickett, K.; Xing, D.; Eastoe, J.; Enick, R. M.; Mohamed, A.; Hollamby, M. J.; Cummings, S.; Rogers, S. E.; Heenan, R. K. *Langmuir* **2010,** *26,* 4732–4737. doi:10.1021/la903690c

103. Missel, P. J.; Mazer, N. A.; Carey, M. C.; Benedek, G. B. *J. Phys. Chem.* **1989,** *93,* 8354–8366. doi:10.1021/j100363a014

104. Xu, X.; Ayyagari, M.; Tata, M.; John, V. T.; McPherson, G. L. *J. Phys. Chem.* **1993,** *97,* 11350–11353. doi:10.1021/j100145a038

105. Hatzopoulos, M. H.; Eastoe, J.; Dowding, P. J.; Grillo, I.; Demé, B.; Rogers, S. E.; Heenan, R. K.; Dyer, R. *Langmuir* **2012,** *28,* 9332–9340. doi:10.1021/la301222m

106. Hatzopoulos, M. H.; Eastoe, J.; Dowding, P. J.; Rogers, S. E.; Heenan, R. K.; Dyer, R. *Langmuir* **2011,** *27,* 12346–12353. doi:10.1021/la2025846

107. Eastoe, J.; Hatzopoulos, M. H.; Dowding, P. J. *Soft Matter* **2011,** *7,* 5917–5925. doi:10.1039/c1sm05138e

108. Tata, M.; John, V. T.; Waguespack, Y. Y.; McPherson, G. L. *J. Phys. Chem.* **1994,** *98,* 3809–3817. doi:10.1021/j100065a042

109. Lin, Y.; Qiao, Y.; Cheng, X.; Yan, Y.; Li, Z.; Huang, J. *J. Colloid Interface Sci.* **2012,** *369,* 238–244. doi:10.1016/j.jcis.2011.11.067

110. Adkins, S. S.; Chen, X.; Chan, I.; Torino, E.; Nguyen, Q. P.; Sanders, A. W.; Johnston, K. P. *Langmuir* **2010,** *26,* 5335–5348. doi:10.1021/la903663v

111. Johnston, K. P.; da Rocha, S. R. P. *J. Supercrit. Fluids* **2009,** *47,* 523–530. doi:10.1016/j.supflu.2008.10.024

112. Stone, M. T.; da Rocha, S. R. P.; Rossky, P. J.; Johnston, K. P. *J. Phys. Chem. B* **2003,** *107,* 10185–10192. doi:10.1021/jp035422k

113. Rogers, R. D.; Seddon, K. R. *Science* **2003,** *302,* 792–793. doi:10.1126/science.1090313

Efficient CO$_2$ capture by tertiary amine-functionalized ionic liquids through Li$^+$-stabilized zwitterionic adduct formation

Zhen-Zhen Yang and Liang-Nian He[*]

Abstract

Highly efficient CO$_2$ absorption was realized through formation of zwitterionic adducts, combining synthetic strategies to ionic liquids (ILs) and coordination. The essence of our strategy is to make use of multidentate cation coordination between Li$^+$ and an organic base. Also PEG-functionalized organic bases were employed to enhance the CO$_2$-philicity. The ILs were reacted with CO$_2$ to form the zwitterionic adduct. Coordination effects between various lithium salts and neutral ligands, as well as the CO$_2$ capacity of the chelated ILs obtained were investigated. For example, the CO$_2$ capacity of PEG$_{150}$MeBu$_2$N increased steadily from 0.10 to 0.66 (mol CO$_2$ absorbed per mol of base) through the formation of zwitterionic adducts being stabilized by Li$^+$.

Introduction

Carbon capture and sequestration (CCS) from flue gas formed by combustion of fossil fuel is a critical part of efforts directed towards the stabilization of atmospheric greenhouse gas levels [1]. In recent years, there has been intense research worldwide aimed at the development of various processes and technologies for efficient CO$_2$ capture. These efforts include the development of liquid and solid absorbents and membranes [2-7].

Ionic liquids (ILs), which have attractive properties such as negligible vapor pressure, a wide liquid temperature ranges, good thermal stability, high ionic conductivity, and versatile solvation properties [8-11], can be designed for task-specific applications through the smart choice of the respective cations and/or anions. Application fields include green solvents for synthesis [9,12-15], efficient catalysts in organic synthesis [2,16,17], media for advanced separation [18,19], novel electrolytes for energy applications [20,21], and efficient absorbents for gas separation [2,22-24]. In particular, amino-functionalized IL [APBIm][BF$_4$] (1-aminopropyl-3-butylimidazolium tetrafluoroborate) and ILs being composed of amino acid (AA) anions and phosphonium or ammonium cations were developed for efficient CO$_2$ chemisorption [23,25-30]. Binary absorbents derived from superbases together with various non-volatile

weak proton donors such as hydroxy-functionalized ILs, imidazolium ILs, fluorinated alcohol, imidazole and phenol, were also found to be efficient liquid absorbents allowing for reversible CO_2 chemisorption [31-35]. In general, two absorbent molecules are involved to react with one CO_2 molecule generating ammonium carbamate (Scheme 1a) or ammonium alkyl formate (Scheme 1b). Hence, increasing the 1:2 (CO_2:absorbent molecule) stoichiometry for the CO_2 capacity to 1:1 is an essential prerequisite for a breakthrough in absorption techniques [23]. In this respect, task-specifically designed absorbents have been successfully synthesized from AAs and applied for 1:1 CO_2 capture through a carbamic acid formation pathway (Scheme 1a, step 1). Notably, equimolar CO_2 absorption was obtained using task-specific ionic liquids (TSILs) with the phosphonium cation containing long alkyl chains and anions derived from AAs (prolinate and methioninate) [36], or AA salts with bulky N-substituents in polyethylene glycol (PEG) solution [37]. However, procedures for the preparation of ILs usually include complicated purification procedures or the use of volatile organic solvents (e.g., toluene, acetonitrile). Recently, Wang et al. developed novel alkanolamine-based ILs through multi-dentate cation coordination between alkanolamine and Li^+ for reversible CO_2 capture, by simple mixing of equimolar amounts of alkanolamines with $LiNTf_2$ [38]. The strong complexation of alkali metal cations by crown ethers could be used to achieve equimolar CO_2 absorption in systems containing crown ethers and easily available alkali metal salts of amino acids, resulting in the respective carbamates (onium salts) [39].

As previously reported, strong amidine and guanidine bases such as 1,5,7-triazabicyclo[4.4.0]dec-5-ene (TBD) can form the base-CO_2 zwitterionic adduct in a 1:1 manner under strictly anhydrous conditions (Scheme 1c) [40,41]. Herein, we present such a method combining the formation of ILs and coordination to achieve equimolar CO_2 capture through zwitterionic adduct formation. The essence of our strategy is to make use of the multisite coordination interaction between Li^+ and organic bases or PEG-functionalized organic bases. The readily prepared ILs were reacted then with CO_2 to form intramolecular zwitterionic adducts.

Results and Discussion

Taking $PEG_{150}MeTMG$ as a neutral ligand (Table 1), coordination effects of various lithium salts were investigated (Table S1, Supporting Information File 1). Only $LiSO_3CF_3$ and $LiNTf_2$ formed complexes with $PEG_{150}MeTMG$ through multisite coordination. Subsequently, different neutral ligands with alkyl chains or PEG chain were selected to evaluate the effect of chelating with $LiNTf_2$ on the physicochemical properties of the resulting ILs as well as the CO_2 capacities (Table 1).

Typical optimized structures of cations derived from chelation between neutral ligands and Li^+ are shown in Figure 1. The geometry optimizations were carried out by performing DFT calculations. Four O atoms in $PEG_{150}Me$ chelate with Li^+ in a quasi-crown ether manner. For neutral ligands with PEG chain ($PEG_{150}MeIm$, $PEG_{150}MeNH_2$, $PEG_{150}MeTMG$ and $PEG_{150}MeBu_2N$), all the O and N atoms coordinate with Li^+ in a quasi-aza-crown ether fashion. OctIm, OctTMG, TMG, DBU and DBN generate complexes whereby Li^+ is bound only to N atoms. In contrast, the coordination ability of the N atom in $OctBu_2N$ is not strong enough to form a homogeneous chelated IL with $LiNTf_2$.
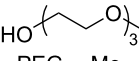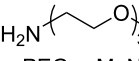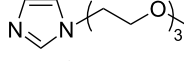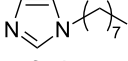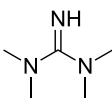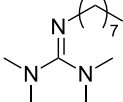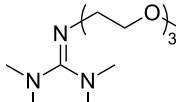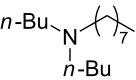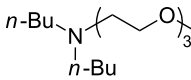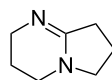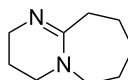
Calculation of the energy of the gas phase reaction between neutral ligands and Li^+ gave a value for the enthalpy change in the range of −41.59 to −106.56 kcal mol^{-1} (Table 1, entries 1–11), indicating that the formation of chelated ILs is feasible.

In addition, PEG-functionalization of the organic base enhanced the complexation ability. For example, ΔH_f decreased from −56.49 kal mol^{-1} (OctIm) to −91.17 kcal mol^{-1} ($PEG_{150}MeIm$) for imidazole (Table 1, entry 2 vs 3), from −47.79 kcal mol^{-1} (OctTMG) to −106.56 kcal mol^{-1} ($PEG_{150}MeTMG$) for guanidine (Table 1, entry 6 vs 7), and from no complexation ($OctBu_2N$) to −96.26 kal mol^{-1} ($PEG_{150}MeBu_2N$) for tertiary amine (Table 1, entry 8 vs 9).
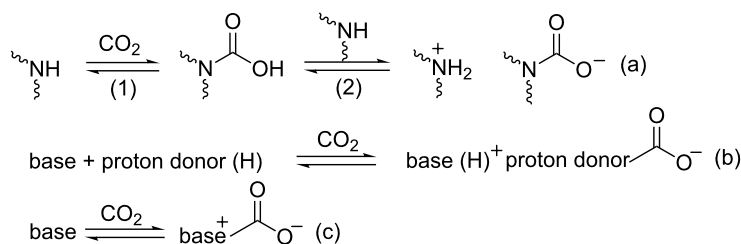
Scheme 1: Reactions of CO_2 with amino-group containing absorbents (a), base/proton donor binary system (b) or strong organic base (c).

Table 1: Stability (ΔH_f) of the cations derived from coordination of Li^+ in $LiNTf_2$ with various neutral ligands and CO_2 capacity of the derived ionic liquids[a].

PEG$_{150}$Me PEG$_{150}$MeNH$_2$ PEG$_{150}$MeIm OctIm

TMG OctTMG PEG$_{150}$MeTMG

OctBu$_2$N PEG$_{150}$MeBu$_2$N DBN DBU

Entry	Ionic liquid	ΔH_f/kcal mol^{-1} [b]	CO_2 capacity[c]
1	[PEG$_{150}$MeLi][NTf$_2$]	−100.94	0.09 (0.9%)
2	[OctImLi][NTf$_2$]	−56.49	0.11 (1.0%)
3	[PEG$_{150}$MeImLi][NTf$_2$]	−91.17	0.16 (1.4%)
4	[PEG$_{150}$MeNH$_2$Li][NTf$_2$]	−89.39	0.45 (4.4%)
5	[TMGLi][NTf$_2$]	−41.59	0.65 (7.1%)
6	[OctTMGLi][NTf$_2$]	−47.79	0.80 (6.8%)
7	[PEG$_{150}$MeTMGLi][NTf$_2$]	−106.56	0.89 (7.1%)
8	OctBu$_2$N/LiNTf$_2$	–	–
9	PEG$_{150}$MeBu$_2$N	–	0.10 (1.6%)
10	[PEG$_{150}$MeBu$_2$NLi][NTf$_2$]	−96.26	0.66 (5.2%)
11	[PEG$_{150}$MeBu$_2$NLi][SO$_3$CF$_3$]	−96.26	0.61 (6.2%)
12	[DBULi][NTf$_2$]	−60.22	0.50 (5.0%)
13	[DBNLi][NTf$_2$]	−60.50	0.75 (8.0%)

[a]Ionic liquids were prepared by mixing of a neutral ligand with $LiNTf_2$ in 1:1 molar ratio. CO_2 absorption was carried out at 25 °C and absorption equilibrium was reached within 20 min. [b]Energy of the gas phase reaction between the neutral ligand and Li^+, was calculated with DFT, using the B3PW91 functional with the 6-311++G (d,p) basis set as implemented in the Gaussian 09 program package. [c]Mol of CO_2 captured per mol of ionic liquid. Results in bracket were grams of CO_2 absorbed per gram of absorbent.

The structures of the chelated ILs were confirmed by thermogravimetric analysis (TGA), NMR (see Supporting Information File 1, Figure S2), in situ FTIR under CO_2 pressure and mass spectrometry. The thermal stability of the chelated ILs was strongly increased compared to the corresponding neutral ligands. The decomposition temperature increased by 90 °C and 60 °C for PEG$_{150}$MeTMG and PEG$_{150}$MeBu$_2$N, respectively, after coordination with $LiNTf_2$ (Figure 2a).

In the ^{1}H NMR spectrum, the proton signals of the four methyl groups in guanidine of PEG$_{150}$MeTMG shifted from 2.63–2.72 ppm to 2.96 ppm after reacting with equimolar amounts of $LiNTf_2$ (Figure 2b). The corresponding anion $CF_3SO_3^-$, the twelve protons moving only from 2.63–2.72 ppm to 2.71–2.75 ppm, indicate that there is only little influence of the anion on the nature of the coordinative bond. In the case of tertiary amines (e.g., PEG$_{150}$MeBu$_2$N), all the protons shifted downfield after forming the chelated IL with $LiNTf_2$. Changing

the anion to $CF_3SO_3^-$ had negligible influence on the coordination ability. All the neutral ligands shown in Table 1 gave a downfield shift in the ^{1}H NMR spectrum after chelating with Li^+, in accordance with the electron density decreasing through coordination. Furthermore, the formation of chelated ILs was also verified by ESI-MS (m/z = 268.27 for [PEG$_{150}$MeTMGLi]$^+$ and m/z = 282.32 for [PEG$_{150}$MeBu$_2$NLi]$^+$) (Figure S3, see Supporting Information File 1). In the in situ FTIR spectrum, the C=N absorption band of the neutral ligand PEG$_{150}$MeTMG was shifted from 1616 cm^{-1} to 1592 cm^{-1} after reacting with equimolar amounts of $LiNTf_2$ as depicted in Figure 3a.

The effect of various chelated ILs on CO_2 absorption was subsequently examined using $LiNTf_2$ as coordinating reagent. The CO_2 absorption capacity, defined as mol of CO_2 captured per mol of IL, was estimated from the weight increase of the reaction mixture. As shown in Table 1, ILs of weak basicity,
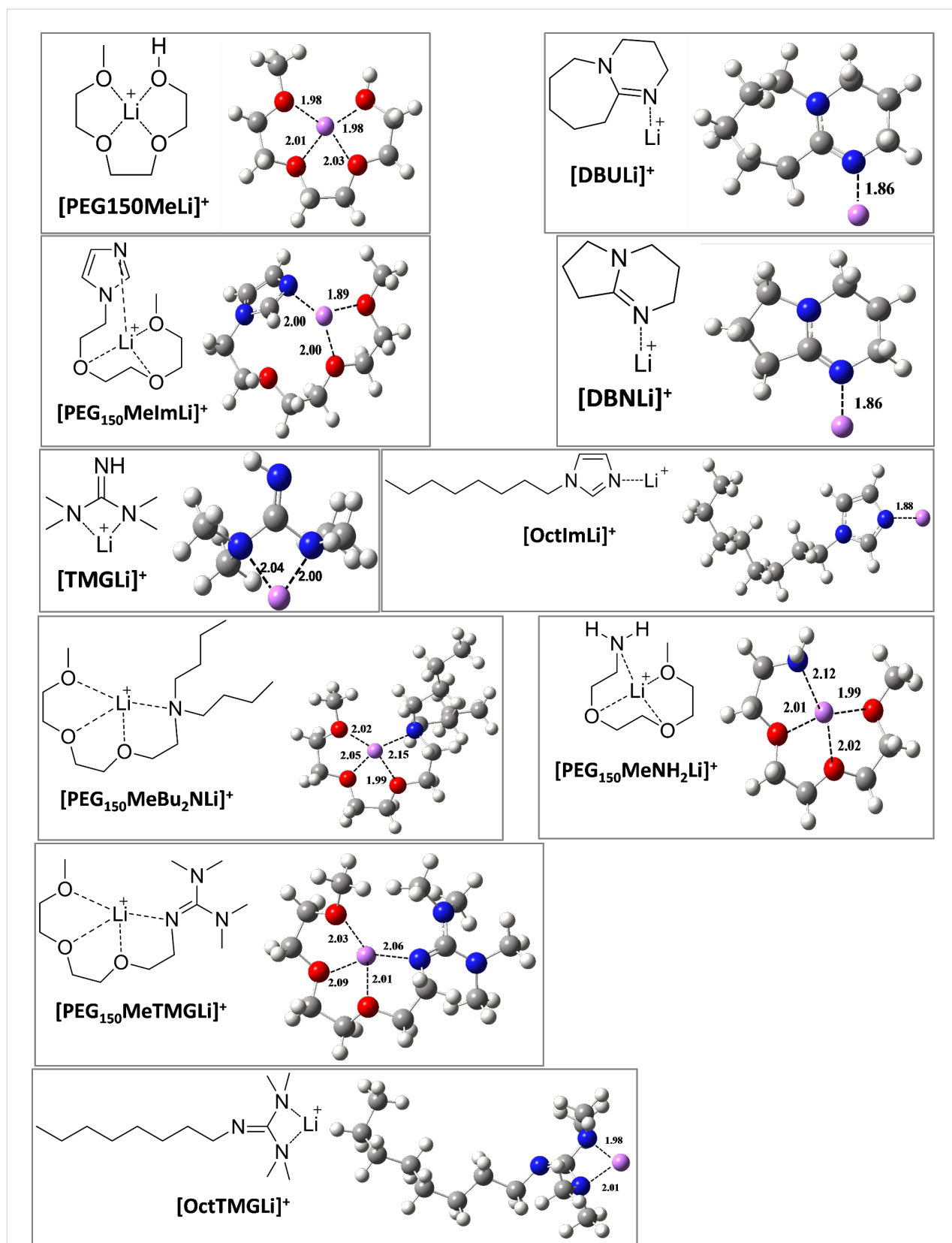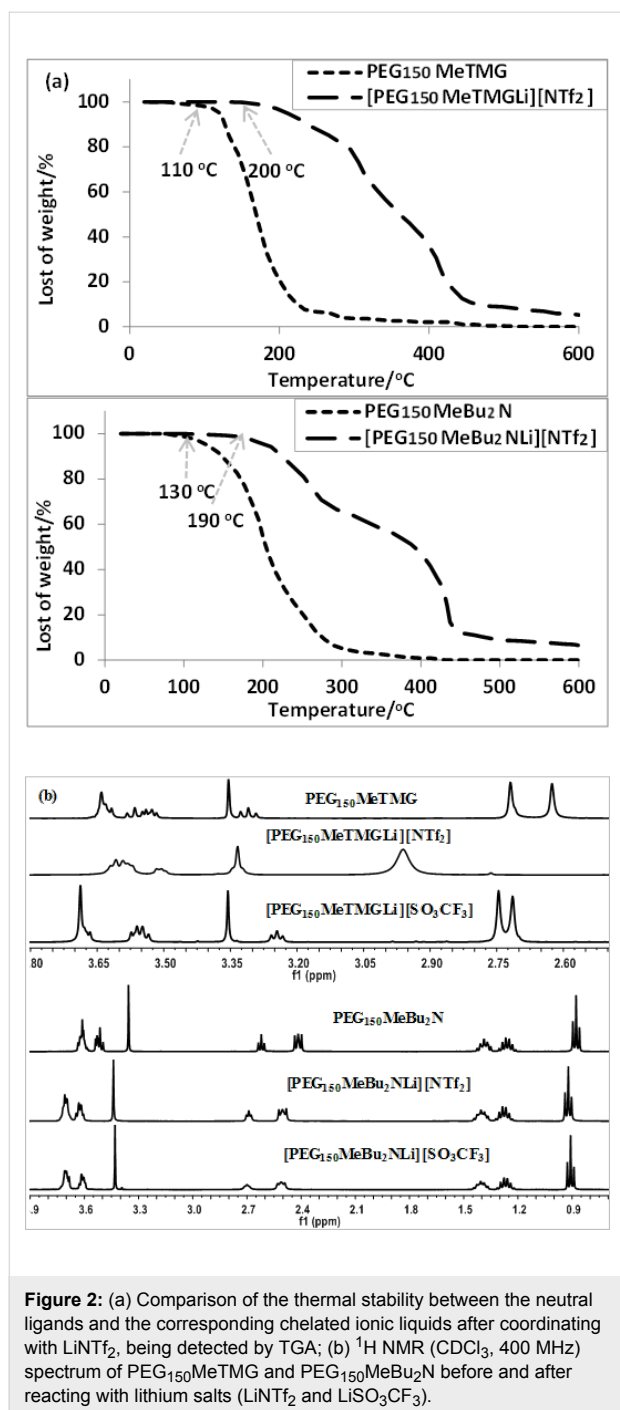
Figure 1: Typical optimized structures of complex cations derived from chelation between Li$^+$ and neutral ligands. H: white, C: grey, O: red, N: blue, Li: purple. Bond lengths are in Å.

Figure 2: (a) Comparison of the thermal stability between the neutral ligands and the corresponding chelated ionic liquids after coordinating with LiNTf₂, being detected by TGA; (b) ^{1}H NMR (CDCl₃, 400 MHz) spectrum of PEG₁₅₀MeTMG and PEG₁₅₀MeBu₂N before and after reacting with lithium salts (LiNTf₂ and LiSO₃CF₃).

Figure 3: In situ FTIR spectra of neutral ligands and the corresponding chelated ionic liquids after reaction with LiNTf₂, as well as the reaction mixture after CO_2 absorption in the absence or presence of water.

such as [PEG$_{150}$MeLi][NTf$_2$], [OctImLi][NTf$_2$] and [PEG$_{150}$MeImLi][NTf$_2$] showed a poor CO_2 sorption capacity, implying that only physical interactions with CO_2 were present (Table 1, entries 1–3). The primary amine-functionalized IL [PEG$_{150}$MeNH$_2$Li][NTf$_2$] gave rise to CO_2 uptake approaching 1:2 stoichiometry (Table 1, entry 4) as expected from the proposed mechanism for the formation of ammonium carbamate as shown in Scheme 1a [38]. Notably, the CO_2 capacity of guanidine-functionalized ILs increased in the order of

[TMGLi][NTf$_2$] (0.65) < [OctTMGLi][NTf$_2$] (0.80) < [PEG$_{150}$MeTMGLi][NTf$_2$] (0.89 mol CO_2 absorbed per mol of base) (Table 1, entries 5–7), indicating that the CO_2-philic nature of the PEG chain facilitates CO_2 sorption. Generally, anhydrous tertiary amines absorb CO_2 only under high CO_2 pressures to form instable zwitterionic alkylcarbonate salts (Table 1, entry 9) [42]. [PEG$_{150}$MeBu$_2$NLi][NTf$_2$] and [PEG$_{150}$MeBu$_2$NLi][SO$_3$CF$_3$] were able to rapidly reach 0.66 and 0.61 CO_2 capacity, respectively. Thus, tertiary amino-functionalized ILs with multidentate cation coordination have a much better performance probably due to the formation of a zwitterionic adduct being stabilized by Li$^+$ (Table 1, entries 10 and 11). Indeed, the CO_2 absorption capacity of [PEG$_{150}$MeBu$_2$NLi][NTf$_2$] increased steadily from 0.10 to 0.66 mol CO_2 absorbed per mol of base when the molar ratio of LiNTf$_2$/PEG$_{150}$MeBu$_2$N was varied from 0 to 1. When the molar ratio was increased to 1.5, no further promotion of the CO_2 capacity was observed (Figure 4). In contrast, when PEG$_{150}$MeTMG was employed as the neutral ligand, the CO_2 capacity decreased from 1.66 to 0.89 mol CO_2 absorbed per mol of base as the molar ratio of LiNTf$_2$/PEG$_{150}$MeTMG was increased from 0 to 1, probably due to decreased basicity of guanidine after coordinating with Li$^+$. At last, ILs

[DBULi][NTf$_2$] (0.50) and [DBNLi][NTf2] (0.75 mol CO$_2$ absorbed per mol of base) had a CO$_2$ capacity below 1:1 stoichiometry expected from the proposed mechanism (Scheme 1c), owing to highly increased viscosity after CO$_2$ absorption (Table 1, entries 12 and 13). Compared on a weight basis, a CO$_2$ capacity of 5.0 wt % to 8.0 wt % was obtained with ILs from neutral ligands/LiNTf$_2$ (Table 1, entries 5–7 and 10–13). This is much higher than for the conventional IL 1-hexyl-3-methylimidazolium hexafluorophosphate (0.0881 wt %) [43], and comparable to amino-functionalized imidazolium-based IL (7.4 wt %) [23] and ILs derived from amino acids [24]. Hence, our IL system has the potential to be utilized for industrialized CO$_2$ absorption processes.

Figure 4: Influence of the ratio of LiNTf$_2$/neutral ligands (PEG$_{150}$MeTMG and PEG$_{150}$MeBu$_2$N) on the CO$_2$ capacity of the coordinating mixtures.
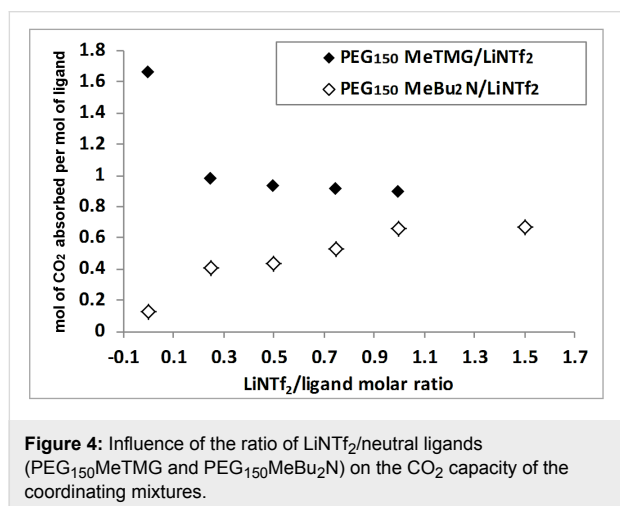
The in situ FTIR spectrum of [PEG$_{150}$MeTMGLi][NTf$_2$] and [PEG$_{150}$MeBu$_2$NLi][NTf$_2$] before and after reaction with CO$_2$ are shown in Figure 3. For [PEG$_{150}$MeTMGLi][NTf$_2$] as absorbent, the C=N stretching band at 1592 cm^{-1} shifted to 1622 cm^{-1} after reaction with CO$_2$. A characteristic peak centered at 1685 cm^{-1} is assigned to the stretching vibration of the carbonyl group in the zwitterionic alkyl carbamate, which is quite different from that in HCO$_3^-$ (1588 cm^{-1}). For the reaction of [PEG$_{150}$MeBu$_2$NLi][NTf$_2$] with CO$_2$, a new band at 1635 cm^{-1} was assigned to the stretching vibration of the C=O bond in the zwitterionic product. In addition, a distinct broad band at around 2118 cm^{-1} corresponding to the ammonium cation was observed in the presence of water.

To gain deeper insight into the reaction mechanism of CO$_2$ absorption with chelated ILs, DFT calculations were carried out. We performed geometry and energy optimizations for the free [BaseLi]$^+$ cation, free CO$_2$ and the [BaseLi]$^+$ + CO$_2$ complex. As shown in Figure 5, the chelated ILs react with CO$_2$ through nucleophilic attack by the N atom, to form the zwitterionic adducts, which are stabilized through coordination

with Li$^+$. In addition, formation of the zwitterionic alkyl carbamate is calculated to be associated with an enthalpy changes of −102.36 kcal mol^{-1} and −89.50 kcal mol^{-1} for [PEG$_{150}$MeTMGLi]$^+$/CO$_2$ and [PEG$_{150}$MeBu$_2$NLi]$^+$/CO$_2$, respectively, indicating that the absorption process is thermodynamically favourable.

Conclusion

In summary, efficient CO$_2$ capture was achieved through formation of zwitterionic adducts with readily synthesized chelated ILs. Multisite coordination interaction between the Li$^+$ cation and organic bases or PEG-functionalized organic bases is thought to be responsible for forming the amidine, guanidine or tertiary amine-functionalized ILs, after reaction with CO$_2$ to form zwitterionic adducts in a 1:1 manner. Coordination effects between various lithium salts and neutral ligands, and the CO$_2$ capacity of the obtained chelated ILs were investigated. Indeed, the thermal stability and the CO$_2$ capacity of the neutral ligands (e.g., PEG$_{150}$MeBu$_2$N) was highly increased after coordination with lithium salts to form chelated ILs (e.g., [PEG$_{150}$MeBu$_2$NLi][NTf$_2$]).

Experimental
Materials
All reagents used in this work were purchased from Sigma-Aldrich and used without further purification. CO$_2$ with a purity of 99.999% was obtained commercially.

Experimental methods
^{1}H NMR spectra were recorded on a Brucker 400 spectrometer in CDCl$_3$. Residual CHCl$_3$ (7.26 ppm) was used as internal reference. ^{13}C NMR spectra were recorded at 100.6 MHz in CDCl$_3$. Residual CHCl$_3$ (77.0 ppm) was used as internal reference. In situ FTIR spectra were collected on a Mettler Toledo React IR ic10, which was equipped with a diamond ATR probe, using an ic IR analysis system. The probe was placed into the absorption mixture. Spectra were collected in situ during CO$_2$ absorption, while the mixture was stirred continuously using a magnetic stir bar. ESI-MS spectra were recorded on a Thermo Finnigan LCQ Advantage spectrometer in ESI mode at a spray voltage of 4.8 kV.

General procedure for CO$_2$ absorption
The CO$_2$ absorption procedure was analogous to the CO$_2$/SO$_2$ absorption procedure we had reported before [35,44]. In a typical procedure, the CO$_2$ capture was carried out in a 10 mL Schlenk flask. The absorbents were charged into the reactor at room temperature. Then, the air in the flask was replaced by passing CO$_2$ through a needle, which was inserted into the bottom of the flask. The absorption was conducted at 25 °C with a CO$_2$ flow rate of 0.1 L/min. The amount of CO$_2$
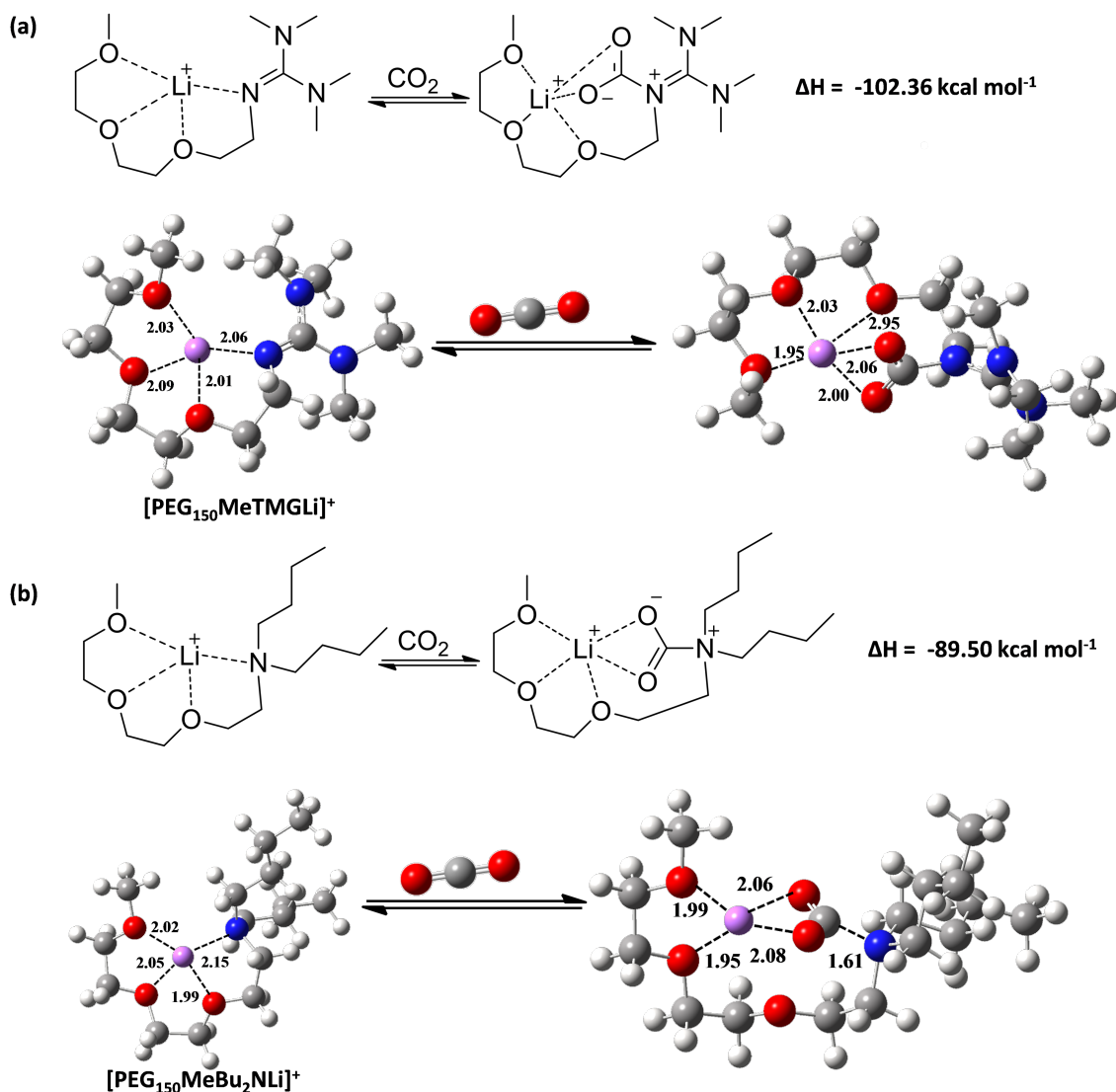
Figure 5: The quantum chemistry calculations (enthalpy changes) of the reaction between CO_2 and $[PEG_{150}MeTMGLi]^+$ (a) or $[PEG_{150}MeBu_2NLi]^+$ (b); H: white, C: grey, O: red, N: blue, Li: purple. Bond lengths are in Å.

absorbed was determined by following the weight of the mixture with an Analytical Balance. Data points were taken with an accuracy of ±0.0001 g every five minutes. Absorption/desorption was determined for at least three cycles.

Supporting Information

Supporting Information File 1

General experimental methods, synthesis and characterization of the neutral ligands, lithium salts and the corresponding chelated ionic liquids.
[http://www.beilstein-journals.org/bjoc/content/supplementary/1860-5397-10-204-S1.pdf]

Acknowledgements

References

1. Raupach, M. R.; Marland, G.; Ciais, P.; Le Quéré, C.; Canadell, J. G.; Klepper, G.; Field, C. B. *Proc. Natl. Acad. Sci. U. S. A.* **2007,** *104,* 10288–10293. doi:10.1073/pnas.0700609104
2. Yang, Z.-Z.; Zhao, Y.-N.; He, L.-N. *RSC Adv.* **2011,** *1,* 545–567. doi:10.1039/c1ra00307k
3. Yang, Z.-Z.; He, L.-N.; Gao, J.; Liu, A.-H.; Yu, B. *Energy Environ. Sci.* **2012,** *5,* 6602–6639. doi:10.1039/C2EE02774G

4. D'Alessandro, D. M.; Smit, B.; Long, J. R. *Angew. Chem., Int. Ed.* **2010,** *49,* 6058–6082. doi:10.1002/anie.201000431

5. Choi, S.; Drese, J. H.; Jones, C. W. *ChemSusChem* **2009,** *2,* 796–854. doi:10.1002/cssc.200900036

6. Wang, Q.; Luo, J.; Zhong, Z.; Borgna, A. *Energy Environ. Sci.* **2011,** *4,* 42–55. doi:10.1039/c0ee00064g

7. Li, L.; Zhao, N.; Wei, W.; Sun, Y. *Fuel* **2013,** *108,* 112–130. doi:10.1016/j.fuel.2011.08.022

8. Welton, T. *Chem. Rev.* **1999,** *99,* 2071–2084. doi:10.1021/cr980032t

9. Wasserscheid, P.; Keim, W. *Angew. Chem., Int. Ed.* **2000,** *39,* 3772–3789. doi:10.1002/1521-3773(20001103)39:21<3772::AID-ANIE3772>3.0.CO ;2-5

10. Petkovic, M.; Seddon, K. R.; Rebelo, L. P. N.; Pereira, C. S. *Chem. Soc. Rev.* **2011,** *40,* 1383–1403. doi:10.1039/c004968a

11. Plechkova, N. V.; Seddon, K. R. *Chem. Soc. Rev.* **2008,** *37,* 123–150. doi:10.1039/b006677j

12. Ma, Z.; Yu, J.; Dai, S. *Adv. Mater.* **2010,** *22,* 261–285. doi:10.1002/adma.200900603

13. Antonietti, M.; Kuang, D.; Smarsly, B.; Zhou, Y. *Angew. Chem., Int. Ed.* **2004,** *43,* 4988–4992. doi:10.1002/anie.200460091

14. Dupont, J.; de Souza, R. F.; Suarez, P. A. Z. *Chem. Rev.* **2002,** *102,* 3667–3692. doi:10.1021/cr010338r

15. Zakrzewska, M. E.; Bogel-Łukasik, E.; Bogel-Łukasik, R. *Chem. Rev.* **2011,** *111,* 397–417. doi:10.1021/cr100171a

16. Miao, C.-X.; He, L.-N.; Wang, J.-Q.; Wang, J.-L. *Adv. Synth. Catal.* **2009,** *351,* 2209–2216. doi:10.1002/adsc.200900285

17. Zhang, Q.; Zhang, S.; Deng, Y. *Green Chem.* **2011,** *13,* 2619–2637. doi:10.1039/c1gc15334j

18. Han, X.; Armstrong, D. W. *Acc. Chem. Res.* **2007,** *40,* 1079–1086. doi:10.1021/ar700044y

19. Berthod, A.; Ruiz-Ángel, M. J.; Carda-Broch, S. *J. Chromatogr., A* **2008,** *1184,* 6–18. doi:10.1016/j.chroma.2007.11.109

20. Armand, M.; Endres, F.; MacFarlane, D. R.; Ohno, H.; Scrosati, B. *Nat. Mater.* **2009,** *8,* 621–629. doi:10.1038/nmat2448

21. MacFarlane, D. R.; Forsyth, M.; Howlett, P. C.; Pringle, J. M.; Sun, J.; Annat, G.; Neil, W.; Izgorodina, E. I. *Acc. Chem. Res.* **2007,** *40,* 1165–1173. doi:10.1021/ar7000952

22. Ramdin, M.; de Loos, T. W.; Vlugt, T. J. H. *Ind. Eng. Chem. Res.* **2012,** *51,* 8149–8177. doi:10.1021/ie3003705

23. Bates, E. D.; Mayton, R. D.; Ntai, I.; Davis, J. H., Jr. *J. Am. Chem. Soc.* **2002,** *124,* 926–927. doi:10.1021/ja017593d

24. Zhang, X.; Zhang, X.; Dong, H.; Zhao, Z.; Zhang, S.; Huang, Y. *Energy Environ. Sci.* **2012,** *5,* 6668–6681. doi:10.1039/c2ee21152a

25. Zhang, J.; Zhang, S.; Dong, K.; Zhang, Y.; Shen, Y.; Lv, X. *Chem. – Eur. J.* **2006,** *12,* 4021–4026. doi:10.1002/chem.200501015

26. Jiang, Y.-Y.; Wang, G.-N.; Zhou, Z.; Wu, Y.-T.; Geng, J.; Zhang, Z.-B. *Chem. Commun.* **2008,** 505–507. doi:10.1039/b713648j

27. Zhang, Y.; Zhang, S.; Lu, X.; Zhou, Q.; Fan, W.; Zhang, X. *Chem. – Eur. J.* **2009,** *15,* 3003–3011. doi:10.1002/chem.200801184

28. Yu, H.; Wu, Y.-T.; Jiang, Y.-Y.; Zhou, Z.; Zhang, Z.-B. *New J. Chem.* **2009,** *33,* 2385–2390. doi:10.1039/b9nj00330d

29. Li, X.; Hou, M.; Zhang, Z.; Han, B.; Yang, G.; Wang, X.; Zou, L. *Green Chem.* **2008,** *10,* 879–884. doi:10.1039/b801948g

30. Luo, X. Y.; Ding, F.; Lin, W. J.; Qi, Y. Q.; Li, H. R.; Wang, C. M. *J. Phys. Chem. Lett.* **2014,** *5,* 381–386. doi:10.1021/jz402531n

31. Wang, C.; Mahurin, S. M.; Luo, H.; Baker, G. A.; Li, H.; Dai, S. *Green Chem.* **2010,** *12,* 870–874. doi:10.1039/b927514b

32. Wang, C.; Luo, H.; Luo, X.; Li, H.; Dai, S. *Green Chem.* **2010,** *12,* 2019–2023. doi:10.1039/c0gc00070a

33. Wang, C.; Luo, H.; Jiang, D.-e.; Li, H.; Dai, S. *Angew. Chem., Int. Ed.* **2010,** *49,* 5978–5981. doi:10.1002/anie.201002641

34. Wang, C.; Luo, X.; Luo, H.; Jiang, D.-e.; Li, H.; Dai, S. *Angew. Chem., Int. Ed.* **2011,** *50,* 4918–4922. doi:10.1002/anie.201008151

35. Yang, Z.-Z.; He, L.-N.; Zhao, Y.-N.; Li, B.; Yu, B. *Energy Environ. Sci.* **2011,** *4,* 3971–3975. doi:10.1039/C1EE02156G

36. Gurkan, B. E.; de la Fuente, J. C.; Mindrup, E. M.; Ficke, L. E.; Goodrich, B. F.; Price, E. A.; Schneider, W. F.; Brennecke, J. F. *J. Am. Chem. Soc.* **2010,** *132,* 2116–2117. doi:10.1021/ja909305t

37. Liu, A.-H.; Ma, R.; Song, C.; Yang, Z.-Z.; Yu, A.; Cai, Y.; He, L.-N.; Zhao, Y.-N.; Yu, B.; Song, Q.-W. *Angew. Chem., Int. Ed.* **2012,** *51,* 11306–11310. doi:10.1002/anie.201205362

38. Wang, C.; Guo, Y.; Zhu, X.; Cui, G.; Li, H.; Dai, S. *Chem. Commun.* **2012,** *48,* 6526–6528. doi:10.1039/c2cc32365f

39. Yang, Z.-Z.; Jiang, D.-e.; Zhu, X.; Tian, C.; Brown, S.; Do-Thanh, C.-L.; He, L.-N.; Dai, S. *Green Chem.* **2014,** *16,* 253–258. doi:10.1039/c3gc41513a

40. Das Neves Gomes, C.; Jacquet, O.; Villiers, C.; Thuéry, P.; Ephritikhine, M.; Cantat, T. *Angew. Chem., Int. Ed.* **2012,** *51,* 187–190. doi:10.1002/anie.201105516

41. Villiers, C.; Dognon, J.-P.; Pollet, R.; Thuéry, P.; Ephritikhine, M. *Angew. Chem., Int. Ed.* **2010,** *49,* 3465–3468. doi:10.1002/anie.201001035

42. Rainbolt, J. E.; Koech, P. K.; Yonker, C. R.; Zheng, F.; Main, D.; Weaver, M. L.; Linehan, J. C.; Heldebrant, D. J. *Energy Environ. Sci.* **2011,** *4,* 480–484. doi:10.1039/c0ee00506a

43. Blanchard, L. A.; Gu, Z.; Brennecke, J. F. *J. Phys. Chem. B* **2001,** *105,* 2437–2444. doi:10.1021/jp003309d

44. Yang, Z.-Z.; He, L.-N.; Zhao, Y.-N.; Yu, B. *Environ. Sci. Technol.* **2013,** *47,* 1598–1605. doi:10.1021/es304147q

Electrocarboxylation: towards sustainable and efficient synthesis of valuable carboxylic acids

Roman Matthessen[1], Jan Fransaer[2], Koen Binnemans[3] and Dirk E. De Vos[*1]

Abstract

The near-unlimited availability of CO_2 has stimulated a growing research effort in creating value-added products from this greenhouse gas. This paper presents the trends on the most important methods used in the electrochemical synthesis of carboxylic acids from carbon dioxide. An overview is given of different substrate groups which form carboxylic acids upon CO_2 fixation, including mechanistic considerations. While most work focuses on the electrocarboxylation of substrates with sacrificial anodes, this review considers the possibilities and challenges of implementing other synthetic methodologies. In view of potential industrial application, the choice of reactor setup, electrode type and reaction pathway has a large influence on the sustainability and efficiency of the process.

Introduction
Carbon dioxide recycling

Implementing sustainable, resource-efficient chemical processes to meet the world's growing demand for energy and chemicals is one of today's major challenges. Depletion of fossil resources and the ongoing increase of atmospheric carbon dioxide levels urge to investigate alternative pathways to close the carbon cycle. The use of carbon dioxide as chemical feedstock is a logical strategy for this purpose, creating economical benefit from its capture. At the moment, only a very minor fraction

(<1%) of anthropogenic CO_2 emissions is actually used [1]. As an end product of combustion, CO_2 has a high thermodynamic stability ($\Delta G_f^\circ = -396$ kJ/mol), often demanding for an energy intensive activation. The hydrogenation of CO_2 to methane for example is an industrial process which requires high temperatures and pressures to activate CO_2 [2,3]. Efficient chemical incorporation of CO_2 is limited to rather reactive substrates, like epoxides [4-6] and amines [7-9] to produce cyclic carbonates

and carbamates, respectively, and even then, elevated reaction temperatures and/or complex catalyst systems are sometimes required. Urea is the main industrial product for which CO_2 is applied as a C_1 building block in a reaction with ammonia, still requiring pressures around 200 bar to drive the equilibrium to acceptable yields [10,11]. Another important end product of CO_2 are inorganic carbonates, like $CaCO_3$, produced by fast reaction with metal hydroxides [12]. Carboxylic acids are an interesting class of products, as important intermediates in the synthesis of polymers and pharmaceuticals. Hydroxybenzoic acids are among the few chemicals that are industrially produced from CO_2, via the Kolbe–Schmidt reaction at high temperatures and CO_2 pressures [13-15]. Sodium phenolate is selectively converted to salicylic acid, a precursor of Aspirin, while potassium phenolate exclusively yields *p*-hydroxybenzoic acid, used in polyester synthesis (Scheme 1) [16-20].

Scheme 1: Synthesis of salicylic acid and *p*-hydroxybenzoic acid via Kolbe–Schmidt reaction [16-20].
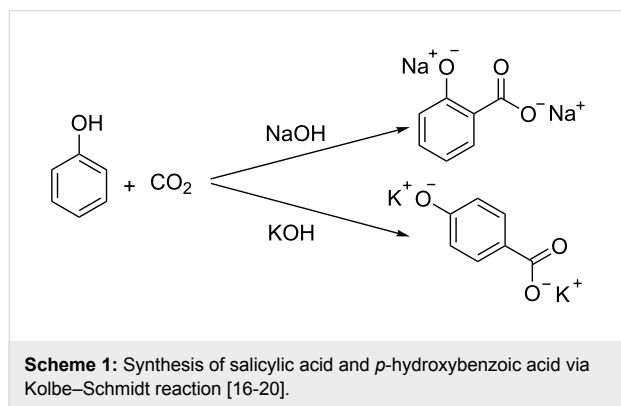
In order to generate carboxylic acids from CO_2 under relatively mild conditions, reactive organometallic nucleophiles such as Grignard reagents can be used, generating a large amount of waste [21-24]. Electroreduction of CO_2 can be a worthy alternative for these dangerous energy-intensive processes, replacing toxic or hazardous reducing agents by clean electrons. In this case, the high thermodynamic stability of CO_2 is by-passed by a simple one-electron reduction at an electrode, leading to in situ generation of reactive intermediates. Often, room temperature conditions are sufficient, considering that the energy of the electrons is determined by the applied voltage [25]. Since the electroreduction takes place on a cathode surface, the need for complex homogeneous organometallic catalysts is minimized. Furthermore, electricity will be increasingly of renewable origin in the future, making organic electrosynthesis a promising technology for environmentally friendly chemical processes [26]. The electroreduction of CO_2 can be applied for the synthesis of fuels like formic acid [27], methanol [28] or methane [29] via two-, six- and eight-electron reductions, respectively (Scheme 2). This way electric energy from periodic sustainable origin, like solar or wind energy, can be stored [30].
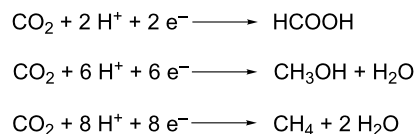
Scheme 2: Electroreduction of carbon dioxide to formic acid, methanol or methane.

Review

In this review, the focus will be on another approach, in which CO_2 is fixed in organic chemicals by means of an energy-efficient reduction process to produce valuable carboxylic acids. This methodology requires only one or two electrons per CO_2 molecule, as shown in Scheme 3 for olefins, with the C–C bond formation highlighted in bold.

Scheme 3: Electrochemical fixation of CO_2 in olefins.
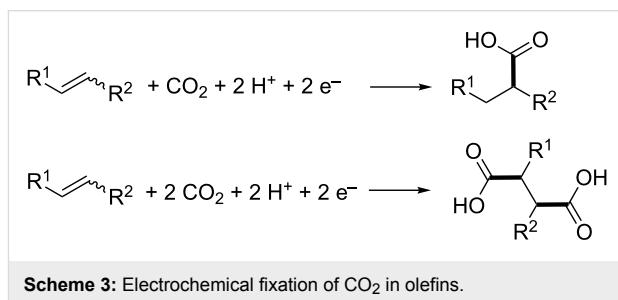
Industrial organic electrosynthesis

The chemical industry is devoting increasing research efforts to the field of organic electrosynthesis [31]. An extended series of electro-organic processes have already been implemented on an industrial scale, like for example the electrohydrodimerisation of acrylonitrile (Scheme 4) [32], or the production of *p*-methoxybenzaldehyde [33].

Scheme 4: Electrohydrodimerisation of acrylonitrile to adiponitrile [32].
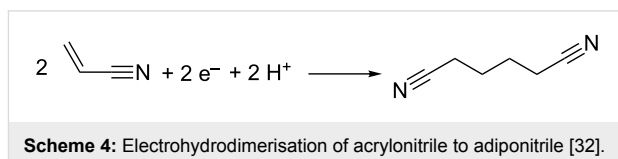
Another interesting industrial process is the simultaneous production of phthalide and *tert*-butylbenzaldehyde dimethylacetal from dimethyl phthalate and *tert*-butyltoluene, respectively (Scheme 5). After separation, by distillation and precipitation, both products can be used in the production of pesticides [34]. This is an example of a paired electrosynthesis, in which the anodic and cathodic reactions simultaneously form compounds that are valuable. This way a combined electrochemical yield, i.e., the fraction of supplied current going to the desired reaction, is achieved, reducing energy consumption and reaction

time. This methodology is very environmentally friendly since there is no generation of toxic wastes, electrical current is used more efficiently and a high atom economy is achievable [35]. The latter being the fraction of the molecular mass of all reactants which is transferred to the desired product(s). In Scheme 5, the total atom efficiency is 100% and the electrochemical yield reaches 180% [34].
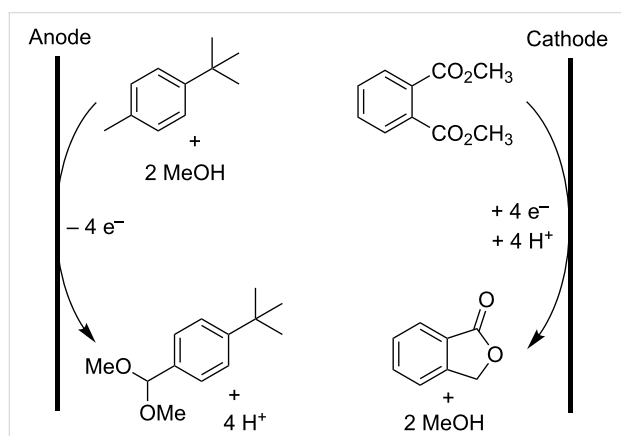

Scheme 5: Parallel paired electrosynthesis of phthalide and *tert*-butyl-benzaldehyde dimethylacetal [34].

Moreover, numerous pilot scale processes have been demonstrated like the electrohydrodimerization of formaldehyde to ethylene glycol [36] or the production of glyoxylic acid [37]. The most important reasons for this raised interest are the higher energy efficiency compared to traditional thermochemical processes, the use of less expensive starting materials, less aggressive reaction conditions, fewer processing steps and the discovery of unique synthesis routes [31].

Despite numerous publications and patents in the field of CO_2 electroreduction, no industrial processes are known in which CO_2 is electrochemically incorporated in organic chemicals producing carboxylic acids. This review will give an overview of various types of electrocarboxylation procedures bearing in mind the requirements for future industrial application. Besides the identification of a profitable market for the product, minimized process costs are the major requirement for potential large scale implementation. Some parameters that influence these costs are current efficiency, reactor design, electrode material and reactant costs.

Electrocarboxylation setups

All electrochemical processes involve an anodic and cathodic reaction in order to close the electron cycle. Electrons supplied at the cathode must emerge from an oxidation reaction occurring at the anode (Scheme 6). The electrochemical system should be optimized to prevent unfavorable interference between both reactions, since such conflicts cause electric current to be lost and lead to a decrease in faradaic efficiency. Electrocarboxylation, the electrochemical fixation of carbon dioxide in organic chemicals, involves the electroreduction of carbon dioxide and/or an organic substrate. For olefins, alkynes, carbonyl compounds, imines and organic halides, this leads to the formation of carboxylate anions. A counter cation is required in order to obtain a stable reaction product and an anodic reaction is necessary to complete the electron cycle. The anodic generation of this counter cation has been a challenging and important point of discussion for many years, as will become clear further in this review. An overview of different possible setups for obtaining carboxylic acids is given in Scheme 6.
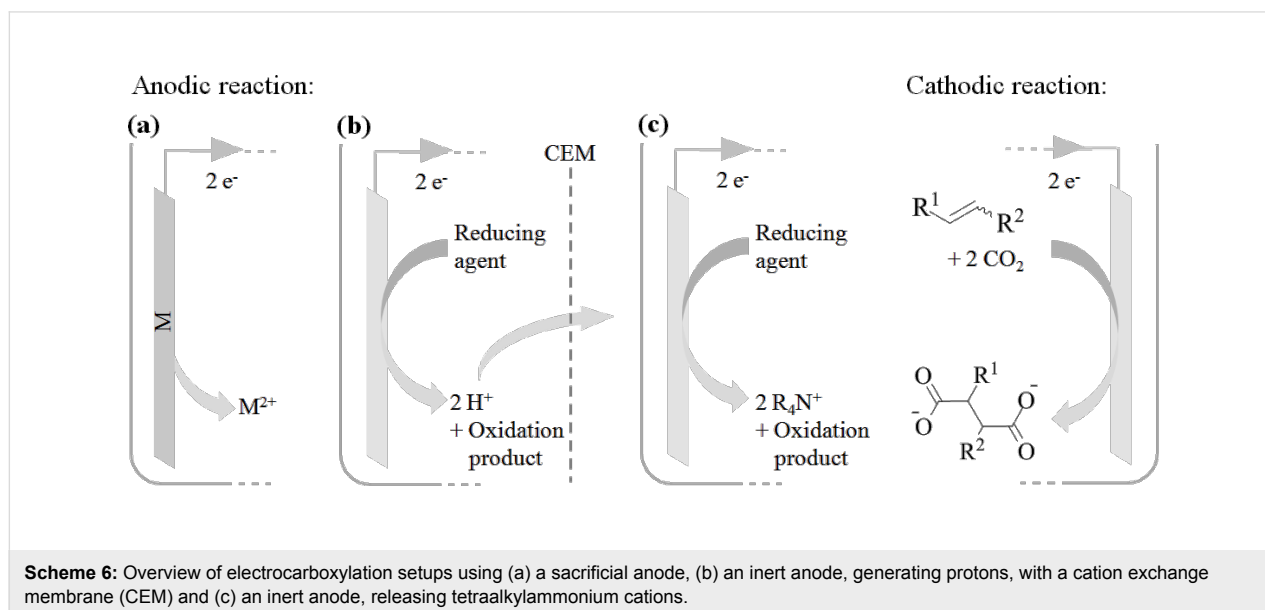
Scheme 6: Overview of electrocarboxylation setups using (a) a sacrificial anode, (b) an inert anode, generating protons, with a cation exchange membrane (CEM) and (c) an inert anode, releasing tetraalkylammonium cations.

Electrocarboxylation reactions can either be conducted with a sacrificial anode, like magnesium or aluminum, or with an inert anode, like platinum or carbon. Most research has been focused on the fixation of CO_2 using sacrificial anodes [38-40] (Scheme 6a). The higher oxidation potential of sacrificial anodes compared to that of the other reaction species makes this setup readily compatible with a simple undivided electrolysis cell, without a membrane separating the catholyte from the anolyte. This way high current densities can be obtained at relatively low potentials leading to minimized energy consumption. The absence of unwanted anodic reactions allows maintaining high current efficiencies without real difficulty. Furthermore, this counter electrode reaction delivers metal cations (Mg^{2+}, Al^{3+}), which rapidly are coordinated by the carboxylate anions formed at the cathode. Finally, the corresponding metal carboxylates can be precipitated from organic solvents allowing easy product isolation. Alongside all the benefits that are associated with these sacrificial anodes, the gradual consumption of the anode material is a major drawback for industrial applications. Not only is it rather expensive to consume such large amounts of metal; it also strongly hinders the implementation of a continuous process. Additionally, in order to obtain the free acids, an acid hydrolysis step is required, complicating product purification, and generating a significant amount of waste. The potential industrial use of electrochemical CO_2 fixation with sacrificial anodes should be found in fine chemical applications, preferably when the carboxylate salt can be used as such.

Considerable efforts have been made in investigating other electrocarboxylation systems. Replacing the sacrificial anode with a stable anode brings along several challenges. First of all, a counter electrode reaction must be identified, delivering counter cations to balance the charge of the carboxylate anions. The anodic reactant should be more easily oxidized than the other species present in the reaction mixture. The possible side product formed in this anodic reaction should either have no effect on the system, or be a useful reactant for the cathodic reaction. The direct formation of free carboxylic acids is a very interesting approach in this respect, minimizing the amount of process steps and waste (Scheme 6b). Protons produced at the anode, however, can have a detrimental effect on the electrocarboxylation efficiency, through cathodic formation of hydrogen, formic acid and other side products [41,42]. Hydrogen formation can be limited by usage of cathode materials with high hydrogen overvoltage like lead and mercury, or more environmentally friendly tantalum and zinc [43]. In order to minimize other side reactions a cation exchange membrane (CEM) is necessary, allowing different conditions in both compartments, giving a controlled supply of protons to the catholyte. Besides the implementation and maintenance costs of such a membrane, it also causes an elevated ohmic resistance between the elec-

trodes decreasing the energy efficiency of the process. Moreover, most membranes have difficulty operating in organic solvents and under high pressure conditions, limiting operational conditions [44]. The anodic oxidation of more reduction stable tetraalkylammonium salts is another approach compatible with non-sacrificial anodes (Scheme 6c). Here, the released tetraalkylammonium cations function as counter ions for the cathodically formed carboxylate anions. If the corresponding oxidation products are not harmful for the cathodic reaction a simple undivided cell can be envisaged. However, this can also be considered as a sacrificial process, since the tetraalkylammonium salts are consumed during the reaction. But more importantly, in contrast to the use of a dissolving anode, this method allows a more efficient implementation of a continuous process.

The first reports on electrocarboxylation date back to the early 1960s with a patent of Loveland, demonstrating the dicarboxylation of 1,3-butadiene in a two-compartment cell with a mercury cathode and a platinum anode, giving a mixture of mono- and dicarboxylic acids. CO_2 bubbling through a catholyte solution of 1 wt % water in DMF, saturated with butadiene, yielded up to 50% of 3-hexenedioic acid [45], a result which unfortunately was difficult to reproduce [42,46]. At that time, various substrates, like olefins, alkynes and aromatic ketones, have been electrocarboxylated in these divided cells [47]. Shortly after, sacrificial anodes made the use of a diaphragm obsolete, giving satisfactory product yields and current efficiencies in an undivided cell [38]. From this point on most of the research in the field of CO_2 fixation was focused on this type of setup.

Electrocarboxylation of conjugated dienes

The electrochemical fixation of carbon dioxide in 1,3-butadiene has been extensively investigated because of the importance of adipic acid for the polymer industry. 1,3-Butadiene is widely available, not only from steam cracking, but increasingly from dehydrogenation of linear butenes. Dicarboxylation of 1,3-butadiene yields a mixture of 3-hexene-1,6-dioic acid isomers, which are only one hydrogenation step removed from adipic acid, a monomer of nylon [41,42,44,48,49]. The general mechanism of CO_2 fixation in conjugated dienes is illustrated in Scheme 7. It is remarkable that only one electron is used per CO_2 molecule which is incorporated, making this a very energy efficient approach. There are two possible pathways to reach the monocarboxylate radical anion intermediate: one in which first CO_2 is reduced to a reactive $CO_2^{\bullet-}$ radical anion, and another one in which a radical anion is formed from the alkene. It has been illustrated that both pathways may be operative at the same time [49,50]. Which mechanism is favored depends amongst other parameters mainly on the diene type [49-51], CO_2 pressure [50] and cathode material [50].
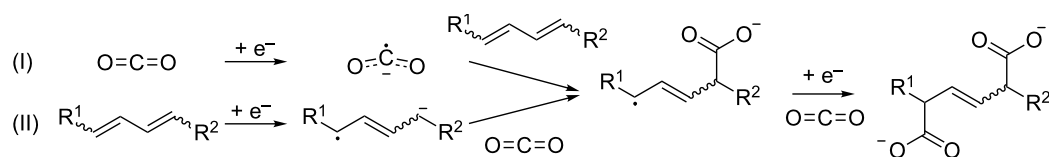
Scheme 7: General mechanism of the electrochemical dicarboxylation of conjugated dienes [49].

The different reactor setups used for the electrocarboxylation of 1,3-butadiene and the effect of the counter cation are illustrated in Table 1.

The different anodic reactions that have been used for the electrocarboxylation of 1,3-butadiene (Table 1) are illustrated in Scheme 8. They are divided into three categories, with (a) the sacrificial anode dissolution, (b) the proton forming reactions and (c) the oxidations evolving other free cations.

In case a stable platinum anode is used, a C5:C6:C10 product mixture is formed, containing isomers of 3-pentenoic acid (C5), 3-hexenedioic acid (C6) and 3,7-decadienedioic acid (C10) (Table 1, entries 1–7). The product distribution is among other things influenced by the water and proton content in the reaction system. In a divided cell, in which the anolyte consists of 1% H_2SO_4 in water, no C6 product is formed (Table 1, entry 1). Only in an anhydrous catholyte and anolyte, applying MgO in the anolyte as reducing agent, the carboxylation becomes more

Table 1: Electrocarboxylation of 1,3-butadiene in different setups.[a]

Entry	Anode	Reducing agent	CEM[b]	Solvent (catholyte – anolyte)	C5:C6:C10[c]	η[d] (%) (Yield (%))	Ref.
1[e]	Pt	H_2O	Yes	$CH_3CN – H_2O$[f]	67:0:33	18 (11)	[41]
2[g]	Pt	dry MgO	Yes	$CH_3CN – CH_3CN$	26:58:16	31 (21)	[41]
3[g]	Pt[h]	H_2	No	CH_3CN	0:0:0	0 (0)	[42]
4[g]	Pt[h]	H_2 + dry MgO	No	CH_3CN	75:25:0	3.7 (–)	[42]
5[g,i]	Pt[h]	H_2O	Yes	$DMF – H_2O$[f]	–:–:–	3.4 (–)	[42]
6[g]	Pt	NH_3	No	CH_3CN	33:54:13	5.8 (–)	[42]
7[j]	Pt	(TEA)$_2$oxalate + TEA formate[k]	No	CH_3CN	36:52:12	39 (98)	[44]
8[l]	Mg	Anode	No	DMF	2:98:0	– (81)	[48]
9[m]	Al	Anode	No	DMF	0:100:0	42 (84)	[49]

[a]Reactions were performed in conditions presented in corresponding references; [b]cation exchange membrane; [c]C5:C6:C10 = 3-pentenoic acid:3-hexenedioic acid:3,7-decadienedioic acid; [d]total current efficiency; [e]mercury cathode; [f]1 wt % H_2SO_4 solution; [g]lead cathode; [h]platinum hydrogen gas-diffusion electrode; [i]NH_3 present in catholyte; [j]carbon felt cathode; [k]TEA = tetraethylammonium; [l]tantalum cathode with 2,4,4-trimethyl-1,5,9-triazacyclododecene nickel(II) tetrafluoroborate mediator; [m]nickel cathode.
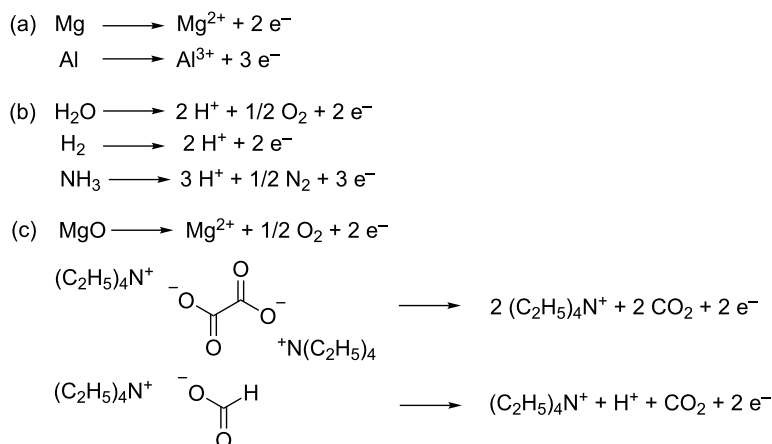
Scheme 8: Reported anodic reactions for the electrocarboxylation of 1,3-butadiene.

selective for C6, reaching appreciable current efficiencies (Table 1, entry 2). Furthermore, the presence of water in the catholyte decreases the total current efficiency, due to the formation of formic acid [41,42]. It must be noted that, when using an aqueous and organic solvent in anolyte and catholyte, respectively, the transfer of hydrated protons through the membrane will cause water to enter the catholyte. Protons in turn can also favor formic acid generation, but on top of that, they promote the C5 and C10 formation [41]. It must be noted that the presence of formic acid illustrates the existence of mechanism I (Scheme 7). When working in an undivided cell and using protons as sole counter cation through hydrogen oxidation in anhydrous conditions, only formic acid is produced (Table 1, entry 3) [42]. The latter stresses the effect of a cation exchange membrane in providing a controlled proton supply to the catholyte, minimizing cathodic formation of formic acid. In these electrosynthesis setups, in which protons are generated at the anode, cathodes with high hydrogen overpotential, like mercury and lead, are necessary to minimize current loss through hydrogen gas formation [41,42].

The counter ion seems to have a significant influence on the fate of the cathodically formed $CO_2^{\bullet-}$ radical anion. For carboxylation of a carbon skeleton to occur, this radical anion needs to react via the radical centered at its carbon atom. Grinberg et al. claim that metal or ammonium cations can cause a reversible migration of the negative charge between the carbon and oxygen atoms, allowing the $CO_2^{\bullet-}$ radical anion to react with its C-centered radical [42]. When this $CO_2^{\bullet-}$ radical anion abstracts a proton from the solvent, proton migration from oxygen to carbon results in formation of a strong covalent CH bond, yielding a formyloxy radical, which is further reduced to a formate anion (Table 1, entry 3). In general terms, one can conclude that the electrocarboxylation of 1,3-butadiene is not efficiently performed in aqueous or protic media. MgO has been considered as an alternative cation source (Table 1, entry 4), but its solubility in organic solvents is low. Using ammonia as proton scavenger, with formation of ammonium counter cations, allows electrocarboxylation of 1,3-butadiene, and can increase the selectivity for the C6 product (Table 1, entries 5 and 6). The faradaic efficiencies, however, are rather low, hence, there has been a search to find alternative reducing agents.

Tetraethylammonium oxalate and formate salts appeared to be very promising for this purpose, fulfilling both the role of electrolyte and reducing agent. Tetraethylammonium cations have high reduction stability, while still possessing good ion pairing properties. The degree of delocalization of the positive charge is large enough to prevent cathodic reduction and small enough to allow a quick and stable interaction with the cathodically

formed carboxylate anions. Furthermore, oxalate and formate are easily oxidized at a Pt anode, gradually releasing the tetraethylammonium cations. The combination of both salts in acetonitrile gives near quantitative yields of the C5:C6:C10 product mixture, with C6 as the main product (Table 1, entry 7) [44]. The anodic reaction produces CO_2 which can directly be used as reactant at the cathode (Scheme 8), sustaining the atom economy of the process. This way, however, there is no net incorporation of gaseous CO_2 into the organic substrate, but only net conversion of more energetic oxalate and formate. On top of that, it is important to realize that both the MgO and the tetraalkylammonium salts can also be considered as sacrificial reducing agents. Their advantage over sacrificial anodes, however, is an easier implementation in a continuous process. The anodic oxidation of formate generates one CO_2 molecule and one proton, giving a controlled supply of protons to the cathode (Scheme 8). Conducting the electrocarboxylation with tetraethylammonium oxalate, without formate salts, increases the amount of C6 compared to C5 and C10 [44]. The use of acetonitrile as solvent is ideal when working in an undivided cell, thanks to its adequate oxidation stability and high dielectric constant. Anhydrous conditions and the easier oxidation of oxalate and formate, at a Pt anode, compared to butadiene and the cathodically generated carboxylates, make the use of a membrane redundant, enabling the use of a simple undivided cell [44]. Moreover, the use of membranes in non-aqueous or aprotic environments is unsatisfactory as they become poorly conducting [44]. This procedure was patented and extended to various other substrates, like activated olefins, imines, carbonyl and halogen compounds, and other anions like an azide, which forms inert N_2 upon oxidation [52].

Eventually the electrocarboxylation of 1,3-butadiene was also conducted with sacrificial anodes, resulting in a high selectivity for the C6 product (Table 1, entries 8 and 9) [48,49]. Working under anhydrous conditions allows using another range of cathode materials, such as nickel, without being limited by the hydrogen overvoltage. The cathode metal has a large effect on the product distribution, acting as a catalyst [44,49]. Secondly, the absence of a membrane allowed the use of high CO_2 pressures, pushing the selectivity towards the C6 product, completely eliminating C10 formation [49]. The above-mentioned benefits of sacrificial anode systems have lead to the electrocarboxylation of various other conjugated dienes [49-51,53,54]. In order to increase the selectivity for the C6 product, dissolved nickel and iron redox mediators have been used [48,53,54]. The need for such organometallic complexes could be eliminated by direct electrocarboxylation on nickel or stainless steel cathode surfaces [49,50]. Substrates with an internal conjugated system appear to be less reactive towards CO_2 fixation, due to steric hindrance and the presence of electron

donating substituents [49,51]. However, working at atmospheric CO_2 pressures and at lower current densities allows effectively performing the double carboxylation of internal conjugated double bonds in open chains. This way, conjugated linoleic acids could be dicarboxylated with a yield approaching 80% at current efficiencies of over 50%, opening the reactant scope to other renewable dienes [50]. The occurrence of mechanism I (Scheme 7) was illustrated via the formation of oxalic acid, the CO_2 dimerization product [50]. Additional insight in the carboxylation mechanism was gained by comparing the reactivity of 1,3-cyclohexadiene with a mixture of 2,4-hexadiene isomers. The fixed cyclic conformation of 1,3-cyclohexadiene increases its reactivity towards CO_2 fixation, explained by a higher adsorption strength on the cathode surface. This suggests that dienes undergo carboxylation according to mechanism II while adsorbed on the surface, combined with mechanism I (Scheme 7). Moreover it was shown that diene configuration has a strong stereoelectronic effect on the rate of the dicarboxylation, with the *Z,Z*-configuration being the most reactive one [50].

Electrocarboxylation of olefins and alkynes

Many reports have been published on the electrocarboxylation of olefins and alkynes [55-74]. Most research has been done using a setup with a sacrificial magnesium or aluminum anode. The general mechanism of alkyne electrocarboxylation to a 1,4-dicarboxylated product is shown in Scheme 9. It is highly similar to the mechanism for electrocarboxylation of olefins. In

these reactions a high selectivity for dicarboxylation can be achieved.

Alkynes and olefins react according to similar pathways, although a separate mechanism has been proposed for selective monocarboxylation of alkynes using nickel mediators, usually with bipyridine or *N,N,N′,N′,N″*-pentamethyldiethylenetriamine ligands [55-60]. These organometallic complexes have also proven their value in increasing the carboxylation efficiency of alkenes, without including a specific selectivity for the monocarboxylic acid [56]. Monocarboxylation can readily occur as a side reaction when a small amount of protons are present in the reaction mixture, or through a proton/hydrogen radical abstraction from the reaction medium. The triple bond of alkynes is more active towards carboxylation than the olefin double bond [56]; furthermore, terminal alkynes are more reactive than internal alkynes [56-58], both leading to highly selective CO_2 fixation. The selectivity towards the dicarboxylation product can be significantly increased by working at higher CO_2 pressures [61,66], although an optimum must be found to minimize oxalic acid formation at high CO_2 pressures by electrodimerization of CO_2 [72]. Under rigorously anhydrous conditions, the dicarboxylation product of alkynes, shown in Scheme 9, can be transformed to a maleic anhydride [61,62]. Alkynes are rather reactive as such; olefins can be rendered more reactive by introduction of electron withdrawing groups [68-71,73,74]. Thus ethyl cinnamate was electrocarboxylated in 78% yield to give a mixture of mono- and dicarboxylated product (Scheme 10) [70].
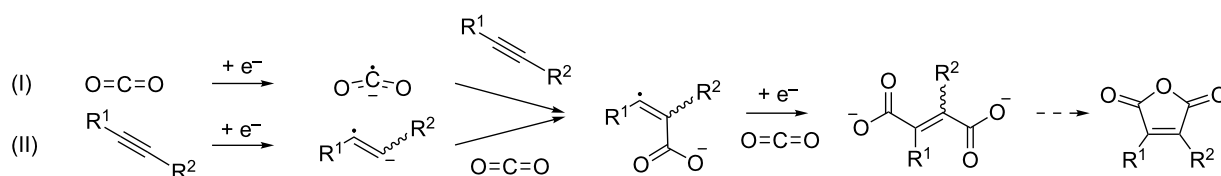
Scheme 9: General mechanism for electrocarboxylation of alkynes.
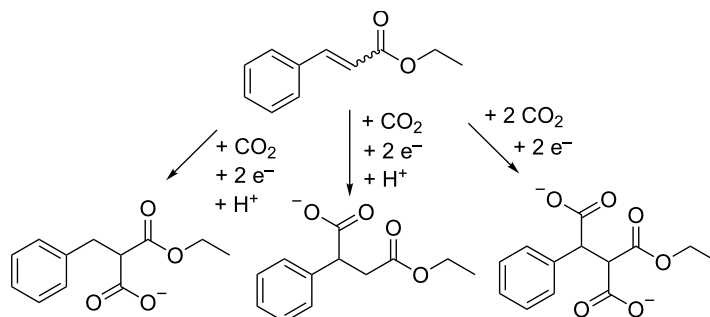
**Scheme 10:** Electrocarboxylation of ethyl cinnamate [70].

Activated olefins like dimethyl maleate and acrylonitrile have also been reacted in a setup with a stable anode utilizing tetraethylammonium oxalate, formate or azide salts as the reductant [52].

## Electrocarboxylation of ketones, aldehydes and imines

As is the case for conjugated dienes, olefins and alkynes, two possible pathways exist for electrocarboxylation of carbonyl and imine compounds. One starts with CO_2 reduction; another starts with reduction of the substrate (Scheme 11). The second route is considered as the predominant one [75]. In case the carbonyl or imine compound is reduced first, the negative charge may reside either on the carbon or on the heteroatom. This results in a first CO_2 fixation on the carbon or on the heteroatom, depending on the electron-withdrawing/electron-donating properties of the substituents R^1 and R^2. In both cases, a second electron reduction in presence of CO_2 yields a carboxylate intermediate with an additional carbonate or carbamate group. The latter is converted to the corresponding α-hydroxy acid or to an α-amino acid after acid hydrolysis in the product work-up [75-77].

An alternative mechanism has been proposed for aliphatic aldehydes, in which not α-hydroxy acids are formed but in which CO_2 is incorporated on the α-carbon according to Scheme 12 [78]. Here, the reduced aldehyde abstracts a proton from the α-carbon of an unreacted aldehyde.

The electrocarboxylation of ketones was first described by Wawzonek, converting benzophenone and acetophenone to benzylic acid and 2-hydroxy-2-phenylpropionic acid, respectively [79]. This offers an electrochemical route for several commercially relevant α-aryl propionic acids, used as non-steroidal anti-inflammatory drugs (NSAIDs) [80]. Therefore, the electrocarboxylation of aromatic ketones with sacrificial anodes has been extensively investigated [75-77,81-98]. Some researchers focused on replacing toxic and volatile organic solvents with ionic liquids [81-83]. Their negligible vapor pressure, large electrochemical window, good intrinsic conductivity and high CO_2 solubility make them interesting solvents for electrochemical CO_2 valorization [81-83,99-101]. Under similar conditions, ketones are carboxylated with higher selectivity for the α-hydroxy acid compared to aldehydes, and especially compared to aliphatic aldehydes, like acetaldehyde, which give
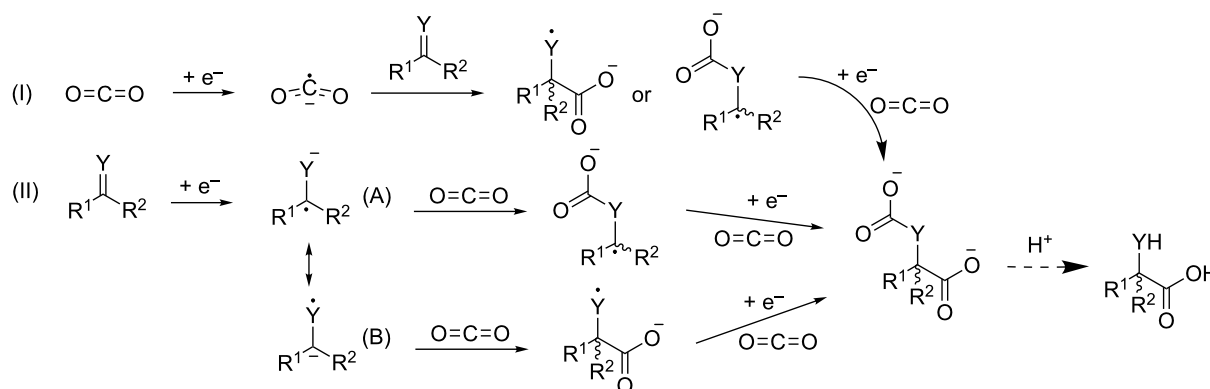
Scheme 11: General electrocarboxylation mechanism for carbonyl compounds (Y = O) and imines (Y = NH) [75-77].
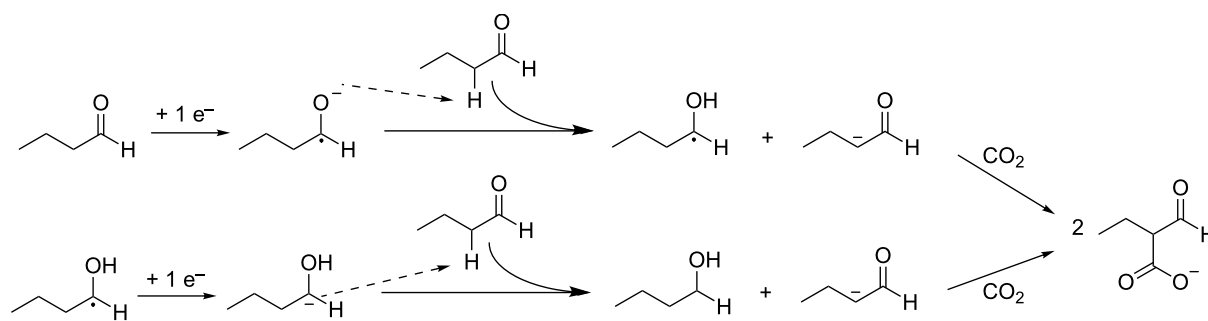
Scheme 12: Electrocarboxylation mechanism of butyraldehyde proposed by Doherty [78].

very poor yields [84]. Since carbonyl compounds have the tendency to accept an electron more easily than CO_2, the reaction mixture contains a lot of carbonyl radical anions, which can form vicinal diol dimers (pinacols) as side product [75,76,83]. The ratio of CO_2 to substrate is of great importance in obtaining a high selectivity for the α-hydroxy acid products. Working at high CO_2 pressures and low carbonyl concentrations gives the highest faradaic efficiencies, minimizing pinacol formation. The presence of protons drastically increases the amount of dimerization product and favors the hydrogenation of the carbonyl group to the alcohol [75,76,82,91]. The cathode material again plays an important role in the electrocarboxylation of carbonyl compounds. Toxic lead cathodes [85] and expensive platinum cathodes [87] can easily be replaced by better performing stainless steel [90] and nickel [75,89]. Concerning the reactivity of carbonyl compounds, it has been demonstrated that the carboxylation rate of benzophenones is decreased by electron donating substituents [90]. The pharmaceutical value of the electrocarboxylation of aromatic ketones to NSAIDs has lead to a significant number of patents using a sacrificial anode [92-95]. Since enantioselectivity is crucial for anti-inflammatory drugs, research has also been performed on the enantioselective electrocarboxylation of aromatic ketones, using chiral alkaloids [96-98].

The most important semi-industrial scale electrocarboxylation processes are related to the synthesis of these NSAIDs. The α-hydroxy acid is an intermediate, still requiring a chemical hydrogenation to obtain the desired product. 2-Acetyl-6-methoxynaphthalene (AMN) can be converted to hydroxy-naproxen (HN), a precursor of naproxen (Scheme 13) [85,86]. Although yields up to 90% were obtained in a 1 L flow reactor, the switch to a 75 L system was accompanied by leaks and

instrument problems resulting in a low yield (58%) and current efficiency (30%) [86].

Besides carbonyl compounds, imines have also shown value as substrates for electrocarboxylation, namely in the synthesis of non-natural amino acids [102-108]. A semi-industrial setup was designed for the electrocarboxylation of benzalaniline (Scheme 14). Scale up was done in a filter press type cell with flow distribution, which is commercially available. The electrodes are pressed together with a PTFE coated glass fibre net between them. This way, the inter-electrode gap remains constant during consumption of the anode. In a 2 L solution with 200 g of reactant, a product yield of 85% and a current efficiency of 80% were obtained [105].

The electrocarboxylation of aromatic ketones was also conducted with stable electrodes as shown in Scheme 15 [94,95]. In these patents *p*-isobutylacetophenone is carboxylated to hydroxyibuprofen, which is readily hydrogenolyzed to ibuprofen. A nafion membrane is used, allowing a selective passage of protons and tetraalkylammonium cations from the anolyte to the catholyte. Cyclohexene is added to the anolyte to scavenge the anodically formed bromine. A current efficiency of up to 90% was reached with a copper cathode and graphite anode. The method appeared also suitable for the synthesis of other NSAIDs like naproxen, cicloprofen, isoprofen, flurbiprofen, fenoprofen and carprofen.
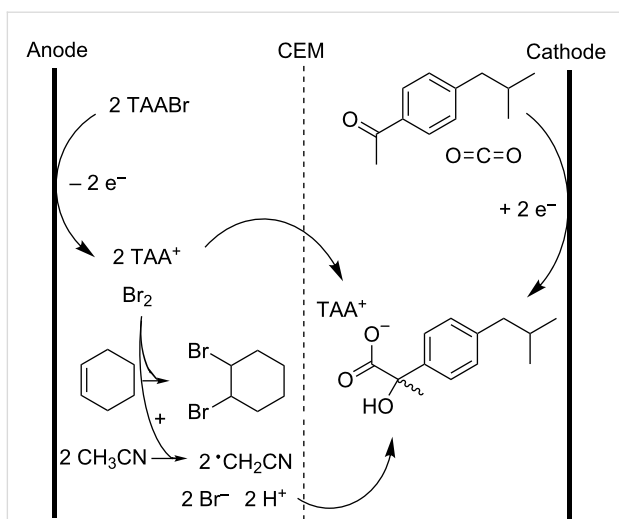
The electrocarboxylation of aliphatic aldehydes was also patented, namely for the production of 2-hydroxy-4-methylmercaptobutyric acid (MHA) by electrochemical carboxylation of 3-methylmercaptopropionaldehyde (MMP), with both a sacrificial anode [109] and a stable anode [110,111] (Scheme 16). The
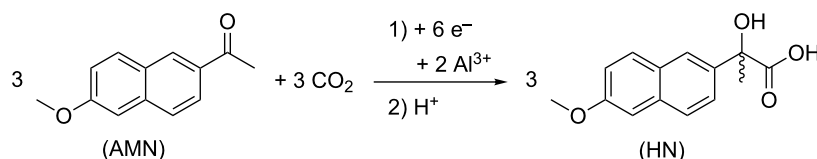
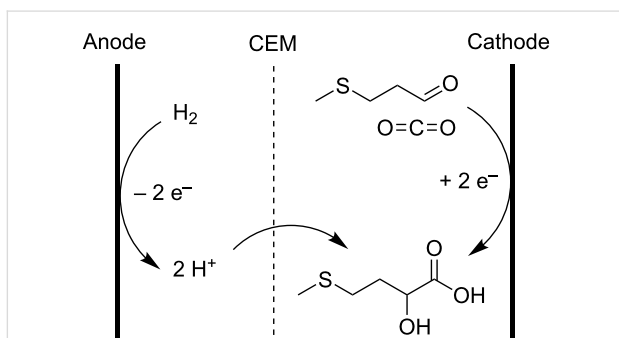**Scheme 13:** Electrocarboxylation of AMN to HN using a sacrificial aluminum anode [86].
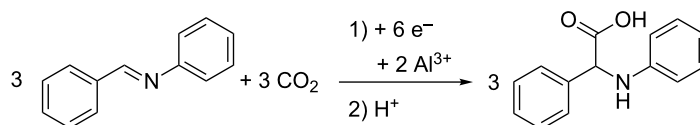
Scheme 14: Electrocarboxylation of benzalaniline using a sacrificial aluminum anode [105].

Scheme 15: Electrocarboxylation of *p*-isobutylacetophenone with stable electrodes [94,95].

system, using the stable electrodes, can be extended to aldehydes, ketones and imines.

**Scheme 16:** Electrochemical carboxylation of MMP to MHA [110,111].

MHA is an industrial scale feed additive, which is conventionally prepared using cyanides. In the proposed setup for the electrocatalytic preparation of MHA, a boron-doped diamond coated permeable cathode and Pt coated permeable anode rest directly on the cation exchange membrane to decrease ohmic resistance by the membrane, minimizing the required voltage. Hydrogen, supplied to the anolyte gives protons, which gradually enter the catholyte to form the free carboxylic acids. Both anolyte and catholyte are based on DMF. Unfortunately, no yields or current efficiencies higher than 30% were obtained [111].

There are also examples in which aromatic ketones and imines are electrocarboxylated in an undivided cell with stable anode. CO_2 fixation in acetophenone was done in good yields in an undivided cell using a quaternary ammonium oxalate as an elec-

trolyte and a sacrificial reducing agent [52,94,95,112,113]. Benzalanilines were carboxylated electrochemically with 79% faradaic yield, using an oxalate electrolyte [52].

Electrocarboxylation of organic halides

Numerous reports have been published on the electrocarboxylation of organic halides [114-146]. In a first step, a one electron reduction causes a halide anion to dissociate, forming a reactive radical. The latter undergoes a second reduction in the presence of CO_2, yielding a monocarboxylate anion (Scheme 17) [122,124-126,128].
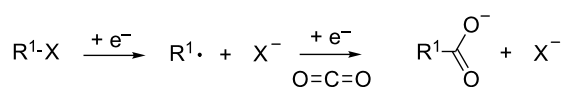
Scheme 17: General mechanism for electrocarboxylation of alkyl halides [122,124-126,128].

The first reactions reported were conducted in a divided cell, giving only moderate yields [114,115]. A drastic increase in efficiency was obtained by employing sacrificial anodes [116], especially magnesium anodes [117,118]. The cathode material is again of great importance, with silver and platinum giving the highest carboxylation selectivity [119-125]. Redox mediators allow working at a less negative cathodic potential, which results in a better energy efficiency and a more selective CO_2 fixation [128]. The most common redox mediators are organometallic nickel [129-131], palladium [132] and cobalt complexes [133-137].

Similar to what was mentioned above for aromatic ketones, benzylic chlorides can also be converted to 2-arylpropionic acids (Scheme 18), with applications in the pharmaceutical industry, mainly as NSAIDs. Here too, some articles described the use of ionic liquids as solvent for electrocarboxylation reactions, in order to increase the safety and efficiency of the process [120,122].
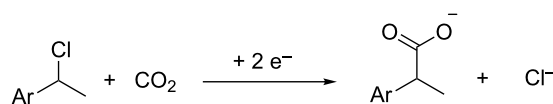
Scheme 18: Electrocarboxylation of benzylic chlorides as synthesis route for NSAIDs.

The industrial potential of this reaction has been assessed in several pilot applications, for example, using a setup with a sacrificial anode. In a 400 L reactor, a narrow and constant interelectrode gap was maintained in time and space, avoiding

an ohmic drop during consumption of the anode material. A polyethylene grid is placed between the electrodes, allowing the anode to press down on the cathode by its own weight. A good agitation is obtained by pumping the reaction mixture through the cell [138]. Unfortunately, industrial production was not developed because of difficulties in the purification of the product, arising from the presence of impurities generated by the degradation of the solvent [139]. Another pilot scale experiment, conducted for the production of NSAIDs, uses a stable graphite anode in an undivided cell. The anodic reaction is the oxidation of lithium oxalate, giving yields up to 85% of 2-phenyl-propionic acid [140]. The same group also investigated a setup in which a metal powder, like zinc, is oxidized at the anode, giving similar results [141].

The electrocarboxylation of organic halides can also be considered as an alternative dechlorination pathway for chlorobenzenes [122] and polychloromethanes [142]. While the synthesis of halogenated reagents is rather hazardous, the electrocarboxylation of organic halides is an interesting method to revalue waste products, like for example carbon tetrachloride, a toxic liquid, causing ozone depletion. In an undivided cell and acetonitrile as solvent, tri- and dichloroacetic acid are formed with current efficiencies between 50 and 60%. The exact anodic reaction(s), however, are not really specified. Oxidation of chloride, which itself originates in the CCl_4 reactant, likely results in partial chlorination of the acetonitrile solvent, releasing protons which in turn cause the formation of chloroform by attacking the cathodically formed carbanions [143].

An undivided electrosynthesis setup with stable anode can also be used for CO_2 fixation in other aliphatic halides. The anodic oxidation of tetraethylammonium oxalate is used in the electrocarboxylation of 1-bromo-2-methylpentane, which is almost quantitatively converted into 3-methylhexanoic acid [52]. The electrocarboxylation of 1,4-dibromo-2-butene is another reaction for which a stable anode and an undivided cell were proposed. The goal here is to form 3-hexenedioic acid, a precursor of adipic acid, although very poor yields and current efficiencies were obtained. Besides 1,4-dibromo-2-butene, 1,3-butadiene is added in the one-compartment cell to capture the bromine generated at the anode, forming the reactant (Scheme 19). The low yields are caused by debromodimerization and oligomerization [144].

A significant effort has been devoted to efficiently produce cyanoacetic acid through CO_2 fixation in chloroacetonitrile, as an alternative for the hazardous synthesis via alkali metal cyanides [137,145,146]. Derivatives of cyanoacetic acid are precious starting materials in pharmaceutical and agrochemical synthesis [137]. When the anodic reaction is the oxidation of a

Scheme 19: Electrocarboxylation of 1,4-dibromo-2-butene [144].
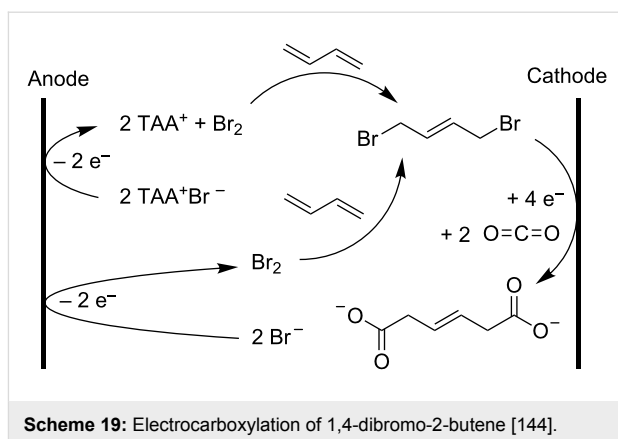
halide, lower current efficiencies can be attributed to a successive oxidation and reduction of respectively halides and halonium species. Therefore, the use of a membrane or glass frit can be interesting to minimize this effect. However, in a divided cell, the electrocarboxylation of chloroacetonitrile to cyanoacetic acid still appeared to give higher current efficiencies when using a sacrificial anode [146]. The major downside in carboxylating organic halides is the release of halides in the system, which can moreover induce a significant number of side reactions in a non-sacrificial setup, and which is in any case disadvantageous for the atom economy.

Innovative electrocarboxylation of other substrates

Besides the electrocarboxylation of chloroacetonitrile, CO_2 can also be incorporated electrocatalytically in acetonitrile itself. Such reaction was successfully conducted in a two-compartment cell divided by a medium porosity glass frit (Scheme 20). This is an interesting alternative for the conventional synthesis of cyanoacetic acid, which is carried out by the reaction of chloroacetic acid and alkaline cyanides [147-149].

Scheme 20: Convergent paired electrosynthesis of cyanoacetic acid, with $X^- = F_4B^-$, ClO_4^-, HSO_4^-, Cl^-, Br^- [147].
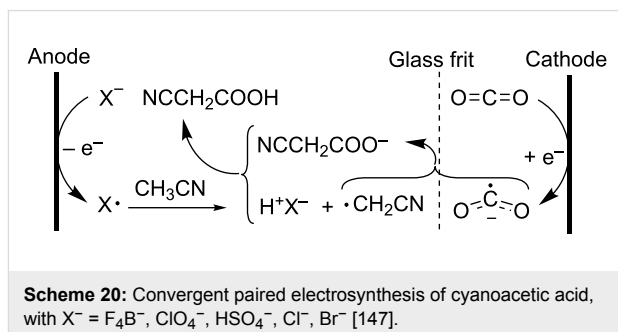
The electrocarboxylation of acetonitrile to cyanoacetic acid is an example of a convergent paired electrosynthesis, meaning that two different substrates undergo either oxidation or reduction to afford products that react among themselves to generate

a single product. Cyanomethyl radicals are formed by anodic oxidation of the supporting electrolyte anion followed by hydrogen radical abstraction from the acetonitrile solvent. These cyanomethyl radicals are then coupled to the $CO_2^{\bullet-}$ radical anion, forming cyanoacetic acid after protonation. The authors claim that the product is solely formed in the anolyte after $CO_2^{\bullet-}$ transport from the catholyte to the anolyte, although transport from cyanomethyl radicals to the catholyte is not excluded. However, product formation through cathodic reduction of acetonitrile is ruled out properly, since no cyanoacetic acid was formed when using a cation-exchange membrane. Since most of the product is present in the anolyte, current yields are rather low (24%). Moreover, the electrolyte anion and the cyanoacetic acid product have similar oxidation potentials. On top of that, some halogenation of the solvent to chloroacetonitrile was observed as a side reaction [147]. This reaction setup was also tested with propionitrile, butyronitrile, benzyl chloride and toluene in the anolyte compartment. Adjacent functional groups weaken C–H bonds, yielding relatively stable radicals, in turn resulting in selective CO_2 fixation [150].

Another patented system uses electrogenerated bases to deprotonate a weakly acidic hydrocarbon group forming anions which are carboxylated in the presence of CO_2. Meanwhile, proton scavengers remove protons released from the anodic regeneration of the base precursors as shown in Scheme 21 [151].

The electrogenerated bases are redox mediators, used as catalysts in the carboxylation process. The net reaction can be written as follows:

RH + CO_2 + scavenger → RCOO⁻ + innocuous scavenger reaction product.

The base precursor should be more easily electroreduced than the weakly acidic hydrocarbon group and carbon dioxide, and should not undergo a nucleophilic attack by either the hydrocarbon anion or the electrogenerated base. Therefore, the base precursor should be sterically hindered at or near the site(s) where reduction will occur. The electrogenerated base must be a strong enough Brønsted base to deprotonate the weakly acidic hydrocarbon group. Ethenetetracarboxylate tetraesters are typical base precursors, suited for the electrocarboxylation of *N*-alkyldiglycolimides (Scheme 22). This process provides a feasible route to methoxymethane-1,1,1'-tricarboxylate salts, which are excellent detergent builders. The reaction should be carried out in strictly anhydrous conditions, since water is a stronger acid than the weakly acidic hydrocarbons employed herein. Electrogenerated bromine is used to regenerate the base precursor. Via a radical bromination, followed by a nucleophilic elimination under alkaline conditions, the alkane is oxidized to the alkene base precursor. These alkaline conditions and the four electron withdrawing ethoxy carbonyl groups (R^1), prevent further bromination of the acquired double bond. Sodium carbonate is a suitable proton scavenger, providing the required alkalinity and being a convenient source of sodium ions. Crown ethers are added to dissolve the alkali metal salts in the organic solvent system. After reaction, anolyte and catholyte are filtered and base precursor and conjugate acid of electrogenerated base must be transferred to the other compartment. In this divided cell a yield of 85% for product (A) could be obtained (Scheme 22). In an undivided setup however, lower yields and current efficiencies were observed [151].

Oxalic acid is another carboxylic acid which can be formed through electrocarboxylation, namely of CO_2 itself. This complexing agent has applications in cleaning industry, dyeing processes and metallurgy [152]. Besides its easy synthesis
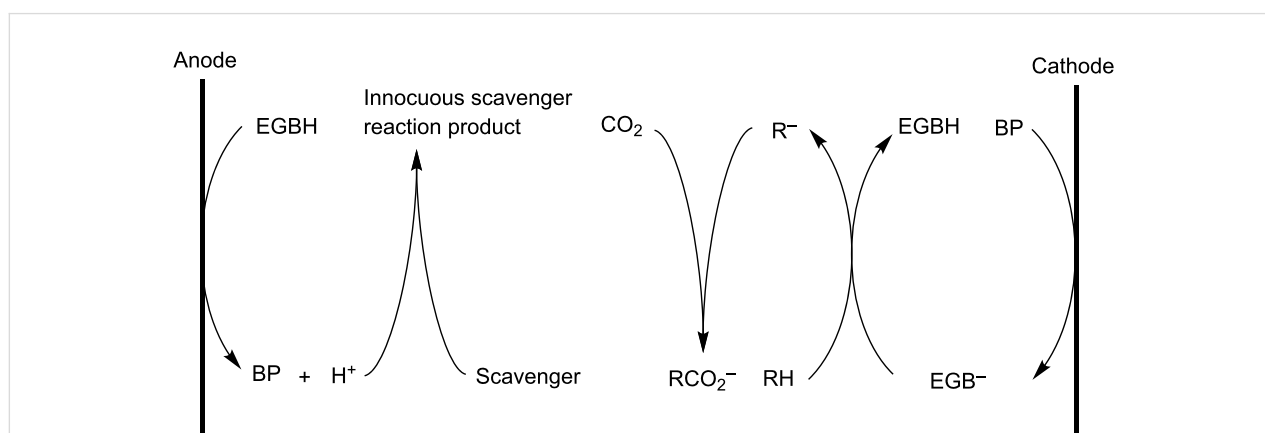

Scheme 21: General scheme of carboxylation of weak acidic hydrocarbons with electrogenerated bases. RH: weakly acidic hydrocarbon; BP: base precursor; EGB⁻: electrogenerated base; EGBH: conjugate acid of electrogenerated base [151].

Scheme 22: Electrocarboxylation of *N*-methyldiglycolimide to methoxymethane-1,1,1'-tricarboxylate precursors. R[1]: ethoxycarbonyl [151].
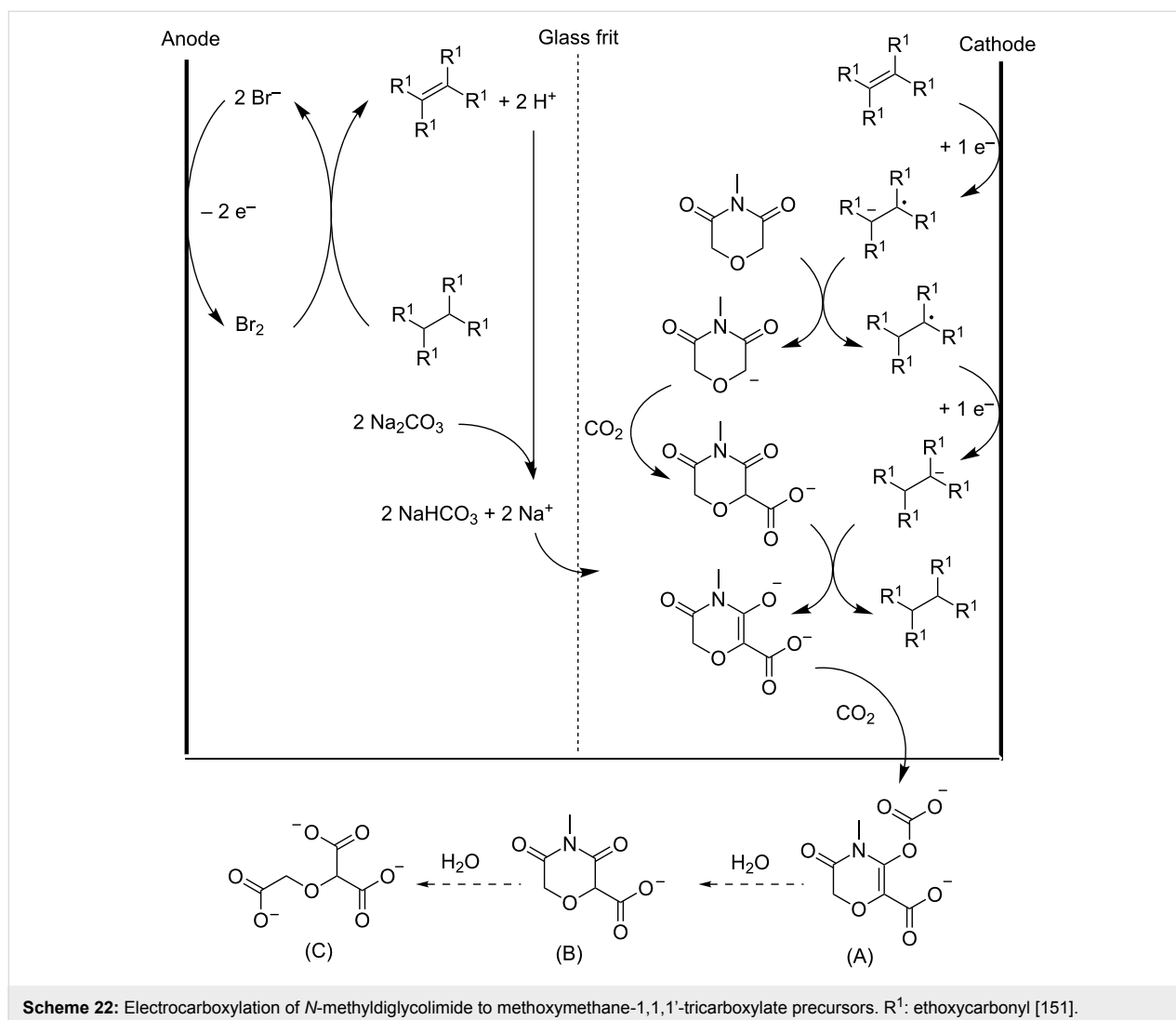
under anhydrous conditions in a cell with sacrificial anode, it can also be produced in a stable electrode setup, with current efficiencies over 50% (Scheme 23) [153]. In the catholyte an organic solvent is used while the anolyte consists of an aqueous NaCl solution. The anodically formed chlorine gas is continuously removed from the anolyte. A cation exchange membrane allows the selective transport of sodium cations to the catholyte. The sodium oxalate that is produced precipitates from the solution. A downside of this setup is the gradual transfer of water from the aqueous anolyte to the organic catholyte, this way steadily lowering the selectivity of the process [153].

Conclusion

Electrochemical reduction is an efficient approach to activate thermodynamically stable CO_2 under relatively mild and safe conditions. Electrocarboxylation allows the production of valuable carboxylic acids, through incorporation of CO_2 in a wide range of organic chemicals. This way, polymer building blocks

Scheme 23: Electrochemical dimerization of CO_2 with stable electrodes [153].
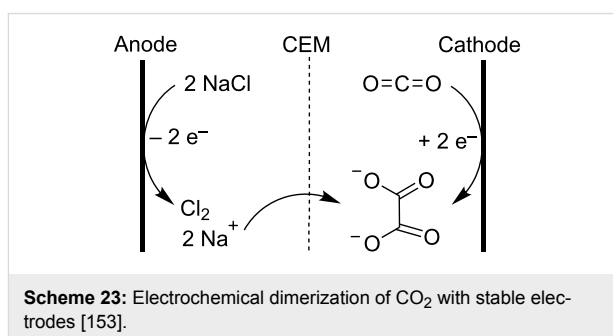
are produced from conjugated dienes, NSAIDs can easily be obtained from aromatic ketones and benzylic halides, and various other interesting applications are possible. Despite the vast amount of papers and patents on this subject, no industrial applications have emerged yet; only a couple of pilot plant scale processes have been demonstrated. The sustainable and efficient formation of carboxylic acids from carbon dioxide

presents many intriguing challenges. The choice of reactor setup, electrode type and reaction pathway, not only affects the implementation cost but also determines operational characteristics like process continuity, atom economy and current efficiency. The shortcomings illustrated in this review emphasize the need for more innovative pathways to invent even more efficient and sustainable electrocarboxylation reactions.

Acknowledgements

References

1. Proceedings of "CO$_2$ Emission from Fuels Combustion: Highlights 2012", October, 2012, Paris, France. http://www.iea.org/publications/freepublications/publication/CO2emissi onfromfuelcombustionhighlightsMarch2013.pdf (accessed October 27, 2014).
2. Hoekman, S. K.; Broch, A.; Robbins, C.; Purcell, R. *Int. J. Greenhouse Gas Control* **2010,** *4,* 44–50. doi:10.1016/j.ijggc.2009.09.012
3. Wang, W.; Wang, S.; Ma, X.; Gong, J. *Chem. Soc. Rev.* **2011,** *40,* 3703–3727. doi:10.1039/c1cs15008a
4. Ion, A.; Parvulescu, V.; Jacobs, P.; de Vos, D. *Appl. Catal., A* **2009,** *363,* 40–44. doi:10.1016/j.apcata.2009.04.036
5. Darensbourg, D. J.; Horn, A., Jr.; Moncada, A. I. *Green Chem.* **2010,** *12,* 1376–1379. doi:10.1039/c0gc00136h
6. Yang, Z.-Z.; Zhao, Y.-N.; He, L.-N.; Gao, J.; Yin, Z.-S. *Green Chem.* **2012,** *14,* 519–527. doi:10.1039/c2gc16039k
7. Tomishige, K.; Yasuda, H.; Yoshida, Y.; Nurunnabi, M.; Li, B.; Kunimori, K. *Green Chem.* **2004,** *6,* 206–214. doi:10.1039/b401215a
8. Ion, A.; Parvulescu, V.; Jacobs, P.; De Vos, D. *Green Chem.* **2007,** *9,* 158–161. doi:10.1039/b612403h
9. Ion, A.; Van Doorslaer, C.; Parvulescu, V.; Jacobs, P.; De Vos, D. *Green Chem.* **2008,** *10,* 111–116. doi:10.1039/b711197e
10. Guyer, A. Process for the manufacture of urea. U.S. Patent 2,854,482, Sept 30, 1958.
11. Krase, N. W.; Gaddy, V. L. *Ind. Eng. Chem.* **1922,** *14,* 611–615. doi:10.1021/ie50151a009
12. Aresta, M.; Dibenedetto, A. *Dalton Trans.* **2007,** 2975–2992. doi:10.1039/b700658f
13. Moore, E. R.; McDonald, D. C.; Willner, J.; Briggs, R. L. Carbonation of alkali metal phenates. U.S. Patent 4,171,453, Oct 16, 1979.
14. Kolbe, H. *Ann. Chem. Pharm.* **1860,** *113,* 125–127. doi:10.1002/jlac.18601130120
15. Schmitt, R. *J. Prakt. Chem.* **1885,** *31,* 397–411. doi:10.1002/prac.18850310130
16. Hunt, S. E.; Jones, J. I.; Lindsey, A. S.; Killoh, D. C.; Turner, H. S. *J. Chem. Soc.* **1958,** 3152–3160. doi:10.1039/jr9580003152
17. Markovic, Z.; Engelbrecht, J. P.; Markovic, S. *Z. Naturforsch.* **2002,** *57,* 812–818.
18. Rahim, M. A.; Matsui, Y.; Matsuyama, T.; Kosugi, Y. *Bull. Chem. Soc. Jpn.* **2003,** *76,* 2191–2195. doi:10.1246/bcsj.76.2191

19. Kosugi, Y.; Imaoka, Y.; Gotoh, F.; Rahim, M. A.; Matsui, Y.; Sakanishi, S. *Org. Biomol. Chem.* **2003,** *1,* 817–821. doi:10.1039/b210793g
20. Marković, Z.; Marković, S.; Manojlović, N.; Predojević-Simović, J. *J. Chem. Inf. Model.* **2007,** *47,* 1520–1525. doi:10.1021/ci700068b
21. Finnegan, R. A.; Altschuld, J. W. *J. Organomet. Chem.* **1967,** *9,* 193–204. doi:10.1016/S0022-328X(00)83721-3
22. Quirk, R. P.; Yin, J.; Fetters, L. J.; Kastrup, R. V. *Macromolecules* **1992,** *25,* 2262–2267. doi:10.1021/ma00034a030
23. Ebert, G. W.; Juda, W. L.; Kosakowski, R. H.; Ma, B.; Dong, L.; Cummings, K. E.; Phelps, M. V. B.; Mostafa, A. E.; Luo, J. *J. Org. Chem.* **2005,** *70,* 4314–4317. doi:10.1021/jo047731s
24. Correa, A.; Martín, R. *Angew. Chem., Int. Ed.* **2009,** *48,* 6201–6204. doi:10.1002/anie.200900667
25. Jitaru, M. *J. Univ. Chem. Technol. Metall.* **2007,** *42,* 333–344.
26. Schäfer, H. J. *C. R. Chim.* **2011,** *14,* 745–765. doi:10.1016/j.crci.2011.01.002
27. Agarwal, A. S.; Zhai, Y.; Hill, D.; Sridhar, N. *ChemSusChem* **2011,** *4,* 1301–1310. doi:10.1002/cssc.201100220
28. Ganesh, I. *Renewable Sustainable Energy Rev.* **2014,** *31,* 221–257. doi:10.1016/j.rser.2013.11.045
29. Cook, R. L.; MacDuff, R. C.; Sammells, A. F. *J. Electrochem. Soc.* **1988,** *135,* 1320–1326. doi:10.1149/1.2095972
30. Olah, G. A.; Prakash, G. K. S.; Goeppert, A. *J. Am. Chem. Soc.* **2011,** *133,* 12881–12898. doi:10.1021/ja202642y
31. Sequeira, C. A. C.; Santos, D. M. F. *J. Braz. Chem. Soc.* **2009,** *20,* 387–406. doi:10.1590/S0103-50532009000300002
32. Danly, D. E. *J. Electrochem. Soc.* **1984,** *131,* 435C–442C. doi:10.1149/1.2115324
33. Matthews, M. A. *Pure Appl. Chem.* **2001,** *73,* 1305–1308. doi:10.1351/pac200173081305
34. Pütter, H.; Hannebaum, H. Preparation of phthalides. U.S. Patent 6,063,256, May 16, 2000.
35. Frontana-Uribe, B. A.; Little, R. D.; Ibanez, J. G.; Palma, A.; Vasquez-Medrano, R. *Green Chem.* **2010,** *12,* 2099–2119. doi:10.1039/c0gc00382d
36. Doherty, A. P.; Christensen, P. A.; Hamnett, A.; Scott, K. *J. Electroanal. Chem.* **1995,** *386,* 39–44. doi:10.1016/0022-0728(94)03816-L
37. Li, J.; Hu, X.; Su, Y.; Li, Q. *Chem. Eng. Sci.* **2007,** *62,* 6784–6793. doi:10.1016/j.ces.2007.02.021
38. Silvestri, G.; Gambino, S.; Filardo, G. *Acta Chem. Scand.* **1991,** *45,* 987–992. doi:10.3891/acta.chem.scand.45-0987
39. Tokuda, M. *J. Nat. Gas Chem.* **2006,** *15,* 275–281. doi:10.1016/S1003-9953(07)60006-1
40. Silvestri, G.; Scialdone, O. Recent Scientific and Technological Developments in Electrochemical Carboxylation Based on Carbon Dioxide. In *Carbon dioxide as Chemical feedstock;* Aresta, M., Ed.; Wiley-VCH: Weinheim, Germany, 2010; pp 317–334. doi:10.1002/9783527629916.ch12
41. van Tilborg, W. J. M.; Smit, C. J. *Recl. Trav. Chim. Pays-Bas* **1981,** *100,* 437–438. doi:10.1002/recl.19811001113
42. Grinberg, V. A.; Koch, T. A.; Mazin, V. M.; Mysov, E. I.; Sterlin, S. R. *Russ. Chem. Bull.* **1999,** *48,* 294–299. doi:10.1007/BF02494552
43. Scott, K. *Dev. Chem. Eng. Miner. Process.* **1993,** *1,* 71–117. doi:10.1002/apj.5500010202
44. Pletcher, D.; Tietje Girault, J. *J. Appl. Electrochem.* **1986,** *16,* 791–802. doi:10.1007/BF01006524
45. Loveland, J. W. Electrolytic production of acyclic carboxylic acids from hydrocarbons. U.S. Patent 3,032,489, May 1, 1962.

46. Neikam, W. C. Electrolytic preparation of carboxylic acids. U.S. Patent 3,344,045, Sept 26, 1967.

47. Tyssee, D. A.; Wagenknecht, J. H.; Baizer, M. M.; Chruma, J. L. *Tetrahedron Lett.* **1972,** *13,* 4809–4812. doi:10.1016/S0040-4039(01)94435-1

48. Bringmann, J.; Dinjus, E. *Appl. Organomet. Chem.* **2001,** *15,* 135–140. doi:10.1002/1099-0739(200102)15:2<135::AID-AOC108>3.0.CO;2-L

49. Li, C.-H.; Yuan, G.-Q.; Ji, X.-C.; Wang, X.-J.; Ye, J.-S.; Jiang, H.-F. *Electrochim. Acta* **2011,** *56,* 1529–1534. doi:10.1016/j.electacta.2010.06.057

50. Zhang, K.; Xiao, Y.; Lan, Y.; Zhu, M.; Wang, H.; Lu, J. *Electrochem. Commun.* **2010,** *12,* 1698–1702. doi:10.1016/j.elecom.2010.09.028

51. Matthessen, R.; Fransaer, J.; Binnemans, K.; De Vos, D. E. *RSC Adv.* **2013,** *3,* 4634–4642. doi:10.1039/c3ra00129f

52. van Tilborg, W. J. M.; Smit, C. J.; Engels, R. A process for the electroreductive preparation of organic compounds. Eur. Patent 0,028,430, May 13, 1981.

53. Ballivet-Tkatchenko, D.; Folest, J.-C.; Tanji, J. *Appl. Organomet. Chem.* **2000,** *14,* 847–849. doi:10.1002/1099-0739(200012)14:12<847::AID-AOC78>3.0.CO;2-7

54. Dérien, S.; Clinet, J.-C.; Duñach, E.; Périchon, J. *Tetrahedron* **1992,** *48,* 5235–5248. doi:10.1016/S0040-4020(01)89021-9

55. Labbé, E.; Duñach, E.; Périchon, J. *J. Organomet. Chem.* **1988,** *353,* C51–C56. doi:10.1016/0022-328X(88)80330-9

56. Duñach, E.; Périchon, J. *J. Organomet. Chem.* **1988,** *352,* 239–246. doi:10.1016/0022-328X(88)83038-9

57. Duñach, E.; Dérien, S.; Périchon, J. *J. Organomet. Chem.* **1989,** *364,* C33–C36. doi:10.1016/0022-328X(89)87156-6

58. Dérien, S.; Duñach, E.; Périchon, J. *J. Am. Chem. Soc.* **1991,** *113,* 8447–8454. doi:10.1021/ja00022a037

59. Dérien, S.; Clinet, J.-C.; Duñach, E.; Périchon, J. *J. Org. Chem.* **1993,** *58,* 2578–2588. doi:10.1021/jo00061a038

60. Saito, S.; Nakagawa, S.; Koizumi, T.; Hirayama, K.; Yamamoto, Y. *J. Org. Chem.* **1999,** *64,* 3975–3978. doi:10.1021/jo982443f

61. Yuan, G.-Q.; Jiang, H.-F.; Lin, C. *Tetrahedron* **2008,** *64,* 5866–5872. doi:10.1016/j.tet.2008.04.053

62. Li, C.; Yuan, G.; Jiang, H. *Chin. J. Chem.* **2010,** *28,* 1685–1689. doi:10.1002/cjoc.201090285

63. Köster, F.; Dinjus, E.; Duñach, E. *Eur. J. Org. Chem.* **2001,** 2507–2511. doi:10.1002/1099-0690(200107)2001:13<2507::AID-EJOC2507>3.0.CO;2-P

64. Senboku, H.; Komatsu, H.; Fujimura, Y.; Tokuda, M. *Synlett* **2001,** 418–420. doi:10.1055/s-2001-11417

65. Wang, H.; Lin, M.-Y.; Fang, H.-J.; Chen, T.-T.; Lu, J.-X. *Chin. J. Chem.* **2007,** *25,* 913–916. doi:10.1002/cjoc.200790177

66. Yuan, G.-Q.; Jiang, H.-F.; Lin, C.; Liao, S.-J. *Electrochim. Acta* **2008,** *53,* 2170–2176. doi:10.1016/j.electacta.2007.09.023

67. Gambino, S.; Gennaro, A.; Filardo, G.; Silvestri, G.; Vianello, E. *J. Electrochem. Soc.* **1987,** *134,* 2172–2175. doi:10.1149/1.2100846

68. Orsini, M.; Feroci, M.; Sotgiu, G.; Inesi, A. *Org. Biomol. Chem.* **2005,** *3,* 1202–1208. doi:10.1039/b500570a

69. Wang, H.; Zhang, G.; Liu, Y.; Luo, Y.; Lu, J. *Electrochem. Commun.* **2007,** *9,* 2235–2239. doi:10.1016/j.elecom.2007.06.031

70. Wang, H.; Du, Y.-F.; Lin, M.-Y.; Zhang, K.; Lu, J.-X. *Chin. J. Chem.* **2008,** *26,* 1745–1748. doi:10.1002/cjoc.200890316

71. Lin, M.-Y.; Wang, H.; Zhang, A.-J.; Zhang, G.-R.; Lu, J.-X. *Chin. J. Org. Chem.* **2008,** *28,* 1572–1577. http://sioc-journal.cn/Jwk_yjhx/EN/abstract/abstract337403.shtml

72. Gambino, S.; Silvestri, G. *Tetrahedron Lett.* **1973,** *14,* 3025–3028. doi:10.1016/S0040-4039(01)96310-5

73. Tyssee, D. A.; Baizer, M. M. *J. Org. Chem.* **1974,** *39,* 2819–2823. doi:10.1021/jo00933a001

74. Tyssee, D. A. Electrolytic monocarboxylation of activated olefins. U.S. Patent 4,028,201, June 7, 1977.

75. Yuan, G.; Li, Z.; Jiang, H. *Chin. J. Chem.* **2009,** *27,* 1464–1470. doi:10.1002/cjoc.200990246

76. Scialdone, O.; Amatore, C.; Galia, A.; Filardo, G. *J. Electroanal. Chem.* **2006,** *592,* 163–174. doi:10.1016/j.jelechem.2006.04.009

77. Pletcher, D.; Slevin, L. *J. Chem. Soc., Perkin Trans. 2* **1996,** 217–220. doi:10.1039/p29960000217

78. Doherty, A. P. *Electrochim. Acta* **2002,** *47,* 2963–2967. doi:10.1016/S0013-4686(02)00196-2

79. Wawzonek, S.; Gundersen, A. *J. Electrochem. Soc.* **1960,** *107,* 537–540. doi:10.1149/1.2427738

80. Rieu, J.-P.; Boucherle, A.; Cousse, H.; Mouzin, G. *Tetrahedron* **1986,** *42,* 4095–4131. doi:10.1016/S0040-4020(01)87634-1

81. Zhao, S.-F.; Wu, L.-X.; Wang, H.; Lu, J.-X.; Bond, A. M.; Zhang, J. *Green Chem.* **2011,** *13,* 3461–3468. doi:10.1039/c1gc15929a

82. Zhao, S.-F.; Horne, M.; Bond, A. M.; Zhang, J. *Green Chem.* **2014,** *16,* 2242–2251. doi:10.1039/c3gc42404a

83. Feng, Q.; Huang, K.; Liu, S.; Yu, J.; Liu, F. *Electrochim. Acta* **2011,** *56,* 5137–5141. doi:10.1016/j.electacta.2011.03.061

84. Silvestri, G.; Gambino, S.; Filardo, G. *Tetrahedron Lett.* **1986,** *27,* 3429–3430. doi:10.1016/S0040-4039(00)84814-5

85. Chan, A. S. C.; Huang, T. T.; Wagenknecht, J. H.; Miller, R. E. *J. Org. Chem.* **1995,** *60,* 742–744. doi:10.1021/jo00108a047

86. Datta, A. K.; Marron, P. A.; King, C. J. H.; Wagenknecht, J. H. *J. Appl. Electrochem.* **1998,** *28,* 569–577. doi:10.1023/A:1003289800341

87. Lateef, S. K.; Raju, R. R.; Mohan, S. K.; Reddy, S. J. *Synth. Commun.* **2006,** *36,* 31–36. doi:10.1080/00397910500328811

88. Zhang, L.; Xiao, L. P.; Niu, D. F.; Luo, Y. W.; Lu, J. X. *Chin. J. Chem.* **2008,** *26,* 35–38. doi:10.1002/cjoc.200890034

89. Zhang, K.; Wang, H.; Wu, L.; Zhang, J.; Lu, J. *Chin. J. Chem.* **2010,** *28,* 509–513. doi:10.1002/cjoc.201090104

90. Zhao, S.-F.; Wang, H.; Lan, Y.-C.; Liu, X.; Lu, J.-X.; Zhang, J. *J. Electroanal. Chem.* **2012,** *664,* 105–110. doi:10.1016/j.jelechem.2011.11.001

91. Scialdone, O.; Galia, A.; Isse, A. A.; Gennaro, A.; Sabatino, M. A.; Leone, R.; Filardo, G. *J. Electroanal. Chem.* **2007,** *609,* 8–16. doi:10.1016/j.jelechem.2007.02.014

92. Silvestri, G.; Gambino, S.; Filardo, G. Process for the electrocarboxylation of carbonyl compounds, for producing alpha-hydoxycarboxylic acids. U.S. Patent 4,708,780, Nov 24, 1987.

93. Maspero, F.; Piccolo, O.; Romano, U.; Gambino, S. New process for the preparation of 2-aryl-propionic acids. U.S. Patent 5,089,661, Feb 18, 1992.

94. Wagenknecht, J. H. Electrochemical carboxylation of *p*-isobutylacetophenone. U.S. Patent 4,582,577, April 15, 1986.

95. Wagenknecht, J. H. Electrochemical carboxylation of p-isobutylacetophenone and other aryl ketones. U.S. Patent 4,601,797, July 22, 1986.

96. Zhang, K.; Wang, H.; Zhao, S.-F.; Niu, D.-F.; Lu, J.-X.
J. Electroanal. Chem. **2009,** *630,* 35–41.
doi:10.1016/j.jelechem.2009.02.013

97. Zhao, S.-F.; Zhu, M.-X.; Zhang, K.; Wang, H.; Lu, J.-X.
Tetrahedron Lett. **2011,** *52,* 2702–2705.
doi:10.1016/j.tetlet.2011.03.076

98. Chen, B.-L.; Tu, Z.-Y.; Zhu, H.-W.; Sun, W.-W.; Wang, H.; Lu, J.-X.
Electrochim. Acta **2014,** *116,* 475–483.
doi:10.1016/j.electacta.2013.11.001

99. Doherty, A. P.; Diaconu, L.; Marley, E.; Spedding, P. L.; Barhdadi, R.;
Troupel, M. *Asia-Pac. J. Chem. Eng.* **2012,** *7,* 14–23.
doi:10.1002/apj.529

100. Barrosse-Antle, L. E.; Compton, R. G. *Chem. Commun.* **2009,**
3744–3746. doi:10.1039/b906320j

101. Snuffin, L. L.; Whaley, L. W.; Yu, L. *J. Electrochem. Soc.* **2011,** *158,*
F155–F158. doi:10.1149/1.3606487

102. Weinberg, N. L.; Hoffmann, A. K.; Reddy, T. B. *Tetrahedron Lett.*
1971, *12,* 2271–2274. doi:10.1016/S0040-4039(01)96837-6

103. Hess, U. *Z. Chem.* **1980,** *20,* 148–149.

104. Hess, U.; Thiele, R. *J. Prakt. Chem.* **1982,** *324,* 385–399.
doi:10.1002/prac.19823240306

105. Silvestri, G.; Gambino, S.; Filardo, G.; Tedeschi, F.
J. Appl. Electrochem. **1989,** *19,* 946–948. doi:10.1007/BF01007947

106. Koshechko, V. G.; Titov, V. E.; Bondarenko, V. N.; Pokhodenko, V. D.
J. Fluorine Chem. **2008,** *129,* 701–706.
doi:10.1016/j.jfluchem.2008.06.010

107. Titov, V. E.; Bondarenko, V. N.; Koshechko, V. G.; Pokhodenko, V. D.
Theor. Exp. Chem. **2010,** *46,* 8–13. doi:10.1007/s11237-010-9113-6

108. Wang, H.; Zhang, K.; Chen, B. L.; Li, R. N.; Zhao, J. Q.; Lu, J. X.
Int. J. Electrochem. Sci. **2011,** *6,* 1720–1729.

109. Lehmann, T.; Schneider, R.; Weckbecker, C.; Dunach, E.; Olivera, S.
Process for the production of 2-hydroxy-4-methylmercaptobutyric acid.
U.S. Patent 6,475,370, Nov 5, 2002.

110. Reufer, C.; Hateley, M.; Lehmann, T.; Weckbecker, C.;
Sanzenbacher, R.; Bilz, J. Process for the preparation of α-substituted
carboxylic acids from the series comprising α-hydroxycarboxylic acids
and n-substituted-α-aminocarboxylic acids. U.S. Patent 7,332,067,
Feb 19, 2008.

111. Hoppe, C.-F.; Nordschild, A.; Jakob, H.; Weckbecker, C.; Roth, P.;
Imad, M. Preparing alpha-substituted carboxylic acids, comprises
cathodic carboxylation of a compound in a conducting salt and an
organic solvent containing catholyte with carbon dioxide at a diamond
cathode layer. Ger. Patent 102,011,078,468, Jan 3, 2013.

112. Engels, R.; Smit, C. J.; van Tilborg, W. J. M.
Angew. Chem., Int. Ed. Engl. **1983,** *22,* 492–493.
doi:10.1002/anie.198304921

113. Ikeda, Y.; Manda, E. *Chem. Lett.* **1984,** *13,* 453–454.
doi:10.1246/cl.1984.453

114. Baizer, M. M.; Chruma, J. L. *J. Org. Chem.* **1972,** *37,* 1951–1960.
doi:10.1021/jo00977a020

115. Wawzonek, S.; Shradel, J. M. *J. Electrochem. Soc.* **1979,** *126,*
401–403. doi:10.1149/1.2129051

116. Silvestri, G.; Gambino, S.; Filardo, G.; Gulotta, A.
Angew. Chem., Int. Ed. Engl. **1984,** *23,* 979–980.
doi:10.1002/anie.198409791

117. Sock, O.; Troupel, M.; Périchon, J. *Tetrahedron Lett.* **1985,** *26,*
1509–1512. doi:10.1016/S0040-4039(00)98538-1

118. Heintz, M.; Sock, O.; Saboureau, C.; Périchon, J. *Tetrahedron* **1988,**
44, 1631–1636. doi:10.1016/S0040-4020(01)86724-7

119. Isse, A. A.; Gennaro, A. *Chem. Commun.* **2002,** 2798–2799.
doi:10.1039/b206746c

120. Gennaro, A.; Sánchez-Sánchez, C. M.; Isse, A. A.; Montiel, V.
Electrochem. Commun. **2004,** *6,* 627–631.
doi:10.1016/j.elecom.2004.04.019

121. Isse, A. A.; Ferlin, M. G.; Gennaro, A. *J. Electroanal. Chem.* **2005,**
581, 38–45. doi:10.1016/j.jelechem.2005.04.007

122. Aishah, A. J.; Hartini, M. A.; Normala, S.; Norhuda, A. M.;
Hanis, H. H. N.; Razif, H. M.; Sugeng, T. *J. Nat. Gas Chem.* **2007,** *16,*
273–277. doi:10.1016/S1003-9953(07)60059-0

123. Niu, D.-F.; Xiao, L.-P.; Zhang, A.-J.; Zhang, G.-R.; Tan, Q.-Y.;
Lu, J.-X. *Tetrahedron* **2008,** *64,* 10517–10520.
doi:10.1016/j.tet.2008.08.093

124. Niu, D.; Zhang, J.; Zhang, K.; Xue, T.; Lu, J. *Chin. J. Chem.* **2009,** *27,*
1041–1044. doi:10.1002/cjoc.200990174

125. Lan, Y.-C.; Wang, H.; Wu, L.-X.; Zhao, S.-F.; Gu, Y.-Q.; Lu, J.-X.
J. Electroanal. Chem. **2012,** *664,* 33–38.
doi:10.1016/j.jelechem.2011.10.011

126. Hiejima, Y.; Hayashi, M.; Uda, A.; Oya, S.; Kondo, H.; Senboku, H.;
Takahashi, K. *Phys. Chem. Chem. Phys.* **2010,** *12,* 1953–1957.
doi:10.1039/b920413j

127. Feng, Q.; Huang, K.; Liu, S.; Wang, X. *Electrochim. Acta* **2010,** *55,*
5741–5745. doi:10.1016/j.electacta.2010.05.010

128. Scialdone, O.; Galia, A.; Silvestri, G.; Amatore, C.; Thouin, L.;
Verpeaux, J.-N. *Chem. – Eur. J.* **2006,** *12,* 7433–7447.
doi:10.1002/chem.200501499

129. Troupel, M.; Rollin, Y.; Périchon, J.; Fauvarque, J. F. *Nouv. J. Chim.*
1981, *2,* 621–625.

130. Amatore, C.; Jutand, A. *J. Am. Chem. Soc.* **1991,** *113,* 2819–2825.
doi:10.1021/ja00008a003

131. Gennaro, A.; Isse, A. A.; Maran, F. *J. Electroanal. Chem.* **2001,** *507,*
124–134. doi:10.1016/S0022-0728(01)00373-4

132. Amatore, C.; Jutand, A.; Khalil, F.; Nielsen, M. F. *J. Am. Chem. Soc.*
1992, *114,* 7076–7085. doi:10.1021/ja00044a018

133. Folest, J.-C.; Duprilot, J.-M.; Périchon, J.; Robin, Y.; Devynck, J.
Tetrahedron Lett. **1985,** *26,* 2633–2636.
doi:10.1016/S0040-4039(00)98122-X

134. Isse, A. A.; Gennaro, A.; Vianello, E. *J. Chem. Soc., Dalton Trans.*
1996, 1613–1618. doi:10.1039/dt9960001613

135. Zheng, G.; Stradiotto, M.; Li, L. *J. Electroanal. Chem.* **1998,** *453,*
79–88. doi:10.1016/S0022-0728(98)00173-9

136. Chung, W.-H.; Guo, P.; Wong, K.-Y.; Lau, C.-P. *J. Electroanal. Chem.*
2000, *486,* 32–39. doi:10.1016/S0022-0728(00)00125-X

137. Fabre, P.-L.; Reynes, O. *Electrochem. Commun.* **2010,** *12,*
1360–1362. doi:10.1016/j.elecom.2010.07.020

138. Chaussard, J.; Troupel, M.; Robin, Y.; Jacob, G.; Juhasz, J. P.
J. Appl. Electrochem. **1989,** *19,* 345–348. doi:10.1007/BF01015234

139. Chanfreau, S.; Cognet, P.; Camy, S.; Condoret, J.-S.
J. Supercrit. Fluids **2008,** *4,* 156–162.
doi:10.1016/j.supflu.2008.04.003

140. Fauvarque, J. F.; Jutand, A.; Francois, M. *J. Appl. Electrochem.* **1988,**
18, 109–115. doi:10.1007/BF01016213

141. Fauvarque, J. F.; De Zelicourt, Y.; Amatore, C.; Jutand, A.
J. Appl. Electrochem. **1990,** *20,* 338–340. doi:10.1007/BF01033614

142. Olloqui-Sariego, J. L.; Molina, V. M.; González-Arjona, D.; Roldán, E.;
Domínguez, M. *J. Electrochem. Soc.* **2010,** *157,* E64–E68.
doi:10.1149/1.3299365

143. Olloqui-Sariego, J. L.; Molina, V. M.; González-Arjona, D.; Roldán, E.;
Domínguezz, M. *J. Electrochem. Soc.* **2008,** *155,* E157–E161.
doi:10.1149/1.2971028

144. Grinberg, K. A.; Koch, T. A.; Mazin, E. M.; Mysov, E. I.; Sterlin, S. R. *Russ. Chem. Bull.* **1997,** *46,* 1560–1564. doi:10.1007/BF02502939

145. Scialdone, O.; Galia, A.; Belfiore, C.; Filardo, G.; Silvestri, G. *Ind. Eng. Chem. Res.* **2004,** *43,* 5006–5014. doi:10.1021/ie034275+

146. Isse, A. A.; Gennaro, A. *J. Electrochem. Soc.* **2002,** *149,* D113–D117. doi:10.1149/1.1490358

147. Batanero, B.; Barba, F.; Sánchez-Sánchez, C. M.; Aldaz, A. *J. Org. Chem.* **2004,** *69,* 2423–2426. doi:10.1021/jo0358473

148. Scialdone, O.; Sabatino, M. A.; Galia, A.; Filardo, G.; Silvestri, G. *J. Electroanal. Chem.* **2008,** *614,* 175–178. doi:10.1016/j.jelechem.2007.11.012

149. Tyssee, D. A. Electrolytic carboxylation of acetonitrile and alpha-substituted acetonitriles. U.S. Patent 3,945,896, March 23, 1976.

150. Otero, M. D.; Batanero, B.; Barba, F. *Tetrahedron Lett.* **2006,** *47,* 2171–2173. doi:10.1016/j.tetlet.2006.01.113

151. Hallcher, R. C.; Baizer, M. M.; White, D. A. Electrolytic carboxylation of carbon acids via electrogenerated bases. U.S. Patent 4,072,583, Feb 7, 1978.

152. Riemenschneider, W.; Tanifuji, M. Oxalic acid. In *Ullmann's Encyclopedia of Industrial Chemistry;* Elvers, B.; Noethe, H., Eds.; Wiley-VCH: Weinheim, Germany, 2002. doi:10.1002/14356007.a18_247

153. Goodridge, F.; Presland, G. *J. Appl. Electrochem.* **1984,** *14,* 791–796. doi:10.1007/BF00615269

An integrated photocatalytic/enzymatic system for the reduction of CO$_2$ to methanol in bioglycerol–water

Michele Aresta[*1,2], Angela Dibenedetto[*3,4], Tomasz Baran[4,5], Antonella Angelini[3,4], Przemysław Łabuz[5] and Wojciech Macyk[5]

Abstract

A hybrid enzymatic/photocatalytic approach for the conversion of CO$_2$ into methanol is described. For the approach discussed here, the production of one mol of CH$_3$OH from CO$_2$ requires three enzymes and the consumption of three mol of NADH. Regeneration of the cofactor NADH from NAD$^+$ was achieved by using visible-light-active, heterogeneous, TiO$_2$-based photocatalysts. The efficiency of the regeneration process is enhanced by using a Rh(III)-complex for facilitating the electron and hydride transfer from the H-donor (water or a water–glycerol solution) to NAD$^+$. This resulted in the production of 100 to 1000 mol of CH$_3$OH from one mol of NADH, providing the possibility for practical application.

Introduction

The reduction of CO$_2$ to fuel is a technology that could contribute to the recycling of large quantities of carbon. Among the various routes, the enzymatic reduction of CO$_2$ in inexpensive H-donor solvents to produce methanol (or other C$_1$ molecules) is an attractive option. Redox enzymes are of industrial interest as they may catalyze reactions in which the use of conventional chemical catalysts is restricted [1]. Unfortunately,

their application is quite limited due to the high cost of their cofactors. A huge effort is being made for the in situ regeneration of these cofactors using various approaches such as: the use of secondary enzymes, electrochemical regeneration, or even the use of living cells. Noteworthy is that the regeneration of the cofactor often involves the potential production of a variety of isomers of the active species or even the formation of dimers

that may not be active in promoting the enzymatic reaction or may even act as inhibitors. In nature, cofactors are usually regenerated via enzymatic reactions. One of the most interesting cofactors is nicotinamide adenine dinucleotide (NAD^+), a cofactor of the oxydoreductase class of enzymes. NAD^+, together with its reduced form, 1,4-NADH, plays an essential role in many metabolic processes of living cells. NADH is also important in industrial biocatalysis, namely in the process of reductive synthesis of chiral organic compounds [2,3].

Currently, the enzymatic reduction of carbon dioxide is under investigation as a possible route for fuel production [4]. A specific application, which leads to the production of methanol, occurs in water through three $2e^-$ steps based on the use of three enzymes, namely: formate dehydrogenase ($F_{ate}DH$), formaldehyde dehydrogenase ($F_{ald}DH$), and alcohol dehydrogenase (ADH). These enzymes promote the cascade reduction of CO_2 to methanol through formic acid ($F_{ate}DH$), formaldehyde ($F_{ald}DH$) and aldehyde (ADH). The reduction process is enabled by NADH, which is oxidized to NAD^+. However, the production of one mole of CH_3OH from CO_2 requires the consumption of three moles of NADH (Figure 1).

Figure 1: CO_2 reduction to methanol in water promoted by $F_{ate}DH$, $F_{ald}DH$ and ADH where three consecutive $2e^-$ steps are involved.
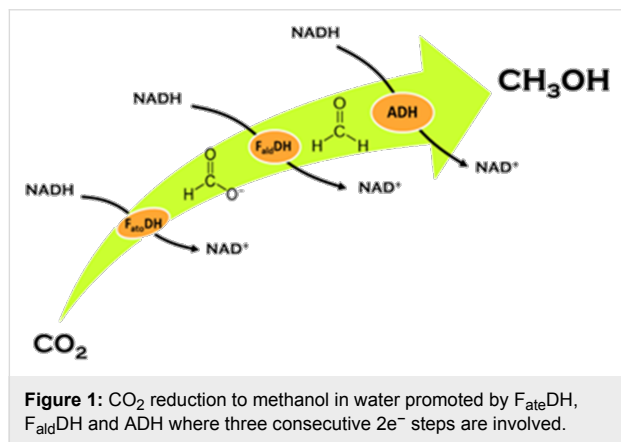
Therefore, the regeneration of NADH is necessary for practical application of the described process. In nature, the endergonic process of NAD^+ reduction to NADH is performed with the help of solar energy during photosynthesis. Presently, a substantial effort is being made for the regeneration of 1,4-NADH using a variety of strategies, including the use of enzymatic catalysis, as well as chemical, electrochemical and photochemical methods [5,6]. For industrial application, such reduction would require implementation of the most energetically and economically convenient technologies, such as visible-light-driven photocatalysis, as chemical methods are either too expensive or not compatible with the enzymes [7]. To date, photocatalysis has shown great potential for photodegradation of environmental pollutants [8,9]. Most interesting is that photo-

catalysis may play a relevant role in the conversion of large quantities of CO_2 into fuel by using water or waste organics as the hydrogen source [7,10,11]. Therefore, integrated photochemical CO_2 reduction/organic oxidation and H_2O splitting have received significant interest due to their potential environmental and resource preservation benefits [12,13]. Interestingly, the oxidized forms of some common waste organics may find practical application.

The use of heterogeneous photocatalysts in the process of NADH regeneration from NAD^+ would be of great interest due to their low cost, moderate (ambient) operational conditions and acceptable environmental impact. The most extensively applied photochemical processes are based on the use of TiO_2 as a photocatalyst in oxidation reactions [14-16]. While pure TiO_2 has a band gap energy of 3.2 eV (which is not compatible for use with visible light), modified TiO_2 is known to be more suitable for carrying out photocatalytic processes utilizing the visible part of the solar spectrum [17].

In previous work, systems based on stable, encapsulated enzymes [7] for the enzymatic reduction of CO_2 to CH_3OH in water combined with the near-UV–vis light driven photoregeneration of NADH for increasing the CH_3OH/NADH molar ratio was described [7]. However, this approach is a hybrid process involving: the enzymatic reduction of CO_2 to CH_3OH promoted by the reduced form of cofactor NADH, and the in situ photocatalytic reduction of NAD^+ to NADH under visible-light irradiation, using semiconductors in water/bioglycerol mixtures. Bioglycerol is being produced in increasing volumes for biodiesel production from oleaginous seeds. New applications for this product are being investigated [7,11,18,19] and its use as a H-source providing its oxidized derivatives (or even C_2 molecules [11]) may be an interesting path for the economically viable use of large volumes of CO_2. Our ultimate goal is to attain a highly efficient and selective reduction of NAD^+ to 1,4-NADH or other equally active isomers upon visible-light irradiation in order to make the enzymatic reduction of CO_2 to CH_3OH viable.

Results and Discussion

In previous work [7] we demonstrated that encapsulated $F_{ate}DH$, $F_{ald}DH$, and ADH enzymes are able to rapidly (<1 min) reduce CO_2 in proton–donor solvents under pH-controlled conditions, resulting in CH_3OH at room temperature. The regeneration of NADH was attempted using both chemical and photochemical techniques. The former affects the enzymes that are quickly deactivated, while the latter techniques are more interesting and produce up to a few mol of methanol per mol of NADH (with respect to 3 NADH per methanol) as shown in Figure 1. As previously discussed [7],

the success of the regeneration depends on the separation of the enzymatic reduction from the photoregeneration of NADH, thus a two-compartment reactor was used (see the Experimental section). In fact, the light most likely affects the enzyme activity by inducing structural modifications. In [7] a photocatalyst was used that operates on the border of the UV–vis spectrum. As described above, the goal of this research is to work in the visible-light range, possibly using direct irradiation with solar light. Therefore, we have synthesized a number of semiconducting materials showing photocatalytic activity under visible-light irradiation. The most active material was selected and fully characterized regarding its photoelectrical- and chemical-properties. Optimal conditions for use with visible light for the reduction of NAD^+ using bioglycerol as a H-donor and a Rh(III)-complex as an e^-–H^+ transfer agent were found. It was shown that the photocatalyst, the electron mediator and the H-donor have suitable energy levels that can be combined together for an effective recycling of NAD^+. The cofactor can be used several times in combination with the encapsulated enzymes, which promote the reduction of CO_2 to methanol. In this work we discuss in detail the utilization of a new TiO_2 photocatalyst (Degussa P25 or 10 nm particles produced in-house [20]) modified with the inorganic complex $[CrF_5(H_2O)]^{2-}$ [20]. Additionally, the properties of other photocatalysts (Cu_2O, $InVO_4$, and TiO_2, which are less active than the Cr-modified TiO_2 photocatalysts), which were modified with the organic compound "rutin", are briefly presented. Figure 2 shows the transformed diffuse reflectance spectra of the photocatalysts converted by the Kubelka–Munk function.

The properties of the photocatalysts used can be summarized as follows. Cu_2O is a visible-light-absorbing, red-colored, *p*-type

Figure 2: Transformed diffuse reflectance spectra of photocatalysts used in the present study.
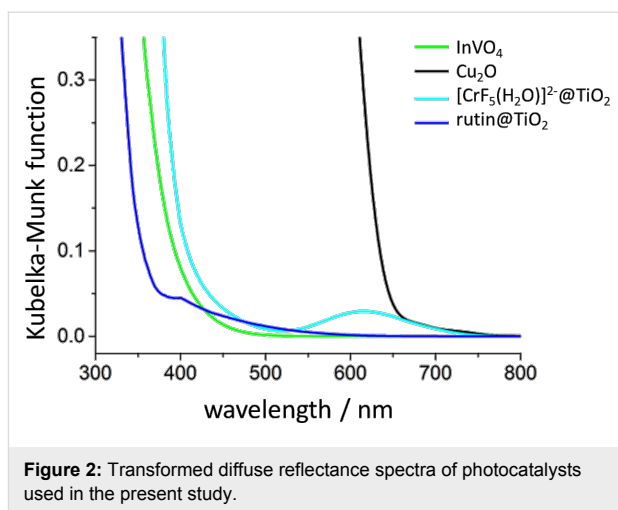
semiconductor with the band gap energy equal of 2.1 eV. $InVO_4$ is an *n*-type semiconductor (E_{bg} = 2.8 eV). TiO_2 modified with the organic compound rutin (rutin@TiO_2) shows an electron injection into the conduction band of TiO_2 as the result of a direct molecule-to-band charge transfer (MBCT) within the surface-formed, colored, charge-transfer complex of titanium(IV) [21]. TiO_2 with an adsorbed chromium(III) anionic complex $[CrF_5(H_2O)]^{2-}$ acts as a photosensitizer by injecting electrons into the conduction band of titania [20].

Photocatalytic tests of NADH regeneration using these materials have been performed using visible light irradiation (λ > 400 nm). The results are summarized in Figure 3.

Figure 3a shows that the conversion yield of NAD^+ into NADH is similar for the various photocatalysts. Additionally, the selec-
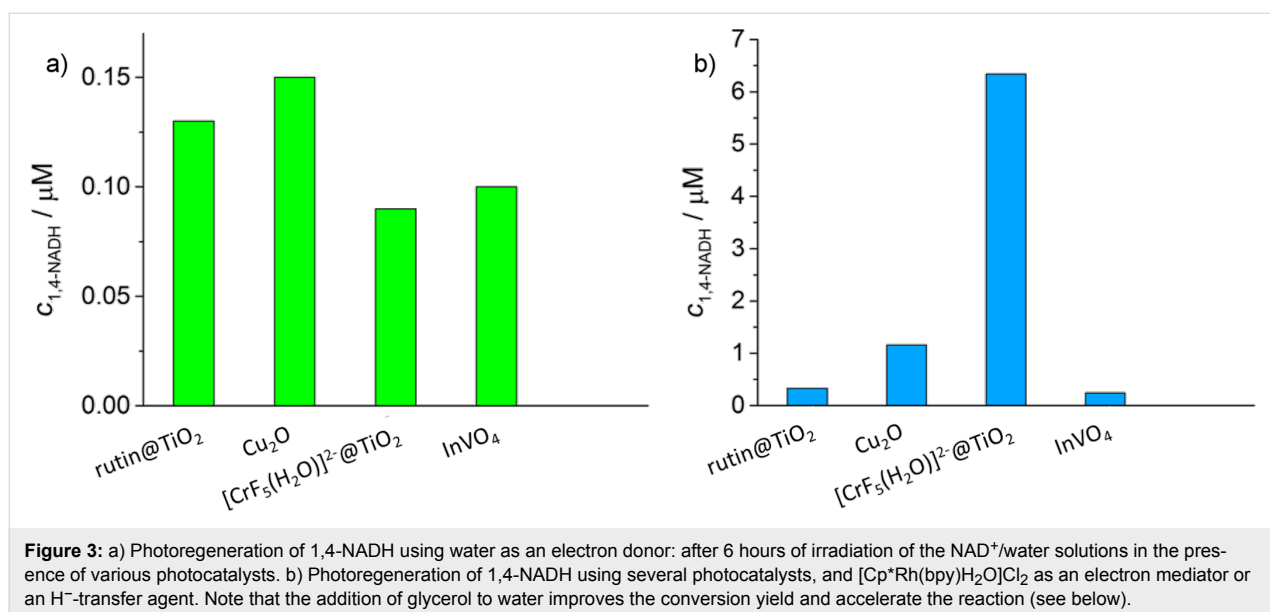
Figure 3: a) Photoregeneration of 1,4-NADH using water as an electron donor: after 6 hours of irradiation of the NAD^+/water solutions in the presence of various photocatalysts. b) Photoregeneration of 1,4-NADH using several photocatalysts, and [Cp*Rh(bpy)H₂O]Cl₂ as an electron mediator or an H^--transfer agent. Note that the addition of glycerol to water improves the conversion yield and accelerate the reaction (see below).

tivity towards 1,4-NADH appears to be not very high. The concentration of the photogenerated, reduced form of the cofactor after 6 hours of visible-light irradiation in the presence of water is within the range of 0.1–0.15 µM. Noteworthy is that no or negligible reaction was observed when any of the components of the system was missing: photocatalyst, light, NAD^+, or water. TiO_2 alone was tested as a reference material yielding only minor traces of a complex mixture of products under the same experimental conditions. HPLC in combination with NMR analysis was employed for the detection of the various isomers of the NAD^+-reduction products, namely the 1,4-NADH, 1,2-NADH, 1,6-NADH, or dimeric species. We have observed that when the photocatalysts alone were used, the selectivity towards 1,4-NADH was significantly lower than 100%. In fact the low amount of 1,4-NADH reported in Figure 3a is due to NAD^+ conversion resulting in a mixture of compounds (including dimers) with a low selectivity (approximately 5%) towards 1,4-NADH. This is most likely due to the fact that the reactions take place on the surface of the photocatalyst without any selectivity. Conversely, the regeneration of 1,4-NADH was much more efficient via an indirect route of H^+–e^- transfer, using hydride-transfer agents coupled to the photocatalytic materials. To implement such a strategy, the above described photoactive materials were coupled to the well-known [22] [Cp*Rh(bpy)(H_2O)]Cl_2 [aquo(2,2'-bipyridine)(pentamethylcyclopentadienyl)]rhodium(III), where Cp* = pentamethylcyclopentadienyl. For comparison we have also used its iridium analog, with phenantroline as a bidentate N-ligand replacing bpy. Iridium showed interesting activity, comparable to that of Rh. A key point in our approach was to demonstrate that the H^+–e^- transfer system (photocatalyst, transition metal complex) we designed had an ideal potential for e^- transfer and could operate in combination with the H-donor and the enzyme to eventually convert CO_2 into CH_3OH. The success of this system was evidenced by measuring the amount of photogenerated 1,4-NADH using water or water/glycerol as electron donor. Figure 3b illustrates the results of the photocatalytic regeneration of NADH in presence of various materials after 6 hours of irradiation. Interestingly, for $[CrF_5(H_2O)]^{2-}$@TiO_2 the yield is 70 times higher in the presence of the electron mediator (under the same experimental conditions). The Cr-modified TiO_2 showed the highest activity among the tested photocatalysts [20] and thus, the focus of the discussion is now shifted to this photocatalyst. Although CrF_3-doped TiO_2 is reported in the literature [8] to be active in oxidation processes of waste organics, neither TiO_2 loaded with anionic $[CrF_5(H_2O)]^{2-}$ nor CrF_3 on TiO_2 (used for reduction purposes) has been described so far.

The ^{19}F NMR spectrum confirms the presence of the anionic form on the TiO_2 surface with a signal at 121 ppm, while free

$[CrF_5(H_2O)]^{2-}$ shows a signal at 122 ppm (see Experimental section). In contrast, CrF_3 has signals in a completely different region (−127 and −128 ppm). Therefore, we conclude that the supported form of Cr on TiO_2 is the anionic complex $[CrF_5(H_2O)]^{2-}$. Another issue in this process was to demonstrate whether the reduction is selective towards 1,4-NADH and no other isomers or if dimers were formed. The answer to this question was provided by using ^1H and ^{13}C NMR in connection with HPLC. The anionic pentafluorochromate-modified TiO_2 coupled to the Rh(Ir)-transition metal complex appeared very selective towards 1,4-NADH, while neither isomers nor dimers were formed. Figure 4 shows typical ^1H NMR spectra recorded during the course of the reduction: a pseudo-quartet centered at 2.65 ppm increases with time showing that the reaction occurs.
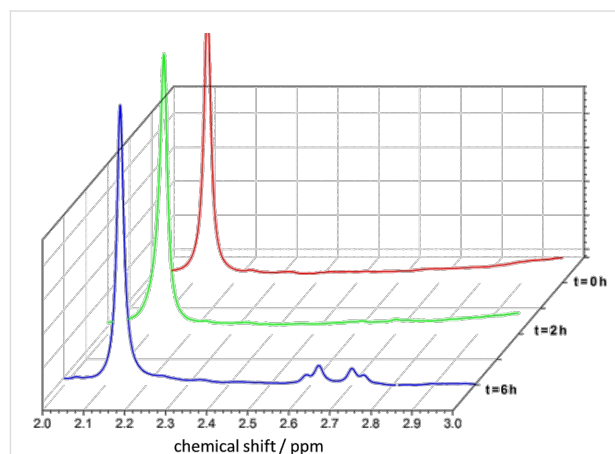

Figure 4: ^1H NMR spectra recorded at *t* = 0, after 2 and 6 h of irradiation in water. The selected range, 2–3 ppm, is diagnostic for NADH H-signals. The signal at 2.1 ppm results from the ribose hydrogen in the cofactor molecule and is taken as a reference peak. The concentration of the rhodium complex is 0.5 mM, with $c_{glycerol}$ = 0.05 M.

This signal is due to 1,4-NADH, as shown in Figure 5. Here, the ^1H NMR spectrum of standard NADH (a commercially available product) is compared with the spectra of the reduction products formed in presence and absence of the hydride-transfer agent used together with the $[CrF_5(H_2O)]^{2-}$@TiO_2 photocatalyst. The green and blue spectra were taken after 6 h of irradiation with solar light or white light under the same operative conditions with and without the Rh complex. They show that the presence of the Rh mediator improves the conversion rate.

It is known that the reduction of the $[Cp*Rh(bpy)(H_2O)]^{2+}$ **1** complex to [Cp*Rh(bpy)] **2** adds a proton and results in the conversion into a hydrido form. This product is an efficient and selective reduction catalysts of NAD^+ to 1,4-NADH [22]. The resulting active hydrido form, [Cp*Rh(bpy)H]+ **3**, transfers a hydride ion to the 4-position of NAD^+ (coordination to the
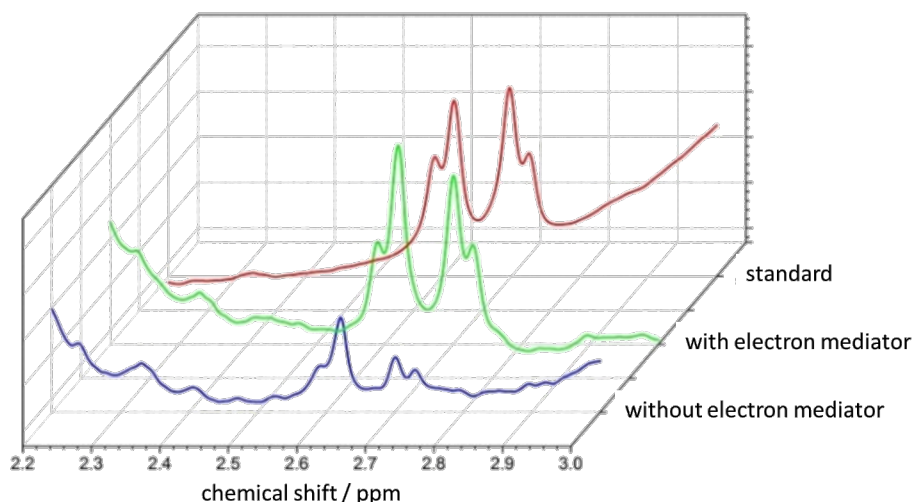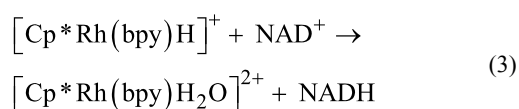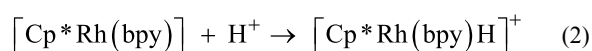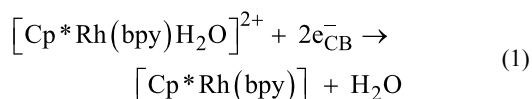
Figure 5: ^{1}H NMR spectrum of a standard 1,4-NADH (red line), and of 1,4-NADH formed from NAD$^+$ upon photocatalysis in the absence (blue) and the presence (green) of the Rh-complex as a mediator and [CrF$_5$(H$_2$O)]$^{2-}$@TiO$_2$ as a photocatalyst.

amide-carbonyl-O-atom) thereby exclusively forming the enzymatically active, reduced 1,4-NADH. The purported mechanism, based on the rhodium complex, has been proposed elsewhere [16,23], and is shown in Equations 1–3.

$$\left[Cp*Rh(bpy)H_2O \right]^{2+} + 2e^-_{CB} \rightarrow$$
$$\left[Cp*Rh(bpy) \right] + H_2O \tag{1}$$

$$\left[Cp*Rh(bpy) \right] + H^+ \rightarrow \left[Cp*Rh(bpy)H \right]^+ \tag{2}$$

$$\left[Cp*Rh(bpy)H \right]^+ + NAD^+ \rightarrow$$
$$\left[Cp*Rh(bpy)H_2O \right]^{2+} + NADH \tag{3}$$

We have carried out dedicated experiments to confirm that such a mechanism holds in our conditions, and that the e$^-$-transfer is thermodynamically and kinetically possible. This enables identification of the intermediates in the reaction pathway of the photocatalytic cycle based on [CrF$_5$(H$_2$O)]$^{2-}$@TiO$_2$ as an exciton generator and confirmation that the rhodium complex is an e$^-$-transfer agent. The redox potential of the [Cp*Rh(bpy)H$_2$O]$^{2+}$/[Cp*Rh(bpy)H]$^+$ couple was determined by Steckhan et al. and was shown to be equal to −0.32 V vs NHE. The redox potential of the conduction band of [CrF$_5$(H$_2$O)]$^{2-}$@TiO$_2$ is −0.58 V vs NHE, as measured in the present study using a previously published methodology [24]. The electrode covered by [CrF$_5$(H$_2$O)]$^{2-}$@TiO$_2$ generates a photocurrent upon visible light irradiation, proving a photoinduced electron transfer from the excited chromium(III) com-

plex to the conduction band of TiO$_2$ (Figure 6). The following step, that is, the transfer of electrons from the conduction band of the photocatalyst to the oxidized form of the rhodium complex (according to Equation 1), is thus thermodynamically feasible.
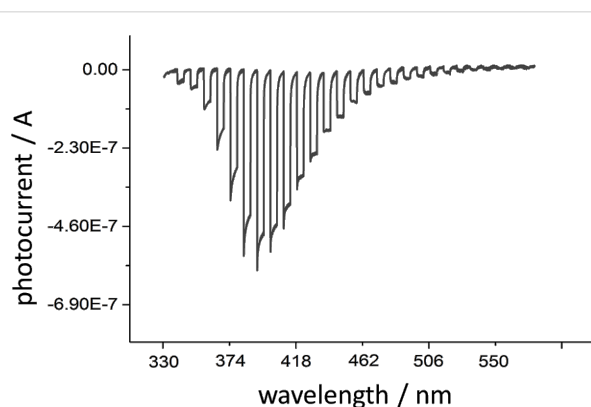
Figure 6: Photocurrent generated at the [CrF$_5$(H$_2$O)]$^{2-}$@TiO$_2$ electrode as a function of the wavelength of the incident light, recorded at constant potential of 500 mV vs Ag/AgCl. The spikes originate from the opening and closing of the shutter.

The photogenerated holes can regain electrons via the oxidation of glycerol. The reduced complex (Rh(I)) reacts with a proton yielding a Rh(III)-hydrido species (Equation 2). The resulting Rh-hydrido-species transfers the hydride to NAD$^+$ affording NADH (Equation 3 and Figure 7).

Such steps, already hypothesized in the literature [23,25], are clearly demonstrated in the present work through the following

Figure 7: Expected role of the rhodium complex as an electron mediator.
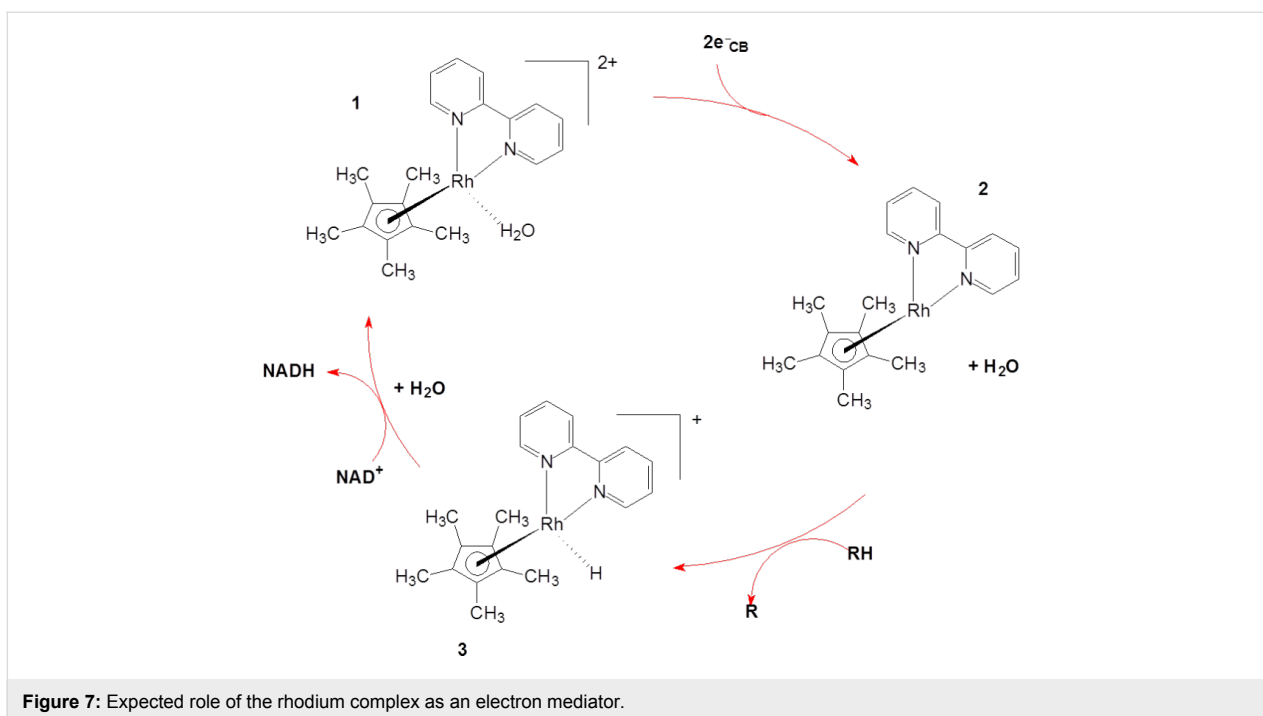
experiments. First, $[Cp*Rh(bpy)H_2O]^{2+}$ was converted into $[Cp*Rh(bpy)H]^+$ upon reaction with elemental hydrogen. The UV–vis absorption spectrum recorded after the reaction shows the appearance of a band at 521 nm that is characteristic of the formation of the rhodium hydride. This was confirmed by taking the spectrum of the isolated complex. The addition of NAD^+ resulted in NADH formation (a band at around 344 nm) in concurrence with the disappearance of the 521 nm band (Figure 8). The formation–disappearance of the hydride was further confirmed by ^1H NMR where a signal at −7.5 ppm (in the same region as the analog $[Cp*Rh(6,6'-dimethyl-2,2'-bipy)H]^+$ [22]) was evident. This ^1H NMR signal was correlated with the disappearance of the 521 nm band in the UV–vis spectrum, along with the appearance of the characteristic band at approximately 344 nm. The process was cyclic and the appearance–disappearance of the hydride signal followed the change in position of the UV–vis band from 521 to 344 nm and back.

The spectral changes in the spectrum of $[CrF_5(H_2O)]^{2-}$ are reported in Figure 9 together with the cyclic voltammograms.

The new combined system described in this paper has very high activity and specificity upon visible light irradiation. The extraordinary activity of $[CrF_5(H_2O)]^{2-}@TiO_2$ can be explained by an efficient photoinduced electron transfer from Cr(III) to the conduction band of TiO_2 and further to the adsorbed rhodium complex. A hindered back electron transfer from the Rh species to the photocatalyst can also be responsible for the overall effi-
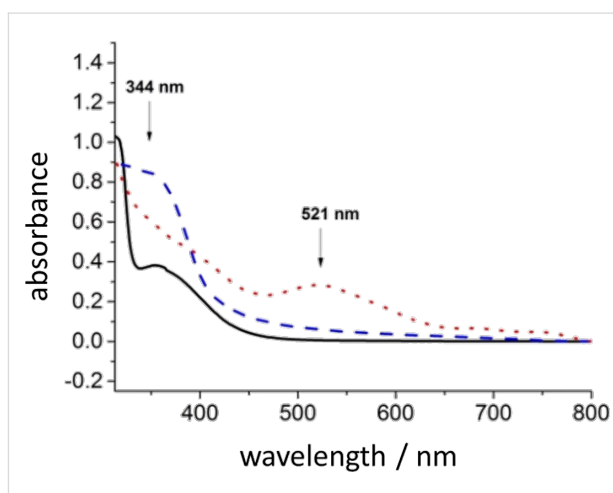
Figure 8: UV–vis absorption spectra of an aqueous solution of $[Cp*Rh(bpy)(H_2O)]^{2+}$. Continuous black line: spectrum of the starting rhodium complex in water. Dotted red line: spectrum of the rhodium complex after treatment with hydrogen. Dashed blue line: spectrum of the rhodium-hydrido complex after addition of NAD^+: the band at 521 nm disappears and the band at 344 nm attributed to NADH appears.

ciency of the process. Substitution of Rh with Ir and of bipyridine with phenanthroline did not improve the yield to appreciable extent, thus the Rh-complex was used. Other photomaterials which are active upon visible light irradiation were also tested, such as Fe/ZnS, Co/ZnS, Ag/ZnS, $ZnBiO_4$, $AgVO_4$, NiO, $CrF_3@TiO_2$, tiron@TiO_2. However, they did not show significant activity in the NADH photoregeneration process when compared to the $[CrF_5(H_2O)]^{2-}@TiO_2$ photocatalyst.

Figure 9: Spectral changes of the [Cp*Rh(bpy)(H₂O)]²⁺ solution as a function of the applied potential (left). Cyclic voltammogram and corresponding changes in absorbance recorded at 521 nm (right). For simplicity, only the part of the potential scan (the reduction process from −0.4 to −1.4 V and back) is shown.
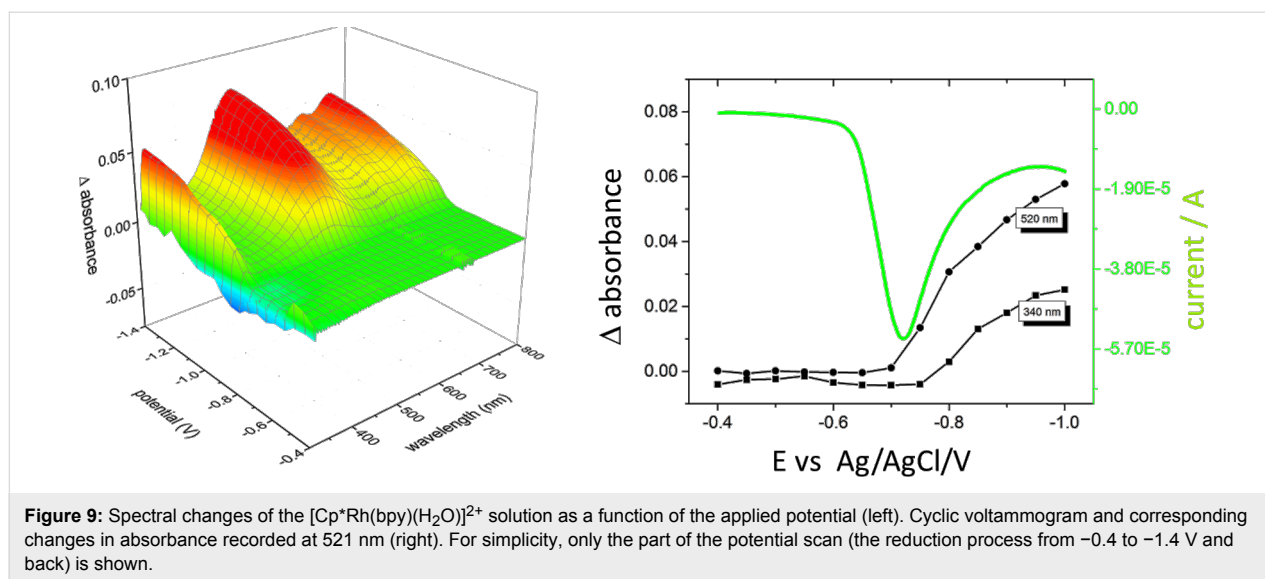
As mentioned above, glycerol was considered as an electron donor in aqueous solution. When only water was used in the photoreduction, the reaction rate was very low due to the weak ability of H_2O to transfer electrons. Figure 10 shows the influence of the nature of the electron donor and the concentration of the electron mediator, on the reduction rate.

Figure 10: Photoreduction of NAD^+ as a function of concentration of glycerol (black line) and [Cp*Rh(bpy)H₂O]Cl₂ (red line) under visible light irradiation in the presence of [CrF₅(H₂O)]²⁻@TiO₂ (irradiation time; 6 h).
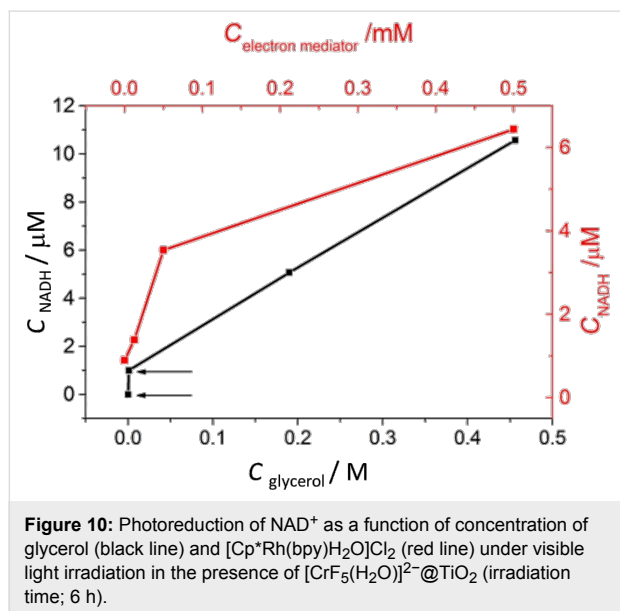
The NADH regeneration rate exhibits a strong dependence on the concentration of glycerol, which plays the crucial role of a sacrificial electron donor. Figure 10 also shows that the increase of the glycerol concentration from 0 M (the lowest point on the black line in Figure 10) to 0.001 M (the second point in the same figure) results in an extremely rapid increase of the reaction rate. It must be emphasized that the reaction in the pres-

ence of other electron donors, such as triethanolamine or isopropanol, was also tested but were not comparable with glycerol. For practical applications the mixture of glycerol 0.1–0.5 M in water was used.

Figure 10 shows also the influence of the concentration of [Cp*Rh(bpy)H₂O]Cl₂ on the reduction of NAD^+ to 1,4-NADH. The rate greatly increases with an increasing concentration of the electron mediator.

These findings demonstrate that the photocatalysts described in this paper are able to utilize visible light for the generation of the electron–hole couples (exciton). The excited electrons are transferred to reaction centers at the surface of the photo-materials, and the conversion of NAD^+ to NADH occurs, involving the electron mediator and the oxidation of glycerol. The overall mechanism is summarized in Figure 11.

Figure 11: The electron flow in the photocatalytic system of NAD^+ reduction composed of the photosensitized TiO₂ photocatalyst, Rh(III)-electron mediator and glycerol as a sacrificial reagent.
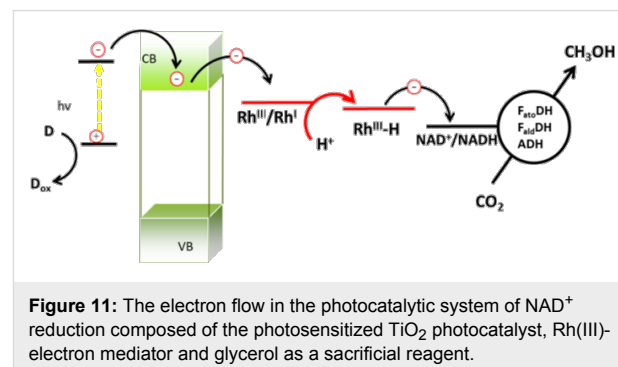
The first and only product of glycerol oxidation is 1,3-di-hydroxyacetone (1,3-DHA), as demonstrated by NMR studies carried out on a fresh reaction mixture (¹H resonances found at

4.34 ppm, as compared with literature data: [1]H at 4.40 ppm) [26]. The dihydroxyacetone species is not very stable and can be easily converted into other monomeric or polymeric species under the reaction conditions. Oxidation of glycerol is still under investigation as the isolation of 1,3-DHA would add value to the process. Other parameters, such as the optimization of the photosystem for a more efficient NAD^+ reduction, the improvement of the reaction selectivity, the increase of the absorption coefficient, and the increase of the chemical stability and photostability of photocatalysts, are also under continuous investigation for their further improvement and bring the whole reaction closer to a potential application.

Conclusion

Titanium dioxide modified with chromium(III) complex, $[CrF_5(H_2O)]^{2-}$@TiO_2, exhibits great ability to drive the in situ selective reduction of NAD^+ cofactor to 1,4-NADH. This process works particularly well in the presence of a $[Cp*Rh(bpy)H_2O]Cl_2$ complex playing the role of the electron transfer mediator. Our studies demonstrate that the photocatalyst is able to utilize visible light for generation of the electron–hole couples. The excited electrons are transferred to an e^--transfer mediator at the surface of the materials, where the conversion of NAD^+ to NADH occurs, involving the eventual oxidation of glycerol. The overall mechanism is summarized in Figure 11.

Anodic photocurrents generated by the photocatalyst upon visible light irradiation suggest the electron transfer from the excited sensitizer (chromium(III) complex) to the conduction band of TiO_2. The reduction of the rhodium complex was confirmed by spectroscopic studies made in the presence of irradiated TiO_2 and upon electrochemical reduction of the complex. Selective reduction of NAD^+ to 1,4-NADH has also been experimentally evidenced by ^{1}H NMR and HPLC measurements. Finally, the enzymatic route of the CO_2 reduction was confirmed to occur as was previously described [7,11]. The novelty of the photochemical NADH regeneration described in this paper consists of the use of visible light and the coupling of an inexpensive photocatalyst with robust e^-- and H^--transfer mediators, which can be used for days. Furthermore, we have demonstrated the entire mechanism of the electron flow from the photo-excited photosensitizer to NAD^+, resulting in NADH generation, which can be further used in enzymatic processes including carbon dioxide reduction.

The product of glycerol oxidation is 1,3-dihydroxyacetone. This species is not very stable and can be converted into other monomeric or polymeric species. Oxidation of glycerol is still under investigation together with other parameters, such as the optimization of the photosystem for a more efficient NAD^+

reduction, the improvement of the reaction selectivity, the increase of the absorption coefficient, and the increase of the chemical stability and photostability of photocatalysts.

The photocatalytic system discussed in this paper is much more effective as compared to ZnS-based photocatalysts as previously presented in [7,11] and represents a significant step towards potential application of this hybrid technology for CO_2 reduction to methanol.

Experimental
Preparation of photocatalysts
Synthesis of photosensitized TiO_2

The modification of TiO_2 with rutin was carried out as reported in the literature [27]. A titanium dioxide powder, P25 Evonik (500 mg), was added to 10 cm^3 of aqueous rutin solution (10^{-2} mol dm^{-3}). The suspension was sonicated (10 minutes) and the colored precipitate was collected, washed 3 times with water and dried in air at 60 °C.

$[CrF_5(H_2O)]^{2-}$@TiO_2 was prepared by impregnation of TiO_2 particles (P25, Evonik or 10 nm particles) [20] by $(NH_4)_2[CrF_5(H_2O)]$ under ultrasonic stirring. The suspension was sonicated for 15 minutes, left for 24 hours, and the nanoparticles were isolated washed with water and dried under vacuum.

Copper(I) oxide was prepared in the reaction of an aqueous solution of glucose (10 mL, 0.8 M) dropped into an alkaline solution of $CuSO_4$ (50 mL, 0.2 M) in presence of polyvinylpyrrolidone K-30 (0.3 g) at 80 °C. After 1 hour a red precipitate was separated by filtration, washed with water and dried.

Vanadates were prepared as reported by Hu et al. [28] with minor modifications: NaOH and V_2O_5 powders in a molar ratio of 6:1 were dissolved together in water and stirred. Subsequently, the solution of $In(VO_3)_3$ or $AgNO_3$ was added. Precipitates, which appeared immediately, were aged at room temperature for 1 hour, washed and dried.

Synthesis of $(NH_4)_2[CrF_5(H_2O)]$

5 mL of an ammonia solution was added to 50 mL of an aqueous solution of $NH_4 \cdot HF$ (15 g). A CrF_3 solution was added dropwise to a hot (363 K) solution of $NH_4 \cdot HF$ in the presence of zinc powder. A green precipitate was obtained, isolated and analyzed, resulting in the title compound.

Synthesis of $[Cp*Rh(bpy)H_2O]Cl_2$

$[Cp*Rh(bpy)H_2O]Cl_2$ was obtained from $[Cp*RhCl_2]_2$ as reported in [29]. Phenanthroline was used instead of bpy to

generate [Cp*Rh(phen)(H$_2$O)]Cl$_2$. The analogous Ir complex was prepared starting from [Cp*IrCl$_2$]$_2$. The hydride [Cp*Rh(bpy)H]$^+$ showed a hydride signal at −7.5 ppm in its ^{1}H NMR spectrum.

UV–vis characterization

The UV–vis diffuse reflectance spectra of the photocatalysts were recorded using a UV-3600 spectrophotometer (Shimadzu) equipped with an integrating sphere. Powder samples were ground with BaSO$_4$ (1:50 wt ratio). Barium sulfate was used as a reference.

Regeneration of NADH from NAD$^+$

Photocatalytic tests of NADH regeneration were performed in a borosilicate glass reactor (V = 10 mL). The photocatalyst (1 g L^{-1}) was suspended in deoxygenated phosphate buffer (pH 7). NAD$^+$ (0.8 mM) was added. Glycerol was used as an electron donor. [Cp*Rh(bpy)H$_2$O]Cl$_2$ was used as electron mediator (concentration range: 0–0.5 µM). The suspension was irradiated in the sealed reactor, under nitrogen atmosphere, using a 50 W LED illuminator (λ > 400 nm) as light source or concentrated solar light. 2 mL samples were collected during irradiation, filtered and analyzed by HPLC (column Zorbax SB-Aq) and NMR.

Reduction of CO$_2$ to CH$_3$OH using the assembled photocatalytic/enzymatic system

The reduction of CO$_2$ to methanol using encapsulated enzymes is described in [7]. Here we recall that the enzymes F$_{ate}$DH, F$_{ald}$DH, and ADH were encapsulated into silicate cages made from Ca alginate and tetraethoxysilanes (TEOS) and used at a controlled pH of 7. CO$_2$ was admitted in a continuous flow reactor at such a rate to generate a 20% excess with respect to the stoichiometric amount required by the enzymes. Excess

CO$_2$ was avoided to prevent its emission into the atmosphere since a goal of the research is to reduce CO$_2$ emissions during the synthesis of methanol. For this reason, the recovery of methanol by stripping was carried out using N$_2$ and not CO$_2$ itself, which would also be possible. A more complex experiment with CO$_2$ recovery is currently under investigation, so that CO$_2$ can be used as reagent and carrier of methanol. In this study, air influenced the enzymes and was not used. The beads (Figure 12) were suspended in water in compartment A of the reaction cell below (Figure 13) in presence of the required amount of NADH, and CO$_2$ was slowly admitted.
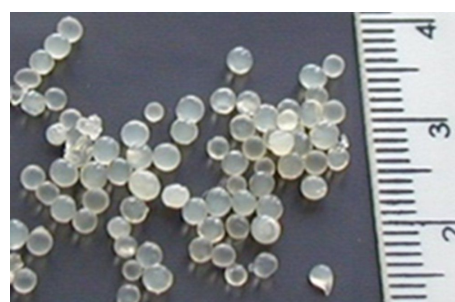
Figure 12: Beads produced from Ca-alginate and TEOS containing co-encapsulated F$_{ate}$DH, F$_{ald}$DH and ADH.

When the formation of methanol (monitored by GC on withdrawn samples of the reaction solution, within 1 min maximum) was at the maximum, the solution was pumped into compartment B, which contained the photocatalyst and the heterogenized Rh complex, while the encapsulated enzymes remained in compartment A. Irradiation (0.5–1 h) with visible light (or solar light) caused the conversion of NAD$^+$ into NADH to occur at the maximum yield (very close to 100%). The solution was again pumped into compartment A where the reduction of CO$_2$
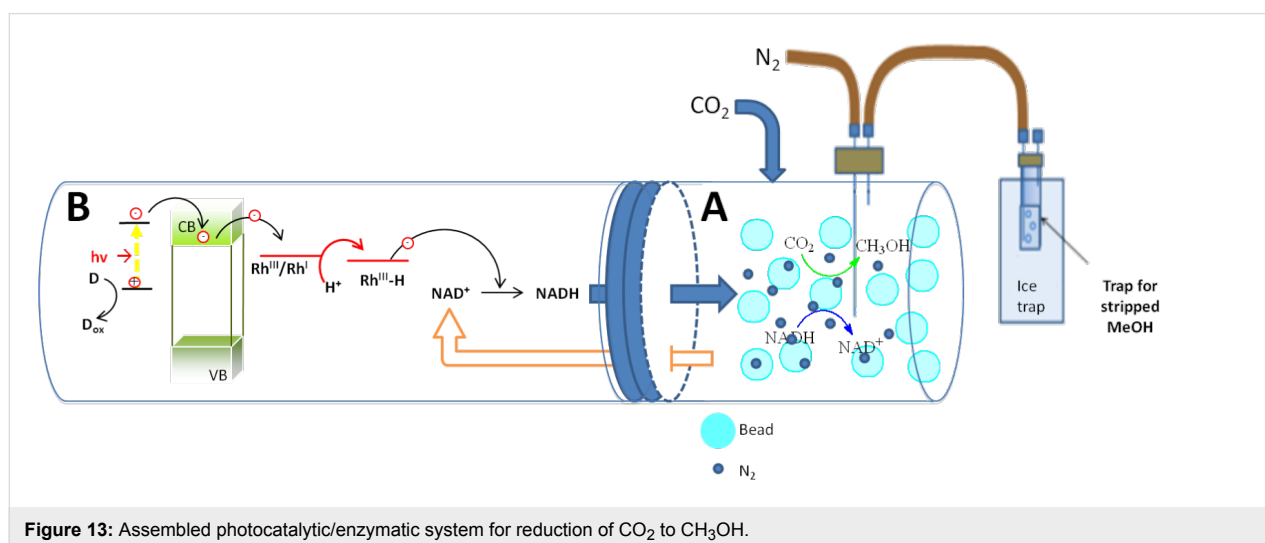

Figure 13: Assembled photocatalytic/enzymatic system for reduction of CO$_2$ to CH$_3$OH.

occurred with formation of CH$_3$OH. The cycle was repeated until no more CH$_3$OH was formed. At given intervals, CH$_3$OH was extracted in compartment B (stripping was realized by bubbling N$_2$ and condensing of the vapors) to avoid an increasing concentration which might block the enzymes. The difference in the rate of the enzymatic reaction and the photo-catalytic regeneration of NADH is a barrier to practical utilization of this hybrid technology. Further efforts for improving the convergence of the time of reaction in the two steps is currently underway.

Acknowledgements

References

1. Gamenara, D.; Seoane, G. A.; Saenz-Méndez, P.; Dominguez de María, P. *Redox Biocatalysis: Fundamentals and Applications;* John Wiley & Sons, Inc.: Hoboken, New Jersey, 2013.
2. Cheikhou, K.; Tzédakis, T. *AIChE J.* **2008,** *54,* 1365–1376. doi:10.1002/aic.11463
3. Patel, R. N. *Biomolecules* **2013,** *3,* 741–777. doi:10.3390/biom3040741
4. Baran, T.; Dibenedetto, A.; Macyk, W.; Aresta, M. *ICCDU XII,* June 23–27, 2013, Alexandria, VA, USA.
5. Siu, E.; Won, K.; Park, C. B. *Biotechnol. Prog.* **2007,** *23,* 293–296. doi:10.1021/bp060247l
6. Soldevila-Barreda, J. J.; Bruijnincx, P. C. A.; Habtemariam, A.; Clarkson, G. J.; Deeth, R. J.; Sadler, P. J. *Organometallics* **2012,** *31,* 5958–5967. doi:10.1021/om3006307
7. Dibenedetto, A.; Stufano, P.; Nocito, F.; Aresta, M. *ChemSusChem* **2011,** *4,* 1311–1315. doi:10.1002/cssc.201000434
8. Baran, T.; Macyk, W. *J. Photochem. Photobiol., A: Chem.* **2012,** *241,* 8–12. doi:10.1016/j.jphotochem.2012.05.008
9. Lettmann, C.; Hinrichs, H.; Maier, W. F. *Angew. Chem., Int. Ed.* **2001,** *40,* 3160–3164. doi:10.1002/1521-3773(20010903)40:17<3160::AID-ANIE3160>3.0.CO;2-Z
10. Maeda, K.; Higashi, M.; Lu, D.; Abe, R.; Domen, K. *J. Am. Chem. Soc.* **2010,** *132,* 5858–5868. doi:10.1021/ja1009025
11. Dibenedetto, A.; Stufano, P.; Macyk, W.; Baran, T.; Fragale, C.; Costa, M.; Aresta, M. *ChemSusChem* **2012,** *5,* 373–378. doi:10.1002/cssc.201100484
12. Sato, S.; Arai, T.; Morikawa, T.; Uemura, K.; Suzuki, T. M.; Tanaka, H.; Kajino, T. *J. Am. Chem. Soc.* **2011,** *133,* 15240–15243. doi:10.1021/ja204881d
13. Aresta, M.; Dibenedetto, A.; Angelini, A. *Philos. Trans. R. Soc., A* **2013,** *371,* No. 1996. doi:10.1098/rsta.2012.0111
14. Bojarska, E.; Pawlicki, K.; Czochralska, B. *J. Photochem. Photobiol., A: Chem.* **1997,** *108,* 207–213. doi:10.1016/S1010-6030(97)00075-0
15. Chen, D.; Yang, D.; Wang, Q.; Jiang, Z. *Ind. Eng. Chem. Res.* **2006,** *45,* 4110–4116. doi:10.1021/ie0600902
16. Shi, Q.; Yang, D.; Jiang, Z.; Li, J. *J. Mol. Catal. B: Enzym.* **2006,** *43,* 44–48. doi:10.1016/j.molcatb.2006.06.005
17. Szaciłowski, K.; Macyk, W.; Drzewiecka-Matuszek, A.; Brindell, M.; Stochel, G. *Chem. Rev.* **2005,** *105,* 2647–2694. doi:10.1021/cr030707e
18. Aresta, M.; Dibenedetto, A.; Nocito, F.; Ferragina, C. *J. Catal.* **2009,** *268,* 106–114. doi:10.1016/j.jcat.2009.09.008
19. Dibenedetto, A.; Angelini, A.; Aresta, M.; Ethiraj, J.; Fragale, C.; Nocito, F. *Tetrahedron* **2011,** *67,* 1308–1313. doi:10.1016/j.tet.2010.11.070
20. Aresta, M.; Dibenedetto, A.; Baran, T.; Macyk, W. Photocatalyst for NAD+ reduction to NADH in hybrid chemo-enzymatic reduction of carbon dioxide to methanol. Pat. Appl. MI2013A001135, 2013.
21. Macyk, W.; Szaciłowski, K.; Stochel, G.; Buchalska, M.; Kuncewicz, J.; Łabuz, P. *Coord. Chem. Rev.* **2010,** *254,* 2687–2701. doi:10.1016/j.ccr.2009.12.037
22. Steckhan, E.; Herrmann, S.; Ruppert, R.; Dietz, E.; Frede, M.; Spika, E. *Organometallics* **1991,** *10,* 1568–1577. doi:10.1021/om00051a056
23. Lo, H. C.; Buriez, O.; Kerr, J. B.; Fish, R. H. *Angew. Chem., Int. Ed.* **1999,** *38,* 1429–1432. doi:10.1002/(SICI)1521-3773(19990517)38:10<1429::AID-ANIE1429>3.0.CO;2-Q
24. Macyk, W.; Burgeth, G.; Kisch, H. *Photochem. Photobiol. Sci.* **2003,** *2,* 322–328. doi:10.1039/b211583b
25. Poizat, M.; Arends, I. W. C. E.; Hollmann, F. *J. Mol. Catal. B: Enzym.* **2010,** *63,* 149–156. doi:10.1016/j.molcatb.2010.01.006
26. http://www.hmdb.ca/spectra/spectra/nmr_one_d/1778.
27. Łabuz, P.; Sadowski, R.; Stochel, G.; Macyk, W. *Chem. Eng. J.* **2013,** *230,* 188–194. doi:10.1016/j.cej.2013.06.079
28. Hu, X.; Hu, C. *J. Solid State Chem.* **2007,** *180,* 725–732. doi:10.1016/j.jssc.2006.11.032
29. White, C.; Yates, A.; Maitlis, P. M.; Heinekey, D. M. (η^5-Pentamethylcyclopentadienyl)Rhodium and -Iridium Compounds. In *Inorganic Syntheses;* Grimes, R. N., Ed.; John Wiley & Sons, Inc.: Hoboken, NJ, USA, 2007; Vol. 29, pp 228–234. doi:10.1002/9780470132609.ch53

Anion effect controlling the selectivity in the zinc-catalysed copolymerisation of CO_2 and cyclohexene oxide

Sait Elmas[1], Muhammad Afzal Subhani[1], Walter Leitner[2] and Thomas E. Müller[*1]

Abstract

The choice of the anion has a surprisingly strong effect on the incorporation of CO_2 into the polymer obtained during the zinc-catalysed copolymerisation of CO_2 and cyclohexene oxide. The product span ranges from polyethercarbonates, where short polyether sequences alternate with carbonate linkages, to polycarbonates with a strictly alternating sequence of the repeating units. Herein, we report on the influence of the coordination ability of the anion on the selectivity and kinetics of the copolymerisation reaction.

Introduction

The fixation of carbon dioxide (CO_2) into polymers [1-3] provides highly promising options for the utilization of CO_2 [4-7]. The copolymerisation of CO_2 with epoxides (Scheme 1) is a prime example of a particularly attractive transformation of CO_2 [8,9] and is at the verge of commercialisation [8]. In this transformation, the low energy level of the CO_2 molecule is overcome by reacting CO_2 with an epoxide as energy-rich comonomer [10]. Homogeneous and heterogeneous catalysts are known to catalyse the copolymerisation reaction [5,11-13]. One lead structure (Scheme 1) for catalysing the reaction is based on binuclear complexes with a macrocyclic ligand

framework (Type I) [14-16]. The macrocyclic ligand L is a 22-membered Robson-type ligand with four secondary amino and two phenoxy donor groups [17]. The binuclear Zn(II) complex ($[LZn_2X_2]$, X = acetate) is substrate specific for the copolymerisation of CO_2 and cyclohexene oxide [16]. Another established common structural motif is based on Salen-type ligands with a central Co(III) [18-20] or Cr(III) [21-24] atom (Type II). Most catalysts based on Salen-type ligands are substrate specific and are most efficient for the copolymerisation of CO_2 with propylene oxide (PO). The use of zinc-based catalysts of Type I appears more favourable from an environmental
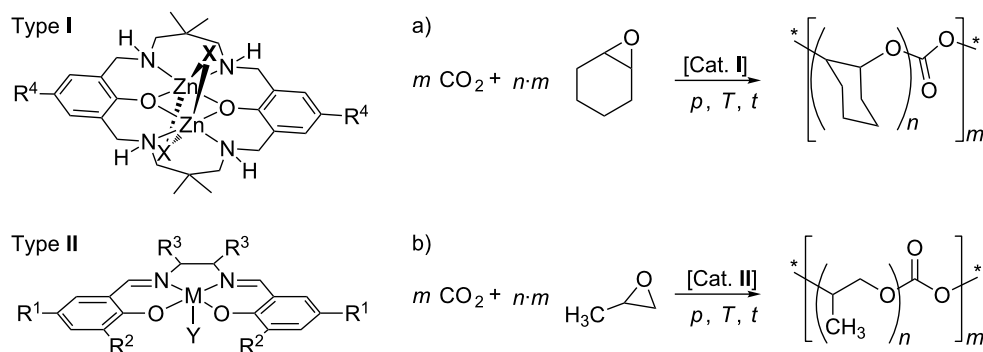
Scheme 1: Structural motif of two important types of catalysts and typical substrate specificity in the copolymerisation of CO_2 and epoxides (*: end groups). Type I: binuclear complexes with a macrocyclic Robson-type ligand framework; Type II: mononuclear complexes with a Salen ligand.

perspective compared to the use of the transition metal cations (Co, Cr) often employed in Type II catalysts, albeit zinc catalysts have lower activity in the copolymerisation of CO_2 and epoxides [16].

The use of catalysts of Types I and II in the copolymerisation of CO_2 and epoxides leads commonly to fully alternating polycarbonates. The polymer backbone of such alternating polycarbonates is relatively stiff due to the restricted rotational freedom in the C–O bonds of the carbonate group. For many applications it would be desirable to have a higher – and adjustable – flexibility of the polymer chain as the latter controls many of the physicochemical properties of the polymer, such as the glass-transition temperature (T_g). With incorporated ether linkages, a molecular weight in the oligomer range and at least two terminal OH groups, polyethercarbonates are interesting polyol building blocks in polyurethane chemistry [8].

To keep the catalyst loading during the synthesis of such polyols low, chain transfer between the growing polymer chain and free alcohol groups needs to be realised. In this study, we have addressed such immortal copolymerisation of CO_2 and epoxides with zinc catalysts. In the Type I lead catalyst [LZn$_2$(OAc)$_2$] [15], the two acetate counter ions may also act as a starter initiating the polymerisation reaction giving rise to polycarbonates with an acetate end group. Furthermore, these anions strongly coordinate in a bridging fashion to the zinc centre. In consequence, the Lewis acidic zinc centre is initially not accessible for coordination of the substrate giving rise to a certain inhibiting effect. So far, the role of the anion and its effect on the activity and selectivity of the zinc catalysts in the copolymerisation of CO_2 and epoxides has not yet been fully understood. To study and unravel the role of the anion, we have replaced the two acetate counter anions in the complex [LZn$_2$(OAc)$_2$] by essentially non-coordinating trifluoromethyl sulphonate ($CF_3SO_3^-$) or weakly coordinating *p*-toluene-
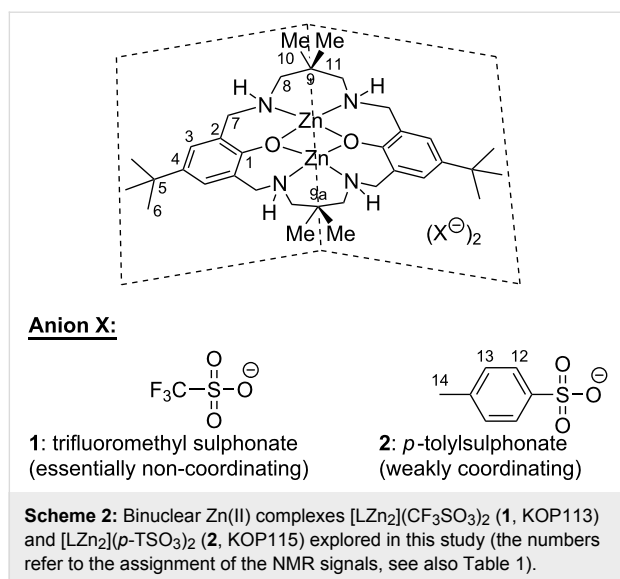
sulphonate anions (*p*-TSO$_3^-$). Herein, we report on the effect of the choice of the counter anion on the product selectivity and the activity of the complexes in catalysing the reaction of CO_2 with cyclohexene oxide.

Results and Discussion
Synthesis and characterisation of binuclear [LZn$_2$](X)$_2$ complexes

Complexes [LZn$_2$](CF$_3$SO$_3$)$_2$ (**1**) and [LZn$_2$](*p*-TSO$_3$)$_2$ (**2**) (Scheme 2) were prepared by reacting the corresponding zinc salt with the deprotonated macrocyclic ligand H$_2$L. Successful complexation was confirmed by the high-field shift of the ^{13}C and ^{1}H NMR resonances assigned to the aromatic groups of **1** and **2** relative to those of the free ligand. Inspection of the ^{13}C APT NMR spectra showed that the position of the signal of the aromatic carbon 2 (for assignment, refer to Scheme 2) was slightly shifted to higher field for **1** (122.0 ppm) relative to **2** (123.0 ppm), suggesting an increased shielding due to lower electron density in the aromatic ring of **1**. This is consistent with the weaker coordinating character of the trifluoromethyl-sulphonate anion (essentially non-coordinating) in comparison to the *p*-toluenesulphonate anion (weakly coordinating). This interpretation is supported by the IR spectra, where the position of one of the two characteristic S=O stretch vibration bands was significantly red-shifted for **1** (1005 cm^{-1}) relative to **2** (1040 cm^{-1}), while the position of the second S=O stretch vibration band remained essentially unchanged (**1**: 1190 cm^{-1}, **2**: 1180 cm^{-1}).

A closer inspection of the ^{13}C NMR spectra revealed two clearly separated signals for the methyl groups 10 and 11 (**1**: 28.2 and 20.8 ppm, **2**: 28.3 and 21.2 ppm, respectively), while only one signal at 25.2 ppm was observed for the methyl groups 10 and 11 in the free ligand H$_2$L. Also in the ^{1}H NMR spectra, the position of the signals assigned to the two methyl groups 10 and 11 was distinctly different (**1**: 0.9 and 1.2 ppm;

Anion X:

1: trifluoromethyl sulphonate
(essentially non-coordinating)

2: *p*-tolylsulphonate
(weakly coordinating)

Scheme 2: Binuclear Zn(II) complexes [LZn$_2$](CF$_3$SO$_3$)$_2$ (**1**, KOP113) and [LZn$_2$](*p*-TSO$_3$)$_2$ (**2**, KOP115) explored in this study (the numbers refer to the assignment of the NMR signals, see also Table 1).

2: 0.8 and 1.1 ppm). Similarly, two separate signals were observed for the methylene protons 8 in the ^{1}H NMR spectra of **1** (2.6 and 3.1 ppm) and **2** (2.4 and 2.5 ppm), while only one signal was observed for the methylene group in the ^{13}C NMR spectra. Such an NMR pattern could arise when the ligand in **1** and **2** adopts a roof-shaped geometry, as indicated in Scheme 2. An alternative explanation may be anisotropic effects induced by the sulphonate anion through formation of a tightly associated ion pair in the relatively non-polar solvent CDCl$_3$.

For **1** and **2**, mass spectrometry revealed characteristic series of salt-like agglomerates [LZn$_2$]X, [LZn$_2$]$_2$X$_3$, [LZn$_2$]$_3$X$_5$ and [LZn$_2$]X$_3$, [LZn$_2$]$_2$X$_5$, [LZn$_2$]$_3$X$_7$ consistent with weak coordination of the anion to the metal centre. For **1**, an additional signal assigned to the parent divalent cation [LZn$_2$]$^{2+}$ was observed, whereas the signal was absent for **2**, which is consistent with the slightly more coordinating nature of the *p*-toluenesulphonate anion. In comparison, the acetate reference complex gave rise to a prevailing signal corresponding to the mass of the non-dissociated complex [LZn$_2$(OAc)$_2$] [15] which is in full agreement with the strongly coordinating nature of the acetate anion.

Copolymerisation of CO$_2$ and cyclohexene oxide with binuclear [LZn$_2$](X)$_2$ complexes

Complexes **1** and **2** were then evaluated as catalysts in the copolymerisation of CO$_2$ and cyclohexene oxide CHO (Scheme 3). To obtain insight into the kinetics, the progress of the reactions was monitored with in situ IR spectroscopy and the results are collected in Table 2 (entries 1–4).

Under the applied conditions (100 °C, 20 bar), both **1** and **2** afforded high conversion of CHO. A polymer with the expected molecular weight in the oligomer range and a narrow molecular weight distribution was obtained (Table 2, entries 1 and 2). Closer analysis of the polymer obtained with catalyst **1** revealed that a polyethercarbonate characterised by surprisingly long polyether segments interspaced by carbonate groups was obtained (ratio of carbonate to ether moieties *m*/*n* 4.5/95.5, Table 2, entry 1). This is in agreement with a relatively small consumption of CO$_2$ during the reaction. The polymer was obtained in excellent selectivity and only traces of cyclic cyclo-

Table 1: Position and assignment of the NMR signals of complexes **1** and **2** in comparison to the parent macrocyclic ligand H$_2$L.

Assignment[a]	[L$_2$Zn](CF$_3$SO$_3$)$_2$ (**1**)		[L$_2$Zn](p-TSO$_3$)$_2$ (**2**)		LH$_2$	
	^{1}H	^{13}C	^{1}H	^{13}C	^{1}H	^{13}C
1	–	n.o.[b]	–	n.o.[b]	–	154.6
2	–	122.0	–	123.0	–	124.2
3	6.88	128.0	6.80 or 7.67	127.7	6.94	125.0
4	–	n.o.[b]	–	n.o.[b]	–	140.8
5/9	–	33.5	–	33.5	–	33.9
		33.6		33.7		34.6
6	1.25	31.5	1.28	31.8	1.26	31.6
7	4.30	55.9	4.08	55.8	3.74	53.3
8	3.10	63.2	2.44	63.0	2.52	59.8
	2.62					
10/11	1.18	28.2	1.02	28.3	1.01	25.2
	0.97	20.8	0.89	21.2 or 21.3		
12/13	–	–	7.67 or 6.80	128.3	–	–
14	–	–	2.19	21.3 or 21.2	–	–
-OH/-NH	2.86	–	2.84	–	n.o.[b]	–

[a]For the numbering refer to Scheme 2; [b]n.o. not observed.
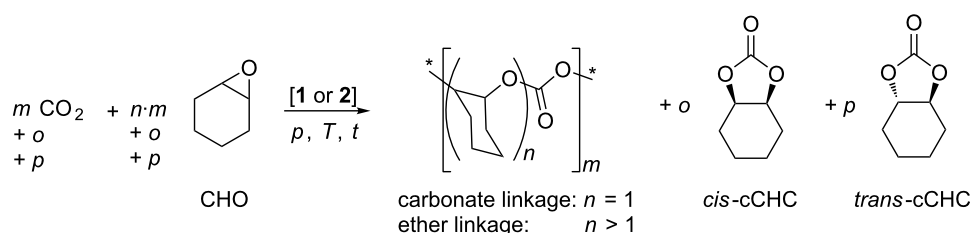
Scheme 3: Copolymerisation of CO_2 and cyclohexene oxide (*: end groups of the polymer chain).

Table 2: Yield and selectivity in the copolymerisation of CO_2 and CHO using complexes **1** and **2** as catalysts and analytical data for the polymers obtained.

Entry	Catalyst	Alcohol (equiv)	Yield[a] (%)	Selectivity[b]		M_n (g/mol)	PDI
				$(o+p)/m$	m/n		
1	**1**	–	94	<0.01	4.5/95.5	3082	1.64
2	**2**	–	74	0.26[c]	>99.0/1.0	2735	1.33
3	**1**	0.01[d]	72	<0.01	6.6/93.4	3567	1.75
4	**2**	0.01[d]	55	0.02	>99.0/1.0	2019	1.24
5[e]	[LZn$_2$(OAc)$_2$]	–	59	>0.08	>99.0/1.0	–	–
6 [15]	[LZn$_2$(OAc)$_2$]	–	55	<0.11	~100/0	–	–

[a]Yield of polymer; [b]$(o+p)/m$: ratio of cyclic cyclohexene carbonate to carbonate linkages in the polymer; m/n: ratio of carbonate to ether linkages in the polymer; [c]high selectivity to polycarbonate (low value for $(o+p)/m$) during the initial phase of the reaction, see Figure 2; [d]Molar ratio of α,ω-dihydroxy-polypropylene oxide to CHO 1/72, corresponding to 1 OH group per 36 CHO molecules; [e]reaction at 90 °C.

hexene carbonate (cCHC) were formed as byproduct ($(o+p)/m$ <0.01).

Analysis of the in-situ IR spectra recorded during the reaction revealed the evolution of an intensive band at 1080 cm^{-1} characteristic for the C–O–C bending vibration assigned to the ether linkages, while the intensity of the signal at 805 cm^{-1} characteristic for CHO decreased in parallel (Figure 1). At 1746 cm^{-1}, the typical carbonate band [ν_{st}(C=O)] [25] appeared with low intensity. Quantitative analysis of the time-resolved IR spectra (Figure 2) revealed a profile of epoxide consumption consistent with a first order reaction in both CO_2 and epoxide. The initial rate for the consumption of CHO was 5.03 mol$_{CHO}$·(mol$_{cat}$·h)$^{-1}$. Ether and carbonate linkages in the polyethercarbonate product were formed in parallel in a ratio of 9.8. The catalyst was still active after 19 hours reaction time and higher yields can be achieved at prolonged reaction times.

In contrast, with complex **2**, a fully alternating polycarbonate with a high fraction of carbonate linkages was obtained (m/n >99.0/1.0, Table 2, entry 2). A considerable pressure drop was observed during the reaction consistent with a consumption of CO_2 in a stoichiometric ratio to CHO. Considerable amounts of cCHC were found as byproduct at the end of the reaction ($(o+p)/m$ 0.26, vide supra). This chemoselectivity was
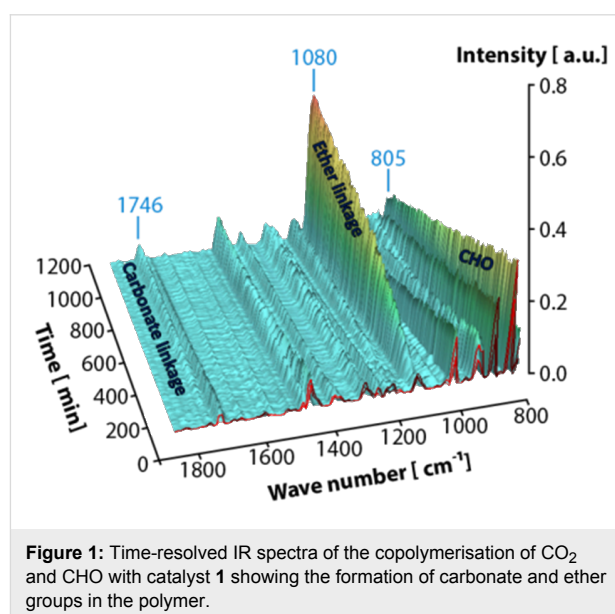

Figure 1: Time-resolved IR spectra of the copolymerisation of CO_2 and CHO with catalyst **1** showing the formation of carbonate and ether groups in the polymer.

similar to [LZn$_2$(OAc)$_2$], where a mixture of alternating polycarbonate (m/n >99.0/1.0) and cCHC was obtained ($(o+p)/m$ <0.08, Table 2, entries 5 and 6).

The results clearly show that the selectivity with respect to the obtained incorporation of CO_2 into the polymer chain is
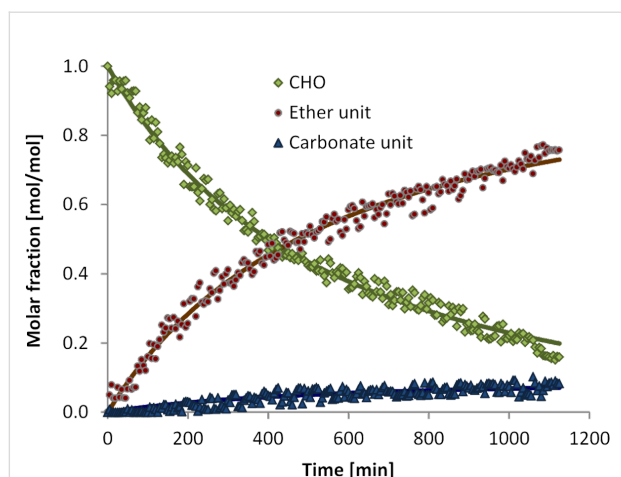
Figure 2: Time–concentration profile of the copolymerisation of CO_2 and CHO in the presence of catalytic amounts of complex **1** and fit according to a first order kinetic in CO_2 and in epoxide.
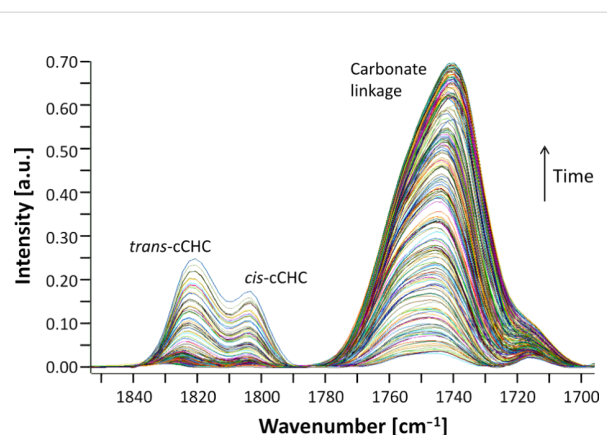

Figure 3: Carbonate region of the time-resolved IR spectra recorded during the copolymerisation of CO_2 and cyclohexene with catalyst **2**.
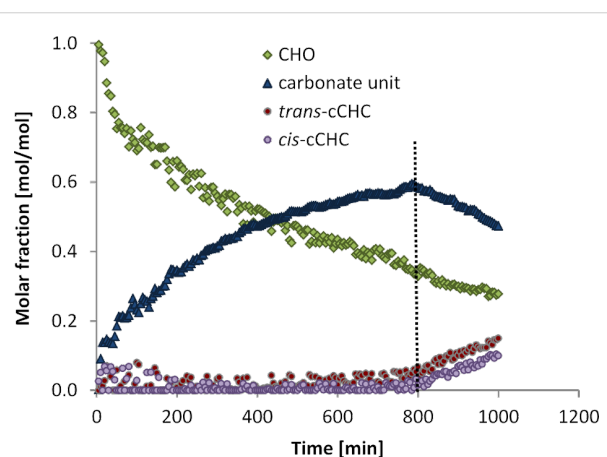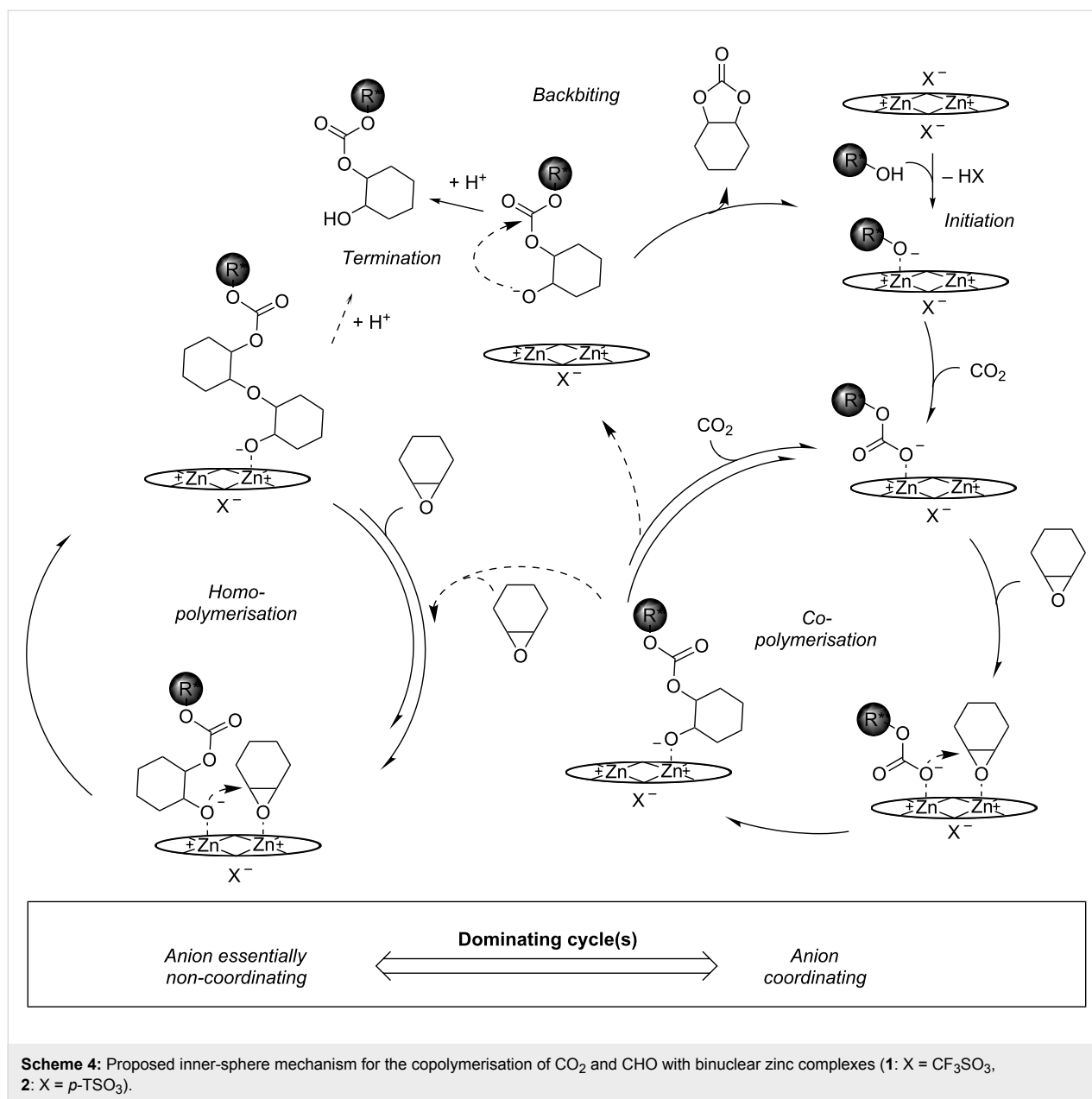

Figure 4: Time–concentration profile of the copolymerisation of CO_2 and CHO in the presence of catalytic amounts of complex **2**.

reversed for complexes **1** and **2**. This is particularly surprising due to the similarity of the sulphonate counter anions and suggests that CO_2 incorporation is related to subtle differences between the two catalysts. Most likely the differences in coordination strength of the anion to the zinc centre account for this change in selectivity.

The time-resolved IR spectra recorded during the reaction using catalyst **2** indicate a very different regime compared to the reaction with catalyst **1**. During the initial period CHO was consumed with a rate of 13.7 $mol_{CHO} \cdot (mol_{cat} \cdot h)^{-1}$. In parallel, two bands with high intensity appeared at 1746 cm^{-1} and 1225 cm^{-1} (Figure 3), which are typical for the $[v_{st}(C=O)]$ and $[v(C–O)]$ vibration of polycarbonates, respectively [25]. After 800 min of reaction time, two further carbonate bands assigned to *cis*- and *trans*-cCHC commenced to develop at 1820 cm^{-1} and 1803 cm^{-1}, respectively. In parallel, the concentration of polycarbonate decreased (Figure 4). This is consistent with back-biting of free polymer chains, which might be induced by the increasing polarity of the reaction medium leading to an enhanced probability that the polymer chains detach from the zinc centres.

To explore the possibility of an immortal polymerisation [26,27], the reactions were repeated in the presence of an alcohol (α,ω-dihydroxypolypropylene oxide, 1 OH group per 36 CHO molecules). Catalyst **1** afforded essentially the same homopolymerisation product (Table 2, entry 3) albeit in a slightly lower yield (72%). Also, the reaction profile was nearly identical. Analogously, a very similar product was obtained with catalyst **2** when the reaction was performed in the presence of the alcohol (55% yield in polymer, Table 2, entry 4).

These observations are readily explained by a similar mechanism as described for the heterogeneous $Zn[Co(CN)_6]$ double metal cyanide (DMC) catalyst [8,28], for which an active site comprising two Lewis acidic zinc centres in vicinity had been proposed [29]. Three catalytic cycles, copolymerisation, homopolymerisation and formation of cyclic carbonate are closely linked (Scheme 4) [28]. The reaction is initiated by coordination of an alcoholate to one of the zinc centres. Insertion of CO_2 into the metal–alcoholate bond provides a coordinated carbonate species [15]. An epoxide molecule coordinates to a neighbouring zinc centre and the nucleophilic attack by the neighbouring carbonate species leads to chain growth. Insertion of the next CO_2 molecule into the zinc–alcoholate bond closes the copolymerisation cycle. The latter competes with coordination of another epoxide molecule at the zinc centre next to the zinc–alcoholate. Nucleophilic attack of the alcoholate species and coordination of another epoxide molecule on the neigh-

Scheme 4: Proposed inner-sphere mechanism for the copolymerisation of CO_2 and CHO with binuclear zinc complexes (**1**: X = CF_3SO_3, **2**: X = *p*-TSO_3).

bouring zinc centre closes the homopolymerisation cycle. The cyclic carbonate is formed by backbiting of a terminal alcoholate, when the chain becomes released after preceding insertion of CO_2. Chains, which dissociate from the surface of the catalyst, restart a catalytic cycle when they re-attach to a free zinc site or react with a coordinated epoxide molecule, while protonation terminates the growth of this particular chain.

In such an inner-sphere mechanism the epoxide molecules compete with the anion in coordination to the zinc centres. In particular, coordination of the epoxide to a zinc centre neighbouring a zinc–carbonate or –alcoholate becomes less likely as coordinating anions are present in the reaction mixture. This

readily explains the differences between the $CF_3SO_3^-$ and the *p*-TSO_3^- complex. In the presence of a $CF_3SO_3^-$ anion (essentially non-coordinating) coordination of the epoxide to a neighbouring zinc centre is facile. In consequence, the homopolymerisation cycle prevails and mainly polyether segments interspersed with carbonate linkages are formed. In the presence of the *p*-TSO_3^- anion (weakly coordinating), the lower concentration of epoxide molecules coordinating to a neighbouring zinc centre leads to an increase in the probability that a CO_2 molecule is inserted into the zinc–alcoholate bond. In consequence, the copolymerisation cycle dominates leading with high selectivity to the alternating polycarbonate. In the presence of the OAc^- anion, a similar pathway as for the *p*-TSO_3^- anion may

be followed or an outer-sphere mechanism with external attack of a chain dissociated from the surface of the catalyst on a co-ordinated epoxide molecule may be present [5]. The propensity to dissociation of the polymer chain depends strongly on the polarity of the reaction medium. The probability that the growing polymer chain detaches increases with the polarity of the medium leading to backbiting as observed with catalyst **2** at higher conversions.

An alternative model may involve a parallel cationic polymerisation mechanism of cyclohexene oxide with the more Lewis acidic complex **1**, which competes with the regular insertion mechanism depicted above. In contrast to $CF_3SO_3^-$, the p-TSO_3^- anion may be sufficiently nucleophilic to open an epoxide molecule coordinated to the Zn cation, consequently initiating the growth of the polymer chain in an analogous manner to acetate. Conversely, the less nucleophilic $CF_3SO_3^-$ cannot open a coordinated epoxide molecule and a cationic homopolymerisation of cyclohexene oxide becomes the prevailing chain-growth mechanism. It is important to note that in a cationic mechanism, CO_2 molecules cannot be inserted as easily, hence, leading to the incorporation of negligible amounts of CO_2.

Non-coordinating anions lead to a more electrophilic zinc centre with a stronger Lewis acidity, thereby triggering the homopolymerization in case of the $CF_3SO_3^-$ anion. In this context, it is known that the rate of the CO_2 insertion into metal–oxygen bonds depends critically on the nucleophilicity of the metal centre [26]. Nevertheless, it is surprising how sharply the selectivity of the CO_2/epoxide coupling reaction reverses upon a slight change in the anion.

Conclusion

In summary, the nature of the anion has a striking effect in the copolymerisation of CO_2 and cyclohexene oxide with binuclear zinc catalysts of Type I. The proposed mechanistic model readily explains the outstanding selectivities observed with complexes [LZn_2]X_2 (**1**: X = CF_3SO_3, **2**: X = p-TSO_3) to the polymeric product. With **1**, the formation of polyethercarbonates is preferred, whereas with **2** and the reference catalyst [$LZn_2(OAc)_2$], polycarbonates with a strictly alternating sequence of the repeating units are obtained.

Supporting Information

Supporting Information File 1
Experimental.
[http://www.beilstein-journals.org/bjoc/content/supplementary/1860-5397-11-7-S1.pdf]

References

1. Peters, M.; Köhler, B.; Kuckshinrichs, W.; Leitner, W.; Markewitz, P.; Müller, T. E. *ChemSusChem* **2011**, *4*, 1216–1240. doi:10.1002/cssc.201000447
2. Müller, T. E. *Preprints Symp., Am. Chem. Soc., Div. Fuel Chem.* **2008**, *53*, 317.
3. Peters, M.; Müller, T. E.; Leitner, W. *Tce* **2009**, *813*, 46–47.
4. Keim, W.; Hölscher, M.; Gürtler, C.; Peters, M.; Müller, T. E.; Leitner, W. *Z. Naturforsch.* **2012**, *67b*, 1–15.
5. Coates, G. W.; Moore, D. R. *Angew. Chem., Int. Ed.* **2004**, *43*, 6618–6639. doi:10.1002/anie.200460442
6. Pescarmona, P. P.; Taherimehr, M. *Catal. Sci. Technol.* **2012**, *2*, 2169–2187. doi:10.1039/c2cy20365k
7. Kember, M. R.; Buchard, A.; Williams, C. K. *Chem. Commun.* **2011**, *47*, 141–163. doi:10.1039/c0cc02207a
8. Langanke, J.; Wolf, A.; Hofmann, J.; Böhm, K.; Subhani, M. A.; Müller, T. E.; Leitner, W.; Gürtler, C. *Green Chem.* **2014**, *16*, 1865–1870. doi:10.1039/c3gc41788c
9. Inoue, S.; Koinuma, H.; Tsuruta, T. *J. Polym. Sci., Part C: Polym. Lett.* **1969**, *7*, 287–292. doi:10.1002/pol.1969.110070408
10. Markewitz, P.; Kuckshinrichs, W.; Leitner, W.; Linssen, J.; Zapp, P.; Bongartz, R.; Schreiber, A.; Müller, T. E. *Energy Environ. Sci.* **2012**, *5*, 7281–7305. doi:10.1039/c2ee03403d
11. Darensbourg, D. J.; Holtcamp, M. W. *Coord. Chem. Rev.* **1996**, *153*, 155–174. doi:10.1016/0010-8545(95)01232-X
12. Ikpo, N.; Flogeras, J. C.; Kerton, F. M. *Dalton Trans.* **2013**, *42*, 8998–9006. doi:10.1039/c3dt00049d
13. Buchard, A.; Bakewell, C. M.; Weiner, J.; Williams, C. K. *Top. Organomet. Chem.* **2012**, *39*, 175–224. doi:10.1007/978-3-642-28288-1_5
14. Lehenmeier, M. W.; Bruckmeier, C.; Klaus, S.; Dengler, J. E.; Deglmann, P.; Ott, A.-K.; Rieger, B. *Chem. – Eur. J.* **2011**, *17*, 8858–8869. doi:10.1002/chem.201100578
15. Elmas, S.; Subhani, M. A.; Vogt, H.; Leitner, W.; Müller, T. E. *Green Chem.* **2013**, *15*, 1356–1360. doi:10.1039/c3gc40147b
16. Kember, M. R.; Knight, P. D.; Reung, P. T. R.; Williams, C. K. *Angew. Chem.* **2009**, *121*, 949–951. doi:10.1002/ange.200803896
17. Dutta, B.; Bag, P.; Adhikary, B.; Flörke, U.; Nag, K. *J. Org. Chem.* **2004**, *69*, 5419–5427. doi:10.1021/jo049787s
18. Lu, X.-B.; Wang, Y. *Angew. Chem., Int. Ed.* **2004**, *43*, 3574–3577. doi:10.1002/anie.200453998
19. Darensbourg, D. J.; Wilson, S. J. *J. Am. Chem. Soc.* **2011**, *133*, 18610–18613. doi:10.1021/ja208711c
20. Lu, X.-B.; Darensbourg, D. J. *Chem. Soc. Rev.* **2012**, *41*, 1462–1484. doi:10.1039/c1cs15142h
21. Qin, Z.; Thomas, C. M.; Lee, S.; Coates, G. W. *Angew. Chem., Int. Ed.* **2003**, *42*, 5484–5487. doi:10.1002/anie.200352605

22. Darensbourg, D. J.; Andreatta, J. R.; Jungman, M. J.;
Reibenspies, J. H. *Dalton Trans.* **2009,** 8891–8899.
doi:10.1039/b911061e
23. Elmas, S.; Subhani, M. A.; Harrer, M.; Leitner, W.; Sundermeyer, J.;
Müller, T. E. *Catal. Sci. Technol.* **2014,** *4,* 1652–1657.
doi:10.1039/c3cy01087b
24. Vagin, S. I.; Reichardt, R.; Klaus, S.; Rieger, B. *J. Am. Chem. Soc.*
2010, *132,* 14367–14369. doi:10.1021/ja106484t
25. Ren, W.-M.; Liu, Z.-W.; Wen, Y.-Q.; Zhang, R.; Lu, X.-B.
J. Am. Chem. Soc. **2009,** *131,* 11509–11518. doi:10.1021/ja9033999
26. Luinstra, G. A.; Haas, G. R.; Molnar, F.; Bernhart, V.; Eberhardt, R.;
Rieger, B. *Chem. – Eur. J.* **2005,** *11,* 6298–6314.
doi:10.1002/chem.200500356
27. Müller, T. E.; Gürtler, C.; Kermagoret, A.; Dienes, Y.; Busygin, I.;
Köhler, B.; Leitner, W. Method for producing polycarbonate polyols by
the immortal Polymerization of cyclic carbonates. WO Pat. Appl.
WO2012059550 A1, May 10, 2012.
28. Dienes, Y.; Leitner, W.; Müller, M. G. J.; Offermans, W. K.; Reier, T.;
Reinholdt, A.; Weirich, T. E.; Müller, T. E. *Green Chem.* **2012,** *14,*
1168–1177. doi:10.1039/c2gc16485j
29. Penzien, J.; Abraham, A.; van Bokhoven, J. A.; Jentys, A.;
Müller, T. E.; Sievers, C.; Lercher, J. A. *J. Phys. Chem. B* **2004,** *108,*
4116–4126. doi:10.1021/jp0373043

License and Terms

DBU-promoted carboxylative cyclization of *o*-hydroxy- and *o*-acetamidoacetophenone

Wen-Zhen Zhang[*], Si Liu and Xiao-Bing Lu

Abstract

The carboxylative cyclization of *o*-hydroxy- and *o*-acetamidoacetophenone with carbon dioxide promoted by the organic base 1,8-diazabicycloundec-7-ene (DBU) is reported. This reaction provides convenient access to the biologically important compounds 4-hydroxy-2*H*-chromen-2-one and 4-hydroxy-2(1*H*)-quinolinone in moderate to good yields using carbon dioxide as the carboxylation reagent. An acyl migration from nitrogen to carbon is observed in the reaction of *o*-acetamidoacetophenone.

Introduction

4-Hydroxy-2*H*-chromen-2-ones and 4-hydroxy-2(1*H*)-quinolinones are key structural subunits found in many natural products [1], commercial drugs [2,3] and pharmacologically potent compounds (Figure 1) [4,5]. Warfarin, for example, is an anticoagulant widely used to prevent thrombosis [2]; Novobiocin has long been established as an aminocoumarin antibiotic [3]. Recent studies revealed that the anticoagulant Dicumarol is able to inhibit the growth of pancreatic cancer [4]. Roquinimex was reported as an antineoplastic agent [5]. Traditional methods for accessing these compounds rely heavily on cyclization reactions using diethyl carbonate in the presence of inorganic bases [6,7] or Friedel–Crafts reactions using strong and corrosive acids [8]. In terms of availability and toxicity of the starting materials, environmental benignity and economical concerns, the

development of an alternative method for the synthesis of these compounds using carbon dioxide as the carboxylation reagent [9-16] is highly desirable.

It was previously reported that the α C–H bond in aromatic ketones readily undergoes a carboxylation reaction with carbon dioxide in the presence of a suitable base, producing β-ketocarboxylic acids [17-20]. Given that *o*-hydroxy- or *o*-acetamidoacetophenone is used as the starting material to react with carbon dioxide, the intramolecular carboxylative cyclization might provide a convenient access to 4-hydroxy-2*H*-chromen-2-one and 4-hydroxy-2(1*H*)-quinolinone. Indeed, Da Re and Sandri reported in 1960 that *o*-hydroxyacetophenone derivatives react with carbon dioxide (4 MPa) in the presence of
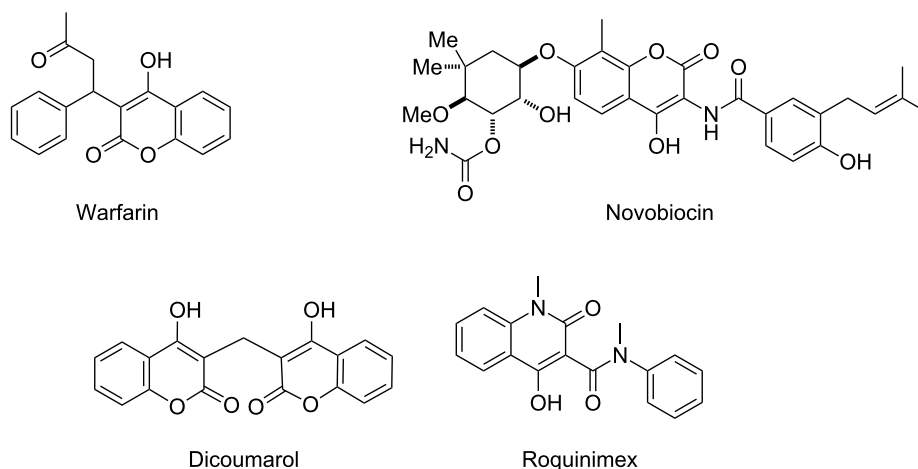
Figure 1: Selected examples for biologically active 4-hydroxy-2*H*-chromen-2-one and 4-hydroxy-2(1*H*)-quinolinone compounds.

3 equivalents of potassium carbonate at 130–170 °C, yielding 4-hydroxy-2*H*-chromen-2-ones in moderate yields [21]. From the viewpoints of solubility, efficiency, and ease of recovery and reuse, the use of an organic base rather than potassium carbonate in this reaction would be more promising. DBU and MTBD were previously reported as suitable bases to promote the carboxylation of α-C–H bonds in aromatic ketones with carbon dioxide [17-20]. In extension of our continuous efforts in developing catalytic transformations of carbon dioxide into value-added fine chemicals [20,22,23], we report herein the DBU-promoted carboxylative cyclization of *o*-hydroxy-

and *o*-acetamidoacetophenones with carbon dioxide to give 4-hydroxy-2*H*-chromen-2-ones and 4-hydroxy-2(1*H*)-quinolinones, respectively, in moderate to good yields under mild reaction conditions. An acyl migration from the nitrogen to carbon is observed in the reaction of *o*-acetamidoacetophenone.

Results and Discussion

We started our investigation with the carboxylative cyclization of *o*-hydroxypropiophenone (**1a**) with carbon dioxide to identify the optimal organic base and reaction conditions (Table 1). The use of potassium carbonate as base in DMF at 100 °C gave

Table 1: Optimization of the reaction conditions.[a]

Entry	Base	Solvent	T/°C	$p(CO_2)$/MPa	Yield/%[b]
1	K$_2$CO$_3$	DMF	100	3	29
2	DBU	DMF	100	3	49
3	MTBD	DMF	100	3	65
4	MTBD	DMSO	100	3	68
5	DBU	DMSO	100	3	75
6	DBU	DMAc	100	3	32
7	DBU	THF	100	3	10
8	**DBU**	**DMSO**	**80**	**3**	**87**
9	DBU	DMSO	60	3	65
10	DBU	DMSO	80	2	53
11	DBU	DMSO	80	0.1	<1

[a]Reaction conditions: *o*-hydroxyacetophenone (**1a**, 0.5 mmol), base (1 mmol), solvent (2 mL), 24 h; then *n*-BuI (1.0 mmol), 80 °C, 4 h. [b]Isolated yield.

29% yield of product **2a** (Table 1, entry 1). When DBU and MTBD were used in this reaction instead of potassium carbonate, a significantly increased yield of **2a** was obtained (Table 1, entries 2 and 3). When switching the solvent to DMSO, further increased yields were obtained, whereby DBU showed a higher efficiency than MTBD (Table 1, entries 4 and 5). Other solvents such as DMAc and THF gave dramatically decreased yields (Table 1, entries 6 and 7). Unexpectedly, we found that a decrease of temperature from 100 °C to 80 °C in DMSO led to a higher yield (87%) of **2a** (Table 1, entry 8). The reaction was found to be sensitive to the carbon dioxide pres-

sure and performing the reaction at a lower pressure gave a distinctly decreased yield (Table 1, entry 10). When the reaction was conducted under atmospheric carbon dioxide, no carboxylative cyclization product was obtained (Table 1, entry 11). Therefore, the optimal reaction conditions were established as following: 2.0 equiv DBU as base, 3.0 MPa of carbon dioxide, DMSO as solvent at 80 °C for 24 h.

Under the optimal reaction conditions, the substrate scope was then investigated (Table 2). Compared with *o*-hydroxypropiophenone, *o*-hydroxyacetophenone gave a slightly lower yield of

Table 2: Carboxylative cyclization of various *o*-hydroxyacetophenones with carbon dioxide.[a]

Entry	Substrate	Product	Yield/%[b]
1	**1a**	**2a**	87
2	**1b**	**2b**	79
3	**1c**	**2c**	56
4	**1d**	**2d**	45
5	**1e**	**2e**	49
6	**1f**	**2f**	36

908

Table 2: Carboxylative cyclization of various *o*-hydroxyacetophenones with carbon dioxide.[a] (continued)

| 7 | **1g** | **2g** | 65 |
| 8 | **1h** | **2h** | 42 |
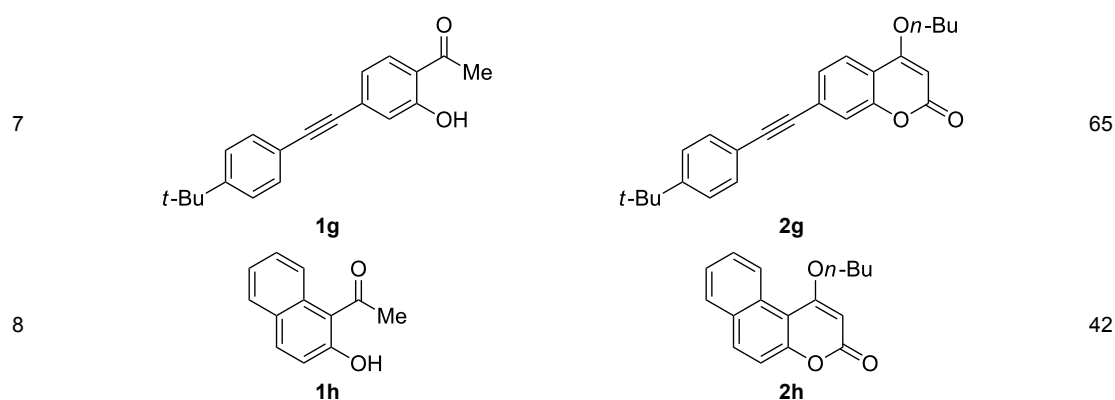
[a]Reaction conditions: *o*-hydroxyacetophenone (**1**) (0.5 mmol), DBU (1.0 mmol), CO_2 (3.0 MPa), DMSO (2 mL), 80 °C, 24 h; then *n*-BuI (1.0 mmol), 80 °C, 4 h. [b]Isolated yield.

the 2*H*-chromen-2-one product (Table 2, entries 2 and 4). *o*-Hydroxyacetophenone bearing electron-donating alkyl and ether groups, or electron-withdrawing fluoro and bromo groups undergoes the carboxylative cyclization reaction smoothly, affording the corresponding 4-butoxy-2*H*-chromen-2-ones **2b**–**2f** in moderate to good yields (Table 2, entries 2–6). The bromo group in product **2f** and the alkyne group in product **2g** offer opportunities for further functionalization of these 2*H*-chromen-2-ones using well-established methods [24]

(Table 2, entries 6 and 7). 2-Hydroxy-1-acetylnaphthalene (**1h**) participates in the carboxylative cyclization reaction to furnish the tricyclic product **2h** in moderate yield (Table 2, entry 8).

With the successful DBU-promoted carboxylative cyclization of *o*-hydroxyacetophenone at hand, we then extended this strategy to *o*-acetamidoacetophenone to synthesize 4-hydroxy-2(1*H*)-quinolinone (Table 3). Using 4 equivalents DBU as base in DMSO at 80 °C, *o*-acetamidoacetophenone (**3a**) underwent the

Table 3: Carboxylative cyclization of various *o*-acetamidoacetophenones with carbon dioxide.[a]
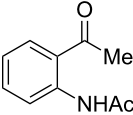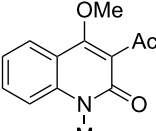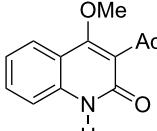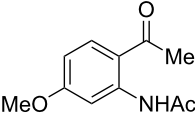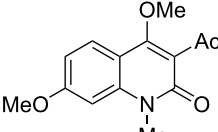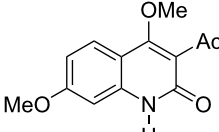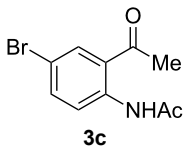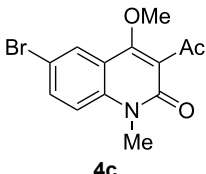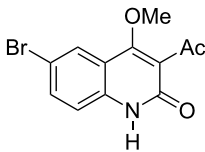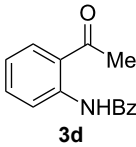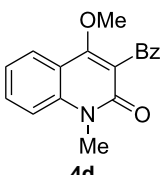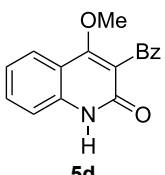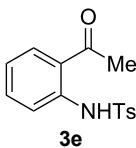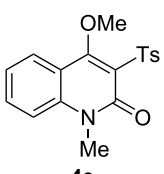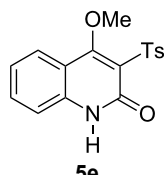

Entry	Substrate	Product		Yield/%
		4	**5**	**4 + 5**
1	**3a**	**4a**	**5a**	42 + 35
2	**3b**	**4b**	**5b**	38 + 37

Table 3: Carboxylative cyclization of various *o*-acetamidoacetophenones with carbon dioxide.[a] (continued)

[a]Reaction conditions: *o*-acetamidoacetophenone (**3**, 0.5 mmol), DBU (2.0 mmol), CO_2 (3.0 MPa), DMSO (2 mL), 80 °C, 24 h; then MeI (2.0 mmol), 30 °C, 4 h. [b]Isolated yield of separated products.

carboxylative cyclization reaction to provide 3-acetyl-4-methoxy-2(1*H*)-quinolinones **4a** and **5a** (Table 3, entry 1). Noteworthy, the acyl group was no longer bound to nitrogen in the product, which implies that a nitrogen to carbon acyl migration occurred during the reaction. The derivatization reaction using iodide compounds at higher temperature led to complex product mixtures. *o*-Acetamidoacetophenone substrates containing methoxy (**3b**) and bromo (**3c**) groups also reacted smoothly to afford the corresponding products (Table 3, entries

2 and 3). The reactions using benzamido- (**3d**) and *p*-toluenesulfonamido- (**3e**) acetophenone gave complex mixtures and no carboxylative cyclization product was observed (Table 3, entries 4 and 5).

A likely mechanism for the carboxylative cyclization of *o*-acetamidoacetophenone with carbon dioxide is proposed as shown in Scheme 1. The reaction can evolve along two pathways: in path **A**, deprotonation of *o*-acetamidoacetophenone by
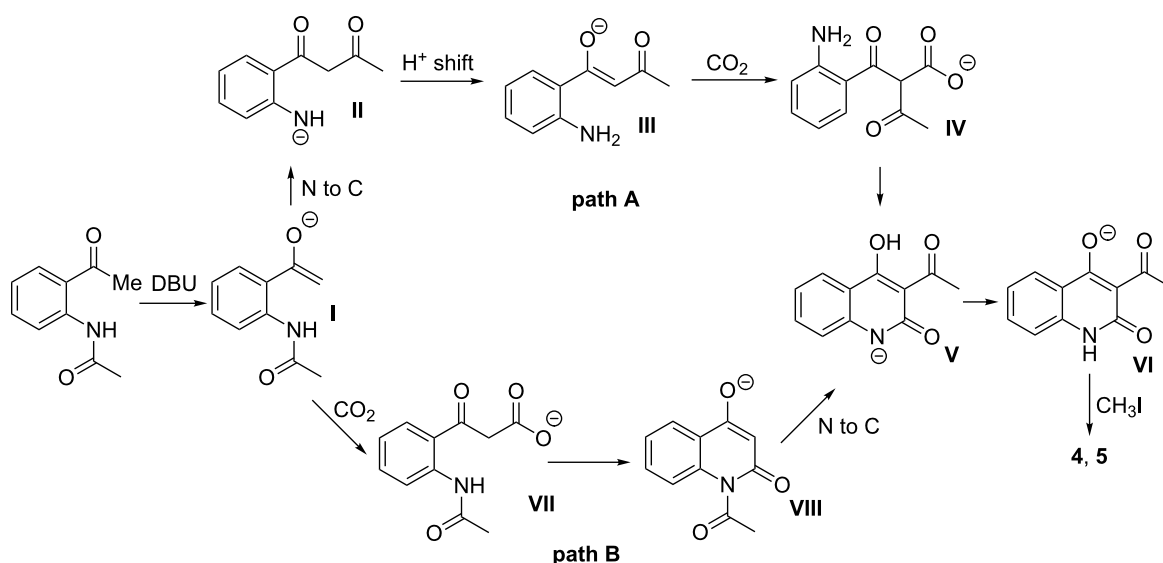
Scheme 1: Possible mechanism for the carboxylative cyclization of *o*-acetamidoacetophenone.

DBU gives enolate **I**, which undergoes an acyl migration from nitrogen to carbon [25,26] similar to the Baker–Venkataraman O to C acyl migration [27]. After a proton shift from the enol to nitrogen, the resultant intermediate **III** is carboxylated with carbon dioxide in the presence of DBU to afford intermediate **IV**, which subsequently undergoes a cyclization reaction to give **V**. The product is obtained after derivatization with methyl iodide. Also, path **B** in which the N to C acyl migration occurs after the carboxylative cyclization cannot be excluded.

We also conducted a cross experiment as shown in Scheme 2. When compounds **3b** and **3f** were reacted concomitantly, the corresponding carboxylative cyclization products **4b** and **4f** were obtained. No cross products **6** and **7** were detected, which implies that the N to C acyl shift occurred intramolecularly, not intermolecularly.

Conclusion
In summary, we have developed a DBU-promoted carboxylative cyclization of *o*-hydroxy- and *o*-acetamidoacetophenones with carbon dioxide. This methodology provides a convenient access to the biologically important 4-hydroxy-2*H*-chromen-2-ones and 4-hydroxy-2(1*H*)-quinolinones in moderate to good yields under mild reaction conditions. While there are precedents for the carboxylation of enolates, a practical protocol was developed that relies on in situ cyclization to form thermodynamically stable coumarins. Importantly, the use of an intramolecular in situ trap avoids the problem of decarboxylation during workup. In case of *o*-acetamidoacetophenones, an acyl migration from nitrogen to carbon was observed. The cross experiment showed that the N to C acyl shift occurred intramolecularly.

Experimental
Similarly as described in our previous paper [22], a 20 mL oven-dried autoclave containing a stirring bar was charged with *o*-hydroxyacetophenone (**1**) or *o*-acetamidoacetophenone (**3**) (0.5 mmol), DBU (1.0 mmol for **1**, 2.0 mmol for **3**), and 2 mL dry DMSO. After purging the autoclave with CO_2 three times, the sealed autoclave was pressurized to the appropriate pressure with CO_2. The reaction mixture was stirred at 80 °C for 24 h, then the autoclave was cooled to room temperature and the remaining CO_2 was vented slowly. Then *n*-BuI (1.0 mmol for **1**) or MeI (2.0 mmol for **3**) was added into the autoclave and the reaction mixture was stirred at 80 °C (for **1**) or at 30 °C (for **3**) for 4 h. The reaction mixture was then diluted with water (30 mL) and extracted with ethyl acetate (3 × 30 mL). The combined organic layers were washed with water and brine, dried over Na_2SO_4 and filtered. The solvent was removed under vacuum. The product was isolated by column chromatography on silica gel (hexane/ethyl acetate 2:1).
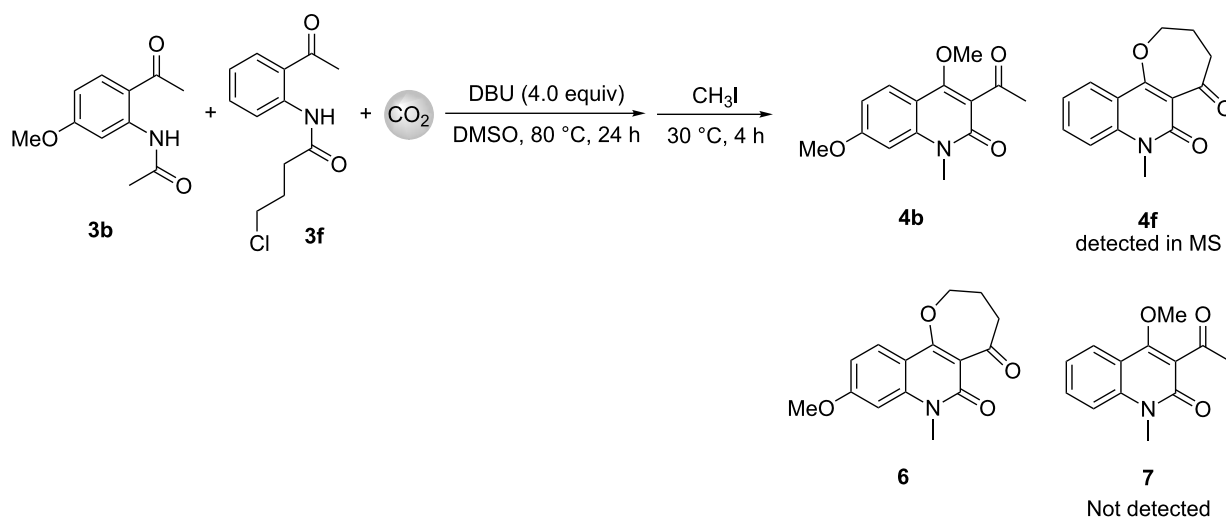
Supporting Information

Supporting Information File 1
Experimental procedures, spectroscopic and analytical data, and copies of NMR spectra of the products.
[http://www.beilstein-journals.org/bjoc/content/supplementary/1860-5397-11-102-S1.pdf]

Acknowledgements

Scheme 2: Cross carboxylative cyclization reaction.

References

1. Pratap, R.; Ram, V. J. *Chem. Rev.* **2014,** *114,* 10476. doi:10.1021/cr500075s
   See for a review.
2. Holbrook, A. M.; Pereira, J. A.; Labiris, R.; McDonald, H.; Douketis, J. D.; Crowther, M.; Wells, P. S. *Arch. Intern. Med.* **2005,** *165,* 1095. doi:10.1001/archinte.165.10.1095
3. Hoeksema, H.; Johnson, J. L.; Hinman, J. W. *J. Am. Chem. Soc.* **1955,** *77,* 6710. doi:10.1021/ja01629a129
4. Cullen, J. J.; Hinkhouse, M. M.; Grady, M.; Gaut, A. W.; Liu, J.; Zhang, Y. P.; Weydert, C. J. D.; Domann, F. E.; Oberley, L. W. *Cancer Res.* **2003,** *63,* 5513.
5. Jönsson, S.; Andersson, G.; Fex, T.; Fristedt, T.; Hedlund, G.; Jansson, K.; Abramo, L.; Fritzson, I.; Pekarski, O.; Runström, A.; Sandin, H.; Thuvesson, I.; Björk, A. *J. Med. Chem.* **2004,** *47,* 2075. doi:10.1021/jm031044w
6. Hack, D.; Chauhan, P.; Deckers, K.; Hermann, G. N.; Mertens, L.; Raabe, G.; Enders, D. *Org. Lett.* **2014,** *16,* 5188. doi:10.1021/ol502551u
7. Prousis, K. C.; Tzani, A.; Avlonitis, N.; Calogeropoulou, T.; Detsi, A. *J. Heterocycl. Chem.* **2013,** *50,* 1313. doi:10.1002/jhet.1869
8. Ambre, P. K.; Pissurlenkar, R. R. S.; Wavhale, R. D.; Shaikh, M. S.; Khedkar, V. M.; Wan, B.; Franzblau, S. G.; Coutinho, E. C. *Med. Chem. Res.* **2014,** *23,* 2564. doi:10.1007/s00044-013-0850-7
9. Sakakura, T.; Choi, J.-C.; Yasuda, H. *Chem. Rev.* **2007,** *107,* 2365. doi:10.1021/cr068357u
10. Riduan, S. N.; Zhang, Y. *Dalton Trans.* **2010,** *39,* 3347. doi:10.1039/b920163g
11. Huang, K.; Sun, C.-L.; Shi, Z.-J. *Chem. Soc. Rev.* **2011,** *40,* 2435. doi:10.1039/c0cs00129e
12. Cokoja, M.; Bruckmeier, C.; Rieger, B.; Herrmann, W. A.; Kühn, F. E. *Angew. Chem., Int. Ed.* **2011,** *50,* 8510. doi:10.1002/anie.201102010
13. Zhang, W.; Lü, X. *Chin. J. Catal.* **2012,** *33,* 745. doi:10.1016/S1872-2067(11)60390-2
14. Tsuji, Y.; Fujihara, T. *Chem. Commun.* **2012,** *48,* 9956. doi:10.1039/c2cc33848c
15. Zhang, L.; Hou, Z. *Chem. Sci.* **2013,** *4,* 3395. doi:10.1039/c3sc51070k
16. Aresta, M.; Dibenedetto, A.; Angelini, A. *Chem. Rev.* **2014,** *114,* 1709. doi:10.1021/cr4002758
17. Flowers, B. J.; Gautreau-Service, R.; Jessop, P. G. *Adv. Synth. Catal.* **2008,** *350,* 2947. doi:10.1002/adsc.200800516
18. Kikuchi, S.; Sekine, K.; Ishida, T.; Yamada, T. *Angew. Chem., Int. Ed.* **2012,** *51,* 6989. doi:10.1002/anie.201201399
19. Sekine, K.; Takayanagi, A.; Kikuchi, S.; Yamada, T. *Chem. Commun.* **2013,** *49,* 11320. doi:10.1039/c3cc47221c
20. Zhang, W.-Z.; Shi, L.-L.; Liu, C.; Yang, X.-T.; Wang, Y.-B.; Luo, Y.; Lu, X.-B. *Org. Chem. Front.* **2014,** *1,* 275. doi:10.1039/c3qo00047h
21. Da Re, P.; Sandri, E. *Chem. Ber.* **1960,** *93,* 1085. doi:10.1002/cber.19600930514
22. Guo, C.-X.; Zhang, W.-Z.; Liu, S.; Lu, X.-B. *Catal. Sci. Technol.* **2014,** *4,* 1570. doi:10.1039/c3cy00858d
23. Zhang, W.-Z.; Xia, T.; Yang, X.-T.; Lu, X.-B. *Chem. Commun.* **2015,** *51,* 6175. doi:10.1039/c5cc01530h
24. Wu, X.-F.; Anbarasan, P.; Neumann, H.; Beller, M. *Angew. Chem., Int. Ed.* **2010,** *49,* 9047. doi:10.1002/anie.201006374
    See for a review.
25. Zhang, Z.; Fang, S.; Liu, Q.; Zhang, G. *J. Org. Chem.* **2012,** *77,* 7665. doi:10.1021/jo3010217
26. Strumfs, B.; Hermane, J.; Belyakov, S.; Trapencieris, P. *Tetrahedron* **2014,** *70,* 355. doi:10.1016/j.tet.2013.11.052
27. Ameen, D.; Snape, T. J. *Synthesis* **2015,** *47,* 141. doi:10.1055/s-0034-1379498

Surprisingly facile CO_2 insertion into cobalt alkoxide bonds: A theoretical investigation

Willem K. Offermans[1], Claudia Bizzarri[1], Walter Leitner[2] and Thomas E. Müller[*1]

Abstract

Exploiting carbon dioxide as co-monomer with epoxides in the production of polycarbonates is economically highly attractive. More effective catalysts for this reaction are intensively being sought. To promote better understanding of the catalytic pathways, this study uses density functional theory calculations to elucidate the reaction step of CO_2 insertion into cobalt(III)–alkoxide bonds, which is also the central step of metal catalysed carboxylation reactions. It was found that CO_2 insertion into the cobalt(III)–alkoxide bond of [(2-hydroxyethoxy)Co^{III}(salen)(L)] complexes (salen = N,N''-bis(salicyliden-1,6-diaminophenyl)) is exothermic, whereby the exothermicity depends on the *trans*-ligand L. The more electron-donating this ligand is, the more exothermic the insertion step is. Interestingly, we found that the activation barrier decreases with increasing exothermicity of the CO_2 insertion. Hereby, a linear Brønsted–Evans–Polanyi relationship was found between the activation energy and the reaction energy.

Introduction

Carbon dioxide (CO_2) has been known to be an attractive carbon source for decades [1-6]. Even so, industrial processes using CO_2 as chemical feedstock are limited to the production of few large scale chemicals such as urea, methanol, salicylic acid as well as inorganic and organic carbonates [5]. Since CO_2 is captured in huge amounts from the flue gases of fossil fuel combustion, it would be very beneficial to harness a part of this stream for producing valuable products [7]. From a thermodynamic point of view, however, CO_2 is highly stable and, thus, shows low reactivity. One way to overcome this thermodynamic hurdle is to react carbon dioxide with relatively high-energy molecules such as ammonia, hydrogen, epoxides or

lactones [8]. Nevertheless, the reactions frequently involve a substantial kinetic barrier or are accompanied by side reactions that, so far, have resulted in insufficient yields and/or selectivities. Even though there are numerous compounds that might react with CO_2, active and selective catalysts for these reactions are scarce [9].

The reaction of CO_2 with epoxides yields alternating polycarbonates, polyethercarbonates or cyclic carbonates (Scheme 1). The production of CO_2-based polymers is considerably more challenging compared to the formation of cyclic carbonates. In consequence, industrially relevant catalysts, combined with efficient processes, have only recently emerged for the manufacture of alternating polycarbonates [10] and polyethercarbonates [11]. The respective research has mainly focussed on homogeneous zinc–alkoxide complexes [12] and chromium– [13-18] and cobalt–salen complexes [19-22] and heterogeneous double metal cyanide (DMC) catalysts [11,23-26]. In comparison, industrially well-established catalysts are available to accelerate the production of cyclic carbonates [27-29]. As the CO_2-based polymers are thermodynamically less stable than cyclic carbonates, a kinetic control must be attained to direct the reaction to the polymeric products. To selectively lower the activation barrier towards polycarbonates, a rational development of suitable catalysts is essential. This current study aims to elucidate the reaction step of CO_2 insertion, catalysed by

cobalt(III)–salen complexes, using density functional theory calculations (DFT).

Results and Discussion
Background research: Formation of CO_2-based polymers

The catalytic pathways for producing polycarbonate and polyethercarbonates have been explored in several studies.

Rieger et al. studied the mechanisms of the copolymerisation by homogeneous chromium(III)– and aluminium(III)–salen complexes and by heterogeneous zinc-dicarboxylates [30,31]. Experimental work on the chromium(III)– and aluminium(III)–salen complexes was combined with a theoretical study, in which the initiation and propagation steps of the copolymerisation were addressed. The initiation started with the coordination of epoxide at a penta-coordinated metal–salen complex, followed by a nucleophilic, S_N2-like, back-side attack on such a coordinated epoxide. The propagation comprised a *syn*-insertion of CO_2 into the metal–alkoxide bond and a bimolecular chain transfer of a metal-bound, carbonate-terminated, growing chain to a metal-coordinated and, thus, activated epoxide (see Scheme 2). For hepta-coordinated Cr(III)– and Al(III)–salen complexes, the CO_2 insertion requires considerable energy, and it was concluded to be the rate-determining step especially at low CO_2 concentrations.

n = 1: Alternating polycarbonate
n > 1: Polyethercarbonate
* End groups of polymer chain
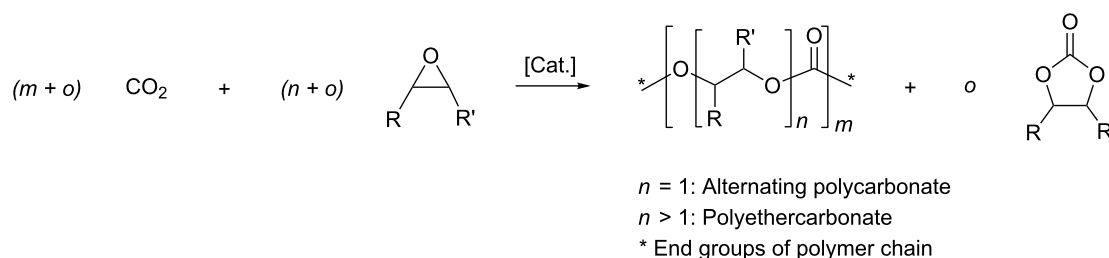
**Scheme 1:** Reaction of carbon dioxide with epoxide to yield alternating polycarbonates, polyethercarbonates or cyclic carbonates.

M = Cr(III) or Al(III)

= salen ligand
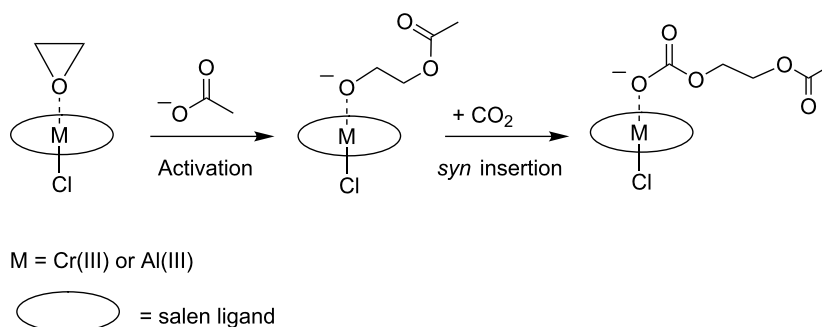
Scheme 2: Epoxide and CO_2 copolymerisation by homogeneous Cr(III)– and Al(III)–salen complexes.
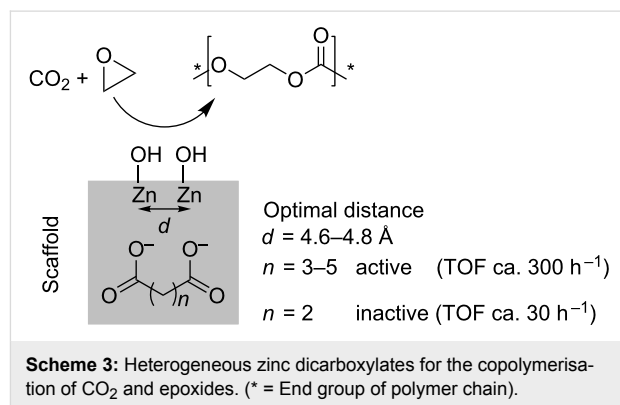
A mechanism for the copolymerisation of epoxides and CO_2, catalysed by cobalt(III)–salen complexes was proposed by Lu et al. [32]. The authors stated that a general mechanism with pending (re)attachment of growing carbonate chains or units might explain the stability, activity and selectivity of the cobalt(III)–salen complexes. Even though CO_2 insertion plays a key role in this mechanism, it is only schematically depicted.

The mechanism of the Zn(II)-catalysed copolymerisation of CO_2 and cyclohexene oxide was the subject of a molecular orbital study on the tri-coordinated di-iminate zinc–alkoxide complex [(BDI)ZnOCH$_3$], whereby BDI is *N*-(2,6-iPr$_2$C$_6$H$_3$C(Me)-CHC(Me)-*N*-(2,6-iPr$_2$C$_6$H$_3$) (see Figure 1) [33]. The study was based on the ONIOM [34,35] method, which is a computationally intricate method applied to atoms directly involved or in close vicinity of the reaction center, but involves less demanding calculations for the outer periphery.


Figure 1: The tri-coordinated di-iminate zinc–alkoxide complex [(BDI)ZnOCH$_3$].
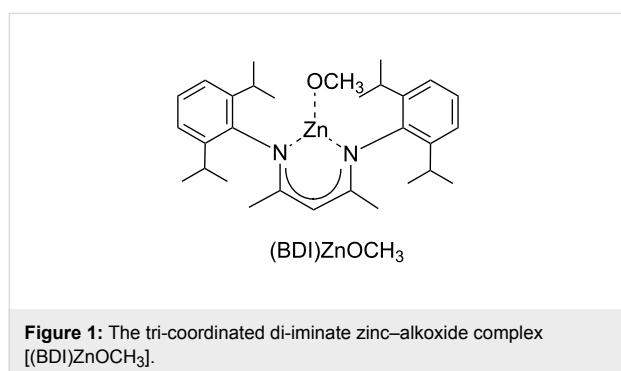
Though kinetically favoured, the insertion of CO_2 into the zinc–alkoxide bond turned out to be thermodynamically less favourable than the insertion of epoxide. A low activation barrier found for the CO_2 insertion into the zinc–alkoxide bond may be related to the use of a relatively high energy unsaturated 16-electron complex. In the reaction mixture of neat cyclohexene oxide, the complex will readily coordinate additional cyclohexene oxide as solvent molecule(s). Accompanied by high activation barriers, the ring opening of the epoxide and the electrophilic insertion into either the zinc–alkoxide or zinc carbonate bond occur consecutively. Only if the ring is pre-activated by, for example, sufficient ring strain, the polymerisation reaction does become feasible.

In mechanistic studies on zinc dicarboxylates and their application in the heterogeneously catalysed copolymerisation of CO_2 and epoxides a bimetallic mechanism was proposed [31]. As post-modification of the prepared catalysts with water proved to be important for the activity of the catalysts, the presence of ZnOH groups at the surface may be inevitable for the catalysis. Two zinc atoms, in a distance of approximately 4.6–4.8 Å, are present at the surfaces of zinc glutarate, zinc adipate and zinc pimelate (Scheme 3). This spatial conformation of two zinc atoms is not present on the surface of zinc succinate. This was used to explain the activity of the former three and the inactivity of the latter. Theoretical calculations revealed a decrease in the activation barrier for the homopolymerisation as well as the copolymerisation step with increasing metal–metal distance. Moreover, the difference in activation barriers between the homo- and copolymerisation decreased with an increase in the metal–metal distance, but levelled at distances above 5 Å. Thus, a distance of 4.6–4.8 Å is a good compromise to avoid the homopolymerisation and to enhance the catalytic activity for the copolymerisation. Involving two proximate zinc atoms, which coordinate the reactants, the ring-opening of epoxides by alkylcarbonates or alkoxides occurs in a bimetallic fashion [31,36]. The insertion of CO_2 was not further addressed and was regarded as facile by the authors.

Scheme 3: Heterogeneous zinc dicarboxylates for the copolymerisation of CO_2 and epoxides. (* = End group of polymer chain).

Background research: Formation of cyclic carbonates

Cyclic carbonates can be formed either by a backbiting mechanism from a growing polymer chain [30] (Scheme 4) or directly by the catalytic cycloaddition of CO_2 and epoxides [27-29].

**Scheme 4:** Backbiting mechanism for the formation of cyclic carbonates.
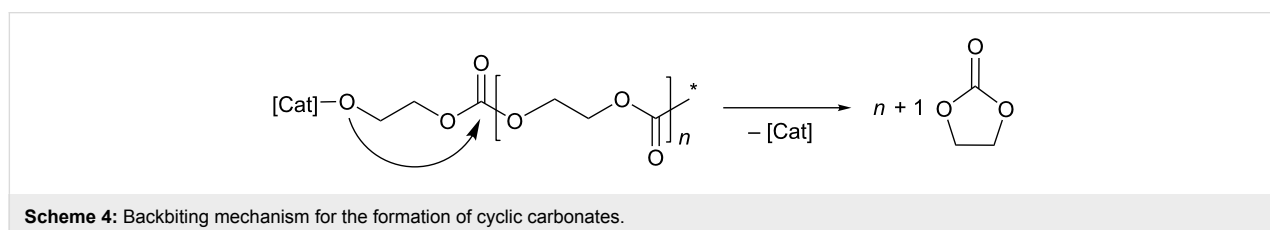
Sun and Zhang modelled the cycloaddition of CO_2 with propylene oxide, catalysed by alkylmethylimidazolium chlorine ionic liquids [37]. They identified competitive three-step and two-step pathways, both having the ring opening of propylene oxide as the rate-determining step. In the three-step pathway, the ring opening precedes the CO_2 insertion. By contrast, in the two-step pathway, the ring opening and CO_2 insertion occur simultaneously, whereby at a given time three molecules need to orientate themselves into a particular configuration to form the transition state (see Scheme 5). This is demanding with respect to the entropy effects. In both pathways, the CO_2 addition to the epoxide was found to be facilitated considerably by hydrogen bonding interactions. Thus, a scaffold of hydrogen bonds can compensate for the lack of a Lewis acid metal center to activate the CO_2 molecule.

In addition, Zhang et al. investigated the coupling of propylene oxide with CO_2 catalysed by a copper(I)–cyanomethyl complex [38]. They proposed two reaction steps: insertion of carbon dioxide forming a copper(I) cyanoacetate as activated CO_2 carrier that reacts in a second step with propylene oxide (see Scheme 6). Formation of propylene carbonate subsequently involves the oxidative transformation of an eight-membered ring intermediate to a six-membered ring.

Moreover, Wu et al. studied a) the cycloaddition of ethylene oxide and CO_2, catalysed by $Ni(PPh_3)_2$ [39], b) the cycloaddition of chloromethyloxirane and CO_2, catalysed by $Re(CO)_5Br$ [40] and c) the cycloaddition of 4-(phenoxymethyl)-1,3-dioxolan-2-one and CO_2, catalysed by LiBr [41]. The preferred path-

ways principally involve ring opening of the epoxide, followed by CO_2 insertion and ring closure of the cyclic carbonate. Interestingly, in the Re(I)-catalysed reaction (b), an alternative reaction pathway was followed, whereby the first step is CO_2 insertion, induced by the nucleophilic attack of the bromide on the carbon atom of CO_2. The transition state comprised a four membered oxametallacycle (see Scheme 7). The alternative insertion of epoxide into the Re–Br bond was found to be significantly more energy demanding.
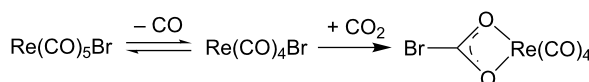
Scheme 7: Activation of CO_2 by nucleophilic attack of bromide in the Re(I)-catalysed cycloaddition.

Background research: Activation of CO_2 by insertion into metal–H and metal–R bonds

The insertion of CO_2 into metal–alkoxide bonds is believed to be a key step in the aforementioned catalytic routes to polycarbonates and cyclic carbonates. In this context, several studies on the activation of CO_2 and insertion into metal–H and metal–X bonds have been reported [42,43] (see Scheme 8).

The reaction of CO_2 with metal alkoxides is reversible as the metal–oxygen bond strengths of metal alkoxides and of metal carbonates are similar [44,45]. The theoretically derived mechanism points out an intermediate encounter complex between CO_2 and metal alkoxide. Formation of this associative complex
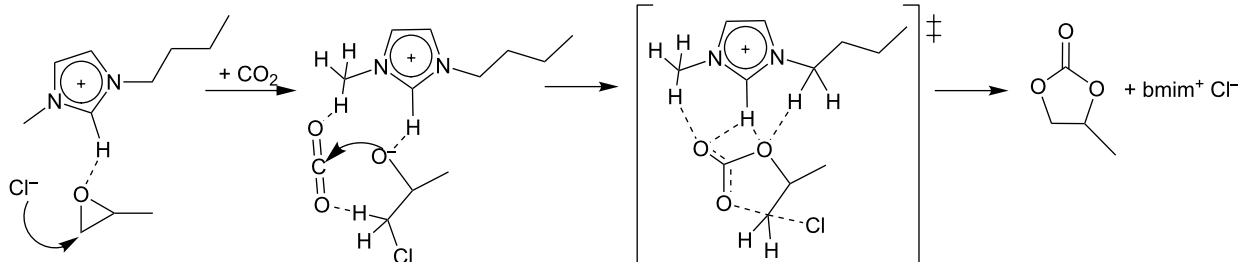
Scheme 5: Two-step pathway for the cycloaddition of propylene oxide and CO_2 in the ionic liquid 1-butyl-3-methylimidazolium chloride ($bmim^+$ Cl^-).
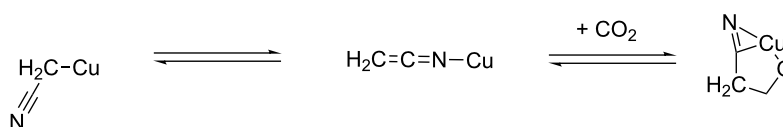
Scheme 6: Formation of copper(I) cyanoacetate for the activation of CO_2.

Scheme 8: Direct catalytic carboxylation of aliphatic compounds and arenes by rhodium(I)– and ruthenium(II)–pincer complexes, respectively.
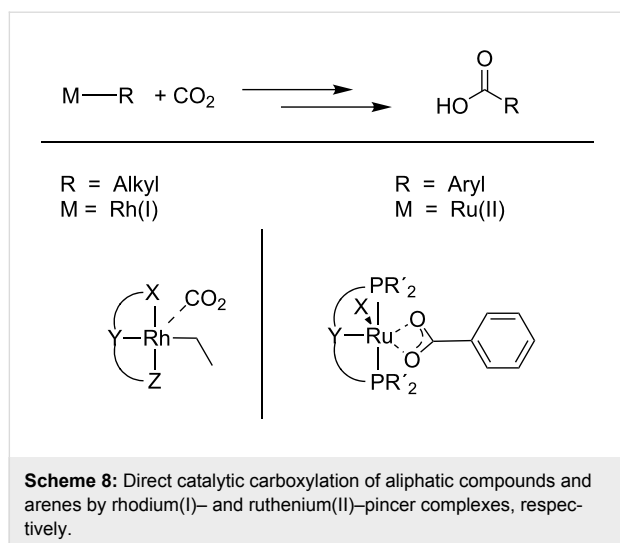
is endergonic due to the entropy effects [45]. The transition state for the CO_2 insertion into metal–oxygen bonds has been postulated to be a four-membered ring consisting of the metal, the carbon and two oxygen atoms (Scheme 9) [44]. For this cycloaddition pathway, a vacant coordination site at the metal center is not necessary.

Scheme 9: Insertion of carbon dioxide into a metal–oxygen bond via a cyclic four-membered transition state. R is either an aliphatic or aromatic group.

Kato et al. reported on the facile uptake of CO_2 into zinc–alkoxide bonds leading to zinc-coordinated monoalkyl carbonates by zinc(II)–tetraazacycloalkane complexes (Scheme 10) in the presence of alcohols [46]. Here, the uptake

of CO_2 from the air was found to occur spontaneously, even in neutral solution and low temperatures below 10 °C. This clearly exemplifies the high reactivity of the CO_2 molecule under appropriately chosen conditions.
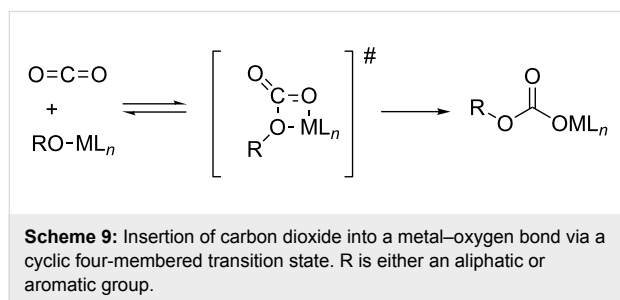
Later, Kunert et al. investigated the mechanism of CO_2 insertion into zinc(II)-phenoxide to form zinc(II)–phenylcarbonate [47]. The CO_2 insertion was found to take place via electrostatic interactions between the electron lone pairs of the zinc-bonded oxygen and the carbon of CO_2, forming an intermediate that finally produces a stable insertion product.

Current research: CO_2 Insertion into cobalt–alkoxide bonds

Even though CO_2 insertion into metal–oxygen bonds plays a key role in the mechanistic pathways for the copolymerisation of epoxides and CO_2, this elementary step is only schematically depicted. Consequently, there is still a lack of understanding of the CO_2-insertion step on a molecular or atomic level. In particular, a detailed study of CO_2 insertion into cobalt–alkoxide bonds is still missing.

This present work aims to investigate CO_2 activation, in general, and the insertion step in the copolymerisation of CO_2 and epoxides, in particular, by DFT methods, using the cobalt(III)–salen complex illustrated in Figure 2 as a model for the catalyst. For the sake of simplicity, the salen ligand is depicted as a circle, although in the discussed calculations the salen ligand is represented by its correct nuclei and electrons. For most calculations the substituents were taken as protons (R^{1-6} = H, salen ligand **1**). To test the validity of the model with respect to the relative energies and geometries, the salen ligand sphere was extended to a cyclohexyl backbone ($R^1\frown R^2$ = $-C_4H_8-$) with the substituents R^{3-6} = H (salen ligand **1a**) and R^{3-6} = *t*-Bu (salen ligand **1b**). The ligand L was varied in the calculations from stronger electron-donating nucleophiles, such as chloride and acetate, to weaker electron-donating ligands, such as 2,4-dinitrophenolate.
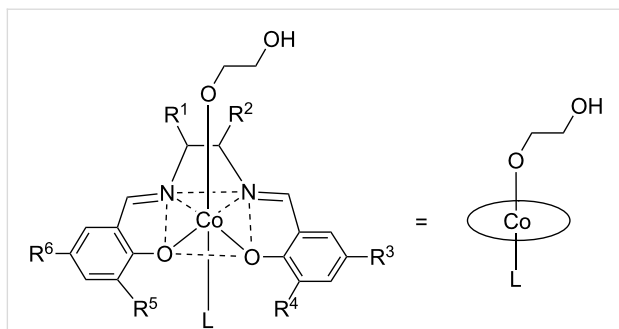

Scheme 10: Facile CO_2 uptake by zinc(II)–tetraazacycloalkanes.
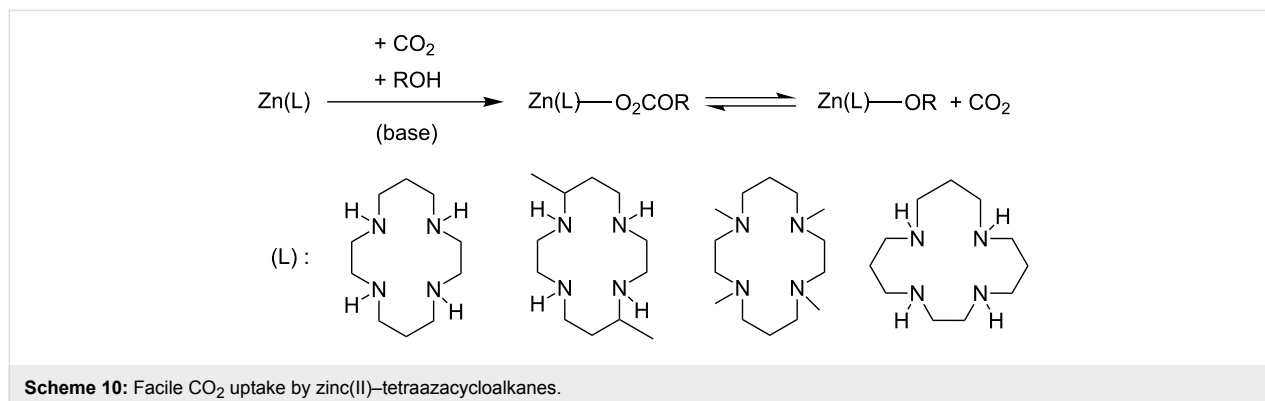
Figure 2: The [(2-hydroxyethoxy)Co^{III}(salen)(L)] complex chosen as catalyst model for the calculations; **1**: R$^{1–6}$ = H; **1a**: R^{1}⌢R^{2} = -C$_4$H$_8$-, R$^{3–6}$ = H; **1b**: R^{1}⌢R^{2} = -C$_4$H$_8$-, R$^{3–6}$ = *t*-Bu.

The salen ligand can assume different configurations relative to the cobalt center [48]. To test the significance of the *mer,mer*- and the *mer,fac*-configuration (Figure 3), the total energy was calculated. It was found that the *mer,mer*-configuration was significantly more stable than the *mer,fac*-configuration. The difference in total energy was 96 kJ·mol^{-1} for chloride and 30 kJ·mol^{-1} for 2,4-dinitrophenolate. Therefore, the further study was limited to models with *mer,mer*-configuration. Here, the salen ligand coordinates the central cobalt atom in a square-planar fashion, whereby the *trans*-ligand L is located in the lower and 2-hydroxyethoxide in the upper hemisphere, respectively.

The modelling of the insertion reaction started with the geometry optimization of a free CO_2 molecule and the parent [(2-hydroxyethoxy)Co^{III}(salen)(L)] complex. This is indicated as the reactant state (**RS**) in Figure 4. We found a linear CO_2 molecule (179.998°) with a bond distance of 1.177 Å, which is in good agreement with experimental and theoretical data [37]. In the [(2-hydroxyethoxy)Co^{III}(salen)(L)] complex, the cobalt atom was located at the center of the salen ligand. The distances between the cobalt center and the nitrogen and oxygen atoms of the salen ligand were 1.92 Å and 1.94 Å, respectively. This is consistent with the single crystal solid-state structure reported for [Co^{III}(salen)(dinitrophenolate)] [49]. The distance between cobalt and the oxygen atom of the alkoxide chain was 1.9–1.94 Å, with a small yet systematic variation in dependence on the nucleophilicity of L. The more nucleophilic L was, the longer the Co–OR distance was. The Co–L bond length was calculated to be 2.03–2.13 Å for L with a coordinating oxygen-atom and 2.35 Å for chloride. The calculated Mulliken charge was 0.7–0.72 C on the cobalt center for L with a coordinating oxygen atom and 0.64 C for chloride consistent with a more nucleophilic character of chloride.

In a search for possible interactions between CO_2 and the cobalt-salen-alkoxide complex, the calculations revealed a precursor state, formed during the approach of CO_2 to the [(2-hydroxyethoxy)Co^{III}(salen)(L)] complex (Figure 4). Inspection
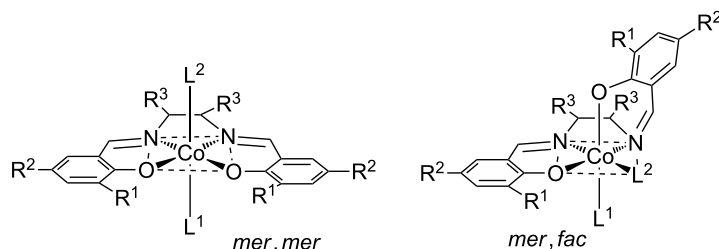

Figure 3: The two most relevant configurations of [(2-hydroxyethoxy)Co^{III}(salen)(L)] complexes. The left-hand model shows a *mer,mer*-configuration, while the right-hand models shows a *mer,fac*-configuration of the salen ligand.
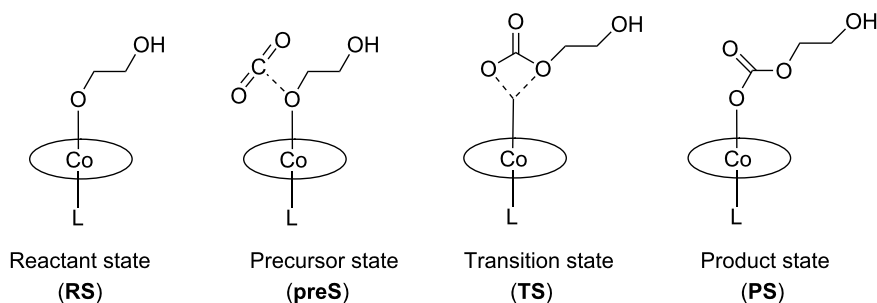

Figure 4: Carbon dioxide insertion into the cobalt(III)–alkoxide bond of [(2-hydroxyethoxy)Co^{III}(salen)(L)] complexes.

Table 1: Relative energies with respect to free CO_2 and free cobalt(III)–salen complex of the precursor, transition and product state of the CO_2 insertion reaction as shown in Figure 4.

Salen ligand	*trans*-Ligand	Precursor state[a] (**preS**)	Transition state[a] (**TS**)	Product state[a] (**PS**)	Activation barrier	Reaction energy
		[kJ·mol^{-1}]	[kJ·mol^{-1}]	[kJ·mol^{-1}]	[kJ·mol^{-1}]	[kJ·mol^{-1}]
1	chloride	−14	31	−47	45	−33
1	$CH_3C(O)O^-$	−14	45	−30	59	−16
1a[b]	$CH_3C(O)O^-$	−12	41	−31	53	−19
1b[c]	$CH_3C(O)O^-$	−11	39	−37	50	−26
1	*p*-methoxyphenolate	−14	41	−33	55	−19
1	$CCl_3C(O)O^-$	−21	34	−30	55	−9
1	2,4-dinitrophenolate	−22	68	−29	90	−7
1	2,4,6-trinitrophenolate	−11	79	−16	90	−5
1	TBD[d]	−14	65	−29	79	−15
1	none	−13	58	−6	71	7
1	ethylene oxide	−17	100	−8	117	9

[a]Potential energies relative to free CO_2 and the free cobalt(III)–salen complex, i.e., the reactant state was set to zero for each *trans*-ligand L.
[b]Salen with cyclohexyl backbone, $R^1\frown R^2 = -C_4H_8-$, $R^{3-6} = H$
[c]Salen with cyclohexyl backbone, $R^1\frown R^2 = -C_4H_8-$, $R^{3-6} = t$-Bu
[d]TBD = 1,5,7-triazabicyclo[4.4.0]dec-5-ene.

of the geometry revealed that the closest intermolecular distance was between the carbon atom of CO_2 and the oxygen atom of the alkoxide chain; the shortest distance was for chloride (1.67 Å) and the longest for a pending 1,5,7-triazabicyclo[4.4.0]dec-5-ene group (TBD) as ligand L (3.59 Å, see Supporting Information File 1). The change in the CO_2 bond angle with respect to linear CO_2 was marginal (2° to 6°). For the chloro complex [(2-hydroxyethoxy)Co^{III}(salen)(Cl)], the potential energy surface was found to be extremely flat with respect to the O–CO_2 distance, meaning that minimum states with a 40° bent CO_2 molecule and states with a practically linear CO_2 molecule have almost equal energy. We noticed a similar configuration of the four atoms in the transition state (vide infra). The geometry in the cobalt–salen complexes was very similar to the reactant state; solely the cobalt–alkoxide bond length increased slightly yet systematically. For each L, the precursor state (**preS**) was 10–20 kJ·mol^{-1} more stable than the reactant state (**RS**). Thus, the change in energy was small with respect to the reactant state. Consistent with an associative step, the entropy change was negative and the change in free energy was positive. Consistent with the weak interaction between CO_2 and the [(2-hydroxyethoxy)Co^{III}(salen)(L)] complex, the calculated Mulliken charge on the metal center and its surrounding geometry hardly changed with respect to the reactant state. Similar precursor states were reported for a supramolecular complex of ethylmethylimidazolium chloride, CO_2, and propylene oxide (complex c in [37]) and for the association complex of [Ni(OH)(pincer ligand)] and CO_2 [50].

The calculations for the product state (**PS**) revealed an optimized structure for each ligand L, whereby the carbonate chain was coordinated in a mono-dentate fashion to the cobalt center (Figure S1 in Supporting Information File 1). The calculated Co^{III}–L bond lengths were 1.95–2.08 Å, when the coordinating atom was oxygen, and 2.29 Å, when it was chloride. In general, these bond lengths were shorter than in **RS** (by 0.03–0.06 Å). Independently of the choice of L, the cobalt atom was located in the center of the salen ligand at an average distance of 1.93(2) Å from the coordinating atoms. Thus, there was only a minor geometrical change in respect to the lower hemisphere of the [(2-hydroxyethoxy)Co^{III}(salen)(L)] complex. The distance of the newly formed Co^{III}–O bond varied from 1.99 Å to 1.93 Å depending on the nucleophilicity of L: the less nucleophilic the ligand L was, the shorter the Co^{III}–O bond was. The carbon–oxygen bond lengths within the carbonate unit were 1.294(5) Å for C1–O3, 1.236(3) Å for C1–O4, and 1.392(11) Å for C1–O5, with only little variation in length upon variation of L. Hence, the carbon–oxygen bond lengths were clearly lengthened relative to the CO_2 molecule. The energies of the product states were lowered with respect to the reactant states. The less nucleophilic the ligand L was, the less stabilized the carbonate species was with respect to free CO_2 and the [(2-hydroxyethoxy)Co^{III}(salen)(L)] complex. The respective Mulliken charge on the cobalt atom was 0.71(1) C in the case of L having an oxygen-coordinating atom and 0.62 C for L being chloride. Consequently, there was no change in the charge of cobalt with respect to the **RS**.

Using the precursor and product states as the anchor points, the transition states were located for each L. All determined transition states were geometrically similar, depicting a cyclic arrangement around the cobalt(III) atom, an oxygen and carbon atom of CO_2 and the oxygen atom of the original Co–O alkoxide bond (Figure 4). These configurations were identical to the arrangement of the reactive atoms in the transition states of the reaction between [Ni(OH)(pincer ligand)] complexes and CO_2 [50]. Since the configurations of the reactive atoms are essentially identical in the reactant, precursor, transition and product states, we conclude that the mechanism of the CO_2 insertion reaction is very similar for cobalt-alkoxide and nickel-hydroxide complexes.

In the case of Cr(III)–salen complexes, it was found [18] that in the transition state of the CO_2 insertion step, the Cr–O bond is elongated (from 1.96 Å to 2.12 Å) as well as the CO_2 molecule is bent (OCO angle 146.7°). The new C–O and Cr–O bonds (after CO_2 insertion) form synchronously, without prior activation by binding to the Lewis acidic Cr(III) center, as the coordination sphere of chromium is saturated.

Regarding Al(III)–salen complexes, the insertion step into an Al(III)-alkoxide bond is a simple intramolecular process with a small activation energy ($\Delta E^{\#}$ = 9.12 kcal/mol) [30,51]. Nevertheless, a bimetallic aluminium complex is considered in the mechanism. Since it is a bimolecular reaction, the Gibbs energies will be higher. Carbon dioxide insertion may well be the rate-determining step, certainly at lower CO_2 pressure.

Also in the transition state (**TS**) the cobalt atom was located at the center of the coordination sphere at a distance of 1.9 Å from the salen ligand. Thus, there is no significant movement of the cobalt center during the reaction with CO_2. The Co^{III}–L bond lengths were calculated to be 1.90–1.98 Å for the coordinating atom being oxygen and 2.24 Å for chloride. The Co^{III}–L bond distances were found to shorten from **RS** to **preS** and **TS**. Although this bond elongates from **TS** to **PS**, the length is still shorter than in **RS**. As these systematic changes were only in the 0.01–0.10 Å range, the geometrical changes in the lower hemisphere of the cobalt(III)–salen complex are only minor during the CO_2 insertion. This is consistent with the changes of the calculated Mulliken charge on the cobalt center. The charge at the transition state was 0.7–0.73 C for L with an oxygen-coordinating atom and was 0.6 C for chloride. The changes over the different states were only noticeable on the scale of 0.01–0.1 C.

Focussing on the arrangement of the four reactive atoms in the transition state and, in particular, on the forming carbonate unit, it is noteworthy that the distance between the carbon atom of CO_2 and the oxygen atom of the alkoxide chain was only slightly larger in the transition state than in the product state. This applies to the carbon–oxygen bond length of the carbonyl group as well. By contrast, the bond length between the carbon atom of CO_2 and the oxygen atom of the forming Co–O–C moiety was slightly shorter in the transition state than in the product state. Although the changes in the bond lengths of the forming carbonate unit were systematic for all L, the changes were small (0.01–0.05 Å). This is consistent with the minor changes in the (O–C–O) angle of the forming carbonate unit between **TS** and **PS**. This means that the configuration of the carbonate unit in the transition state is already very close to the one in the product state. Hence, the major geometrical rearrangement from the transition to product state is concentrated in the O–Co–O configuration, i.e., in the change of the hapticity of the cobalt center from η^2 to η^1 and the inherent changes in bond lengths. The cobalt(III)–alkoxide bond breaks and the newly formed Co^{III}–O bond is shortened by ca. 0.8–1.4 Å in the switchover from **TS** to **PS**. Particular attention ought to be given to the cobalt–oxygen bond lengths of the different L = $CH_3C(O)O^-$ models. In the transition state, there was no difference between the minimal model (salen ligand **1**) and the extended model with only the cyclohexyl backbone (salen ligand **1a**). However, the introduction of the additional *t*-Bu groups (salen ligand **1b**) led to a significant increase of ca. 0.5 Å in these lengths. This is remarkable, since the bond lengths and the respective relative energies in the reactant, precursor and product states were quite similar for all L = $CH_3C(O)O^-$ models. This means that the coordinated L = $CH_3C(O)O^-$ has no significant influence on the CO_2 insertion itself, but only on the relative energy of the cobalt–salen complex. Since the variation in the cobalt–oxygen bond lengths of the O–Co^{III}–O units over all nucleophiles L was relatively large, roughly 2.5–3.5 Å for both bonds, and not systematic for the various ligands L, we assume that this reduced influence of the nucleophile L on the CO_2 insertion applies to the other ligands L as well. This is also consistent with the minor changes in the geometry of the lower hemisphere of the [(2-hydroxy-ethoxy)Co^{III}(salen)(L)] complexes during CO_2 incorporation and in the Mulliken charge on the cobalt center.

Current research: Brønsted–Evans–Polanyi relationship

The relative energies of the precursor, transition and product states with respect to the reactant state are listed in Table 1. The energy difference between the product state and transition state relative to the reactant state in **preS** is the reaction energy and activation barrier, respectively. In Figure 5 the activation barrier is plotted as a function of the reaction energy. Clearly, the values of both energies depend on the choice of the nucleophile L. The more electron-donating the ligand is, the smaller the ac-
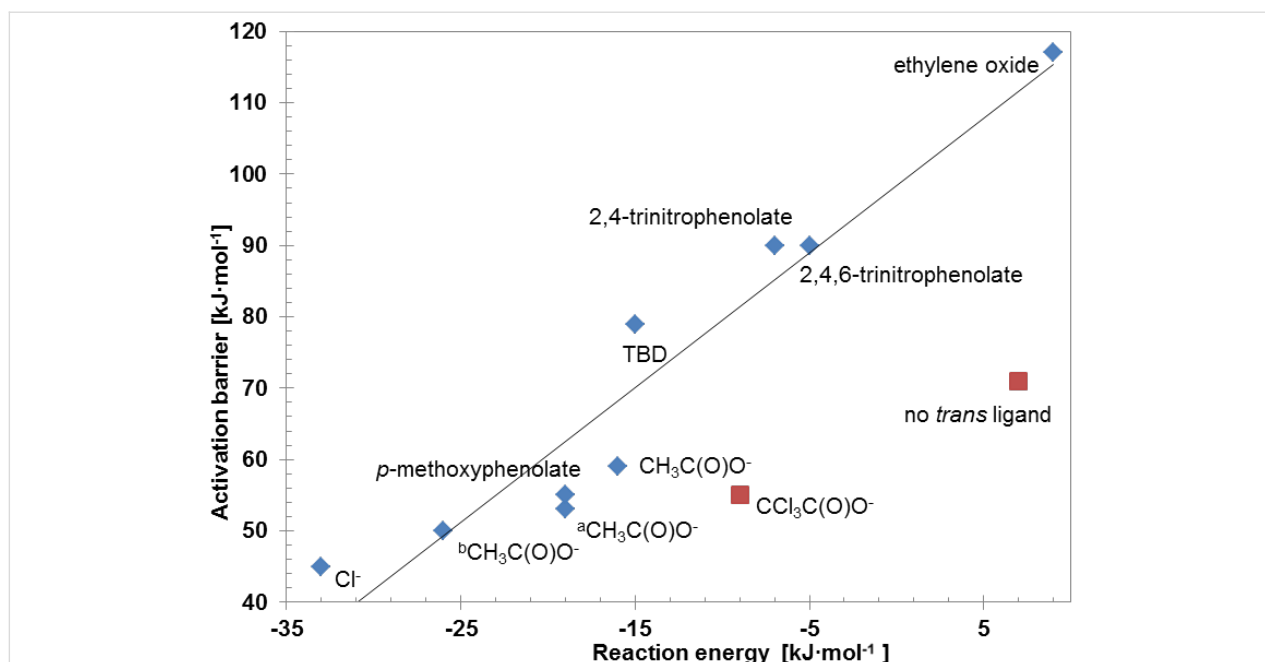
Figure 5: Energy relationship between the activation barrier and the reaction energy of the CO_2 incorporation reaction. Plotted are the results for different nucleophiles L, attached to the Co^{III}–salen base structure as depicted in Figure 2; [a]salen ligand **1a**: $R^1{\frown}R^2$ = $-C_4H_8$-, R^{3-6} = H; [b]salen ligand **1b**: $R^1{\frown}R^2$ = $-C_4H_8$-, R^{3-6} = *t*-Bu. The energies calculated for those ligands depicted with a red square do not follow the BEP relationship (for details, see text). The line represents the equation E_a = (1.9 ± 0.2)·ΔE + (99 ± 4) [kJ·mol^{-1}].

tivation barrier is and the more exothermic the reaction energy is. This linear relationship between the activation barrier and reaction energy is an example of the Brønsted–Evans–Polanyi (BEP) relationship [52]. Mostly, the reaction energy is exothermic, which implies that the cobalt–carbonate bond is stronger than the cobalt–alkoxide bond. Since the alkoxide is a stronger Lewis base than the carbonate, we calculated an increase in bond strength between the carbonate unit and cobalt center with respect to the cobalt(III)–alkoxide bond, depending on the nucleophilicity of the ligand L. This corresponds to a decrease in the Lewis acidity of the cobalt center.

Consequently, the picture evolves to the reaction of an electrophilic CO_2 molecule with a nucleophilic alkoxide chain connected to a cobalt(III) center. The CO_2 molecule reacts via the carbon atom with the oxygen atom of the alkoxide chain to a carbonate unit. Here, the distance to the metal center does not seem to be energetically important, and the geometrical changes within the carbonate unit are similar for all considered *trans*-ligands L. Therefore, we assume that the significant energy differences in the activation and the reaction energy arise from the differing ability of the *trans*-ligand L to stabilize the cobalt(III)–salen complexes.

The energies calculated for L = $CCl_3C(O)O^-$ and for the absence of a *trans*-ligand do not follow the BEP relationship. This is readily explained by the electronic state and the

HOMO–LUMO gap of these complexes [53]. Penta-coordinated cobalt(III)–salen complexes are high-spin complexes and spin-restricted calculations are insufficient to describe their electron configuration. In the hexa-coordinated [(2-hydroxyethoxy)Co^{III}(salen)(trichloroacetate)] complex, the trichloroacetate ligand is so weakly coordinating that the same argument applies.

Thus, neither coordination of CO_2 prior to the insertion of CO_2 into a metal–X bond [50,53,54] nor activation of CO_2 by a base (co-catalyst) is required. The base merely helps to open the epoxide, while CO_2 being a weak electrophile, it requires a strong Lewis base in order for CO_2 to react [54]. Addition of CO_2 to the activated epoxide then occurs with a very low activation barrier [55]. In contrast, it has been generally believed up to now that, in the catalysed reaction of CO_2 and epoxides, both reactants need to be activated [16,56].

Conclusion

We found that CO_2 readily inserts into the cobalt(III)–alkoxide bond of [(2-hydroxyethoxy)Co^{III}(salen)(L)] complexes. Since the insertion occurs in a *syn* fashion via a four-membered ring structure, it does not need a free coordination site at the cobalt(III) center. We further found that the reaction energy of the CO_2 insertion into the cobalt(III)–alkoxide bond is exothermic and that its magnitude depends on the *trans*-ligand coordinated to the cobalt(III)–salen complex. The more elec-

tron-donating this ligand is, the more exothermic the reaction energy is. Moreover, we found that the activation energy decreases with increasing exothermicity of the CO_2 insertion. Thereby, a linear relationship between the activation energy and the reaction energy – a so-called Brønsted–Evans–Polanyi relationship – was found. This relationship enables one to predict the activation barrier from the reaction energy. Since the calculation of the former can be a delicate undertaking and the calculation of the latter is much easier, the relationship can be used to estimate the activation barrier for CO_2 insertion into cobalt(III)–alkoxide bonds of similar, yet unknown complexes. Since we found a linear relationship between the reaction energy and activation energy and that the reaction is more exothermic for stronger electron-donating ligands, we logically conclude that the CO_2 insertion is more facile for more electron-donating ligands. Since it was experimentally shown that cobalt(III)–salen complexes coordinated by electron-withdrawing ligands, are more active in the carbonate formation from epoxides and CO_2, our findings indicate that the CO_2 insertion cannot be the rate-determining step in these reactions.

Experimental

Electronic structure calculations within the framework of density functional theory (DFT) were performed by using the DMol3 program [57,58]. The Perdew–Burke–Ernzerhof functional to account for the exchange correlation of the electrons was applied [59]. A double numerical basis set plus a polarization d-function on all non-hydrogen atoms and a polarization p-function on all hydrogen atoms was used to expand the one-electron Kohn–Sham eigenfunctions. If not otherwise stated, then full electron, spin-restricted calculations were performed. No constraints were applied during geometry optimisation. All reactant and product states were shown to be minima by a normal mode frequency analysis. The synchronous-transit method was applied to localize possible transition states [60]. These states were further optimized by following eigenvectors to gain the best predicted configuration of the transition state. Transition states were analysed by a normal mode frequency analysis and confirmed by only one imaginary frequency. It was confirmed by the calculation of the minimum energy path that the transition state connected the reactant and product state on the potential energy surface. Tests on several molecules showed that the electronic configuration can be trustfully determined by spin-restricted calculations. This is consistent with diamagnetic, low-spin, hexa-coordinated cobalt(III)–salen complexes, observed by Kemper et al. [61], and the results of DFT calculations of similar, hexa-coordinated cobalt(III)–salen complexes by Sun et al. [62]. In the spin-unrestricted calculations, a triplet state was considered and the minima of the corresponding spin-restricted calculations were used as initial structures. It turned out that the total energy of the geometrical optimised structures with triplet state was higher than the total energy of the spin-restricted calculations. A geometrical change was observed as well. The hexa-coordinated cobalt(III)–salen complex changed into a penta-coordinated, quadratic pyramidal structure. This is consistent with the observations and calculations of Kemper et al. and confirms that paramagnetism and penta-coordination of cobalt(III)–salen complexes are related. Solvent effects were not considered in the present study.

Supporting Information

Supporting Information File 1
Atomic coordinates, calculated bond lengths and bond angles as well as calculated Mulliken charges for the reactant state, the precursor state, the transition state and the product state.
[http://www.beilstein-journals.org/bjoc/content/supplementary/1860-5397-11-144-S1.pdf]

Acknowledgements

References

1. Aresta, M.; Dibenedetto, A. *Dalton Trans.* **2007,** 2975–2992. doi:10.1039/b700658f
2. Leitner, W. *Coord. Chem. Rev.* **1996,** *153,* 257–284. doi:10.1016/0010-8545(95)01226-5
3. Aresta, M. *Carbon Dioxide as Chemical Feedstock;* Wiley-VCH: Weinheim, Germany, 2010. doi:10.1002/9783527629916
4. Baiker, A. *Appl. Organomet. Chem.* **2000,** *14,* 751–762. doi:10.1002/1099-0739(200012)14:12<751::AID-AOC85>3.0.CO;2-J
5. Peters, M.; Köhler, B.; Kuckshinrichs, W.; Leitner, W.; Markewitz, P.; Müller, T. E. *ChemSusChem* **2011,** *4,* 1216–1240. doi:10.1002/cssc.201000447
6. Kember, M. R.; Buchard, A.; Williams, C. K. *Chem. Commun.* **2011,** *47,* 141–163. doi:10.1039/C0CC02207A
7. Markewitz, P.; Kuckshinrichs, W.; Leitner, W.; Linssen, J.; Zapp, P.; Bongartz, R.; Schreiber, A.; Müller, T. E. *Energy Environ. Sci.* **2012,** *5,* 7281–7305. doi:10.1039/c2ee03403d
8. Sakakura, T.; Choi, J.-C.; Yasuda, H. *Chem. Rev.* **2007,** *107,* 2365–2387. doi:10.1021/cr068357u
9. Coates, G. W.; Moore, D. R. *Angew. Chem., Int. Ed.* **2004,** *43,* 6618–6639. doi:10.1002/anie.200460442
10. Lu, X.-B.; Darensbourg, D. J. *Chem. Soc. Rev.* **2012,** *41,* 1462–1484. doi:10.1039/C1CS15142H
11. Langanke, J.; Wolf, A.; Hofmann, J.; Böhm, K.; Subhani, M. A.; Müller, T. E.; Leitner, W.; Gürtler, C. *Green Chem.* **2014,** *16,* 1865–1870. doi:10.1039/C3GC41788C
12. Müller, T. E.; Gürtler, C.; Elmas, S.; Köhler, B.; Leitner, W.; Harrer, M.; Sundermeyer, J. Verfahren zur Herstellung von linearen und/oder cyclischen Carbonatestern. Eur. Pat. Appl. EP2700633 A1, Feb 26, 2014.

13. Darensbourg, D. J.; Andreatta, J. R.; Jungman, M. J.; Reibenspies, J. H. *Dalton Trans.* **2009,** 8891–8899. doi:10.1039/b911061e

14. Darensbourg, D. J.; Fang, C. C.; Rodgers, J. L. *Organometallics* **2004,** *23,* 924–927. doi:10.1021/om034278m

15. Qin, Z.; Thomas, C. M.; Lee, S.; Coates, G. W. *Angew. Chem., Int. Ed.* **2003,** *42,* 5484–5487. doi:10.1002/anie.200352605

16. Paddock, R. L.; Nguyen, S. T. *J. Am. Chem. Soc.* **2001,** *123,* 11498–11499. doi:10.1021/ja0164677

17. Eberhardt, R.; Allmendinger, M.; Rieger, B. *Macromol. Rapid Commun.* **2003,** *24,* 194–196. doi:10.1002/marc.200390022

18. Adhikari, D.; Nguyen, S. T.; Baik, M.-H. *Chem. Commun.* **2014,** *50,* 2676–2678. doi:10.1039/c3cc48769e

19. Ready, J. M.; Jacobsen, E. N. *J. Am. Chem. Soc.* **2001,** *123,* 2687–2688. doi:10.1021/ja005867b

20. Ready, J. M.; Jacobsen, E. N. *Angew. Chem., Int. Ed.* **2002,** *41,* 1374–1377. doi:10.1002/1521-3773(20020415)41:8<1374::AID-ANIE1374>3.0.CO; 2-8

21. Nakano, K.; Kamada, T.; Nozaki, K. *Angew. Chem., Int. Ed.* **2006,** *45,* 7274–7277. doi:10.1002/anie.200603132

22. Lu, X.-B.; Ren, W.-M.; Wu, G.-P. *Acc. Chem. Res.* **2012,** *45,* 1721–1735. doi:10.1021/ar300035z

23. Chen, S.; Hua, Z.; Fang, Z.; Qi, G. *Polymer* **2004,** *45,* 6519–6524. doi:10.1016/j.polymer.2004.07.044

24. Qin, Y.; Wang, X. *Biotechnol. J.* **2010,** *5,* 1164–1180. doi:10.1002/biot.201000134

25. Dharman, M. M.; Ahn, J.-Y.; Lee, M.-K.; Shim, H.-L.; Kim, K.-H.; Kim, I.; Park, D.-W. *Green Chem.* **2008,** *10,* 678–684. doi:10.1039/b801132j

26. Dienes, Y.; Leitner, W.; Müller, M. G. J.; Offermans, W. K.; Reier, T.; Reinholdt, A.; Weirich, T. E.; Müller, T. E. *Green Chem.* **2012,** *14,* 1168–1177. doi:10.1039/c2gc16485j

27. Fujita, S.-I.; Arai, M.; Bhanage, B. M. Direct Transformation of Carbon Dioxide to Value-Added Products over Heterogeneous Catalysts. *Transformation and Utilization of Carbon Dioxide;* Green Chemistry and Sustainable Technology; Springer-Verlag: Berlin Heidelberg, 2014; pp 39–53. doi:10.1007/978-3-642-44988-8_2

28. North, M. *Chim. Oggi* **2012,** *30,* 3–5.

29. Peppel, W. J. *Ind. Eng. Chem.* **1958,** *50,* 767–770. doi:10.1021/ie50581a030

30. Luinstra, G. A.; Haas, G. R.; Molnar, F.; Bernhart, V.; Eberhardt, R.; Rieger, B. *Chem. – Eur. J.* **2005,** *11,* 6298–6314. doi:10.1002/chem.200500356

31. Klaus, S.; Lehenmeier, M. W.; Herdtweck, E.; Deglmann, P.; Ott, A. K.; Rieger, B. *J. Am. Chem. Soc.* **2011,** *133,* 13151–13161. doi:10.1021/ja204481w

32. Ren, W.-M.; Liu, Z.-W.; Wen, Y.-Q.; Zhang, R.; Lu, X.-B. *J. Am. Chem. Soc.* **2009,** *131,* 11509–11518. doi:10.1021/ja9033999

33. Liu, Z.; Torrent, M.; Morokuma, K. *Organometallics* **2002,** *21,* 1056–1071. doi:10.1021/om0110843

34. Svensson, M.; Humbel, S.; Froese, R. D. J.; Matsubara, T.; Sieber, S.; Morokuma, K. *J. Phys. Chem.* **1996,** *100,* 19357–19363. doi:10.1021/jp962071j

35. Humbel, S.; Sieber, S.; Morokuma, K. *J. Chem. Phys.* **1996,** *105,* 1959–1967. doi:10.1063/1.472065

36. Luinstra, G. A.; Molnar, F. *Macromol. Symp.* **2007,** *259,* 203–209. doi:10.1002/masy.200751324

37. Sun, H.; Zhang, D. *J. Phys. Chem. A* **2007,** *111,* 8036–8043. doi:10.1021/jp073873p

38. Guo, C.-H.; Wu, H.-S.; Zhang, X.-M.; Song, J.-Y.; Zhang, X. *J. Phys. Chem. A* **2009,** *113,* 6710–6723. doi:10.1021/jp809471s

39. Guo, C.-H.; Zhang, X.-M.; Jia, J.-F.; Wu, H.-S. *J. Mol. Struct.: THEOCHEM* **2009,** *916,* 125–134. doi:10.1016/j.theochem.2009.09.020

40. Guo, C.-H.; Song, J.-Y.; Jia, J.-F.; Zhang, X.-M.; Wu, H.-S. *Organometallics* **2010,** *29,* 2069–2079. doi:10.1021/om100020s

41. Ren, Y.; Guo, C.-H.; Jia, J.-F.; Wu, H.-S. *J. Phys. Chem. A* **2011,** *115,* 2258–2267. doi:10.1021/jp104184v

42. Uhe, A.; Hölscher, M.; Leitner, W. *Chem. – Eur. J.* **2012,** *18,* 170–177. doi:10.1002/chem.201102785

43. Ostapowicz, T. G.; Hölscher, M.; Leitner, W. *Chem. – Eur. J.* **2011,** *17,* 10329–10338. doi:10.1002/chem.201101463

44. Ferro, L.; Hitchcock, P. B.; Coles, M. P.; Cox, H.; Fulton, J. R. *Inorg. Chem.* **2011,** *50,* 1879–1888. doi:10.1021/ic102273n

45. Darensbourg, D. J.; Mueller, B. L.; Bischoff, C. J.; Chojnaoki, S. S.; Reibenspies, J. H. *Inorg. Chem.* **1991,** *30,* 2418–2424. doi:10.1021/ic00010a035

46. Kato, M.; Ito, T. *Inorg. Chem.* **1985,** *24,* 504–508. doi:10.1021/ic00198a015

47. Kunert, M.; Bräuer, M.; Klobes, O.; Görls, H.; Dinjus, E.; Anders, E. *Eur. J. Inorg. Chem.* **2000,** *2000,* 1803–1809. doi:10.1002/1099-0682(200008)2000:8<1803::AID-EJIC1803>3.0.CO; 2-L

48. Elmas, S.; Subhani, M. A.; Vogt, H.; Leitner, W.; Müller, T. E. *Green Chem.* **2013,** *15,* 1356–1360. doi:10.1039/c3gc40147b

49. Zhuang, X.; Oyaizu, K.; Niu, Y.; Koshika, K.; Chen, X.; Nishide, H. *Macromol. Chem. Phys.* **2010,** *211,* 669–676. doi:10.1002/macp.200900472

50. Huang, D.; Makhlynets, O. V.; Tan, L. L.; Lee, S. C.; Rybak-Akimova, E. V.; Holm, R. H. *Proc. Natl. Acad. Sci. U. S. A.* **2011,** *108,* 1222–1227. doi:10.1073/pnas.1017430108

51. Wang, T.-T.; Xie, Y.; Deng, W.-Q. *J. Phys. Chem. A* **2014,** *118,* 9239–9243. doi:10.1021/jp506124h

52. Bligaard, T.; Nørskov, J. K.; Dahl, S.; Matthiesen, J.; Christensen, C. H.; Sehested, J. *J. Catal.* **2004,** *224,* 206–217. doi:10.1016/j.jcat.2004.02.034

53. Pápai, I.; Schubert, G.; Mayer, I.; Besenyei, G.; Aresta, M. *Organometallics* **2004,** *23,* 5252–5259. doi:10.1021/om049496+

54. Cokoja, M.; Bruckmeier, C.; Rieger, B.; Herrmann, W. A.; Kühn, F. E. *Angew. Chem., Int. Ed.* **2011,** *50,* 8510–8537. doi:10.1002/anie.201102010

55. Wang, J.-Q.; Dong, K.; Cheng, W.-G.; Sun, J.; Zhang, S.-J. *Catal. Sci. Technol.* **2012,** *2,* 1480–1484. doi:10.1039/c2cy20103h

56. Lu, X.-B.; Zhang, Y.-J.; Jin, K.; Luo, L.-M.; Wang, H. *J. Catal.* **2004,** *227,* 537–541. doi:10.1016/j.jcat.2004.07.018

57. Delley, B. *J. Chem. Phys.* **1990,** *92,* 508–517. doi:10.1063/1.458452

58. Delley, B. *J. Chem. Phys.* **2000,** *113,* 7756–7764. doi:10.1063/1.1316015

59. Perdew, J. P.; Burke, K.; Ernzerhof, M. *Phys. Rev. Lett.* **1996,** *77,* 3865–3868. doi:10.1103/PhysRevLett.77.3865

60. Govind, N.; Petersen, M.; Fitzgerald, G.; King-Smith, D.; Andzelm, J. *Comput. Mater. Sci.* **2003,** *28,* 250–258. doi:10.1016/S0927-0256(03)00111-3

61. Kemper, S.; Hrobárik, P.; Kaupp, M.; Schlörer, N. E. *J. Am. Chem. Soc.* **2009,** *131,* 4172–4173. doi:10.1021/ja806151g

62. Sun, K.; Li, W.-X.; Feng, Z.; Li, C. *Chem. Phys. Lett.* **2009,** *470,* 259–263. doi:10.1016/j.cplett.2009.01.044